# UNIVERSITÉ DE STRASBOURG

*ÉCOLE DOCTORALE PHYSIQUE ET CHIMIE-PHYSIQUE*

**ICPEES Institut de Chimie Pour l'Energie, l'Environnement et la Santé**

# THÈSE présentée par :

**Salima NEDJARI**

Soutenue publiquement le : **21 octobre 2014**

pour obtenir le grade de : **Docteur de l'Université de Strasbourg**

DISCIPLINE : PHYSIQUE-CHIMIE

SPECIALITE : BIOMATERIAUX

# Microstructuration of nanofibrous membranes by electrospinning: Application to tissue engineering

**Membres du jury:**

| | |
|---|---|
| **M. Guy SCHLATTER** | Professeur, Université de Strasbourg<br>**Directeur de Thèse** |
| **M$^{me}$ Karen DE CLERCK** | Professeur, Université de Gent<br>**Rapporteur externe** |
| **M. Christophe EGLES** | Professeur, Université de Technologie de Compiègne<br>**Rapporteur externe** |
| **M. Luc AVEROUS** | Professeur, Université de Strasbourg<br>**Examinateur interne** |

*A Papa et Maman, mes parents bien-aimés,*

*A ma grande soeur Fatiha chérie,*

*A mes petits choux qui grandissent,*

*A ma cousine Rachida, paix à son âme,*

# Remerciements

*Mes travaux de thèse ont été effectués au sein de l'Institut de Chimie et Procédés pour l'Environnement, l'Energie et la Santé (ICPEES) UMR7515 et également au sein de l'unité de Médecine Nano-Régénérative U1109 de l'INSERM.*

*J'exprime une profonde gratitude et mes très sincères remerciements à Monsieur le Professeur Guy Schlatter, mon directeur de thèse. Je le remercie pour sa gentillesse, sa disponibilité et pour m'avoir si bien encadrée et guidée durant ces années de recherches. Je suis très heureuse d'avoir pu travailler avec lui et je pense avoir beaucoup appris à son contact. Il a su me transmettre son esprit passionné pour l'électrospinning et je l'en remercie sincèrement.*

*Je souhaite également remercier très sincèrement le Docteur Anne Hébraud pour m'avoir encadrée durant ma thèse et pour m'avoir appris tant de choses. Je la remercie pour sa gentillesse, sa disponibilité et les précieux conseils qu'elle m'a donnés.*

*J'adresse mes sincères remerciements aux membres du jury qui ont accepté d'évaluer mon travail de thèse :*
*Mme Karen De Clerck, professeur à l'Université de Gent, et Mr Christophes Egles, professeur à l'Université de Technologie de Compiègnes pour avoir accepté d'être de participer à mon jury de thèse en tant que rapporteurs externes.*
*Mr Luc Averous, professeur à l'Université de Strasbourg, pour avoir accepté de participer à mon jury de thèse en tant qu'examinateur.*
*Mme Anne Hébraud et Mme Nadia Benkirane-Jessel pour avoir accepté de participer à mon jury de thèse en tant que membres invités.*

*Je souhaiterai particulièrement remercier les partenaires du projet NeoTissage, projet dans lequel s'inscrit ma thèse.*
*Tout d'abord, je remercie très sincèrement le Docteur Nadia Benkirane-Jessel de l'INSERM pour m'avoir accueilli au sein de son équipe, pour ses encouragements et ses précieux conseils.*
*Je remercie très chaleureusement le Docteur Ségolen Geffray de l'IRMA, pour son incroyable gentillesse et sa bonne humeur. Son aide et ses explications m'ont étaient très précieux pour ma thèse.*

*Enfin, je remercie particulièrement le Docteur Sandy Eap de l'INSERM pour notre très fructueuse et très agréable collaboration. Je la remercie pour son écoute et son aide dans mes travaux de recherches.*

*Je tiens également à adresser mes sincèrement remerciements à Mr Nabyl Khenoussi, Maitre de Conférences à l'ENSISA pour m'avoir fait découvrir les nanofibres, pour sa gentillesse et pour m'avoir encouragée tout au long de ma thèse.*

*Ensuite, je souhaiterai adresser mes profonds remerciements au personnel technique de l'ICPEES sans qui je n'aurai pas pu avancer aussi bien dans ma thèse : Sabine Siegwald, Romain Bernard (IPCMS), Christophe Mélart, Christophe Sutter et Thierry Djekkriff. Je suis très reconnaissante pour toute l'aide qu'ils m'ont apporté et je l'ai remercie pour l'incroyable bonne humeur dans laquelle on a travaillé.*
*Je remercie également Chheng Ngov, Sébastien Gallet et Catherine Kientz pour leur gentillesse, leur aide et leur disponibilité.*
*Je remercie également Badi Triki pour les très bons moments qu'on a passés ensemble au laboratoire d'électrospinning.*

*Au sein de l'ICPEES, je remercie très chaleureusement l'ensemble des doctorants, post-doctorants, stagiaires que j'ai pu rencontrer et qui m'ont apporté beaucoup de joie durant ces années de thèse: Allan, Anna, Bilal, Bruno, Camille, Cannan, Cédric, Dambarudhar, Deepak, Dhriti, Dias, François-Xavier, Ikram, Inès, Jon, Julianna, Julianno, Lukas, Marie, Marina, Matthieu, Nancy, Rigoberto, Rogério, Rouba, Simon, Shugai, Stéphanie, Stéphane, Thibaud, Victor, Wei et Yuefengh.*

*Au sein de l'unité de médecine régénérative U1109, je remercie Sabine Bopp-Kuchler, Arielle Ferrandon, Tunay, Laeticia, et Stéphanie pour leur bonne humeur.*

*Je remercie également mes amies : Sarah, Jessica et Nour. Merci de m'avoir motivée pendant toutes ces années.*

*Enfin, je remercie ceux qui m'ont toujours encouragée et soutenue durant toutes ces années d'études et que j'aime très fort : mes parents Abdelkader Nedjari et Khedouja Nedjari pour leur amour et leur générosité. Et également un immense merci à ma grande sœur Fatiha Nedjari que j'aime très très fort : merci infiniment pour ton amour inconditionnel et pour avoir si bien veillé sur moi.*

Titre français :

Micro-structuration de membranes nanofibreuses par électrospinning : application à l'ingénierie tissulaire

---

Cette thèse de doctorat a été rédigée en utilisant, pour chaque chapitre, le format habituellement adopté dans les articles scientifiques paraissant dans des revues à comité de lecture. L'indulgence du lecteur est ainsi sollicité pour les répétitions et redites inhérentes à la forme de rédaction choisie.

---

Le présent mémoire de thèse a été rédigé en langue anglaise, conformément à l'autorisation délivrée par Monsieur le Professeur Éric WESTHOF, professeur des Universités à l'université de Strasbourg, et vice-président de l'université de Strasbourg, chargé de la recherche et de la formation doctorale, le 08 juillet 2008.

**REMERCIEMENTS** ..... **5**

**RESUME** ..... **15**

**ABSTRACT** ..... **17**

**ABBREVIATIONS, ACRONYMS AND SYMBOLS** ..... **19**

**GENERAL INTRODUCTION** ..... **21**

**CHAPTER 1: AN INTRODUCTION TO ORGANIZED NANOFIBERS : FROM 1D TO 3D** ..... **35**

1. ELECTROSPINNING PROCESS ..... 37

*1.1 Electrospinning theory* ..... *37*

*1.2 Electrospinning setup* ..... *39*

*1.3 Electrospinning parameters* ..... *40*

2. ORGANIZED ASSEMBLY OF ELECTROSPUN NANOFIBERS: FROM 1D TO 3D ..... 48

*2.1 Fiber Alignment* ..... *49*

2.1.1 Electrostatic Forces ..... 49

2.1.2 Magnetic Forces ..... 53

2.1.3 Mechanical forces ..... 54

*2.2 2D Patterned Nanofibrous Membranes* ..... *59*

2.2.1 2D Composites formed from 1D aligned fibers ..... 59

2.2.2 Complex 2D patterned membranes by precise control of electrostatic forces ..... 60

2.2.3 Self-assembly of electrospun fibers ..... 64

*2.3 Towards 3D Nanofibrous Constructs* ..... *69*

2.3.1 Specific electrospinning processes for 3D constructs ..... 69

2.3.2 3D Cm-thick scaffolds from self-assembled electrospun fibers ..... 70

*2.4 Conclusions of the structuration* ..... *73*

3. CONCLUSIONS OF CHAPTER 1 ..... 74

# CHAPTER 2: MONOCOMPONENT 2D AND 3D ARCHITECTURED NANOFIBROUS SCAFFOLDS FOR BONE REGENERATION..... 77


1. INTRODUCTION ..... 79

2. MATERIALS AND METHODS ..... 80

*2.1 Photolithographic processes ..... 80*

2.1.1 Principle ..... 80

2.1.2 Main steps in photolithography process used during this work. ..... 81

*2.2 Polymers for bone tissue engineering applications ..... 84*

2.2.1 PCL ..... 85

2.2.2 PLA ..... 86

3. ELECTROSPINNING OF PCL AND PLA ..... 89

*3.1 Electrospinning of PCL ..... 89*

*3.2 Electrospinning of PLA ..... 93*

4. 2D STRUCTURATION ..... 96

*4.1 Electrospinning on block collectors ..... 96*

*4.2 Electrospinning on honeycomb micropatterned collectors ..... 100*

*Electrospun Honeycomb as Nests for Controlled Osteoblast Spatial Organization ..... 100*

4.2.1 Introduction ..... 101

4.2.2 Experiments ..... 103

4.2.3 Results and Discussion ..... 106

4.2.4 Conclusions ..... 116

4.2.5 Supporting informations ..... 117

5. 3D STRUCTURATION ..... 122

*5.1 Introduction ..... 122*

*5.2 Materials and Methods ..... 123*

5.2.1 Fabrication of honeycomb micropatterned collector ..... 123

5.2.2 Electrospinning of 3D Scaffold ..... 123

5.2.3 Scanning electron microscopy (SEM) and X-ray microcomputed tomography ..... 124

*5.3 Results and Discussions ..... 124*

*5.4 Conclusions ..... 128*

*5.5 Supporting informations ..... 129*

6. CONCLUSIONS OF THE CHAPTER TWO ..... 131

# CHAPTER 3: COMPOSITE 2D AND 3D ARCHITECTURED NANOFIBROUS SCAFFOLDS ..... 134

1. INTRODUCTION ..... 136

2. ELECTROSTATIC TEMPLATE-ASSISTED DEPOSITION OF MICROPARTICLES ON ELECTROSPUN NANOFIBERS: APPLICATION TO THE FABRICATION OF BIOCHIPS FOR THE SCREENING OF COMPOSITE MICROSTRUCTURED MATERIALS FOR BONE REGENERATION ..... 137

*2.1 Introduction ..... 137*

*2.2 Electrostatic template-assisted deposition of microparticles on electrospun nanofibers ..... 140*

2.2.1 Electrospraying of hydroxyapatite ..... 140

2.2.2 Electrospinning and cross-linking of Alginate nanofibers ..... 142

2.2.3 Selected experimental conditions ..... 147

2.2.4 Controlled deposition of hydroxyapatite particles on electrospun fibers ..... 147

*2.3 Biochip by electrospinning and electrospraying: application for the screening of PCL/HA microstructured composites for bone regeneration ..... 150*

2.3.1 Protocols ..... 152

2.3.2 Results and discussions ..... 153

*2.4 Screening of composite fibrous structured materials for bone regeneration: preliminary results ..... 161*

2.4.1 Protocols for biological characterization ..... 161

2.4.2 Results and discussion ..... 163

*2.5 Conclusions ..... 170*

3. 3D COMPOSITE ELECTROSPUN SCAFFOLD WITH CONTROLLED PORE SIZE ..... 172

*3.1 Introduction ..... 172*

*3.2 Experimental Section ..... 174*

3.2.1 Materials ..... 174

3.2.2 Fabrication of the collectors ..... 174

3.2.3 Electrospinning / electrospraying ..... 175

3.2.4 SEM analysis ..... 175

3.2.5 Mechanical characterization ..... 176

*3.3 Results and discussion ..... 177*

*3.4 Conclusion* ..... *188*

4. CONCLUSIONS OF THE CHAPTER THREE ..... 189

**GENERAL CONCLUSION AND PERSPECTIVES ..... 191**

CONCLUSIONS AND PERSPECTIVES ..... 192

**REFERENCES ..... 199**

**PUBLICATIONS LISTS AND COMMUNICATIONS ..... 215**

# Résumé

L'objectif de cette thèse était de développer de nouveaux biomatériaux nanofibreux architecturés (2D ou 3D) grâce à la méthode d'électrospinning puis d'étudier l'influence de ces structures nanofibreuses sur le comportement des cellules osseuses. L'électrospinning est une technique qui permet d'obtenir des nanofibres en projetant sous l'action d'un champ électrique intense une solution de polymère sur un collecteur. Le jet de la solution de polymère, émanent de l'émetteur (une aiguille métallique soumis à une tension de plusieurs kV), subit des mouvements de fouet violents qui conduisent à la réduction du diamètre et à l'évaporation du solvant. Les nanofibres sont alors généralement disposées aléatoirement sous forme de mats (ou scaffolds). Ces scaffolds trouvent des applications en ingénierie tissulaire grâce à leur structure mimant la matrice extracellulaire des tissus vivants. Toutefois, il a été montré que lorsque le collecteur est micro-structuré, il est alors possible de contrôler l'organisation des fibres lors de leur dépôt grâce à la perturbation locale du champ électrique au voisinage de la surface du collecteur. Ces collecteurs architecturés jouent ainsi le rôle de « templates » électrostatiques. C'est dans ce contexte que s'est inscrit ce sujet de thèse.

Dans un premier temps, nous avons développé des scaffolds 2D nanofibreux monocomposants en forme de nids d'abeilles grâce à l'utilisation d'un collecteur micro-structuré en nids d'abeilles lors du procédé d'électrospinning. Ces scaffolds ont été développés à partir de deux biopolyesters le poly(ε-caprolactone) (PCL) ou le poly(lactic acid) (PLA). Nous avons prouvé que la morphologie des nanofibres de PCL (distribution bimodale du diamètre des fibres) conduisait à un scaffold présentant un relief beaucoup plus marqué alors qu'avec les fibres de PLA, qui présentent une distribution monomodale du diamètre des fibres, les scaffolds obtenus sont beaucoup plus plats. Puis nous avons montré qu'il est possible de contrôler l'organisation spatiale de cellules osseuses de type MG-63, des ostéoblastes, en jouant sur le relief et l'architecture du scaffold.

Puis, nous avons cherché à développer des matériaux 3D en utilisant des collecteurs micro-structurés afin d'ouvrir de nouvelles voies pour l'élaboration de matériaux de comblement pour la régénération osseuse. Nous avons démontré qu'en couplant la micro-structuration des nanofibres de PCL (par l'utilisation d'un collecteur en nid d'abeilles lors du procédé d'électrospinning) avec les propriétés d'auto-assemblage du PCL, nous pouvions élaborer de nouveaux scaffolds nanofibreux 3D ayant la particularité de présenter des pores de tailles contrôlées ainsi qu'un gradient de porosité dans l'épaisseur du scaffold.

Puis nous nous sommes intéressés à l'élaboration de membranes composites micro-structurées 2D et 3D. En couplant le procédé d'électrospinning avec le procédé d'électrospraying sur des collecteur micro-structurés, nous avons démontré que nous pouvions déposer de manière contrôlée les particules spécialement sur les murs des nids d'abeilles grâce notamment à la présence d'une très fine couche de fibres électrospinnées au préalable sur le collecteur. Cette fine couche de nanofibres joue le rôle de « template électrostatique » pour le dépôt des particules.

Nous avons ensuite appliqué cette technique pour développer des membranes composites nanofibreuses bicouches à base de nanofibres de PCL et de microparticules d'hydroxyapatite (HA). Ces membranes composées de 21 microarchitectures différentes (barres, plots, hexagones, labyrinthe) ont ensuite été intégrées dans des mini plaques de culture cellulaire, formant ainsi un nouveau type de biopuce, pour le screening d'architectures nanofibreuses. En effet, ces biopuces appelées biochip ont prouvé qu'elles permettaient de réaliser le screening de microarchitectures nanofibreuses composites afin d'identifier la plus pertinente pour la régénération osseuse. Il s'est avéré que la structure HA hexagonale (avec un diamètre moyen de 300 µm) ainsi que les structures HA circulaires (avec un diamètre moyen 150 µm environ) sont celles qui améliorent le mieux le processus de minéralisation des cellules osseuses.

Enfin, nous avons montré qu'il est possible d'élaborer des scaffolds composites 3D en combinant simultanément l'électrospinning de nanofibres et l'électrospraying de particules sur des collecteur micro-structurés en nid d'abeilles. Il est possible de contrôler la taille des pores cylindriques de ces composites 3D de quelques dizaines de microns à quelques centaines de microns en changeant la taille du nid d'abeilles du collecteur.

## Abstract

The aim of this thesis was to develop new architectured nanofibrous biomaterials (2D or 3D) using the electrospinning method and to study the influence of these nanofibrous structures on bone cells behaviors. Electrospinning is a technique allowing the production of nanofibers by projecting, under the action of a strong electric field, a polymer solution on a collector. The jet of the polymer solution, emitted from a metalic needle subjected to a voltage of several kV, undergoes strong whipping movements, resulting in the evaporation of the solvent and the reduction of the diameter of the nanofiber. The nanofibers are generally randomly deposited and form mats or scaffolds. These scaffolds are interesting for tissue engineering applications because of their structure mimicking the extracellular matrix of living tissues. However, it has been shown that when the collector is microstructured, it is possible to control the organization of the fibers during their deposition through the local perturbation of the electric field at the vicinity of the surface of the collector. These micropatterned collectors act as "electrostatic templates".

First, 2D honeycomb nanofibrous scaffolds were elaborated using micropatterned honeycomb collectors during the electrospinning process. These scaffolds were made either with poly(ε-caprolactone) (PCL) or poly(lactic acid) (PLA). We showed that the morphology of the PCL nanofibers (bimodal distribution of the fiber diameter) led to a scaffold with a strong relief. Despite, with PLA fibers which presented a monomodal distribution of the fiber diameter, the obtained scaffolds were much flatter. It was possible to control the spatial organization of bone-like cells MG-63 (osteoblasts), playing on the relief and the architecture of the scaffold.

Subsequently, 3D materials were elaborated using micropatterned collectors in order to open new paths for the development of filling materials for bone regeneration. Microstructuration of PCL nanofibers (by the use of micropatterned honeycomb collector during the electrospinning process) coupled with the self-assembling properties of the PCL lead to the development of new 3D nanofibrous scaffolds, with controlled pore size and porosity gradient in the thickness of the scaffold.

Afterwards, micropatterned composite 2D and 3D membranes were elaborated. By coupling the process of electrospinning with the process of electrospraying on micropatterned collector, we demonstrated that we can deposit the particles in a controlled way, especially on the walls of honeycomb patterns thanks to the presence of a thin fiber layer first deposited on

the collector. This thin nanofiber layer plays the role of an "*electrostatic template*" for the particles deposition.

Thereafter, this technique was applied to develop bilayers composite nanofibrous membranes containing PCL nanofibers and hydroxyapatite (HA) microparticles. These membranes consisted of 21 different microarchitectures (bars, blocks, hexagons, maze) were then incorporated into a small cell culture plate, thereby forming a new type of biochip for the screening of nanofibrous architectures. Indeed, these biochips allowed the screening of nanofibrous microarchitectures to identify the most relevant for bone regeneration. It turned out that the HA hexagonal structures (with an average diameter of 300 microns) and circular HA structures (with an average diameter of 150 microns) are the structures that enhance the most the mineralization process of bone cells.

Finally, by combining simultaneously electrospinning nanofibers and electrospraying particles on micropatterned honeycomb collector, 3D composite scaffolds were elaborated. It was possible to control the size of cylindrical pores of these 3D composite from tens to hundreds of microns by changing the size of the honeycomb patterns of the collector.

# Abbreviations, acronyms and symbols

| | |
|---|---|
| AA | Acetic Acid |
| Al | Alginate |
| BSPII | Bone SialoProtein II |
| C | Concentration |
| $Ca(OH)_2$ | Calcium Hydroxyde |
| $Ca_{10}(PO_4)_6(OH)_2$ | Hydroxyapatite |
| $CHCl_3$ | Chloroform |
| $CaCl_2$ | Calcium Chloride |
| DCM | Dichloromethane |
| DMF | Dimethylformamide |
| DW | Deionized Water |
| EtOH | Ethanol |
| FA | Formic Acid |
| FDA | Food and Drug Administration |
| GTA | Glutaraldehyde |
| HA | Hydroxyapatite |
| HFIP | Hexafluoropropan-2-ol |
| $H_3PO_4$ | Orthophosphoric acid |
| OCN | Osteocalcin |
| PBS | Phosphate Buffer Saline |

| | |
|---|---|
| PCL | Poly(ε-caprolactone) |
| PDMS | Polydimethylsiloxane |
| PEG | Poly(ethylene glycol) |
| PEO | Polyethylene Glycol |
| PFA | Paraformaldehyde |
| PGA | Polyglycolic Acid |
| PLA | Poly(lactic acid) |
| PMMA | Poly(methyl methacrylate) |
| PS | Polystyrene |
| PVA | Polyvinyl alcool |
| SEM | Scanning Electron Microscopy |
| TFE | 2,2,2-trifluoroethanol |
| $T_g$ | Glass Temperature |
| THF | Tetrahydrofuran |
| $T_m$ | Melting point |
| $\varepsilon_r$ | Resistivity |

# General Introduction

**Context:**

Currently, global population is ageing and new health challenges have emerged. Indeed, while in the past, people were dying of infectious diseases, nowadays, the number of chronic diseases is increasing and has become responsible of health loss and death. Contrary to infectious diseases which are cured by antibiotics, the chronic diseases should be cured by regenerative approaches [1].

Among these chronic diseases, bone diseases represent a big challenge due to apparent inability of bone to self-repair. Indeed, there is no effective therapy available and patients can only be helped by surgical joint replacement. An inherent major concern is the limited availability of autografts, which significantly reduces the number of treatable defects. Therefore, tissue engineering for bone regeneration appears as the most promising alternative.

The term "Tissue engineering" was firstly used by Dr. Fung from California University during the National Science Foundation Meeting in 1987 [2]. The official definition dates to 1988 and was published in 1988 by Skalak and Fox, after the Tissue engineering meeting held in USA this year [3].

Tissue engineering refers to an "interdisciplinary field that applies the principles of engineering and life sciences toward the development of biological substitutes that restore, maintain or improve tissue function" [4]. In 1993, Langer and Vacanti introduced three different strategies of tissue engineering [3] (**Figure 1**):

(a) The development of cell therapy : infusion of cells at the lesion place (like stem cells)
(b) The development of specific molecules (such as growth factor, small molecules which promote several effects on the cells)
(c) The development of scaffold or matrices, which are placed at the lesion, and which enhances and promotes the regeneration process.

While research has been made about cells and specific molecules, the degree of success of tissue engineering is still highly dependent on the properties of the scaffold.

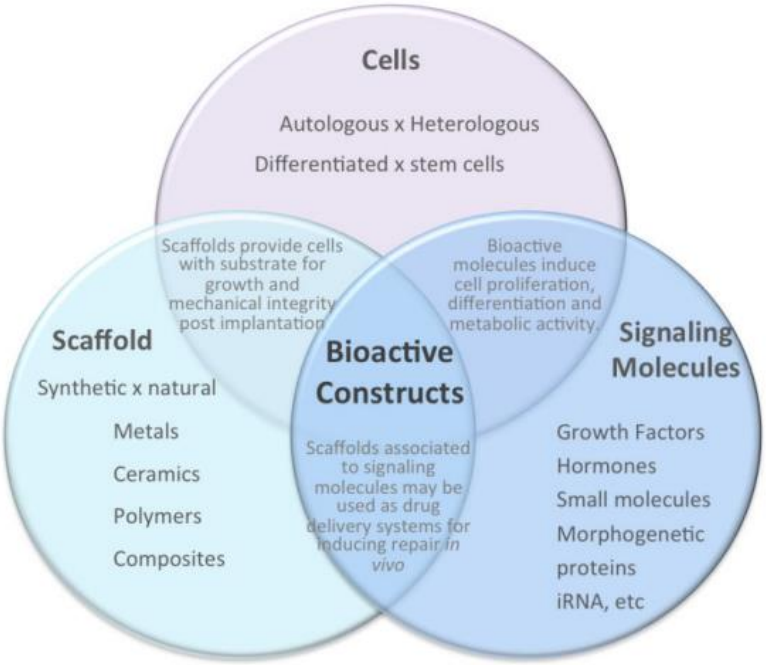


**Figure 1: Tissue engineering strategies: As proposed by Langer and Vacanti [5, 6], tissue engineering can be performed by different approaches. Combining cells, scaffolds and signaling molecules can be the best association for tissue regeneration.**

It is now very important to develop efficient biomaterials for bone regeneration. Efforts have to be made on the Achilles' hill of tissue engineering: the scaffold. The main challenge relies upon the design of ideal scaffold/ synthetic matrices that can mimic the structure and biological functions of the natural extracellular matrix.

The scaffold plays a key role as it must guide the cell growth, allow the synthesis of extracellular matrix and other biological molecules and facilitate the formation of new functional tissue. There are several basic and important requirements for the design of bone regeneration scaffold. It should:

(a) Be biocompatible : the scaffold should not be rejected when it is put at the lesion place

(b) Be biodegradable : it should degrade with the same speed (rate) than the new tissue is growing

(c) Present good mechanical properties, near to the native mechanical properties of the native organ

(d) Have a good porosity, which will allow nutrients intakes and cell penetration deeper in the scaffold

(e) Present functional character in order to enhance bone cells-scaffold interactions such as adhesion, growth, migration, differentiation function, and bio-mineralization.

(f) Mimic well the structure of the native tissue

It is also well known that because the extracellular matrix is made of collagen nanofibers, the scaffold must show specific fibrous morphology. Besides, one of the most promising techniques to develop nanofibrous scaffold for tissue engineering is electrostatic spinning also called electrospinning.

Electrospinning was invented and patented in 1902 by Cooley [7] and Morton [8]. This technology allows the production of nanofibers by the projection of a polymer solution under a high electrical field in order to produce nanofibers with a diameter ranging from few tens of nm to few microns.

Electrospinning was patented in 1934 by Formhals [9]. However, due the incapacity to observe the obtained nanofibers, scientists were not interested by this technique.

It is only in the 1990's that electrospinning was rediscovered. Renecker *et al.* showed that electrospun fabrics are promising materials due to their high surface to volume ratio and their capability to mimic natural tissues [10, 11].

Furthermore, this technique is applicable with any kind of polymer which can be dissolved in a solvent or molten by heating. Therefore, electrospinning can be used in many domains such as filtration [12, 13], protective clothes [14, 15], environmental engineering [16, 17], electronics [18, 19], and of course biomedical [20-22] and tissue engineering [23, 24]. For all these reasons, electrospinning presents a growing interest for researchers around the world (**Figure 2**).

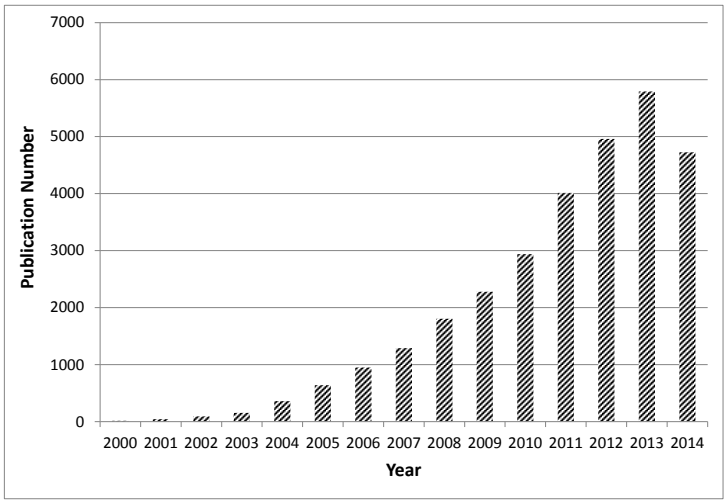


**Figure 2: Plot of annual research publications concerning electrospinning studies. Search data from http://www.scopus.com, years 2000–2014, using "electrospinning" or "electrospun," as article title, abstract, or keywords.**

**Structuration of electrospun nanofibers:**

Many tissues or organs (heart, nerves, and skin) have a native complex structure and bones are among them. Effective regeneration process of these complex tissues could only be possible with scaffolds that are able to mimic as closely as possible the native structure of these tissues.

Electrospinning is a very interesting technique in the field of tissue regeneration due to its capability to structure the nanofibers from one dimension to three dimensions. Indeed, while with a classical electrospinning setup, fibers are generally collected in a random way on the collector (generally an aluminum foil), it is possible to structure the electrospun mat by just changing the nature of the collector. Researchers have developed different kinds of collectors in order to organize the nanofibers from simply aligned nanofibers to complex three dimensional nanofibrous scaffolds [25]. Now, architectured electrospun scaffolds with fibrous/ porous/ roughness morphology (from several nm to hundreds µm length scales) can be obtained. They are used in different fields of tissue engineering. Thanks to *in vitro* an *in vivo* studies, the efficiency of these electrospun architectured scaffolds is evaluated. Despite, very often, the influence of the electrospun scaffold morphology on cells behaviors is not very well explained and understood.

This thesis seeks to elaborate and to study new kinds of micropatterned scaffolds obtained by electrospinning process for bone regeneration applications. The control of the architecture of electrospun scaffolds is explained. The influence of different micropatterned electrospun structures on osteoblast cells behaviors such as spatial organization and mineralization is studied.

The first chapter of this work is a review of all the methods existing to organize the nanofibers from 1D to 3D dimensions with the electrospinning process. The effect of the different forces acting on the fiber structuration during the process is explained.

In the second chapter, the elaboration of monocomponent micropatterned electrospun scaffold is presented. The first part of this chapter deals with 2D monocomponent micropatterned scaffolds. Thanks to photolithographic processes, micropatterned collectors were obtained (block collector and honeycomb collector). Two kinds of biopolyesters were then tested for the fabrication of the electrospun membranes. After optimization of the electrospinning parameters, honeycomb electrospun scaffolds were elaborated either with poly(ε-caprolactone) (PCL) either with poly(lactic acid) (PLA). First, the effect of the fiber morphology on the morphology at the scaffold's length scale was discussed. Then, the

influence of honeycomb structure of the electrospun scaffold on osteoblast cells organization was showed. In the second part of the Chapter 2, elaboration of 3D monocomponent micropatterned scaffolds is presented. We demonstrate that by using honeycomb collector and the self-assembling properties of fibers, we were able to fabricate a new kind of 3D electrospun scaffold. The mechanism of formation of such 3D electrospun scaffold is explained. This scaffold has the particularity to present porous columns and porosity gradient with controlled pore size, which could be useful for bone regeneration applications.

The third chapter deals with composites micropatterned electrospun membranes elaborated with nanofibers (PCL, alginate or PLA) and microparticles (hydroxyapatite or poly(ethylene oxide) (PEO)). In the first part of this chapter, we present a new kind of 2D composite electrospun microstructured membrane. First, we explained the "electrostatic template effect" leading to the local controlled deposition of particles on an electrospun thin membrane deposited on a micropatterned collector. This kind of composite membranes were used in a new device called a biochip. The biochip was dedicated for screening application for bone regeneration. This device was made for testing different nanofibrous structures at the same time. It was developed in order to find quickly which kind of architecture of the nanofibrous membranes can induce the best bone regeneration process. Therefore, a biochip was an on-chip small cell culture plate with 21 different wells. In each well, a specific architecture made by PCL nanofibers and hydroxyapatite microparticles is included. The smaller size of the biochip and the screening of the different micropatterned composite electrospun membranes (located in each well) made this device a new tool for rapid diagnosis in bone tissue regeneration. On the second part of the third chapter, we present new kind of 3D composite micropatterned membrane. These 3D composite construct were elaborated by alternately electrospraying and electrospinning onto a honeycomb micropatterned collector. We showed that these scaffolds presented cylindrical pores with an internal diameter that could be tuned precisely from tens to hundreds microns. Tensile measurements showed good mechanical properties of these scaffolds, promoting their use in tissue regeneration applications.

Finally, general conclusions and perspectives of this work are presented.

## Contexte:

Actuellement, la population mondiale vieillit de plus en plus, et de nouveaux défis de santé ont vu le jour. En effet, alors que dans le passé, les gens mouraient de maladies infectieuses, de nos jours, le nombre de maladies chroniques augmente et est devenu le principal facteur de décès de la population. Contrairement aux maladies infectieuses qui sont soignées par la prise d'antibiotiques, les maladies chroniques doivent être soignées par des approches régénératives [1].

Parmi ces maladies chroniques, les maladies osseuses représentent un important défi en raison de l'incapacité apparente de l'os à s'auto-réparer. En effet, il n'existe aucun traitement efficace disponible à ce jour et les patients ne peuvent être aidés que par des arthroplasties chirurgicales. Une des préoccupations majeures qui en découle est la disponibilité limitée des autogreffes, ce qui réduit considérablement le nombre de patients traitables. Par conséquent, l'ingénierie tissulaire apparaît comme la solution la plus prometteuse pour la régénération osseuse.

Le terme «ingénierie tissulaire » a d'abord été utilisé par le Dr Fung de l'Université de Californie lors de l'Assemblée National Science Foundation en 1987 [2]. La définition officielle remonte à 1988 et a été publié en 1988 par Skalak et Fox, après la conférence sur l'ingénierie tissulaire tenue aux Etats-Unis cette même année [3].

L'ingénierie tissulaire se réfère à un "domaine interdisciplinaire qui applique les principes d'ingénierie et de sciences de la vie afin de développer des substituts biologiques qui peuvent restaurer, maintenir ou améliorer la fonction des tissus" [4]. En 1993, Langer et Vacanti introduisent trois stratégies différentes en ingénierie tissulaire [3] (**Figure 1**):

(a) Le développement de la thérapie cellulaire: injection de cellules à l'endroit de la lésion (comme des cellules souches par exemple)

(b) La mise au point de molécules spécifiques (tels que des facteurs de croissance, des petites molécules qui favorisent différents effets sur les cellules)

(c) Le développement de scaffolds ou matrices, qui sont mis en place au niveau de la lésion, et qui améliorent et favorisent le processus de régénération.

Bien que beaucoup de recherche ait été faite au sujet de la thérapie cellulaire et également au sujet de l'élaboration de nouvelles molécules spécifiques, le degré de succès de l'ingénierie tissulaire dépends encore très fortement des propriétés du scaffold qui est introduit au niveau de la lésion.

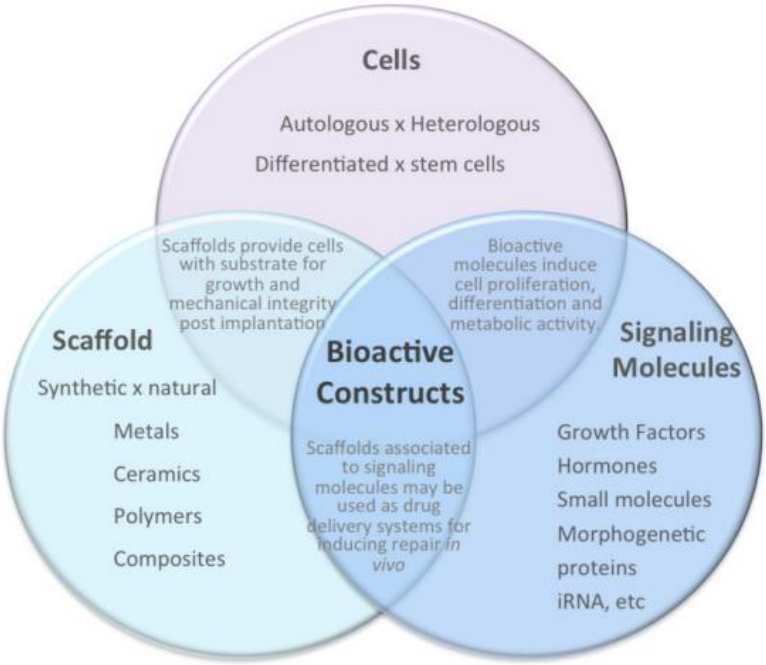


**Figure 1 : Les stratégies en ingénierie tissulaire: Comme proposé par Langer et Vacanti [ 5 , 6 ], l'ingénierie tissulaire peut être effectuée par différentes approches. Combiner à la fois la thérapie cellulaire, l'utilisation de scaffolds ainsi que des molécules spécifiques peut représenter la meilleure association pour parfaire la régénération des tissus.**

Il est maintenant très important de développer des biomatériaux efficaces pour la régénération osseuse. Des efforts doivent être faits en ce qui concerne le talon d'Achille de l'ingénierie tissulaire, à savoir le scaffold. Le principal défi repose sur la conception du scaffold idéal / des matrices synthétiques qui peuvent imiter à la fois la structure et les fonctions biologiques de la matrice extracellulaire naturelle.

Le scaffold joue un rôle essentiel car il doit promouvoir la croissance des cellules, permettre la synthèse de la matrice extracellulaire et d'autres molécules biologiques et également faciliter la formation d'un nouveau tissu fonctionnel. Il y a plusieurs exigences fondamentales et nécessaires pour la conception d'un scaffold dédié à la régénération osseuse. Il doit :

(a) Être biocompatible: le scaffold ne doit pas être rejeté quand il est mis en place au niveau de la lésion.

(b) Être biodégradable: le scaffold doit se dégrader à la même vitesse que le nouveau tissu qui est en train de se former.

(c) Présenter de bonnes propriétés mécaniques, proche des propriétés mécaniques de l'organe qu'il vise à régénérer.

(d) Avoir une bonne porosité, ce qui permettra l'apport de nutriments et une pénétration cellulaire plus profonde dans le scaffold.

(e) Présenter certains propriétés spécifiques afin d'améliorer les intéractions cellules osseuses –scaffold telle que l'adhésion, la croissance, la migration, la différenciation et la bio-minéralisation.

(f) Bien imiter la structure native du tissu.

Il est également bien connu que la matrice extracellulaire est constituée de nanofibres de collagène. Afin d'optimiser le processus de régénération, le scaffold doit présenter une morphologie fibreuse qui tend à mimer la structure fibreuse de la matrice extracellulaire. L'une des techniques les plus prometteuses pour développer des scaffolds nanofibreux pour l'ingénierie tissulaire est le filage électrostatique également appelé électrofilage ou électrospinning.

L'électrospinning a été inventé et breveté en 1902 par Cooley [7] et Morton [8]. Cette technologie permet la production de nanofibres par la projection d'une solution de polymère sous un champ électrique élevé afin de produire des nanofibres ayant un diamètre allant de quelques dizaines de nm à quelques microns.

L'électrospinning a été breveté en 1934 par Formhals [9]. Toutefois, en raison de l'incapacité des scientifiques à observer les nanofibres obtenues, ils ne se sont pas intéressés à cette technique.

Ce n'est que dans les années 1990 que l'électrospinning a été redécouvert. Renecker et al. ont montré que les non-tissés obtenus par électrospinning sont des matériaux prometteurs en raison de leur rapport élevé surface / volume ainsi que leur capacité à mimer les tissus vivants [10, 11].

De plus, cette technique peut être appliquée à tout type de polymère qui peut être dissous dans un solvant ou fondue par chauffage. Par conséquent, l'électrospinning peut être utilisé dans de nombreux domaines tels que la filtration [12, 13], les vêtements de protection [14, 15], le génie environnemental [16, 17], l'électronique [18, 19], et bien sûr le domaine biomédical [20-22] et l'ingénierie tissulaire [23, 24]. Pour toutes ces raisons, l'électrospinning présente un intérêt croissant pour les chercheurs du monde entier (**Figure 2**).

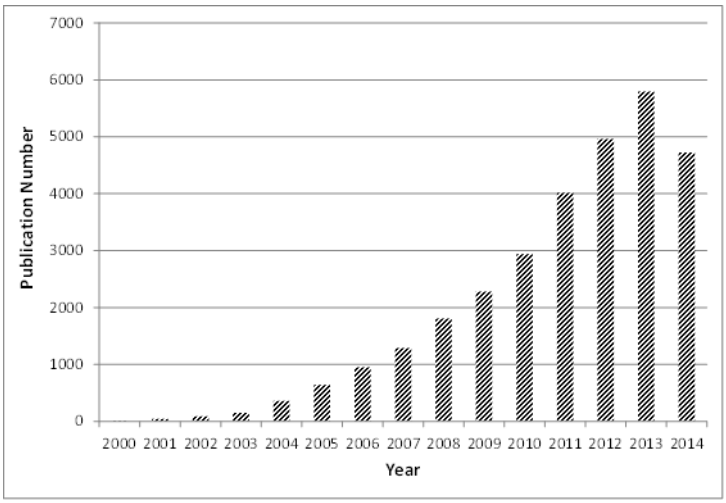


**Figure 2 : Nombre de publications annuels concernant les études portant sur l'électrospinning Recherche des données sur http://www.scopus.com, années 2000-2014, en utilisant les termes « electrospinning » ou « electrospun », comme titre d'article, de résumé, ou de mots-clés.**

## Structuration des nanofibres obtenues par électrospinning :

Beaucoup de tissus ou d'organes (tels que le cœur, les nerfs et la peau par exemple) présentent naturellement une structure complexe. Les os sont également des tissus naturellement structurés. Le processus de régénération de ces tissus ne peut être efficace que si les scaffolds employés sont capable de mimer le plus fidèlement possible la structure native de ces tissus.

L'électrospinning est une technique très intéressante dans le domaine de la régénération des tissus en raison de sa capacité à permettre la structuration de nanofibres d'une dimension à trois dimensions. En effet, en utilisant un montage d'électrospinning classique, les fibres sont généralement collectées de manière aléatoire sur le collecteur (qui est en général une feuille d'aluminium). Cependant il est possible de structurer le tapis de nanofibres en changeant simplement la nature du collecteur. Les chercheurs ont développé différents types de collecteurs afin d'organiser les nanofibres : ils ont pu réaliser à la fois des fibres simplement alignées (1D) jusqu'à l'élaboration de scaffolds 3D nanofibreux complexes [25]. De nos jours, des scaffolds présentant des morphologies à la fois nanofibreuses, poreuses et ayant une rugosité de surface ont pu être obtenus. Ils sont utilisés dans différents domaines de l'ingénierie tissulaire. Grâce aux études *in vitro* et *in vivo*, l'efficacité de ces scaffolds architecturés obtenus par électrospinning a pu être évaluée. Cependant, très souvent, l'influence de la morphologie du scaffold nanofibreux sur les comportements cellulaires n'est pas bien expliquée et pas bien comprise par les chercheurs.

Cette thèse vise à élaborer et à étudier de nouveaux types de scaffolds micro-structurés obtenus par le procédé d'électrofilage (ou électrospinning) pour des applications en régénération osseuse. Le contrôle de l'architecture des scaffolds nanofibreux est expliqué. L'influence des différentes structures nanofibreuses sur les comportements des cellules osseuses (telles que l'organisation spatiale et la minéralisation des ostéoblastes) est étudié.

Le premier chapitre de ce travail recense toutes les méthodes existantes pour organiser les nanofibres d'une dimension à trois dimensions (1D à 3D) avec le processus d'électrospinning. L'effet des différentes forces agissant sur la structuration de la fibre pendant le procédé est expliqué.

Dans le deuxième chapitre, l'élaboration de scaffolds micro-structurés nanofibreux monocomposants est présentée. La première partie de ce chapitre traite des scaffolds 2D monocomposants micro-structurés. Grâce aux procédés de lithographie, des collecteurs micro-architecturés ont été obtenus (des collecteurs plots et des collecteur en nid d'abeilles). Deux types de biopolyesters ont ensuite été testés pour la fabrication des membranes nanofibeuses. Après optimisation des paramètres d'électrofilage, les scaffolds en nid d'abeilles ont été élaborées soit avec du poly (ε-caprolactone) (PCL), soit avec du poly (acide lactique) (PLA). Premièrement, l'effet de la morphologie de la fibre sur la morphologie à l'échelle du scaffold a été discuté. Ensuite, l'influence de la structure en nid d'abeilles du scaffold nanofibreux sur l'organisation spatiale des cellules osseuses a été étudiée. Dans la deuxième partie du chapitre 2, l'élaboration de scaffolds 3D monocomposant micro-structuré est présenté. Nous démontrons qu'à l'aide d'un collecteur en nid d'abeilles et grâce aux propriétés d'auto-assemblage des fibres de PCL, nous avons été en mesure de fabriquer un nouveau type de scaffold 3D par électrospinning. Le mécanisme de formation de ces scaffolds 3D est expliqué. Ces scaffolds ont la particularité de présenter des colonnes poreuses avec une taille de pores contrôlée et un gradient de porosité dans l'épaisseur du scaffold, ce qui pourrait être très utile pour les applications en régénération osseuse.

Le troisième chapitre traite des membranes composites micro-structurées élaborées à partir de nanofibres (PCL, alginate ou PLA) et de microparticules (hydroxyapatite ou poly (oxyde d'éthylène) (PEO)). Dans la première partie de ce chapitre, nous présentons un nouveau type de membrane composite 2D micro-structurée. Tout d'abord, nous expliquons l'effet de « template » électrostatique d'une fine membrane de nanofibres (électrospinnée sur un collecteur micro-structuré) sur le dépôt contrôlé local de particules. Ce type de membranes composites ont été utilisés par la suite dans un nouveau type de biopuce appelé biochip. Le biochip a été conçu pour réaliser du screening dans le domaine de la régénération osseuse. Ce

dispositif permet de tester différentes structures nanofibreuses en même temps. Il a été développé dans le but de trouver rapidement quel est le type d'architecture nanofibreuse qui permet d'induire le meilleur processus de régénération osseuse. De ce fait, le biochip est une mini plaque de culture cellulaire constituée de 21 puits différents. Dans chaque puit se trouve une membrane composite nanofibreuse faite de nanofibres de PCL et de microparticules d'hydroxyapatite. Dans chaque puit, la membrane présente une architecture différente. La taille réduite de ce biochip et le fait qu'il permette de tester un grand nombre de structures nanofibreuses en même temps ont fait de ce dispositif un nouvel outil de diagnostic rapide dans le domaine de la régénération du tissu osseux.

Dans la deuxième partie du troisième chapitre, nous présentons nouveau type de membrane 3D composite micro-structurée. Ces scaffolds 3D composites ont été élaborés en réalisant alternativement l'électrospinning de nanofibres et l'électrospraying de microparticules sur des collecteurs micro-structurés en nid d'abeilles. Nous avons montré que ces scaffolds présententt des pores cylindriques avec un diamètre intérieur qui peut être de quelques dizaines à quelques centaines de microns. Des mesures en traction ont permis de mettre en évidence les bonnes propriétés mécaniques de ces scaffolds, favorisant ainsi leur utilisation dans des applications de régénération tissulaire.

Enfin, les conclusions générales et les perspectives de ce travail sont présentées.

# Chapter 1: An introduction to organized nanofibers : from 1D to 3D

# 1. Electrospinning process

## 1.1 Electrospinning theory

Electrospinning is a way of obtaining nanofibers that can be used with a wide variety of polymers. Applying the electrostatic force for drawing a pendant droplet of polymer solution, to form fibers in sub-micron scale, is the electrospinning theory. In fact, the polymer solution is placed in a syringe connected to a needle. An automatic pump feeds the polymer solution into the metallic needle. A drop of polymer solution is suspended from the needle tip which is in contact with a high voltage electrode. The electric charges overcome the surface tension and a jet of solution is ejected at high velocity (**Figure 3**). In 1969, Taylor presented his theory about the behavior of pendant polymer droplet at the end of the spinning capillary [26]. In fact, Taylor determined that in order to balance the polymer solution surface tension with the electrical forces, a cone angle of 98.6° (49.3° between the cone axis and the cone apex) is essential (**Figure 4**).

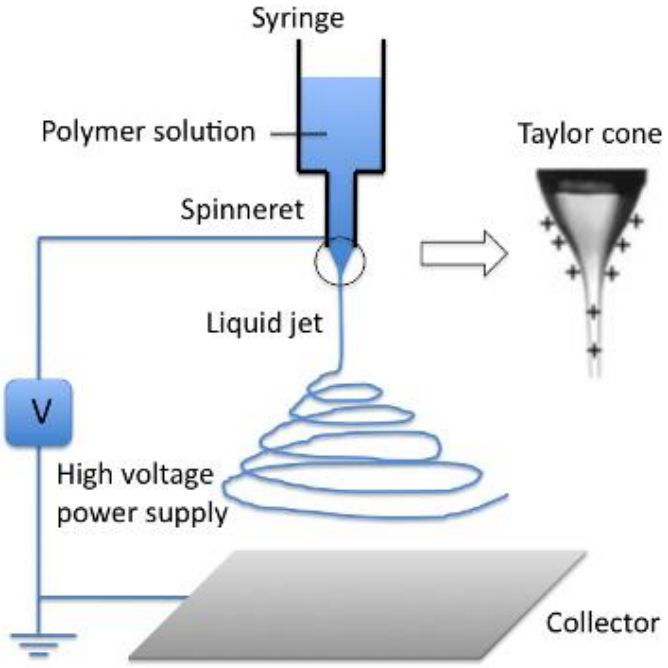


**Figure 3 : Electrospinning set up (Reproduced from [27])**

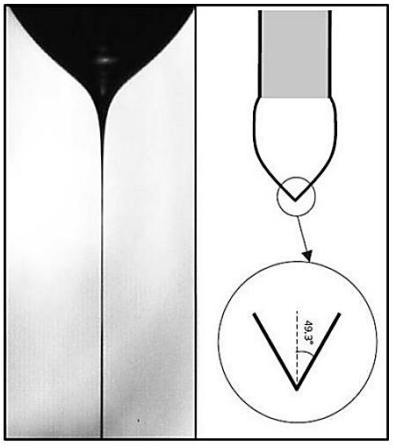


**Figure 4: Taylor Cone [28, 29]**

During the process, the jet passes through the distance between the needle and the second electrode, which acts as a collector. Between the two electrodes, the jet is stretched by two combined phenomena: first, the repulsion between the positive charges and second, the strong attraction of the collector. Although the setup of the electrospinning device seems simple, its principle is rather complicated. Until 1999, most of researches thought that the repulsion between the charged polymer charges was the reason of splitting and splaying of the polymer solution and theirs ultrathin structure formation [30] [31]. Recent studies show that the bending instability of electrified jets is the main reason of thinning of jet during their transition from spinneret to collector [30].

**Figure 5-a** shows the picture of an electrospun jet and **Figure 5-b** shows the conical shape of a single electrospun jet. Obviously, it can be seen that the jet, at first, is a straight line and then becomes unstable. The picture **5-b** demonstrates that the conical region in electrospinning process contains only a single, rapidly bending or whipping fiber [31].

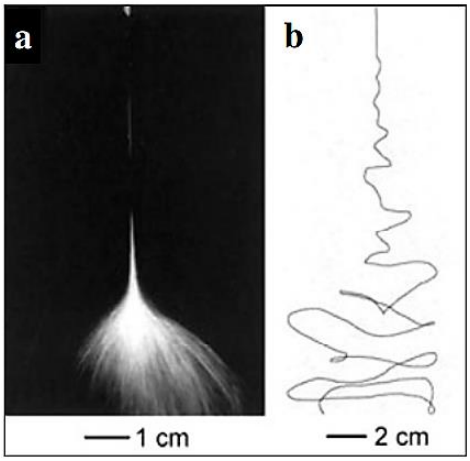


**Figure 5 : a) Conical instability of jet; b) Single jet ( from [31])**

The high frequency of whipping makes impossible to see the single jet with conventional cameras and gives impression that the initial jet divides and splits into multiple branches as they move forward the collector.

## 1.2 Electrospinning setup

Technically, electrospinning is a relatively simple spinning process that could be used with a large range of polymer solutions. A simple electrospinning device is composed of:

- A high voltage system
- A pump
- A metallic needle
- A syringe
- The feeding tubes
- A metallic collector

The high voltage system should prepare the electrical field in the range of 1kV/cm. Normally, a metallic needle is used as electrospinning capillary, although there are some electrospinning systems which used more than one needle and are called multi jet electrospinning. The feed rate of pumping must be controllable with a high precision and adapted with the rate imposed by the electric field. For the feeding tubes, it is better to use the Teflon tubes to avoid the reaction

between tube and polymer solution. The metallic collector may be of various shapes, flat, circular, tubular, and it can be static or rotary.

Other set ups were also designed and built to increase the production rate. For example needleless devices were developed to improve the electrospinning productivity, such as the one supplied by Elmarco Company (**Figure 6)**.


**Figure 6: Needleless electrospinning system presented by Elmarco Co.**

## 1.3 Electrospinning parameters

It is very important to optimize the electrospinning process conditions to obtain homogeneous electrospun nanofibers in a reproducible way. A large number of researchers have focused their studies to investigate the parameters that affect the homogeneity and reproducibility of electrospinning process. The major known defects which occurred in electrospinning process are:

- branched nanofibers
- beaded nanofibers
- buckled nanofibers
- flat (ribbon like) nanofibers

Different parameters affect the electrospinning condition which could be classified in three general categories. Generally, researches sorted these parameters by following order:

- Polymer solution parameters (such as: concentration, viscosity, molar mass, surface tension, conductivity and the ions addition)

- Process parameters (such as: applied voltage, distance, feed rate, polarity, needle properties)
- Ambient parameters (such as: temperature, humidity)

Optimization of these parameters leads to product defect-free electrospun nanofibers. Moreover, by understanding and controlling the influence of these effective parameters on nanofibers properties, it will be possible to create targeted electrospun nanofibers in term of morphological and physical properties. All three mentioned categories consist of different parameters which will be described.

**The concentration, the viscosity and the molar mass**

Concentration is one of the most important parameter which affects electrospun nanofibers properties. The effect of this parameter was studied for many polymers (PCL [32], PLA [33], PEO [34], PA-6 [35], silk [36], PMMA [37], PVA [37]). It is in general one of the first parameter that is varied to optimize the morphology of the nanofibers. The investigation of the effect of polymer solution concentration on beading during electrospinning shows that by increasing the solution concentration, the amount of beads disappear and the average diameter of the fibers increases. Also, the shape of the fibers appears to be more elongated [35]. By increasing the concentration of the polymer solution, the viscosity of the solution increases too. The polymer solution viscosity has same effect as the polymer solution concentration on electrospun nanofibers. By increasing the viscosity, beads and beaded fibers disappear and the diameter of the fibers increases [38]. Furthermore, for a given concentration, the viscosity of the solution also increases with the molar weight of the polymer. The relation between the intrinsic viscosity [η] and the molar weight $M_w$ is given by the Mark–Houwink equation, also known as the Mark–Houwink–Sakurada equation:

$$[\eta] = K M_w^{\alpha}$$

The polymer chain entanglements insure the stability of the electrospun jet and prevent the droplet formation and consequently control the morphological properties of resultant nanofibers, such as beading, branching and diameter uniformity [39]. In fact, it was demonstrated that the fiber morphology, and thus the electrospinning regime, depends on the product of the intrinsic viscosity and the solution concentration [η]C (**Figure 7**) [40-42] . The product [η]C is equivalent to the ration C/C*, where C* is the critical chain overlap concentration, i.e the cross-

over concentration between the dilute and semi-dilute regimes [41]. A decrease of [η]C directly relates to a decrease of the viscosity of the solution and thus a reduction of the fiber diameter. They showed that in case of dilute system, when [η]C< 1, PCL could only be electrosprayed: there are not enough entanglements between the polymers chains and therefore, instead of forming nanofibers, particles are formed and electrospinning becomes electrospraying. Furthermore, for their studied PCL solutions in acid solvents, Lavielle et al. [40] demonstrated that for 1< [η]C< 3, the solution was defined as being in the range of semidilute, unentangled regime, leading also to only electrospraying. Finally, for [η]C> 3, which was considered as the entrance of the semidilute, entangled domain, their PCL solutions led to beaded fiber formation. Only higher degree of entanglements in the PCL solution led to form bead-free fibers ([η]C> 10). However, nanofibers could be obtained until the product [η]C < 21, otherwise, the solution was too viscous to produce fibers under the applied electrospinning conditions. Such electrospinning regimes are always observed, however, the critical values of [η]C which bounded the regimes strongly depends on the polymer-solvent system.

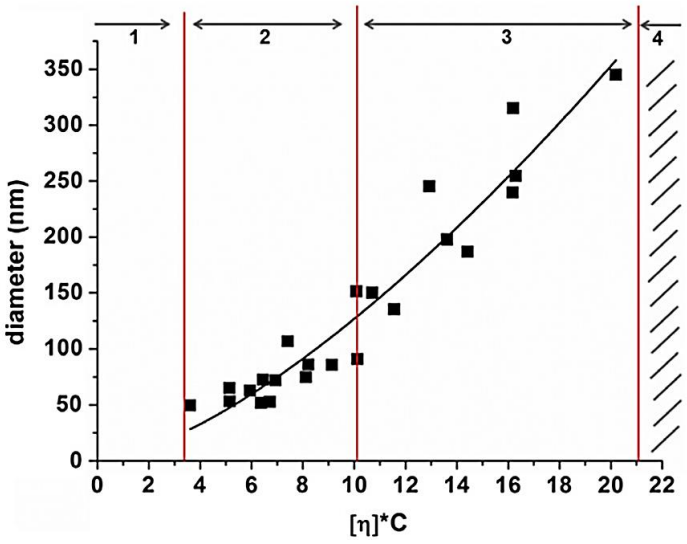


**Figure 7: Variation of fibers average diameter with [η]*C (■): zone 1: electrospraying, zone 2: beaded electrospun fibers, zone 3: bead-free electrospun fibers and zone 4: no electrospinning. Equation of power law dependency ( ▬): diameter = 4.2 ([η]*C)1.5 (R2 = 0.92) from [40].**

**The voltage**

The effect of the electric field on the processability and on the electrospun nanofibers morphology was one of the most studied parameters. The voltage is one of the most primordial parameter of the electrospinning process since the voltage allows the formation of the Taylor cone and the ejection of the solution at high velocity. Indeed, the electrospinning only happens when the electrical charges at the surface of the droplet overcome the surface tension of the solution. The voltage should overcome a threshold value so that the Taylor cone could be formed. But in the same time, the voltage should not be too high to not make the Taylor cone instable. Indeed, if the stability of the Taylor cone is not guaranteed, then an intermittent jet could appear, leading to the formation of beaded fibers. For example, Deitzel J. M. *et al*. demonstrated the effect of applied voltage variation on the shape of the Taylor Cone [43] in the case of poly ethylene oxide (PEO) dissolved in water. They concluded that above a critical electrical field, the shapes of origination jet are significantly changed and these changes correspond to an increase in amount of beaded nanofibers.

**The surface tension**

The surface tension of a polymer solution depends on the solvent properties. The surface tension plays a key role on the Taylor cone shape and therefore the initiation of the jet but also on the diameter of the fibers. In general, a high surface tension prevents the electrospinning process, makes irregular Taylor cone shape, creating instabilities of solution jet during the process and therefore beaded fibers. Conversely, studies show that by reducing the polymer solution surface tension, the nanofibers could be produced without beads and the average diameter of nanofibers increases [35, 38].

Different ways were presented to change the polymer solution surface tension. For example, addition of solvent with a low surface tension helps formation of smooth nanofibers. Another way to decrease the surface tension is to add surfactant to the solution. It was found that, the addition of surfactant helps to produce more uniform nanofibers [44].

**The conductivity and ions addition**

The charged ions in the polymer solutions have a great influence on the jet formation. The existence of ions increases the charge carrying capacity of the jet and creates higher tension with applied electric voltage [45].

The addition of ions can change the conductivity of the polymer solution. It has been found that the polymer solution conductivity mainly affects the morphology of the fibers by decreasing the average of their diameter [46]. Beachley V. and Wen X. [32] reported that by increasing NaCl concentration in polycaprolactone, a decrease of nanofibers diameter was observed and beaded fibers were produced only when NaCl was not present in the polymer solution. Similarly, Mit-Uppatham C. *et al*. have investigated the effect of solution conductivity on nanofibers diameter; they found that by increasing the polymer solution conductivity, the average of nanofibers diameter decreases significantly [35].

**Needle tip-to-collector distance**

The most important aspect of this parameter concerns the evaporation of solvent during electrospinning process. To obtain defect free electrospun nanofibers, a sufficient residence time between the needle tip and the collector is essential for an efficient evaporation of the solvent. This residence time is determined by the needle tip-to-collector distance.

**Figure 8** demonstrates the effect of the needle tip-to-collector distance on the morphology of electrospun SLPF (Silk Like Polymer Fibronectin functionalized) [47]. Two different structures from two different distances were obtained. For **Figure 8-a**, the needle tip-to-collector distance was 2 cm and for **Figure 8-b** was 0.5 cm. By applying a larger distance between needle tip and collector the evaporation time increases and the electrospinning process leads to produce fibers (**Figure 8-a**), but the smaller distance does not allow a complete evaporation of the solvent leading to fiber fusion (**Figure 8-b**).

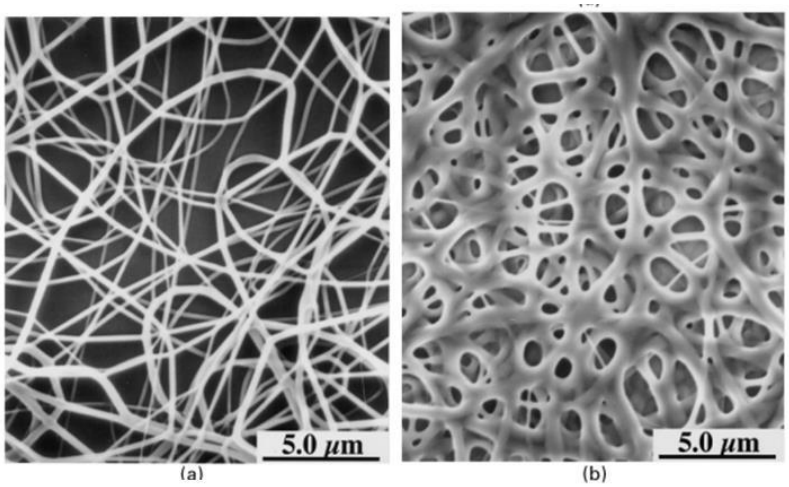


**Figure 8: Deposition distance morphology of SLPF fibers a) with a distance = 2 cm; b) with a distance =0.5 cm ([47])**

## Feed rate

For a given applied voltage, an increase in feed rate increases the nanofibers diameter [33]. Touny A. H. *et al*. investigated this effect on poly(lactic acid) (PLA) electrospun nanofibers. They showed that a decrease in the polymer solution feed rate leads to decrease the nanofiber diameter. Another advantage of decreasing the feed rate is the complete evaporation of solvent from nanofibers and the reduction of the beading problem. Therefore, lower feed rate is more desirable for defect free nanofibers [33]. In the same time, a minimum of feed rate is essential to maintain the Taylor cone shape during production. Higher feed rate provides more polymer solution volume than needed and further increase leads to projection of polymer solution droplet toward the collector.

## Collector

Collector design and composition are the most important parameters to determine the nanofibers organization. The different methods to structure the nanofibers from aligned fibers to complex 3D structures are explained in details in the second part of this chapter.

## Temperature

The change in polymer solution temperature can make the changes in solution properties such as viscosity, surface tension and conductivity. The changes in these parameters, as

mentioned before, affect the electrospinning process and electrospun nanofibers morphology [35].

**Humidity**

It is well known that humidity plays a key role on the production stability during electrospinning. The effect of humidity largely depends on the polymer/solvent system. Electrospinning in very low humidity makes clogging in the needle and thus prevents the polymer solution jet formation.

Humidity affects the evaporation speed of the solvent. As an example, for aqueous polymer solutions, humidity affects the drying of electrospun nanofibers. Tripanatasuwan *et al*. noticed that by increasing humidity during the electrospinning of poly(ethylene oxide) (PEO) in water, a decrease of the evaporation rate from the fluid jet is observed, which allowed the charged jet to remain fluid, to continue to elongate and to become thinner [48]. In the same interval, the surface area increased and the charge per unit area on the surface decreased. Capillary instabilities were developed creating thin fiber segments between beads with diameter larger than the fibers. In another study, Casper C. L. *et al.* demonstrated that the amount of humidity affects the surface morphology of electrospun polystyrene (PS) fibers [49]. The polystyrene was dissolved into tetrahydrofuran (THF). Electrospinning in an atmosphere of less than 25% humidity produced smooth fibers without any surface features. When the humidity is above 30%, pores begin to be formed on the surface of the fiber. Increasing the amount of humidity causes an increase in the number of pores on the surface, the pores diameter, and the pores size distribution (**Figure 9**).

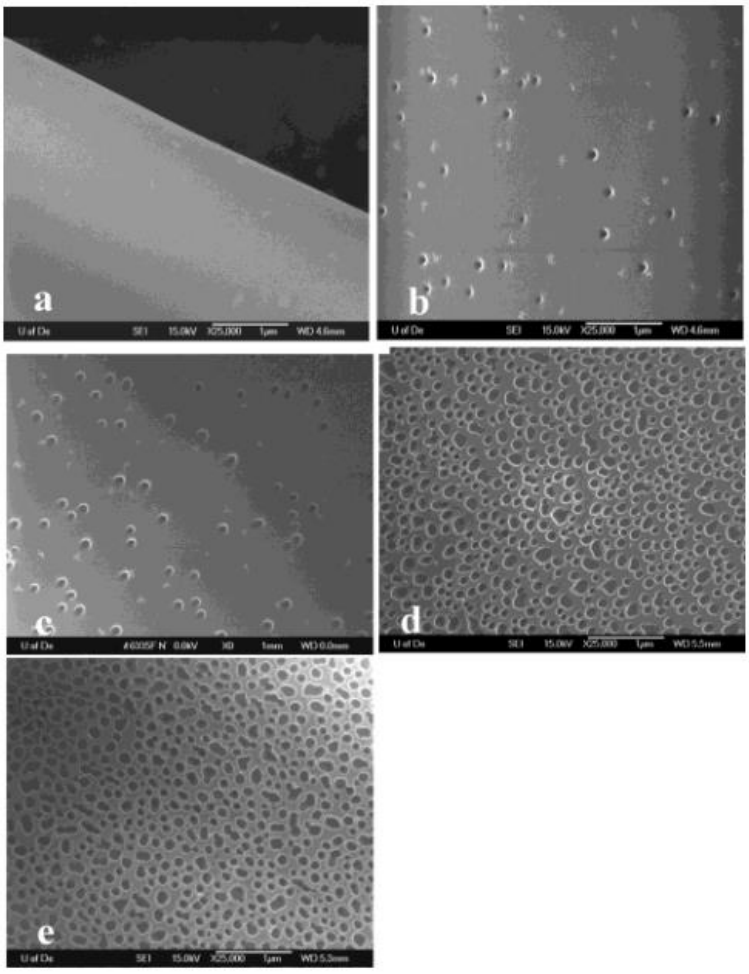


**Figure 9: FESEM micrographs of 190 000 g/mol PS/THFfibers electrospun under varying humidity: (a) <25%, (b) 31-38%, (c) 40-45%, (d) 50-59%, (e) 60-72%. ([49]).**

They explained the pore formation by two phase separation processes: thermally induced and vapor phase separations. Vapor induced phase separation involves the penetration of a non-solvent vapor causing phase separation of the polymer solution. In their case, water is the non-solvent, which induces the phase separation of the homogeneous mixture of PS and THF. They claimed also that the rapid evaporation of the solvent when the jet is being projected from the needle thus making thermally induced phase separation a viable explanation for pore formation as well. In the case of PS fibers in THF, the phase separation process occurs by the mechanism of spinodal decomposition (SD), thus creating closed pores. Spinodal decomposition is opposed to the other mechanism of phase separation, the nucleation and growth (NG) which leads to an interconnected pore structure.

## 2. Organized assembly of electrospun nanofibers: from 1D to 3D

**Chapter IX of the Book entitled '*Electrospinning, Principles, Practices and Possibilities*', under press, 2014**

***ISBN 13: 9781849735568, ISBN 10: 1849735565, 2014.***

**Salima Nedjari, Anne Hébraud, Guy Schlatter**

**Abstract:**

Although electrospinning is well-known as a process able to produce non-woven mats, researchers have shown from the beginning that fiber alignment can be easily achieved. Indeed, when the charged electrospun jet is landing on a collector with a sharp corner, alignment occurs thanks to favourable electrostatic forces. Starting from these observations, researchers have exploited the versatility of the process to assemble the nanofibers and produce mats with 1D, 2D and even 3D organized architectures. In this objective, they have manipulated electrostatic, magnetic or mechanical forces and adapted the standard electrospinning set up to control the organisation of nanofibers, or taken advantage of the self-assembly of the nanofibers under certain conditions.

The aim of this chapter is to present the mechanisms driving the assembly of electrospun nanofibers. It highlights recent applications proving that the building of complex nanofibrous architectures is an active research field in many areas. In the first part, we will describe the different possible ways allowing an efficient 1D fiber alignment. Then, we will show in the second part that the previous concepts are generalizable to elaborate 2D fibrous structures. Furthermore, a new strategy is also presented to produce 2D structures by self-organisation. In the last third part, we will show that electrospinning can eventually lead in the building of 3D nanofibrous constructs with controlled pore size.

## 2.1 Fiber Alignment

### 2.1.1 *Electrostatic Forces*

Aligned electrospun nanofibers can be obtained by manipulating the electrostatic forces that act on the charged jet. Thus replacing the plane collector by a specially designed one has an effect on the electric field at the vicinity of the collector.

The use of a rectangular collector [50, 51] (**Figure 10-a**) or of a collector consisting of two pieces of electrically conducting substrates separated by a gap [52, 53] (**Figure 10-b**) or an insulating substrate [54] results in the alignment of the electrospun nanofibers.

a) 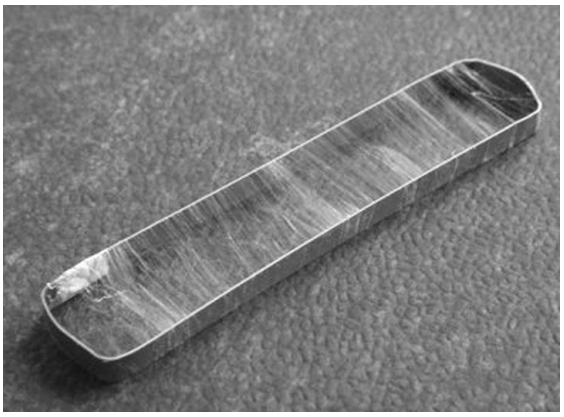 b) 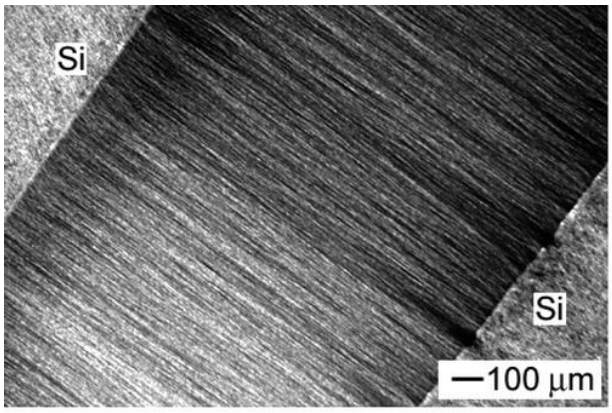


**Figure 10: a) Alignment of electrospun nanofibers over a rectangular frame electrode of 2 x 6 cm, reproduced from ref. [50] b) Nanofibers aligned between two conducting silicon stripes, Reprinted with permission from [52].**

#### *2.1.1.1* Mechanism of alignment

The charged electrospun jet is subject to two kinds of electrostatic forces: forces induced by the external electric field and coulombic interactions between the landing jet and the collector or the already deposited nanofibers. Thus the landing fiber will first follow the direction of the electric field lines towards the two electrodes and will land across the gap (**Figure 11**). Then the induced image charges created at the surface of the grounded electrode by the highly charged fiber will generate coulombic attractive forces between the fiber and the oppositely charged

electrode, stretching the fiber across the gap with perpendicular orientation. Finally, because the middle part of the fiber suspended over the gap remains highly charged, it will induce repulsive coulombic interactions with the subsequent landing fibers and enhance the alignment between them. Thus after a few seconds of deposition, an improvement of the alignment is observed [55].

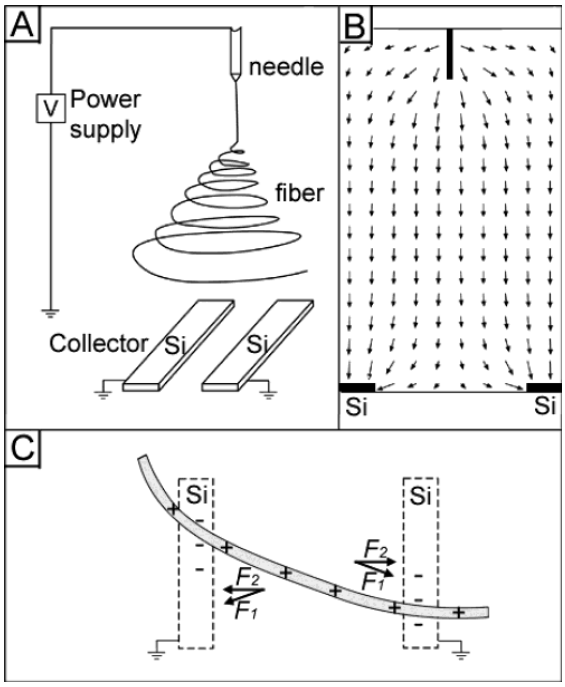


**Figure 11: (A) Schematic illustration of an electrospinning setup with two conducting silicon stripes separated by an air gap. (B) Calculated electric field strength vectors in the region between the needle and the collector. The arrows denote the direction of the electrostatic field lines. (C) Electrostatic force analysis of a charged nanofiber spanning across the gap: the electrostatic force (F1) resulting from the electric field and the Coulomb interactions (F2) between the positive charges on the nanofiber and the negative image charges on the two grounded electrodes. Reprinted with permission from[52] .**

#### *2.1.1.2* Influence of the experimental conditions on the alignment

As alignment of the nanofibers is here exclusively due to electrostatic forces, the relevant parameters to obtain the best possible alignment should have either an influence on the geometry or intensity of the electric field or on the charge density of the landing fiber and already deposited ones. Several parameters play a role in the electric field shape and magnitude.

Besides the voltage, the gap width has a great influence on the local electric field direction and intensity. Indeed, the magnitude of the transversal electric field $E_x$ at the metal edge increases dramatically with the gap width, until the distance between the electrodes is approximately equal to the distance between the needle and collector and then further decrease for larger gaps [54]. However, at the same time, the spatial extent of the stretching forces due to $E_x$ decreases with increasing gap width and while it acts on the whole fiber for gaps lower than 1 mm, efficiently enough to lower the fiber diameter, on the contrary, it only stretches the end of the fiber at the vicinity of the electrodes for gaps larger than 1 cm. Thus an optimal distance is observed of around 1 cm depending on the experimental conditions, for the best alignment of the fibers [51, 54, 56] .

The intensity of the transversal electric field also increases with the electrical permittivity of the electrodes and according to Yan *et al.*[53], it is difficult to get aligned nanofibers when the relative permittivity of the collector is below 5. For example, fibers could be aligned between ferrite electrodes ($\varepsilon_r$=12, **Figure 12-b and 12-d**) while a random mat was obtained when using epoxy electrodes ($\varepsilon_r$=4, **Figure 12-a and 12-c**).

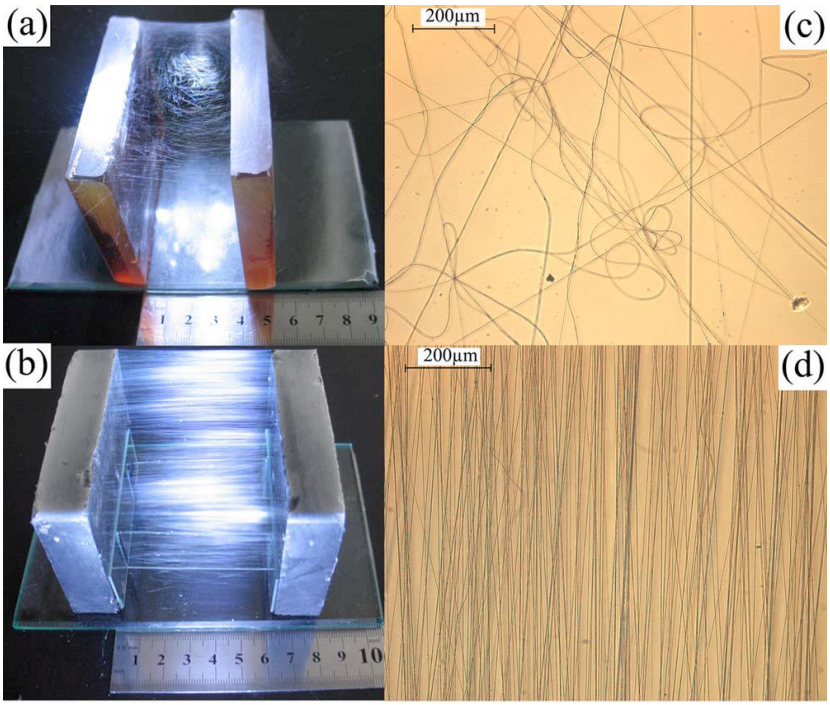


**Figure 12: a) and b) Digital camera Images of prepared nanofiber meshes using epoxy and ferrite as the collectors, respectively. c) And d) are optical micrographs of a) and b) respectively. Reprinted with permission from [53].**

As for the charge density of the electrospun nanofibers and mats, it is influenced by the relative humidity, the electric permittivity of the polymer solution or the conductivity of the insulator between the electrodes. The water molecules in air promote fiber discharging, leading to a decrease of the residual charges on the nanofibers and of the coulombic electrostatic repulsion between fibers. So at high relative humidity, the degree of orientation is reduced [57, 58].

The permittivity of the solvents has also a direct impact on the surface charge density of the fibers. Indeed, increasing the solvents permittivity induces higher charge density, and thus stronger coulombic interactions, resulting finally in a higher degree of orientation. As an example, Zhang *et al.*[59] have electrospun poly(ε-caprolactone (PCL) and D,L-poly(lactic acid) (PDLLA) in a mixture of THF ($\varepsilon_r$=7.4) and DMF ($\varepsilon_r$=36.2) and have observed better alignments for higher DMF/THF ratio i.e. for higher electric permittivity of the polymer solution.

Finally, when using a void gap between electrodes, thinner fibers (inferior to 150 nm in diameter) usually break because they are not enough strong to support their own weight and the repulsion forces between them. To avoid this problem, collectors composed by two conducting strips on an insulating substrate have been used [54, 55]. In this case, alignment of the nanofibers also improves with the insulator resistivity. This confirms the role on the alignment of the fibers, of electrostatic repulsion forces due to residual charges on the deposited fibers across the insulating substrate.

#### *2.1.1.3* Limits of the process

One of the limits of the process is the length of the aligned nanofibers. Indeed, nanofibers align between two electrodes and, as already discussed, the alignment efficiency decreases at large gap width. To our knowledge, the longest aligned fibers using this process in literature were reported by Rafique *et al* .[60], who were able to align nanofibers on length as big as 25 cm. Another solution to this problem was proposed by Katta *et al* .[61] who used a drum composed of parallel copper wires assembled by two plexiglas disks which rotates very slowly (1 rpm). In this case, the nanofiber is attracted by the copper-wire nearest to the needle and because the drum is slowly rotating, the next copper wire attracts the nanofibers which stretch perpendicular to the copper wires to span the gap between them. Another limit of the process is the deposition time. Most of the studies of fiber alignment by electrostatic forces were done on short deposition time.

Indeed alignment is lost after long deposition times [61], certainly due to the accumulation of charges on the whole mat and the modification of the electrostatic fields at the vicinity of the collector after thick mats have been formed.

In conclusion, using electrostatic forces to align electrospun nanofibers is a facile and versatile method as it takes advantage of the high electric charge density of the electrospun jet. Moreover, this method can have a small impact on the morphology of the fibers as in specific cases (gap lower than 1 mm), it can decrease their diameter [54] or align polymer chains parallel to the fiber axis [62].

### 2.1.2 *Magnetic Forces*

Magnetic forces can also be used to align nanofibers, either by taking advantage of the fact that the fibers are electrically charged, and thus are subject to Lorenz forces [63], or by addition of magnetic $Fe_2O_3$ nanoparticles inside the polymer solution [64, 65].

#### *2.1.2.1* Electrospinning using magnetic collectors: application of Lorenz force

Liu *et al.* [63] were able to align nanofibers with very good efficiency by adding two magnets on both sides of a plane aluminium collector, separated from the collector by thick insulators. In this case, the charged jet, moving inside the magnetic field, is subject to radial Lorenz forces that tend to align the nanofibers in the direction of the magnetic field. The nanofibers moreover became more uniform, with less branching and a slightly reduced diameter under magnetic field, compared to nanofibers electrospun in the same conditions in the absence of magnets. The magnetic forces seem to reduce the jet instability and increase the velocity of the jet reaching the substrate.

Finally, Magnetic-Field-Assisted Electrospinning (MFAE) enables the alignment of nanofibers over long deposition times, whereas alignment gradually disappears when parallel auxiliary electrodes are used.

#### *2.1.2.2* Electrospinning using magnetics or paramagnetic Particles in the polymer solutions

In order to reinforce the influence of the magnetic field on the electrospun jet, it is possible to add a small amount of $Fe_2O_3$ magnetic nanoparticles (less than 0.5 %) in the polymer solution [65]. This solution is then electrospun between non conducting magnets, placed on a grounded aluminium plate, forming nanofibers suspended between the two magnets, parallel to the magnetic field lines. The same polymer solution without magnetic nanoparticles does not align between the magnets, but deposit as a random mat on the aluminium plate, confirming the role of the magnetic field in the alignment. Finally, the addition of a larger quantity of magnetic particles (25% of the solid content) in the polymer solution enabled the fabrication of aligned ferrite nanofibers by electrospinning and removal of the polymer by oxygen plasma treatment [64].

### 2.1.3 *Mechanical forces*

Mechanical forces have been used to align nanofibers, collecting the electrospun jet onto a rapidly moving surface.

#### *2.1.3.1* Mechanism of alignment as a function of collector velocity

Matthews *et al.* [66] used a rotating cylinder to collect collagen nanofibers (**Figure 13-a**). They showed that the velocity of the rotating cylinder is crucial to obtain aligned fibers. Indeed, at low velocity, the collected mat still has a random structure due to the jet whipping movements, while at higher velocity, the fibers are aligned perpendicularly to the axis of rotation (**Figure 13-b** and **Figure 13-c**). The critical tangential velocity of the drum, at which the fibers start to be aligned, should be equal to the velocity of the landing nanofibers jet. The nanofiber velocity, $v_f$, can be estimated from mass balance [67], relating the weight of the polymer fibers collected during a short time with the infuse rate of the polymer solution by the syringe pump:

$$v_f = 4\,Q\,\phi_V / (\pi D^2) \qquad (1)$$

were $Q$ is the syringe pump infusion rate, $\phi_V$ is the polymer volume fraction in the solution and $D$ is the landing fiber diameter.

However in some cases, when the applied voltage and infusion rate are high, the calculated nanofibers velocity is so high (even higher than the sound velocity) that one must assume that multiple filaments with lower velocity are landing on the collector [67]. These multiple filaments can be the result of the ejection of several jets from two or more Taylor cones at the same time, or from branching of a single electrospun jet [68].

Finally, when the collector velocity increases, after an optimum alignment, wavy fibers can be observed, probably due to a turbulent air flow near the surface of the collector [69] (**Figure 13-d**).

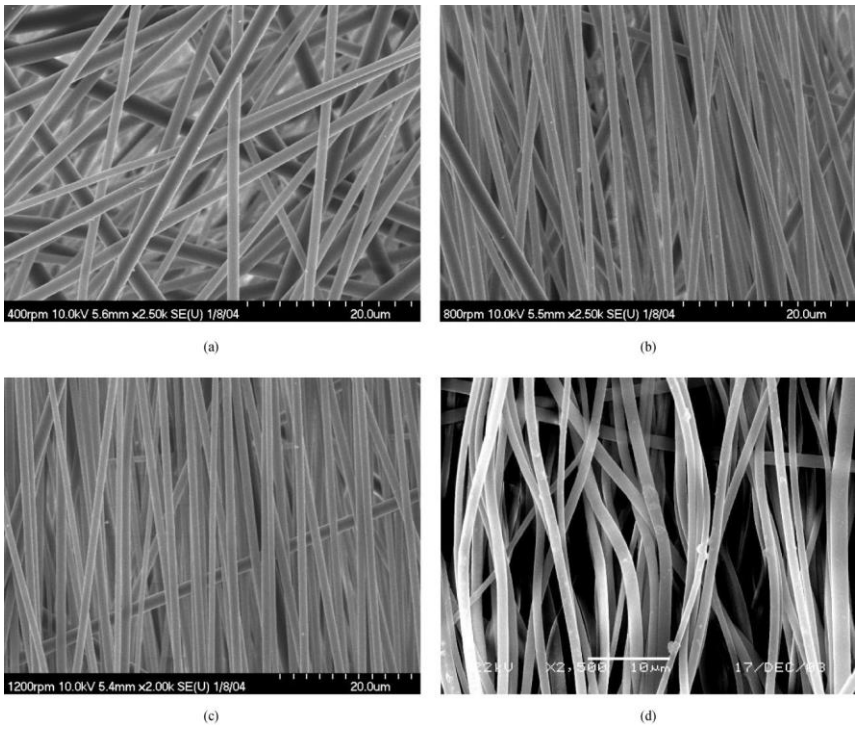


**Figure 13: FE-SEM micrographs of electrospun fiber mats at various surface velocities: (a) 4.3 m/s, (b) 8.6 m/s, (c) 12.9 m/s), and (d) 17.2 m/s. Reprinted with permission from [69].**

At high velocity of the collector surface, the nanofibers are subject to mechanical forces that stretch them, thereby decreasing their diameter [69, 70]. Moreover, the stretching forces acting on the fiber also modify their structure. Indeed, changes in the orientation of polymer crystals in the fibers, necking with the development of fibrillar structures or even breakage have been observed [71-73].

#### *2.1.3.2* Limitations and strategies to improve alignment

Mechanical alignment by using a simple rotating drum is most of the time not perfect [74, 75], as a result of the whipping movements of the landing nanofiber leading to its random orientation just before landing on the collector. To achieve a higher degree of alignment, different strategies have been employed, that aim at reducing or suppressing the whipping movements. The whipping movements are due to a bending instability [76] that develops due to the presence of free charges at the surface of the jet, and their interaction with the external electric field. Hence, it is possible to reduce or suppress it either by decreasing the presence of charges at the surface of the jet, or by modifying the external electric field.

Decreasing the presence of charges at the surface of the jet can be done by choosing very pure solvents with low dielectric constants. It was shown that electrospinning PEO in HPLC grade $CHCl_3$ rather than water, allow the suppression of the whipping movements and the collection of highly aligned fibers [77]. On the contrary, adding organic salts to this PEO in $CHCl_3$ solution results in the appearance of the bending instability and poorer alignments of the fibers. Another way to reduce the global amount of free charges at the surface of the electrospun jet is to use an AC potential instead of a DC potential. By using this technique Kessick *et al.* [78] observed a significant reduction of the bending instability and the deposition of much better aligned nanofibers on a collector, compared to those collected under a DC potential.

A good control of the electric field can also permit the suppression of the whipping movements. For example, the fibers were collected on the edge of a rotating disc leading to focusing of the jet and diminution of whipping movements near the collector [79] (**Figure 14-b**).

Nanofibers were also collected on thin copper wire electrode winded around an insulating cylinder, producing bundles of highly aligned nanofibers [80] (**Figure 14-c**). However the use of a thin disc or a thin copper wire as a collector leads to membranes with small areas, which could be a problem for some applications.

Another similar strategy to control the electric field and reduce the whipping movements is to use of an auxiliary electrode placed inside [81] (**Figure 14-d**), or just behind the rotating drum [82] (**Figure 14-e**), at an electric potential opposite to the one of the electrospinning nozzle. In this last case, the whipping movement is completely suppressed, and the jet follows a straight electric field path toward the auxiliary electrode. The auxiliary electrode can then be moved along the

drum during the process in order to collect fibers on the whole area of the drum. The fibers collected on the drum during the first moments are uniform with uniform spacing, on the order of 5 to 30 μm depending on the electric charge on the fibers that repel each other's.

Kiselev *et al.* [70] (**Figure 14-f**) have used a low electric field near the tip of the needle and at low liquid flow rate; they were able to produce single filament electrospinning, thus allowing the precise matching of the velocity of the collector and the jet production. Furthermore, they have added an electrode plate, positioned behind the electrospinning emitter in order to render the electric field more uniform and to limit whipping movements.

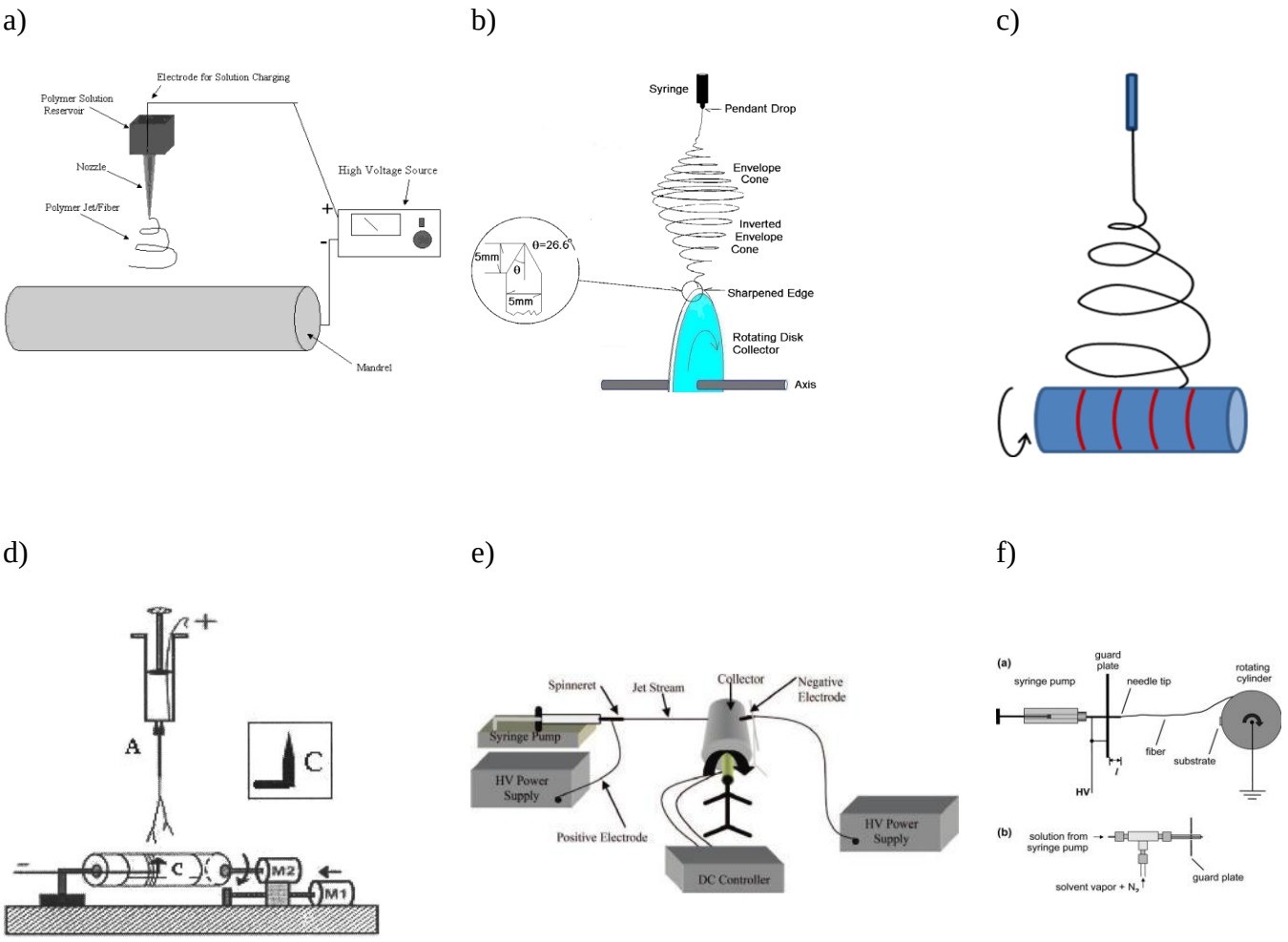


**Figure 14: Different electrospinning setups with rotating collector. From a) Reprinted with permission from Matthew *et al.* [66]. b) From Theron *et al.* [79]. c) Setup of Bhattarai *et al.* [80]. d) Reprinted with permission from Sundaray *et al.* [81]. e) Reprinted with permission from Carnell *et al.* [59]. f) Reprinted with permission from Kiselev *et al.* [70]**

## 2.2 2D Patterned Nanofibrous Membranes

2D patterned complex nanofibrous membranes have been prepared by using the same approaches as described for 1D assemblies. They can be formed by stacking of the 1D aligned nanofibers, or by precise local control of the previous forces. Moreover, a new strategy has emerged recently that uses self-assembly of the nanofibers during electrospinning.

### 2.2.1 *2D Composites formed from 1D aligned fibers*

The easiest way to obtain 2D controlled assemblies of nanofibers is to produce several independent layers of uniaxial aligned fibers, using one of the methods previously described and to stack them with different orientation or positions. This can be done, either by transferring the aligned fibers on a support [65], or by depositing them onto a thin film, that can be turned in another direction before depositing the new layer of aligned nanofibers [82, 83].

Composite structure made of multilayers of aligned fibers can be used in tissue engineering for example. They combine the advantage of alignment of nanofibers, which has shown to favour cell proliferation and induce the formation of anisotropic tissues such as the cardiac muscle [84] or guidance for neural tissue engineering [85], with increased mechanical properties in all directions [86].

When using electrostatic forces, different pairs of electrodes can also be used, that are alternately grounded for a few seconds, changing the alignment orientation of the nanofibers from one layer to the other [55] **(Figure 15**). This approach can be generalized for 2D structures for the fabrication of more complex architectures.

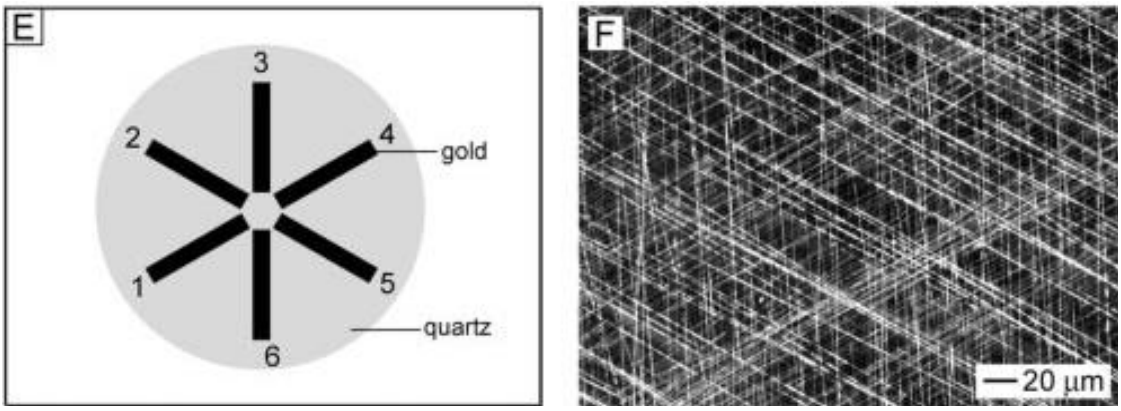


**Figure 15: Gold electrodes patterned on a quartz substrate. The electrode pairs of 1-4, 2-5 and 3-6 were sequentially grounded for 5 s to collect alternating layers with the orientations of their fibers rotated by ~ 60°.Reprinted with permission from [51].**

### 2.2.2 *Complex 2D patterned membranes by precise control of electrostatic forces*

As described in part 2.1, electrostatic forces can be manipulated in order to control the deposition of the nanofibers by designing collectors with particular geometry or different local dielectric properties. This concept has been employed for the preparation of aligned nanofibers mats but can be generalised to more complex 2D patterns. Hence, electrospinning has been performed on various macroscopic substrates, such as metallic grids [87] or the knit pattern of a fabric mesh coated with a conducting gold layer [88]. In these cases, most of the nanofibers deposited on the conducting structure that play the role of a template [89], with some fibers aligned in between.

In order to control the 2D architecture of the electrospun membranes on a smaller scale, various type of collector with micropatterns were designed and prepared by photolithography [83, 90], thermal evaporation [57] or other microfabrication techniques [91]. The effect of the geometry of the substrate: conducting protusions on conducting surfaces [91, 92] and the impact of local differences in electric permittivity of a flat substrate [57, 83] on the structure of the membrane were studied.

When protusions are present on a conducting collector, the electric field at the vicinity of the collector is modified. For truncated pyramidal protusions, a simulation was performed showing that the electric field was higher at the top of the pyramid than in the valley, leading to a

selective deposition on top of the pyramid [91] during the first moments. However, the selectivity of the deposition decreases with time as the deposited fibers mat accumulates charges and becomes repulsive towards incoming fibers, forcing them to land between the protusions. Thus, after a few minutes fibers are deposited on top of the protusions as well as in the valleys provided that spacing between protusions is large enough to allow for fibers deposition in-between. In the case of protusions, close enough to each other, fibers deposit on the top of protusions with aligned fibers suspended between adjacent ones. It has been shown for conducting cylindrical blocks, that the spacing L between blocks had to be lower than 3 times their height H for the fibers to align between blocks [90]. For L>3H, fibers are deposited on top of the plots and in the valley with fibers suspended from the top of the plots to the bottom in the form of a tent (**Figure 16**), as is observed macroscopically when electrospinning on an erected screw [93].

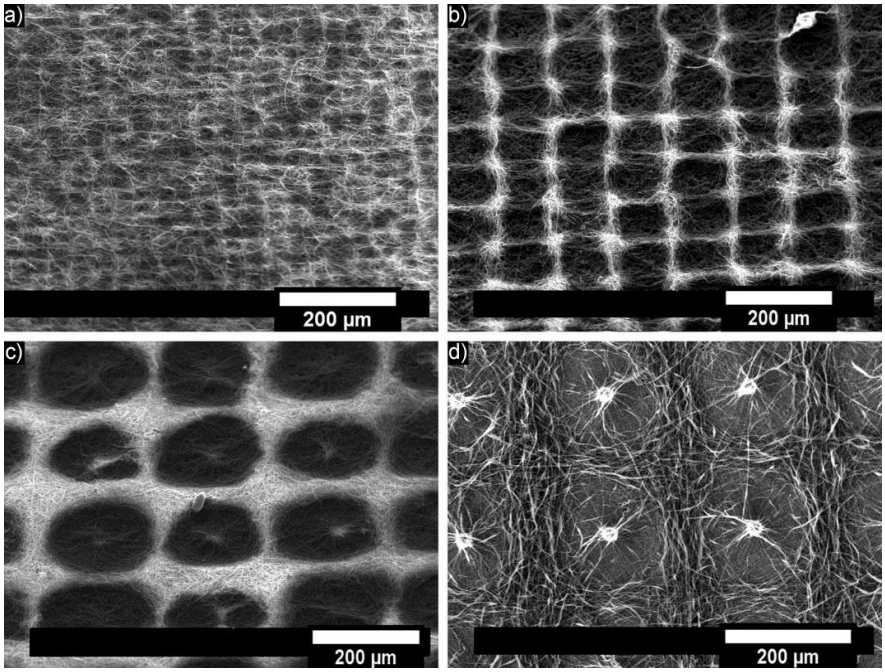


**Figure 16 : Effect of the distance L between conducting 20 µm-in-diameter block and height H=60 µm: (a) downside view of the scaffold showing microgrids with block separation L=0.33H=20 µm after peeling from the collector, (b) downside view (after peeling the scaffold from the collector) of the scaffold with L=1.67H=100 µm, (c) downside view with L=3.67H=220 µm, (d) topside view of the collector after fiber deposition with L=3.67H=220 µm. Scale bars=200 µm. Reprinted with permission from [90].**

As a generalization of the 1D alignment observed on the sharp edge of a rotating disc [79] (**Figure 14-b**), 2D sharp conducting micropatterns can also lead to local fiber alignment by a confinement effect. Indeed, it has been shown that when a collector is made of thin conducting strips surrounded by insulating regions, the nanofibers are confined and mostly aligned along the conducting paths [57].

Similarly, such effect occurs also when using entirely conducting collectors with tall, thin and long patterns. As an example, a patterned collector with thin walls forming a honeycomb structure is shown in the inset of **Figure17-a**. The intense electric field located over the thin walls induces an efficient deposition of the nanofiber over these patterns. Furthermore, because the width of the walls is much smaller than the curvature radius of the loops formed by the whipping movements of the electrospun nanofiber, an efficient alignment is observed between the edges of the walls (**Figure 17-b**).

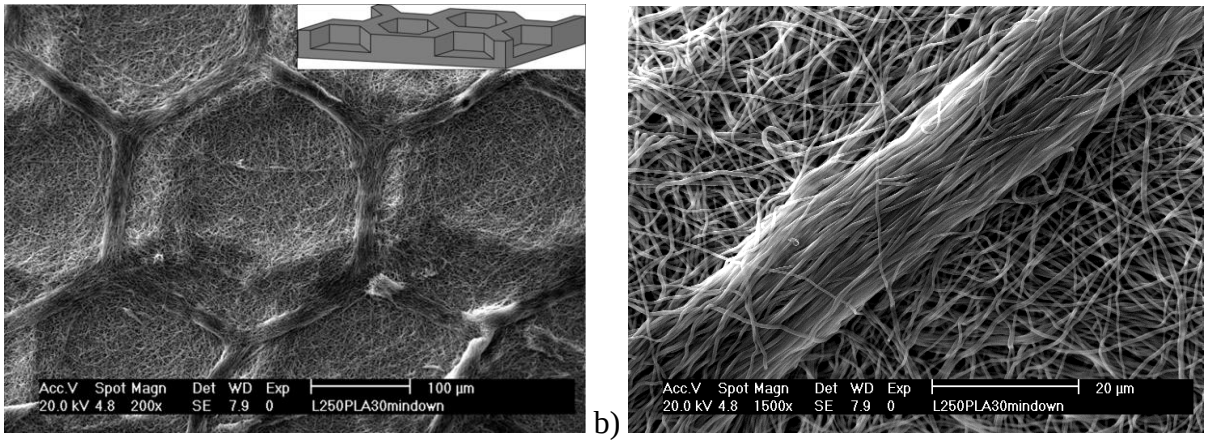


**Figure 17: Downside views (obtained after peeling the scaffold from the collector) showing honeycomb structures of PLA obtained from the deposition onto a honeycomb-like conducting collector. a) Structure of a nanofibrous pattern. The inset shows the structure of the used collector. b) Detail showing that thanks to the confinement effect, the nanofibers align efficiently over the thin conducting walls of the honeycomb collector.**

Selective deposition was also obtained by playing on local electric permittivity differences. It is the case of insulating collectors with a patterned conducting layer evaporated on top of it [57, 83]. In this case, the nanofibers are first randomly deposited on the conducting electrode following its shape (**Figure 18**). Moreover Cho *et al*. [83]. have shown that selectivity could be improved by inversing the polarities of the electrodes, placing the electrospinning needle to the

ground and the collector to a positive electric potential, thus creating a larger potential between the electrode and the surrounding insulator.

By this process, patterns with resolutions as low as 30 μm could be obtained. Finally, by electrospinning on a thin polymer film placed over the patterned collector, more complex patterns can be obtained as it is possible electrospin a second layer with different shape on the top of the first one after placing the film on another patterned collector.

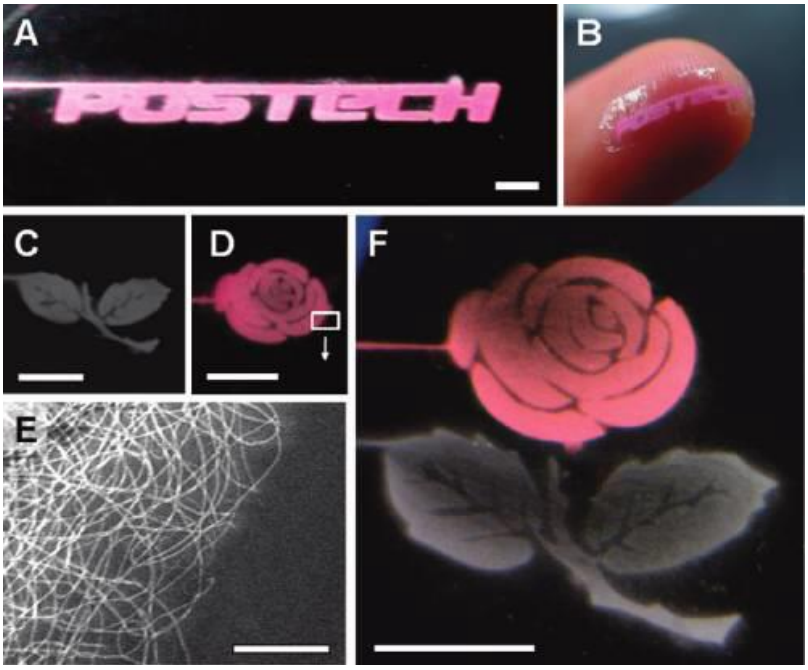


**Figure 18: Complex shapes deposited on a thin flexible film above conducting pattern electrodes. Reprinted with permission from [83].**

As a conclusion, by playing on the geometry and/or the dielectric properties of the collector, very complex 2D architectures can be obtained, as was demonstrated by Zhang *et al.* [59], who prepared structured electrospun tubes for biological applications (**Figure 19**). However, the preparation of an electrospun membrane with small patterns necessitates the fabrication of the corresponding collector by microfabrication techniques and, as for the 1D alignment of nanofibers under electrostatic forces, the structure might be lost after long deposition times, as the electric field is modified by the accumulation of charges on the electrospun mat.

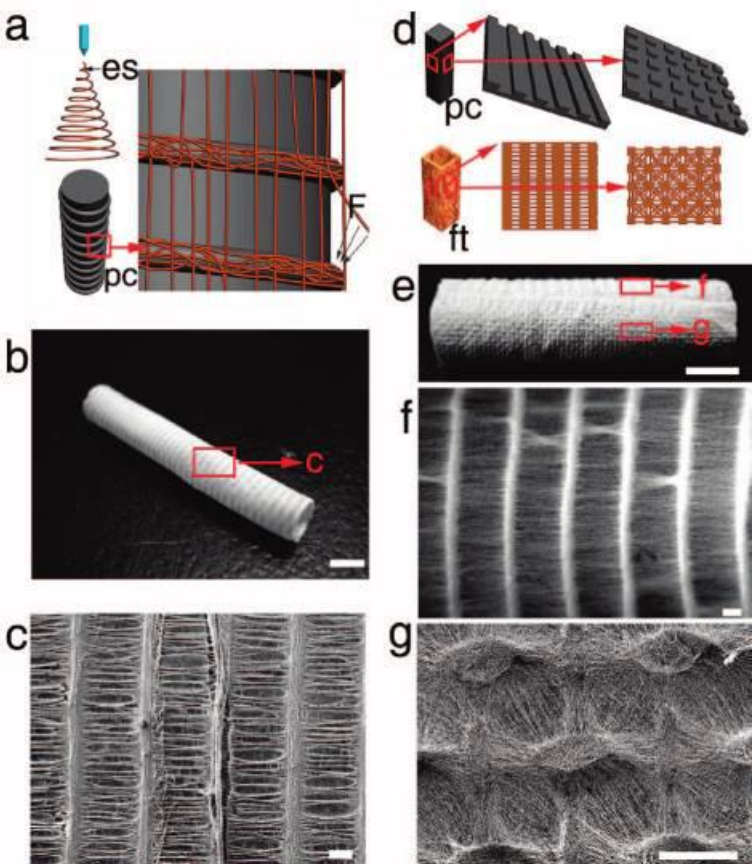


**Figure 19: a) Schematic illustration of collecting process using a cylindrical collector with equally spaced circular protrusions (es, electrospinning process; pc, patterned collector). b) A fibrous tube with patterned architectures (scale bar = 5 mm). c) Magnified image of panel b (scale bar = 200 µm). d) Schematic illustration of collectors with two different patterns and relevant fibrous tube (pc, patterned collector; ft, fibrous tube). e) A fibrous tube with two different patterns (scale bar = 5 mm). f, g) Magnified images of two different patterns of panel (scale bar = 200 µm). Reprinted with permission from [59].**

### 2.2.3 *Self-assembly of electrospun fibers*

As shown in previous sections, many efforts are made to elaborate structured nanofibrous scaffolds by developing specific processing techniques. However, few researchers have shown that under certain conditions, nanofibers can self-organize during their landing on the collector to form aligned fibrous bundles or honeycomb-like fibrous patterns. This strategy is very interesting

because it requires the standard electrospinning setup without any more modification leading thus to the production of structured scaffolds in a very cost-effective way.

Self-assembly has been observed in various conditions, but always with a common feature: the electrospun fibers must present a bimodal distribution in size and/or electric charge when landing on the collector. Deitzel *et al.*[43] reported that irregular fibers with large variation in diameter obtained from low concentrated poly(ethylene oxide) aqueous solutions can lead to the formation of numerous junction and bundles of fibers in the non-woven mat. More recently, Heiden *et al.* [94, 95] observed similar morphologies when electrospinning conducting solutions by adding a salt. The authors explain the formation of bundles by attractive electrostatic forces due to the excess charge provided by the salt. This phenomenon, called by the authors "backbuilding", leads to the appearance of negative charges which are drawn back through the positively charged jet. Thus, the positive portions of the jet are attracted by the negative ones before hitting the collector surface forming bundles of fibers. With similar ionic solutions of chlorinated polypropylene, the formation of bundles of fibers have been observed but moreover they self-organize into honeycomb-like patterns [96]. Microscopic observations reveal that the walls of the honeycomb patterns are formed by the accumulation of the bundles of fibers whereas single isolated fibers are hanging in air between the walls of the honeycomb patterns.

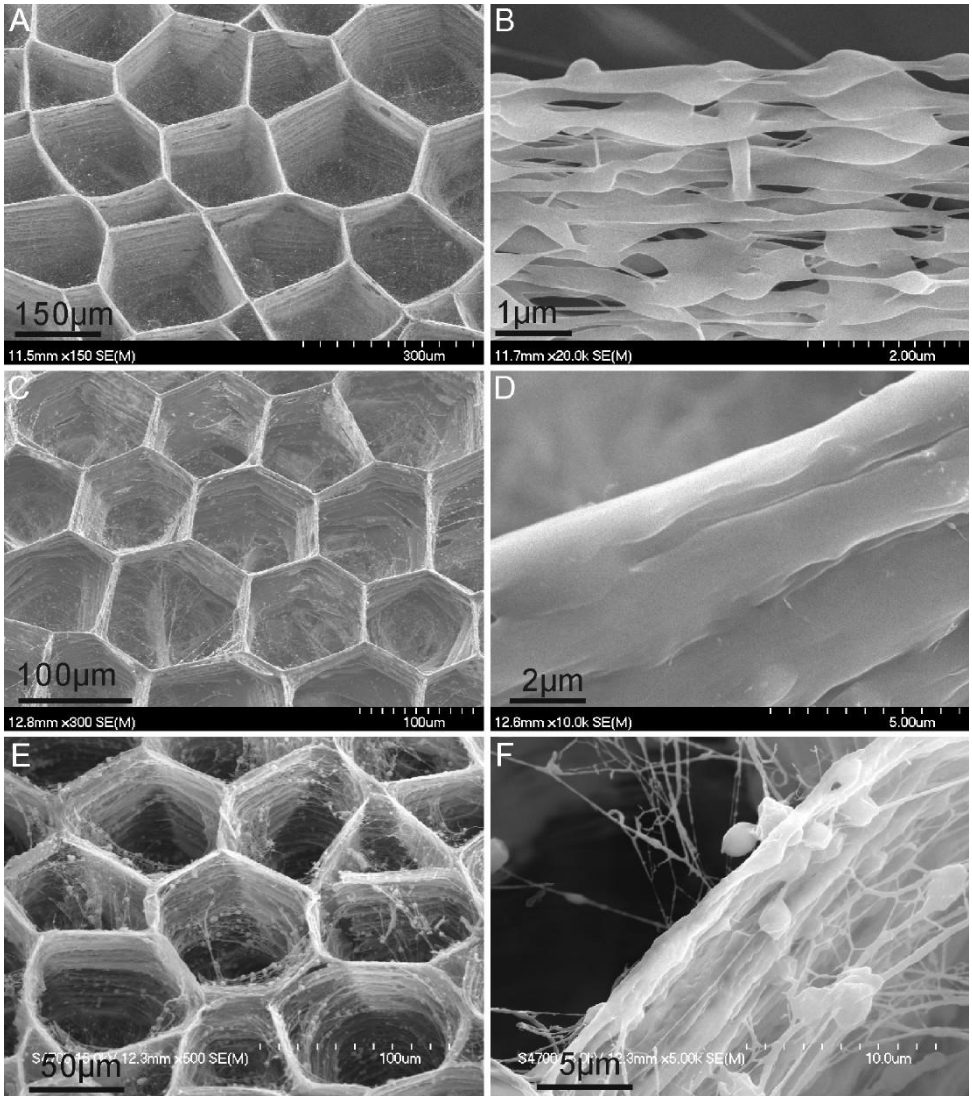


**Figure 20 : SEM images showing the surface morphology and wall structure of the HNFSs of PVA and PEO electrospun at different conditions: (A,B) PVA, concentration 6%, 22 kV, on plastic films; (C,D) PEO, concentration 16%, 22 kV, on Al substrates; (E,F) PEO, concentration 16%, 19 kV, on Al substrates. Reprinted with permission from [97].**

Honeycomb-like structures have also been observed in the case of beaded nanofibers obtained from low concentrated polymer solutions with poor volatile solvents [97, 98]. Yan *et al.*[97] observed very regular patterns (**Figure 20**) for which the walls are formed by the aggregation of the beads whereas thin free-beaded segments of fibers are crossing the honeycomb patterns. The authors explain the self-organization mechanism by the competition between the repulsive Coulomb forces and the attractive capillary forces due to remaining solvent. However, capillary forces can only act at very short distances and in the presence of solvent.

Recently, we observed that electrospinning of poly(ε-caprolactone) (PCL) in a dichloromethane/dimethylformamide (DCM/DMF 50/50) solvent system can also lead to self-assembled honeycomb-like structures. We showed that honeycombs efficiently form when a bimodal distribution of the fiber diameter is observed. This bimodal distribution, explained by the poor solubility of PCL in DMF, leads to a heterogeneous distribution of the electric charges along the electrospun jet. When the jet is landing on the collector, a rough fibrous membrane is formed showing a honeycomb structure. The walls of the honeycombs are formed by thick and wet fibers segments in good contact with the collector (thanks to the remaining DMF) whereas thin and dried fibers are hanging in air between the walls leading to poor electric charge dissipation (**Figure 21**). Thus, the membrane surface is rough and shows attractive (honeycomb walls) and repulsive domains (inside honeycomb patterns).

In conclusion, honeycomb-like structure can be obtained from highly conducting solutions or from low concentrated solutions with poor volatile solvents. The condition for self-organization is the bimodal distribution of the jet diameter (i.e. jet segments of bundles of fibers and single fibers in the case of highly conducting solutions and beaded jet morphology in the other case) which results in a heterogeneous electric charge distribution on the top surface of the fibrous membrane (**Fig. 21-b**) leading to a self-sustained structuration process.

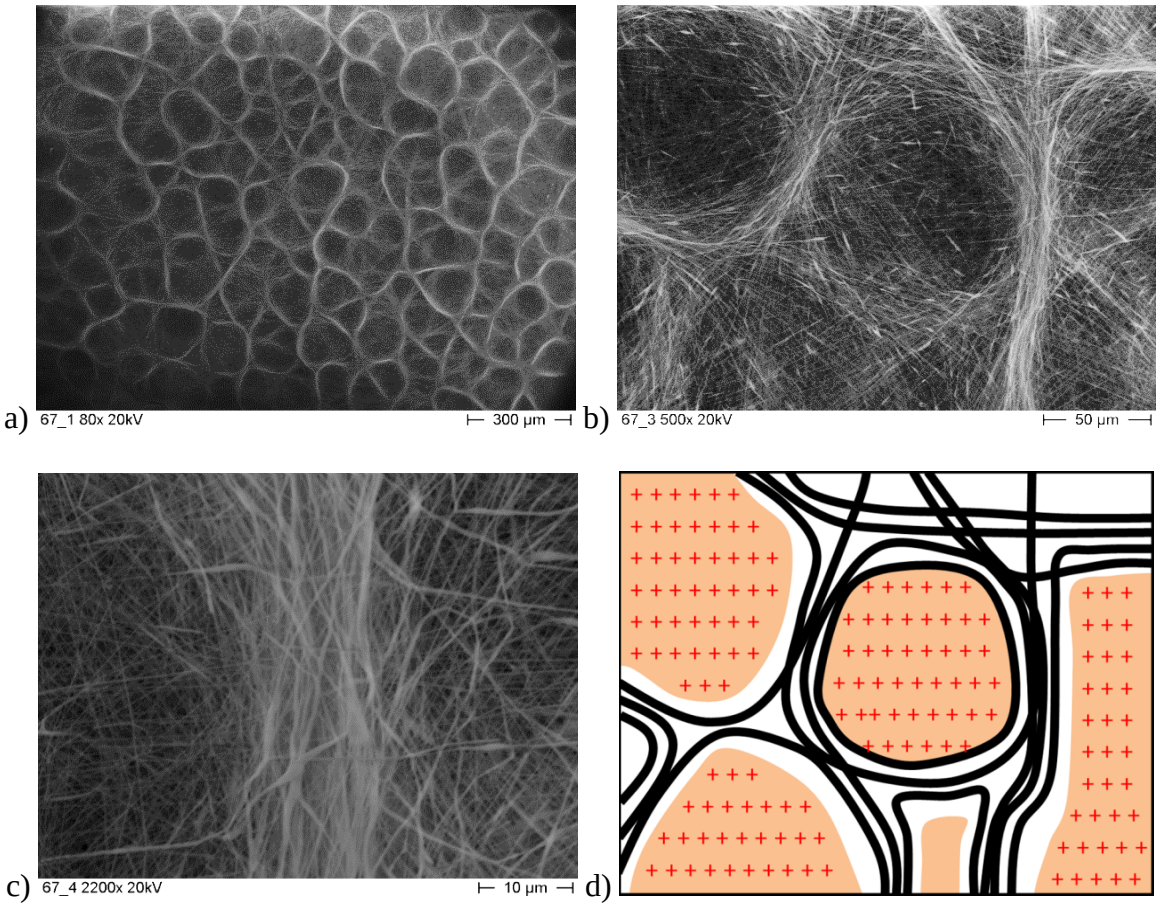


**Figure 21: a-c) Self-assembled PCL-based scaffold at different scales. d) Scheme representing honeycomb patterns with positive charges remaining on the suspended thin membrane suspended in the air and the thick bundles of fibers in good contact with the collector.**
**Reprinted with permission from [99].**

## 2.3 Towards 3D Nanofibrous Constructs

Thick nanofibrous and porous constructs are necessary in some applications such as catalysis or scaffolding for bone regeneration of large defects. In the latter case, porosity and pore size play a crucial role in bone formation. Pore size of few hundreds of microns is required for efficient cell infiltration and but also for vascularisation [100]. However, by nature, electrospinning is a process that generally results to the fabrication of thin 2D mats with pore size typically smaller than 5 µm and a thickness rarely larger than several hundreds of µm. Indeed, the thickness limitation is due to electric charge saturation on top of the mat during electrospinning. This saturation level is reached when the electrostatic field due to the charges on the substrate cancels out the external field imposed by the electrodes and the geometry of the apparatus leading thus to fiber repelling and inefficient deposition [101].

We will show that different kinds of electrospinning processes have been proposed to overcome the limitations of the thickness and pore size. Furthermore, we will present recent results showing that cm-thick 3D open cell foams with pores ranging from µm to few hundreds of µm can be obtained thanks to self-assembly of electrospun nanofibers.

### 2.3.1 *Specific electrospinning processes for 3D constructs*

The use of a chemical blowing agent (azodicarbonamide) in the formulation for the electrospinning was proposed to increase the size of the pores of PCL scaffolds up to 50-70 µm [102]. In this method, the scaffold is subjected to 100°C in a drying oven during few seconds leading to partial blowing of some spots of fibers. The method leads to partial melting of the fibers and moreover, the mesopores formed from the blown spots are not densely distributed in the scaffold. In order to create mesopores of several tens to hundreds of microns, leaching of salt [103] or ice particles [104] (see **Fig. 22-a**) which were previously deposited in the scaffold during electrospinning was proposed. Although this latter method doesn't lead to the fabrication of thick scaffold (i.e. no more than several hundreds of microns), the authors demonstrated that the depth of in vivo cell infiltration were much greater (> 400 µm) for such mesoporous scaffolds compared to standard electrospun scaffolds (< 50 µm). The easiest way to achieve a thick scaffold is to build multilayered constructs. Srouji *et al.*[105] built multilayered constructs with thirty individual PCL and collagen-based electrospun scaffolds which were previously seeded by

human mesenchymal stem cells. They achieved mm-thick of densely-stacked layers. After six week culture period in a bioreactor, the thick multilayered scaffold was implanted in nude mice. Although this strategy doesn't lead to the formation of mesopores, it revealed good cell proliferation and neovascularization.

Tzezana *et al.* [106] developed multilayered hydrospinning technique for which each nanofibrous layer is electrospun onto a water coagulation bath. Thanks to the use of a coagulation bath instead of a standard solid collector, a thin skin of water is surrounding the nanofibers preventing their fusing into each other during the collection process. Then, exposition of the multilayered scaffold in the vacuum for few minutes allows the elaboration of cm-thick scaffolds with pore size up to 100 µm (see **Fig. 21-b**). Moreover, the authors claimed that cells can be seeded during the hydrospinning process but however without sterilization due to technical difficulties.

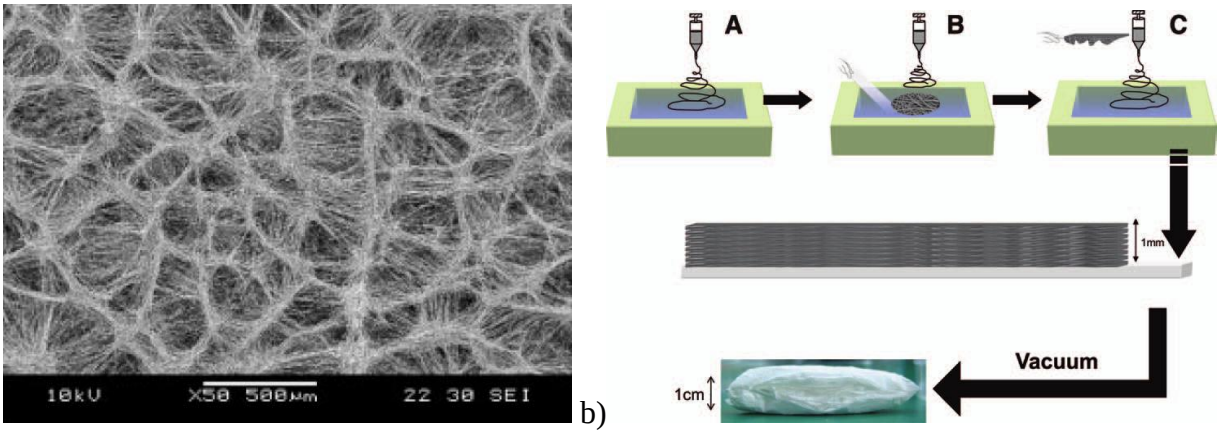


**Figure 22: a) Cryogenic electrospun scaffold showing pores between 10 to 500 µm. (Reprinted with permission from [104]. b) Principle of hydrospinning technique: (A) Electrospinning onto a coagulation bath. (B) A thin layer of nanofibers is collected on the surface of the water. (C) The layer is picked up on a glass slide. Step (C) is repeated and each layer is assembled on top of the previous one. The layered scaffold is put in a vacuum chamber for few minutes, during which its thickness is multiplied by 10. (Reprinted with permission [106])**

### 2.3.2 *3D Cm-thick scaffolds from self-assembled electrospun fibers*

Multilayered electrospinning techniques require a huge number of steps for the production of each layer and thus lead to long time of production. Thus, researchers developed one-step electrospinning processes for the elaboration of thick scaffolds. Blakeney *et al.*[107] used a

specially designed collector made of an array of long stainless steel probes in a non-conducting spherical dish. The electrospun nanofibers were collected on the probes preventing an efficient charge dissipation leading thus to the elaboration of cotton ball-like PCL scaffolds with loose random fiber networks. However no mechanical characterisation was performed on these scaffolds and implanting them *in vivo* might lead to collapse of the structure or delamination.

Recently, we found that cm-thick electrospun scaffolds with suitable mechanical properties and a gradient in porosity and pore size up to several hundreds of microns can be produced thanks to the self-assembly of PCL nanofibers. By focusing the electrospun jet and optimising the process conditions we force the growth of the scaffold in thickness up to the cm-scale. Indeed, as previously mentioned in section 3.3, PCL can self-organized into honeycomb-like structure. This process is stable and efficient for very long deposition times allowing thus the continuous production of stratified honeycomb layers. As it can be seen in **Figure 23**, each honeycomb pattern forms a mesopore. Moreover, the walls of the honeycomb structures are organized in the form of columns (see **Figure 23-d**) which are in good contact with the collector allowing efficient charge dissipation and thus very long deposition times of several hours. Furthermore, water content in the DMF plays a huge role in electric charge repulsion. Thus, the use of non-distilled DMF can lead to the formation of large mesopores up to 500 µm - 1 mm whereas distilled DMF lead to the formation of dense foam (see **Fig. 23-a** and **23-b**). This unique columnar structure of the mesopores leads to good mechanical properties in compression, suitable for handling and implanting the thick scaffold *in vivo*.

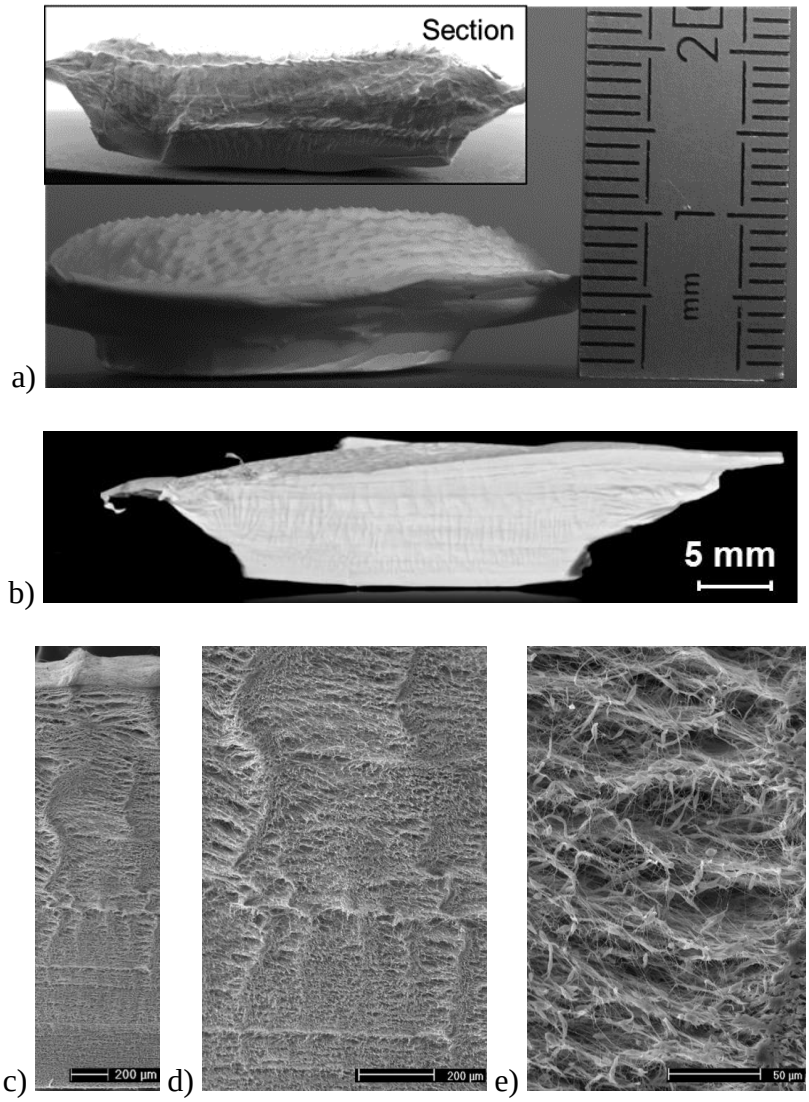


**Figure 23: Sections in the thickness of 3D thick scaffolds obtained thanks to the self-assembly of electrospun nanofibers. a) Macro-photography of a 3D thick scaffold and its section in the inset of a sample of ~10 mm thick showing large meso-pores obtained from non-distilled DMF. b) Macro-photography of the section of a sample of ~10 mm thick showing smaller meso-pores obtained from distilled DMF. c) SEM picture of the whole section of a sample of ~2 mm thick. d) Detail of the previous picture showing the columnar meso-porous structure of the scaffold. e) Detail of the previous picture showing micro and meso-pores. Reprinted with permission of [99].**

## 2.4 Conclusions of the structuration

In this part, we showed that controlled assembly or self-assembly of electrospun fibers can be achieved by the use of electrostatic, mechanical or magnetic forces forming 1D, 2D or 3D well defined fibrous architectures. It then allows the design of the complex architectures necessary for many specific applications such as reinforcement of composites [108], electronics [109] and tissue engineering [110].

For example in tissue engineering, electrospun scaffolds mimic the complex structures of the human body such as bones, skin, heart, vessels and nerves and their structuration is very important [111-115], as it influences the cell activity in various ways. For instance, aligned nanofibers results in a higher production of fibroblasts cells [116] and also improve the cell differentiation of the tendon stem cells [117]. Furthermore, it can guide cell growth in a specific direction in order to obtain the anisotropic structure necessary for heart tissue construction [118] or for nerve regeneration [119]. A double-layered nanofibrous mesh can also provide a good guidance for the neurites to grow into complex patterns and thus improve the nerve repair [120]. Structures like tubes are also often developed for the nerve regeneration and can have great potential in vascular substitutes [121]. At last, in 3D electrospun scaffolds, control of the porosity and improvement of the mechanical properties are the key factors for a better bone regeneration [100].

In conclusion, the ability to organize the nanofibers in highly ordered structures offers a great promise for technical applications especially in tissue regeneration.

## 3. Conclusions of Chapter 1

In this first chapter, we presented briefly the electrospinning theory. We discussed the effect of the different electrospinning parameters on the fiber formation during the process.

In the second part of this chapter, we explained in detail the elaboration of architectured electrospun nanofibers from one dimension to three dimensions. The effect of the different forces acting on the fiber structuration during the process was explained. 1D aligned and highly aligned electrospun nanofibers were first developed by using different kind of forces (electrostatic forces, mechanical forces and magnetic forces). 2D patterned nanofibrous membranes could be obtained by a stacking of the 1D aligned nanofibers. A local control of the electrostatic forces (with micropatterned collectors) is another way to obtain micropatterned electrospun membranes. Finally, we showed that in some case, self-assembly of some polymers during the electrospinning process could also lead to 2D electrospun constructs.

Finally, we presented different electrospinning strategies which were developed to create 3D electrospun scaffolds with open porosity, ideal for tissue regeneration applications.

The aim of the thesis was to elaborate new kinds of architectured electrospun membranes. To do that, we had to choose among all available strategies the best way to organize the nanofibers in 2D and 3D. We decided to use micropatterned collectors to control the fiber structuration. Indeed, the local control of the electrostatic forces at the vicinity of the micropatterned collector will structure the nanofibers and allow the formation of a 2D micropatterned electrospun membrane.

In the chapter two, we present the elaboration of new 2D and 3D monocomponent electrospun membranes thanks to new kind of micropatterned collectors (made by lithographic processes). The effect of the morphology of nanofibers on the topography of the scaffold is explained in detail. Then, the influence of these micropatterned electrospun membranes on bone cells (i.e. osteoblasts) behaviors (proliferation, organization) is studied. Finally, we show that by combining micropatterned collectors and self-assembling properties of electrospun fibers, we can elaborate a new kind of 3D electrospun scaffold with controlled pore size and porosity gradient.

# Chapter 2: Monocomponent 2D and 3D architectured nanofibrous scaffolds for bone regeneration

## 1. Introduction

In this chapter, we present how monocomponent 2D and 3D electrospun membranes can be obtained and how they can be used for bone regeneration applications.

Our first aim was to develop electrospun 2D micropatterned membranes and then, to study the impact of the microstructuration on osteoblasts proliferation. Our second aim was to be elaborate 3D micropatterned electrospun scaffold based on the findings obtained for the membranes.

Our strategy was to use micropatterned collectors during the electrospinning process in order to structure the fibers into a micropatterned nanofibrous mat. Indeed, at the vicinity of the collector, the electrostatic forces are driven by the topography of the micropatterned collector, resulting in the structuration of the jet over the micropatterns of the collector.

Micropatterned collectors were designed by photolithographic processes. Different kinds of collectors (honeycomb collector, grid collector) were elaborated and tested during the electrospinning processes. The 2D electrospun membranes were fabricated with two FDA approved biopolyesters: poly(ε-caprolactone) (PCL) and poly(lactic acid) (PLA). After an optimization of electrospinning conditions of PCL and PLA, different kinds of micropatterned electrospun membranes were fabricated: grids and honeycomb electrospun membranes.
Then, a complete study of PCL and PLA honeycomb micropatterned electrospun membranes and their effect on osteoblast organization was made and published in *Macromolecular Bioscience*.

In the second part of this chapter, we show that by using honeycomb micropatterned collectors and self-assembling properties of PCL electrospun fibers during their deposition, we were able to elaborate 3D mm-thick electrospun scaffold with controlled pore size and porosity gradient in the thickness of the scaffold. This work was submitted to *Material Letters*.

Finally, conclusions of this chapter are given.

# 2. Materials and methods

## 2.1 Photolithographic processes

### 2.1.1 *Principle*

Photolithography (or "optical lithography") is a process used in microfabrication to selectively remove parts of a thin film deposited on a substrate. It uses UV light to transfer a geometric pattern from a photo mask to a light-sensitive chemical "photoresist" on the substrate. A series of chemical treatments then engraves the exposed patterns into the material underneath the photoresist. Patterns of micro and nano size can therefore be fabricated on a flat substrate such as a silicon wafer.

During the lithographic process, a light sensitive chemical photoresist is exposed to UV light (wavelength 365-436 nm) through a mask made of geometric chrome patterns and geometric quartz patterns. The chrome patterns are opaque to UV wavelength and therefore only light transmitted through the geometric quartz patterns could expose the photoresist. After the exposure, a latent image of the patterns is created in the photoresist allowing the selective development in adequate solution.

Different kinds of photoresist are available in the market: positive and negative photoresists. (see **Figure 24**).

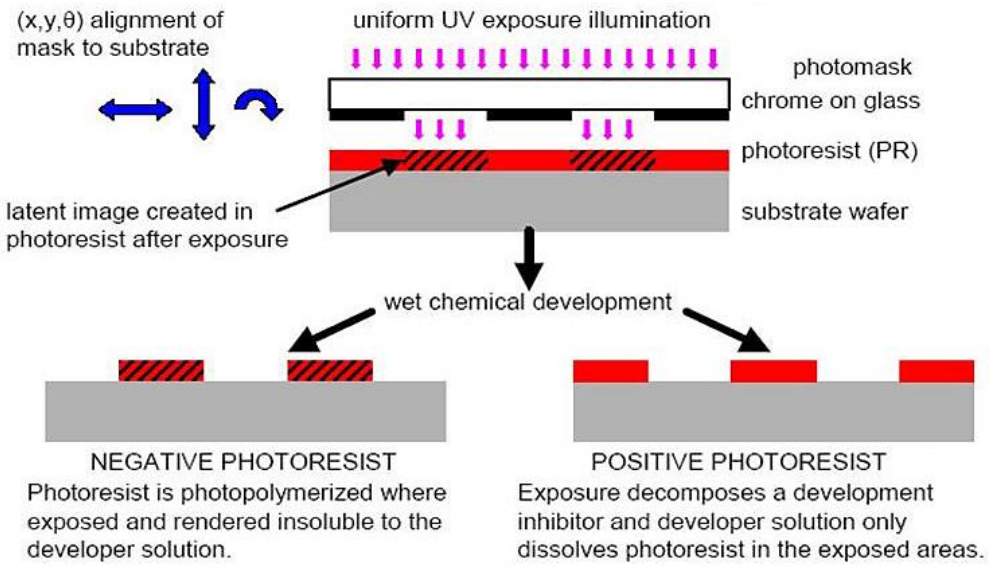


**Figure 24: Differences between a negative photoresist and a positive photoresist during a photolithographic process.**

With a negative photoresist, the exposed areas are cross-linked during a post-exposure bake and become insoluble into the developer solution. Conversely, with a positive photoresist, the UV exposed areas are dissolved in the developer solution (**Figure 24**).

Only one type of photoresist was used during our study: the epoxy-based SU-8 photoresist. This type of photoresist was chosen due to the chemic stability of the SU-8 photoresist. As example, SU-8 is not soluble in many solvents like acetone, ethanol, and isopropanol.

The resistance to solvent is a property required for the photoresist because after the electrospinning process, the collector made by the photoresist is immersed into different kinds of solvents in order to remove the electrospun scaffold. With the SU-8, the patterns will be stable after the peeling operation of the scaffold. The different steps of lithographic processes are summarized on the **Figure 25** and detailed in the next part.

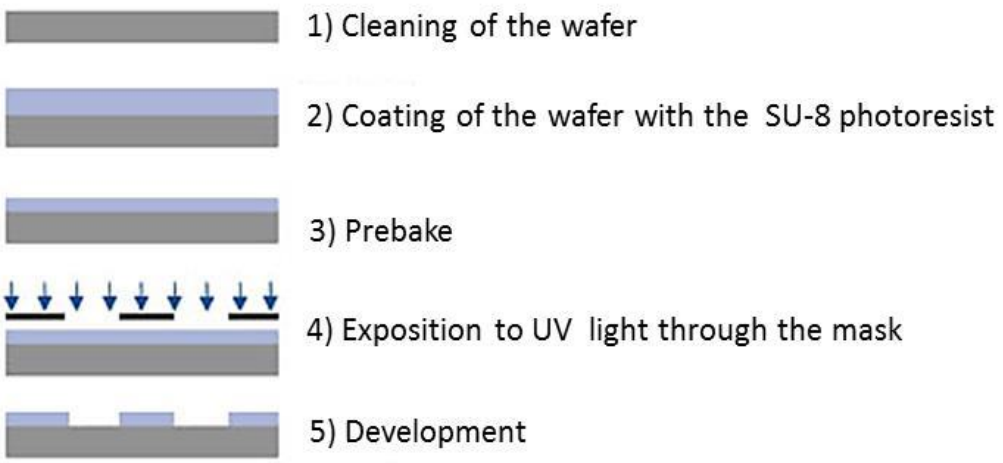


**Figure 25: The different steps of lithographic processes**

### 2.1.2 *Main steps in photolithography process used during this work.*

**1) Treatment of the substrate before the spin coating:**

The contamination of the silicon wafer can create many problems on the next steps of the process of photolithography. The main problems are the decrease of the adhesion of the photoresist to the substrate and also the inclusion of defects. To avoid these defects, the silicon wafer is firstly washed in acetone, ethanol and isopropanol. Humidity is also one the most pollutant during photolithographic processes. The silicon wafers are hydrophilic and thus can adsorb the humidity of the air, increasing the amount of hydroxides on the surface of

the substrate leading adhesion issue with the photoresist. To avoid this phenomenon, the substrate is heated just before the spin coating operation. Once the substrate is dehydrated, a special component, generally hexamethyldisilazane (HMDS) is deposited at the surface of the substrate to promote the adhesion between the photoresist and the substrate, in replacing hydrophilic groups by hydrophobic groups.

**2) Deposition of the photoresist**

The photoresist is deposited by a centrifugation coating (spin-coating) (**Figure 25-2**). The principle consists in spreading a little quantity of a solution of the photoresist on the substrate (silicon wafer) thanks to centrifugal forces, in a spin-coater. The main steps of the process are:

a) Deposition of the photoresist over the wafer
b) Repartition of the photoresist over the wafer by a slow rotation of the spinner
c) Increase of the speed rotation in order to eliminate the overage of the photoresist
d) Rotation with a constant speed in order to evaporate the solvent and also to homogenize the thickness of the deposited photoresist.

The result is a solid film deposited on a wafer. The quality of the film depends on the presence of defects (dust, crater). For SU-8 2050, the photoresist is firstly spread a with a speed of 500 rpm during 5 seconds and then 30 seconds at 2500 rpm in order to obtain patterns with a height of 60 µm.

**3) Baking after spin coating:**

This step follows directly the deposition of the resin on the wafer. This first bake guarantees a rapid elimination of the solvents and also the densification of the matrix. The bake is made on a heating plate. For SU-8 2050, the first bake is made at 65°C during 3minutes and the second bake lasts 7 minutes at 95°C.

**4) Exposition:**

The time of exposition depends directly on the power of the UV lamp. The time of exposition is calculated by through a surface energy ($J/m^2$). The time of exposition fixes the surface energy which the parameter that controls the resolution of the patterns. For the SU-8 2050, for a thickness of 60 µm, a surface energy of 7 $mW/cm^2$ corresponded to 28 s of exposure. A post-exposure bake at 65° C during 2 minutes and followed by 95 °C for 6 minutes is then necessary in order to cross-link the exposed areas (**Figur**e **25-3**).

**5) Development:**

The patterns of the desired height appear during the step of the development (**Figure 25-5**). The wafer is immersed in a developer during a certain period. Immersion for longer periods can partially or fully destroy the patterns. After this step, the wafer has to be rinsed into isopropanol in order to stop the development process. Once the residues of SU-8 have been perfectly removed, patterns with a height of 60 µm are on the surface of the wafer.

**Final Bake:**

Before making any other treatment, the wafer undergoes a final bake in order to harden the photoresist. For SU-8, a final bake during 10 minutes at 150 °C was necessary. Optical images and characteristics of the obtained silicon collectors are presented on **Figure 26** and in **Table 1**.

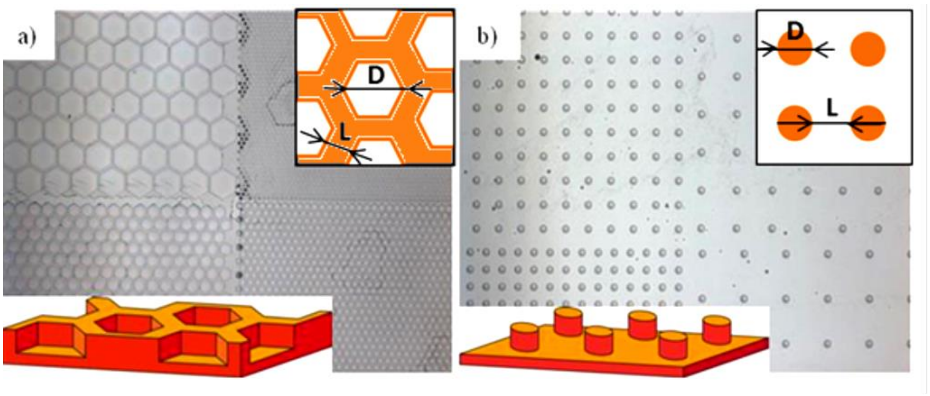


**Figure 26: Optical images of silicon collectors: a) Honeycomb collector: D is the internal diameter of the honeycomb pattern and L is the width the honeycomb wall (space between two honeycomb patterns; b) Block collector: D is the internal diameter of the block pattern block and L is the space between two block patterns**

| Honeycomb collector | Block collector |
|---|---|
| D= 360 µm / L=20 µm | D= 20 µm / L=40 µm |
| D= 160 µm / L=20 µm | D= 20 µm / L=60 µm |
| D= 80 µm / L=20 µm | D=20 µm / L=100 µm |
| D= 40 µm / L=20 µm | D= 20 µm / L=120 µm |

**Table 1: Characteristics of the micro-fabricated collectors: D is the internal diameter of the hexagon or the block and L is the space between two patterns.**

**Gold/ Aluminium deposition**

Finally, the micropatterned collectors are covered by a conductive layer in order to make them conductive as they will be used as collectors during the electrospinning process. To make them conductive, a thin layer of aluminum/ gold (150 nm) was deposited by electron beam deposition machine. After this final step, the collectors can be used for the electrospinning process.

## 2.2 Polymers for bone tissue engineering applications

In tissue engineering, the scaffold that allows the reconstruction of the tissue is introduced in the living body at the lesion place. For consequence, it should be:

- biocompatible: the scaffold should have the ability to be accepted by the living body
- bioresorbable: the scaffold should be able to resorb and to be replaced by the new formed tissue
- biodegradable: the scaffold should break down in physiological environments by macromolecular chain scission into smaller fragments, and ultimately into simple stable end products that are not toxic. The degradation may be due to aerobic or anaerobic microorganisms or biologically active processes (e.g: enzyme reactions) or passive hydrolytic cleavage.

Thus, the chosen polymer to elaborate the electrospun scaffold should respect these requirements but it should also be able to be dissolved in a system of solvents adapted to the process of electrospinning. Finally, the polymer selected should present mechanical properties that allow the manipulation of the electrospun membrane during surgery.

Considering that the extra-cellular matrix (ECM) of the bone tissues presents a fibrillar structure of various type of collagen (collagen type I, II, III), natural polymers (such as collagen[122] or hyaluronic acid [123]) come as the best choice to elaborate such scaffolds. However, the elaboration of electrospun nanofibers with these polymers is not trivial: they are in general polysaccharides or polypeptides that are not soluble in solvents adapted to the process of electrospinning. Moreover, the supply of such natural polymers is more difficult (their price is high) and their properties could be very variable.

In such context, we decided to elaborate our monocomponent electrospun micropatterned scaffolds with synthetic polymers. The synthetic polymers are less expensive than the natural

polymers, their properties are predictable and their elaboration with the electrospinning process is easier than with the natural polymers [21].

Degradable polymers frequently used for tissue engineering applications are linear aliphatic polyesters such as PGA (polyglycolic acid), PCL poly (ε-caprolactone) and PLA poly (lactic acid). They are biocompatible and bioresorbable, and thus ideal for such kind of applications. They differ from each other by their physical properties but also their time of degradation. PCL and PLA present longer time of degradation (superior to 2 years) than PGA (0.5 year-1 year), and this makes them more suitable for bone tissue engineering applications that require a longer time of degradation (superior to 8 months) to allow the formation of the new bone [124].

We decided to work with the PCL and the PLA, that present long degradation rate but also interesting mechanical properties. We used these polymers as homopolymers while in many studies researchers have mixed the two polymers in order to obtain different properties. These two polyesters are presented in the next part.

### 2.2.1 *PCL*

PCL was one of the earliest polymer synthesized by the Carothers group in the early 1930 [125]. It is an aliphatic polyester with a glass transition temperature ($T_g$) of -61°C and a low melting point ($T_m$) (65°C) [126]. PCL is generally prepared by Ring-Opening Polymerization (ROP) of ε-caprolactone in the presence of metal alkoxide (aluminium isopropoxide, tin octoate, etc) [126] (**Figure 27**). It is a semicrystalline polymer and its crystallinity tends to decrease with increasing molar mass [127].

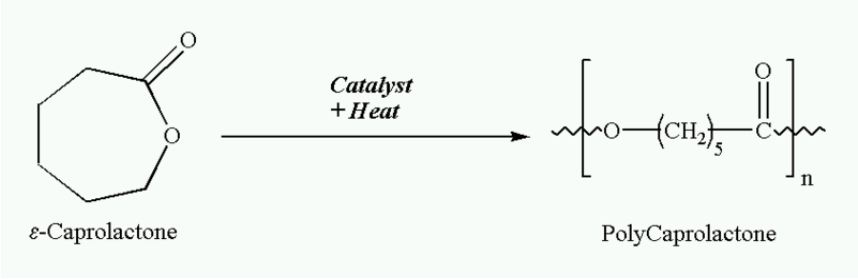


**Figure 27: Ring opening polymerization of poly(ε-caprolactone) from [127].**

PCL is soluble in chloroform, dichloromethane, benzene, toluene, cyclohexanone and 2-nitropropane at room temperature. It has a low solubility in acetone, butanone, ethyl acetate, dimethylformamide and acetonitrile and is insoluble in alcohol, petroleum ether and diethyl ether [128].

PCL is a biocompatible and bioresorbable polymer. It is FDA (Food and Drug Administration) approved [129]: it is already used in clinical applications as a medical suture material (Monocryl®) or drug controlled release material (Capronor®) or even as nerve guide device in nerve regeneration [129]. PCL presents some rheological and viscoelastic properties that allow its processing by electrospinning [130] of course and other techniques like solid freeform fabrication [131], and others. The fact that PCL is easily processed by different techniques makes this material ideal for the elaboration of various types of scaffolds for tissue engineering applications [130]. In electrospinning for example, various PCL scaffolds were developed for cardiac engineering [132], bone and cartilage tissue engineering [133]. Indeed, one advantage of PCL for tissue engineering application is its degradation rate. PCL presents a very slow degradation rate : 2 to 4 years depending on the starting molar mass of the device or implant and on the environment conditions [127]. For example, because of its slow degradation rate, PCL can be used in long time application such as Capronor® which is a contraceptive device implantable for one year [134, 135]. PCL could also be easily enzymatically degraded. Actually, the mechanism of degradation of PCL could be attributed to random hydrolytic chain scission of the esters linkages, which caused a decrease in molar mass [127]. Furthermore, this hydrolytic degradation can be catalyzed under acidic conditions [136]. However, PCL also present some disadvantages like for instance its hydrophobicity [130].The fact that PCL is hydrophobic results in poor wettability, lack of cell attachment and uncontrolled biological interactions with the materials [137]. This inconvenient could be overcome by surface modifications of the PCL such as modifications by covalent chemical bonds, plasma treatment or physical adsorption of proteins [130].

### 2.2.2 *PLA*

PLA is an aliphatic polyester, which is biocompatible and bioresorbable. It was FDA approved for biomedical applications [138] such as sutures, drug delivery systems and implants for tissue engineering [129, 139]. For example, PLA has been used as a copolymer with the glycolic acid to form a suture material (Vicryl®) [140].

The chemistry of PLA involves the processing and polymerization of lactic acid monomer. L-lactide acid and D-lactic acid are the two isomers of lactic acid. Lactic acid is commercially easily prepared by fermentation of molasses or potato starch or of dextrose from corn. Lactic acid can also be prepared via petrochemical feedstocks. The lactic acid produced by the petrochemical route can be L or D isomers whereas the lactic acid produced by fermentation is in majority the L-isomer but D-form is also produced [141].

Polymerization of lactic acid to high molecular weight PLA can be achieved according **Figure 28**.

In direct condensation, solvent is used under vacuum and temperatures for the removal of water produced in the condensation. This technique was used by Carothers and the resultant product is a low to intermediate molar mass material, which can be used as is, or coupled with isocyanates, epoxides or peroxide to obtain high molar mass [141].

In the solvent free process, a cyclic intermediate dimer, the lactide, is produced and purified by distillation. Ring-Opening polymerization of the lactide intermediate results in PLA with controlled molar mass. By controlling residence time and temperatures in combination with the catalyst system and concentration, it is possible to control the ratio and sequence of D- and L-lactic acid units in the final polymer [142, 143].

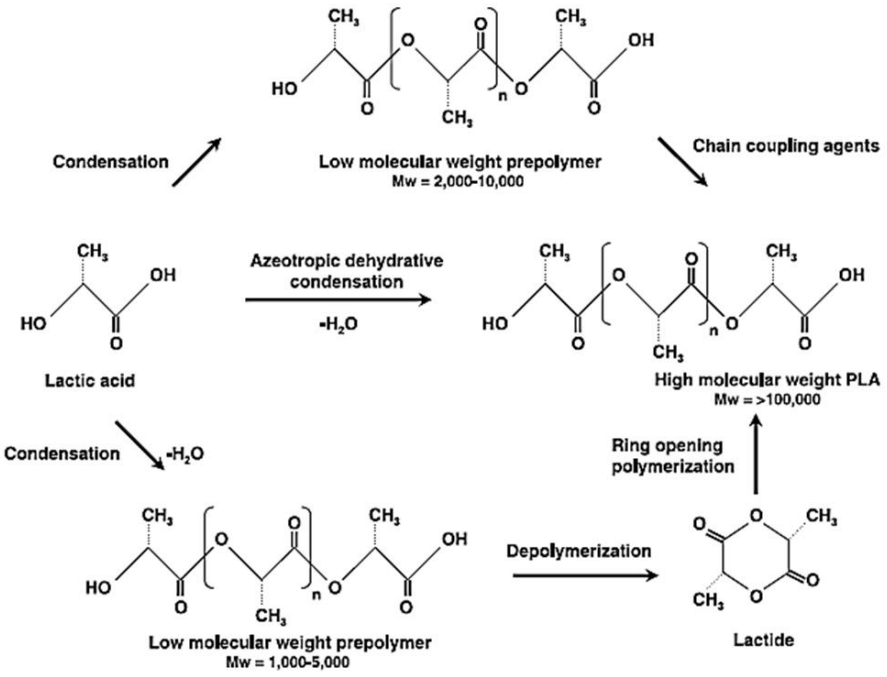


**Figure 28: Synthesis of polylactic acid [143]**

Different PLA structures can be produced such as the poly (D-lactic acid) (PDLA) and the poly (L-lactic acid) (PLLA), which are semi-crystalline material with regular chain structures; the poly (D, L-lactic acid) (PDLLA), which is from semi-crystalline to amorphous according to the L/D ratio. We can also find the specific case of the 1:1 blend of poly (D-lactic acid) with the poly (L-lactic acid) with formation of a stereo-complex. The homopolymer PLA has a Tg of around 58° C and a Tm of around 152°C. PLA is soluble in common solvents like benzene, chloroform, dioxane; etc. and degrade by simple hydrolysis of

the ester bond [139]. The PLA 7000D (containing 7% of D) is a PDLLA, which is amorphous before processing.

Some properties of PLA and PCL are presented on the Table 2, to be compared. At room temperature, PLA is a brittle material (less than 10% elongation at break) whereas PCL is more elastomeric and presents an elongation at break higher than 500 %.Then, PLA presents a high tensile modulus (2050 MPa) compared to PCL (190 MPa). PLA mechanical behavior limit its application when high deformation is required [144]. One way to increase the PLA deformation is the plasticization. Different plasticizers can be used such as PEG, oligomers of lactic acid [145].

| | PCL Solvay (CAPA 680) | PLA Dow-Cargill (Natureworks) |
|---|---|---|
| Density (g/cm$^3$) | 1.11 | 1.25 |
| Melting point (°C)[a] | 65 | 152 |
| Glass transition (°C)[a] | -61 | 58 |
| Crystallinity[b] (%) | 67 | 0-1 |
| Modulus (MPa) ( NFT 51-035) | 190 | 2050 |
| Elongation at break (%) (NFT 51-035) | > 500 | 9 |
| Tensile stress at break or max (Mpa) (NFT 51-035) | 14 | - |
| Water permeability WVTR at 25°C (g/m2/day) | 177 | 172 |
| Surface tension (γ) (mN/m) | 51 | 50 |

[a] : Measured by DSC; [b] : determined on granules, before processing.

**Table 2: Some properties of PCL and PLA (from [126])**

The PLA, likewise the PCL can be processed by different techniques such as the melt-spinning, the dry spinning, the electrospinning, etc. [141]. Different studies proved that PLA is a very promising material in the field of biomedical applications, especially when it plays the role of the support (scaffold) for the cells in the human body [139].

Its bioresorbability property can be observed when PLA filaments were used for regeneration of nerves in paralyzed patients. Schwann cells were growing on the support (functionalized with poly-D-Lysine) that was joining two extremities of the nerves. With the passage of time, the support disappears and leaves behind a continuous channel of nerve cells [146].

Moreover, PLA has already shown favorable results in the case of fractures and osteotomies. For example, PLLA rods, which were manufactured by extrusion and drawing techniques, were used as scaffolds for bone formation in muscle. At 6 weeks after the

implementation, new histologically mature bone had been generated in predesigned cylindrical form [147].

The degradation rate of PLA depends on the crystallinity, the molar mass and its distribution, the morphology, the water diffusion rate into the polymer and the stereoisomeric content [144, 148]. It was proved that PLA implants are reduced in weight by 63.2% within 168 days and that a complete decay would need at least 2 years [149]. This slow degradation rate makes PLA ideal for bone tissue engineering. To obtain desired mechanical properties or desired degradation rate, PLA is often copolymerized with glycolide or caprolactone in order to tailor the final performances of the final biomaterial [150].

## 3. Electrospinning of PCL and PLA

### 3.1 Electrospinning of PCL

PCL has been widely used in electrospinning to produce scaffolds for various applications in tissue engineering, especially in the last decade **[130]** (**Figure 29**).

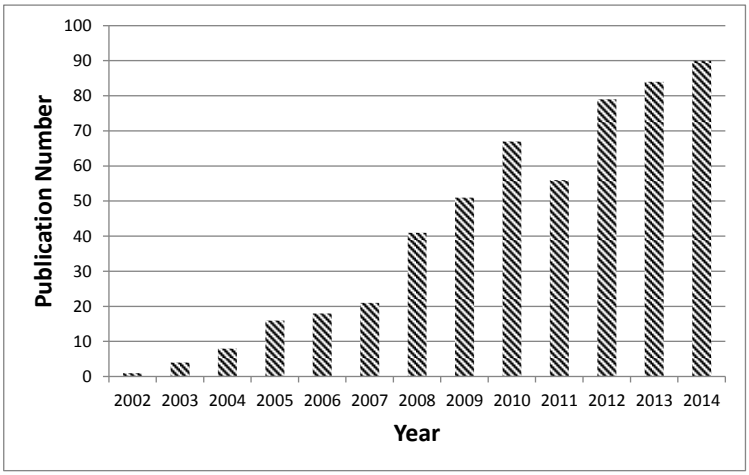


**Figure 29: Publications using PCL electrospun fibers during the last 12 years ( Search date from http://www.scopus.com, years 2002-2014, using " PCL electrospun fibers" [130].**

In the literature, PCL has been electrospun in solvent or mixing of solvents. Unique solvent such as acetone [151], chloroform [152] or dichloromethane (DCM) [153] are good solvents for PCL but they evaporate very quickly. Indeed, their rapid evaporation provoke formation of clogging in the needle, therefore the process is not stable. Fluorinated solvents like hexafluoropropanol (HFIP) [154] or trifluoroethanol (TFE) can be used for the

electrospinning of PCL [155] but they should be avoided because of their high toxicity. Thus, PCL is generally electrospun from the mixing of two solvents.

Acid solvent mixtures can be used. They present advantage for biomedical applications because of their absence of toxicity [136]. However, the acid system accelerate the hydrolytic degradation of PCL [40]. It is thus necessary to perfectly control the duration of immersion of PCL in this kind of solvents systems in order to keep a constant molar mass during the production.

Another kind of solvent system including DMF (dimethylformamide) is often used with PCL. The high dielectric constant of DMF allows a high polarization and therefore a concentration of electrical charges at the surfaces of the droplet. Besides, the saturating vapor tension of DMF is low avoiding a quick evaporation of the solvent mixture, allowing a stable production. In solvent system like DCM/DMF, Ahirwal *et al.* showed that PCL fibers present a bimodal distribution of their diameter [99].

To get more regular PCL fibers, we decided to play on the conductivity of the solvent system. Indeed, Uyar *et al.* showed for instance that conductivity could greatly affect the morphology of polystyrene (PS) fibers. They prepared solutions of PS in DMF with different grades of DMF from different suppliers showing different conductivity. They demonstrated that by electrospinning the solutions of PS under the same conditions, they could manage to obtain beaded or non-beaded PS fibers only by playing on the conductivity of the DMF [156]. Moreover, De Clerck *et al.* proposed a new system of acids solvents (mixture of formic acid/ acetic acid) in which PCL nanofibers had a diameter ten times smaller than the diameter obtained from chloroform solution [136]. But as previously mentioned, PCL is subjected to high degradation rate due to the catalytic effect of acids. Lavielle *et al.* exploited this phenomenon to produce regular thin nanofibers with a diameter as low as 135 nm +/- 70 nm [40].

Based on these studies, we played on the conductivity of the solution in order to optimize the morphology of PCL fibers. We compare three different solvents systems for the solution of PCL:

- DCM/DMF1 (DMF1: ReagentPlus® ≥ 99%, Sigma-Aldrich)
- DCM/DMF2 (DMF2: ACS reagent, ≥99.8%, Sigma-Aldrich)
- DCM/DMF1/Formic Acid (FA): we added 5% wt/wt of FA compared to the total weight of the solution.

The influence of the conductivity of the solutions on the diameter of the fibers is presented on **Table 3** and the **Figure 30**.

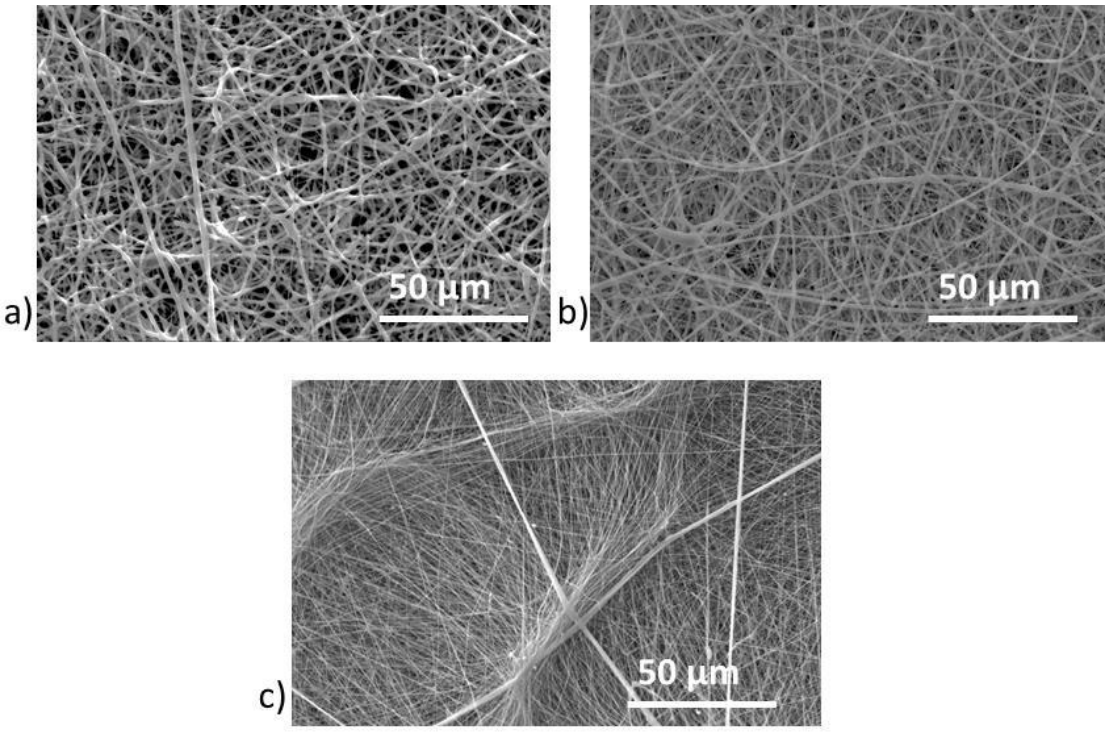


**Figure 30: SEM images of PCL nanofibers: a) 15 wt % PCL solution containing DMF1; b) 15 wt % PCL solution containing DMF2; c) 15 wt % PCL solution containing 5% of Formic Acid.**

| | PCL 15 wt % 60/40 DCM/DMF1 | PCL 15 wt % 60/40 DCM/DMF2 | PCL 15 wt % 60/40 DCM/DMF1/Formic Acid |
|---|---|---|---|
| Average diameter (nm) | 1650 +/- 500 | 950 +/- 450 | 270 +/- 600 |
| Conductivity ($\mu S.cm^{-1}$) | 1 +/- 0.1 | 3 +/- 0.2 | 234 +/- 12 |
| Voltage (kV) | 25/0 | 25/0 | 25/0 |
| Distance (cm) | 13 | 13 | 13,5 |
| Flow rate (mL.h-1) | 1 | 0,9 | 1,1 |
| Temperature (° C) | 25 +/- 1 | 25 +/- 1 | 25 +/- 1 |
| Humidity (HR %) | 33 +/- 3 | 33 +/- 3 | 35 +/- 3 |

**Table 3: Electrospinning conditions of different PCL solutions and diameter of the fibers obtained from these solutions.**

According to the **Table 3** and **Figure 30**, there is a small increase of the conductivity of the solution made with the purest DMF (DMF2). Yet, the nanofibers obtained with the solutions without acid presented quite the same fibers morphology: a bimodal distribution of the fiber diameter with a large amount of thick fibers compared to thin fibers (**Figure 30-a and Figure 30-b**). However, by adding some formic acid in the solution, we increased

significantly the conductivity of the solution from 1 µS.cm$^2$ to 234 µS.cm$^2$ (**Table 3**) and the sample presented bimodal distribution of the diameter of the fibers with a higher amount of thinner and regular fibers (270 nm) fibers (**Figure 30-c**). By increasing the conductivity, we increased the quantity of charges inside the solution. Thus, the rise of charges inside the solution induces an increase of the electrostatic forces: the jet is well stretched and the nanofibers present therefore a smaller diameter.

Because we added formic acid in the solutions, the catalytic hydrolysis of PCL had to occur. To measure the degradation of PCL after 24 hours after FA introduction, the molecular wright was assessed by GPC measurements. It appeared that, after 24 hours, the molar mass of PCL did not much decrease, which proved that the small amount of formic acid added to the solution did not accelerate so much the hydrolysis of PCL during the first 24 h (**Table 4**).

| | PCL 15 wt%<br>60/ 40 DCM/DMF | PCL 15 wt%<br>60/40 DCM/DMF<br>+ 5 % Formic Acid |
|---|---|---|
| $M_w$ (kg/mol) | 75 +/- 8 | 74 +/- 8 |

**Table 4:Molar mass of two different samples of PCL**

Electrospinning was always performed between 20 hours and 24 hours after introduction of FA in the solution.

Finally, we measured also the surface tension of the different solvents system of the PCL solutions to see if an increase in the conductivity could have affected the surface tension. Regarding the **Table 5**, we can conclude that there is no significant difference between the all solutions with or without FA.

| | DCM | DMF | 60/ 40 (V/V)<br>DCM/ DMF | PCL 15 wt%<br>60/ 40 DCM/DMF | PCL 15 wt%<br>60/40 DCM/DMF + 5 %<br>Formic Acid |
|---|---|---|---|---|---|
| Surface Tension (mN.m$^{-1}$ ) | 27 +/- 2 | 36 +/- 2 | 31 +/-2 | 30 +/-2 | 32 +/-2 |

**Table 5: Surface tension of different solvents and different solutions of PCL**

## 3.2 Electrospinning of PLA

To obtain PLA nanofibers, we decided to work in a system of solvent with DCM/ DMF, similar with the one used for PCL but without acid. Indeed, like PCL, DCM is a good solvent of PLA, whereas the addition of DMF in the solution will permit to get of a stable jet during the production.

We prepared different solution of PLA, varying the concentration and the DCM/DMF ratio. The obtained nanofibers are presented on **Figure 31**. As we can see on **Figure 31**, we varied the concentration of PLA from 7 % to 10 %. The ratio DCM/DMF was either 70/30 (V/V) either 50/50 (V/V).

As showed on **Figure 31-a** and **Figure31-b**, concentrations of 7 % of PLA and 8 % PLA in 70/30 (V/V) DCM/DMF leads to beaded fibers. By increasing the concentration to 10 % in 70/30 (V/V) DCM/DMF, the beads disappear but the diameter of the fibers greatly increase due to the increase of the concentration. The diameter of the fibers rises from 110 nm to 1656 nm. However, the ratio 70/30 (V/V) DCM/DMF does not allow long time of production.

By changing the ratio to 50/50 (V/V) DMC/DMF, the jet is stable during long time of production. PLA solution of 10 wt% electrospun with a voltage of 27 kV leads to homogenous regular nanofibers with an average diameter of 477 nm (**Table 6**).

However, we optimize the diameter of the fibers by decreasing the concentration to 8wt % and by applying a negative voltage during the electrospinning process. Indeed, with a PLA concentration of 8.2 % in 50/50 (V/V) DCM/DMF electrospun with a negative voltage, the diameter of the PLA nanofibers reaches 254 nm. Finally, this solution was selected and used for next applications.

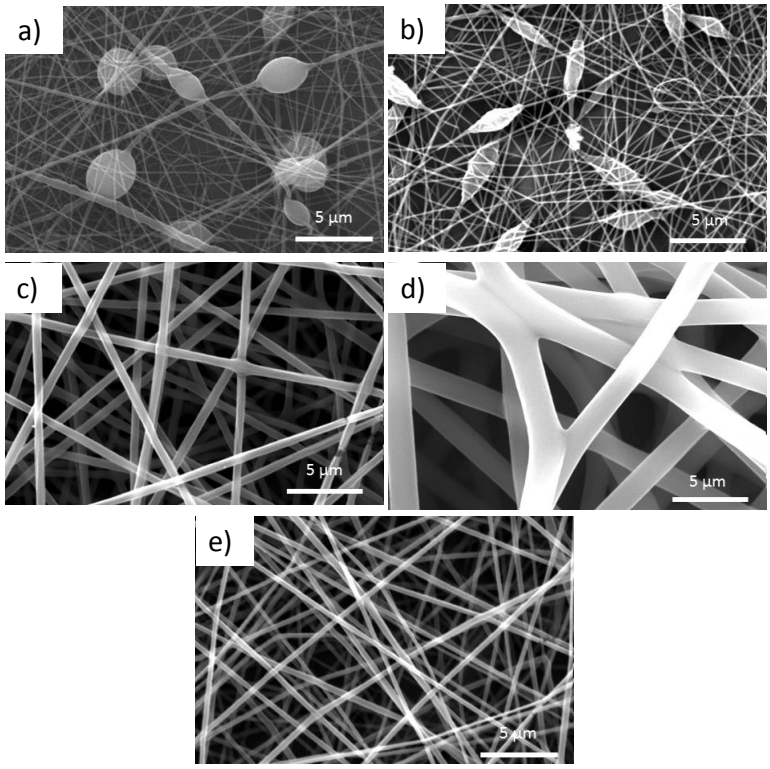


**Figure 31: SEM images of different PLA solutions: a) 7% PLA in 70/30 (V/V) DCM/DMF; b) 8% PLA in 70/30 (V/V) DCM/DMF; c) 8% PLA in 50/50 (V/V) DCM/DMF; d) 10% PLA in 70/30 (V/V) DCM/DMF; e) 8.2 % PLA in 50/50 (V/V) DCM/DMF**

| | PLA 8 wt% | PLA 10 wt% | PLA 8.2% wt% | PLA 10 wt% |
|---|---|---|---|---|
| | 70/30 (V/V) DCM/DMF | 70/30 (V/V) DCM/DMF | 50/50 (V/V) DCM/DMF | 50/50 (V/V) DCM/DMF |
| Diameter (nm) | 110 +/- 23 | 1656 +/- 142 | 254 +/- 34 | 477 +/- 54 |
| Beads | Yes | No | No | No |
| Voltage (kV) | 27/0 | 21/0 | 12/-5 | 27/0 |
| Distance (cm) | 18 | 22 | 18 | 18 |
| Flow rate ($mL.h^{-1}$) | 1 | 1 | 1,2 | 1 |
| Temperature (°C) | 26 +/- 1 | 25 +/-1 | 25 +/-1 | 26 +/-1 |
| Humidity (HR %) | 51 +/-3 | 50 +/-3 | 50 +/-3 | 51 +/-3 |

**Table 6: Electrospinning of different PLA solutions**

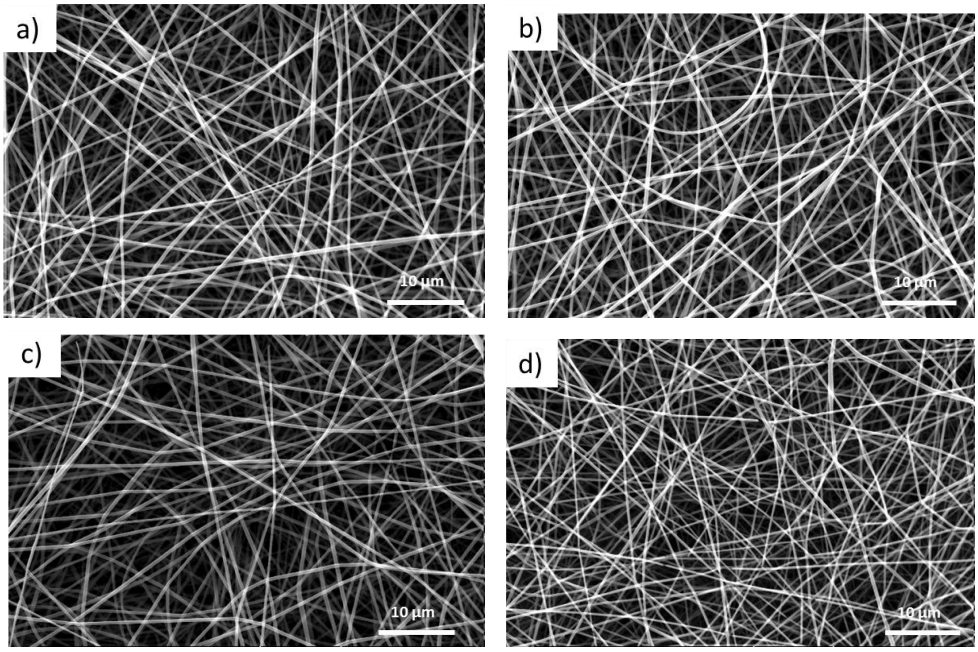


**Figure 32: SEM images of different samples of PLA nanofibers obtained with different PMMA plate: a) without PMMA plate b) with a PMMA plate with an internal hole (diameter of 25 mm) c) with a PMMA plate with an internal hole (diameter of 35 mm); d) with a PMMA plate with with an internal hole (diameter of 55 mm)**

To concentrate the deposition of the nanofibers on the collector (silicon wafer), a poly(methyl methacrylate) (PMMA) plate with an internal hole can be placed over the wafer. The morphology of the fibers could be affected by this PMMA plate. To see the effect of the PMMA plate on nanofibers morphology, we compared the diameter of samples which were electrospun directly on aluminium foil without a PMMA plate above and other samples which were electrospun on aluminium foil with a PMMA plate (with different hole diameters). As showed on **Figure 32**, by varying the PMMA plate diameter hole from 25 mm to 55 mm, the diameter of the fiber is not affected. Therefore, we decided to use the PMMA plate with a diameter of 55 mm to concentrate the deposition of the nanofibers only on the silicon wafer during the electrospinning process.

## 4. 2D Structuration

After optimal electrospinning conditions of PCL and PLA were found, different kinds of micropatterned electrospun membranes were elaborated.

First, we tried to elaborate grid micropatterned scaffolds with block collectors. Indeed, with block collectors, Lavielle *et al.* [90] showed that different kind of micropatterned grids could be obtained. Such kind of structured scaffolds with aligned fibers and good mechanical properties may be interesting for the culture of cells which can be promoted by structural anisotropy [157]. The results obtained with the block micropatterned collector are presented in the next subchapter.

We also developed a new kind of honeycomb micropatterned collector. As it was mentioned in the chapter one, the self-assembling of electrospun fibers in the form of honeycomb-like structures occur [96, 98]. In order to control the size and the morphology of honeycomb structure, we designed a new kind of honeycomb micropatterned collector. We expected that such collector may help to guide the deposition of the nanofibers in the form of regular honeycomb fibrous structure which may mimic the bone structure of osteons. The complete study of the elaboration and application of such membranes was published in *Macromolecular Bioscience* and is presented on next chapter.

### 4.1 Electrospinning on block collectors

The first micropatterned collectors that were tested were block collector with block of 10 µm in diameter. The distance L between two blocks was varied: 20 µm, 40 µm, 90 µm and 120 µm. However, with this kind of micropatterned collector, we were not able to structure the electrospun nanofibers as it is presented on the **Figure 33**. Either with gelatin nanofibers, which are thin fibers (average diameter of 200 nm) (**Figure 33-a**), either with PCL nanofibers which are thicker than gelatin fibers (**Figure 33-b)**, it was not possible to structure the membrane.

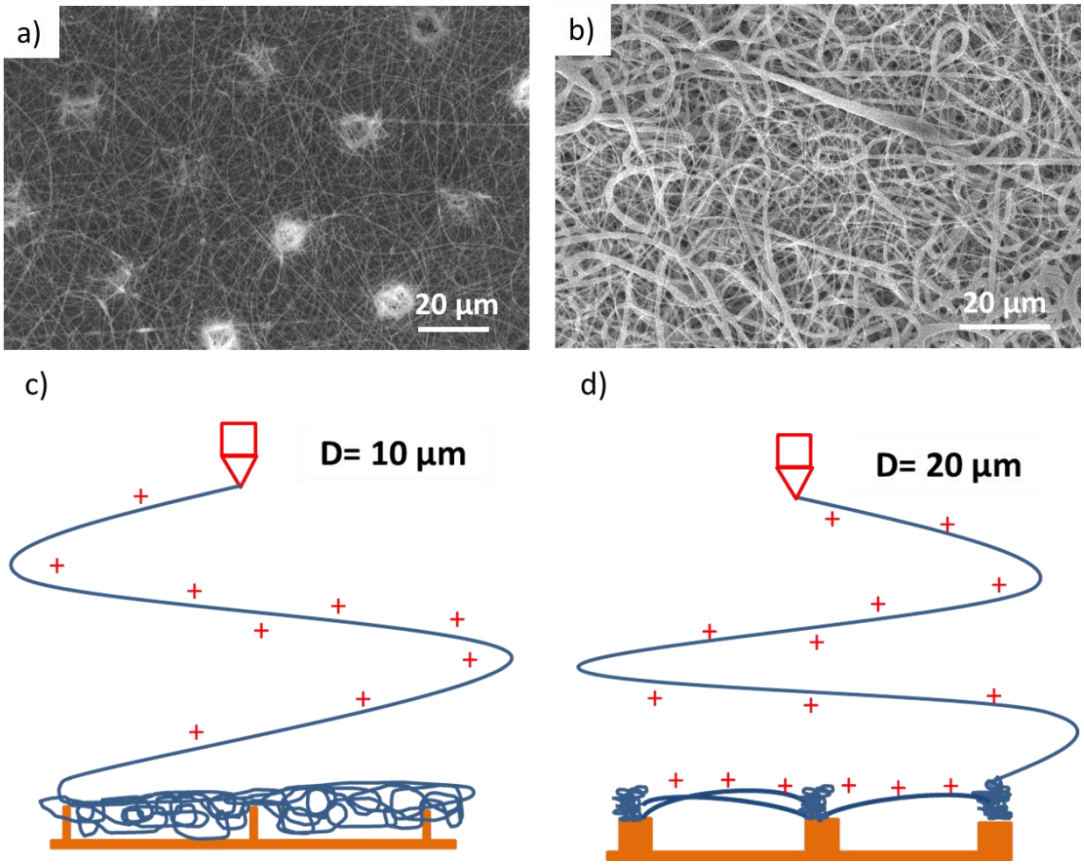


**Figure 33: a) SEM image of gelatin fibers on a block micropatterned collector with an internal diameter D = 10 µm and L= 40 µm after 5 minutes of electrospinning.**
**b) SEM image of PCL fibers on a block micropatterned collector with an internal diameter D = 10 µm and L= 40 µm after 5 minutes of electrospinning**
**c) Proposed mechanism for the deposition of nanofibers on a block micropatterned collector with D= 10 µm**
**d) Proposed mechanism for the deposition of nanofibers on a block micropatterned collector with D= 20 µm**

The microstructuration of a membrane may be obtained when the ratio L/H (where L is the distance between two patterns and H the height of the pattern) is lower or equal to 1.5 [90]. Here, even if the ratio L/H = 40/60= 0.7 is in the range where structuration is possible, structuration of electrospun fibers did not occurred. Normally, the electric field is more intense at the top of the blocks, driving the deposition of the charged jet preferentially on the blocks, leading to the formation of aligned fibers between the blocks and thus an electrospun microgrid (**Figure 33-d**). However, it seems that when the diameter of the blocks is 10 µm, the difference between the electric field at the vicinity of the patterns and the bottom of the collector is not enough. Thus, the charged jet is attracted by the entire surface, no matter the

micropatterns. Therefore, a diameter of 10 µm for a block is the limitation to get microgrids micropatterned membranes.

Thus, we increased the block diameter D to 20 µm. The space L between two blocks varied from 40 µm to 120 µm (60 µm, 100 µm). SEM images of the first moments of nanofiber deposition (**Figure 34**) proved that with these collectors, the micro-structuration of the membrane can be achieved. The fibers deposit preferentially on the top of the blocks, and aligned between two block patterns, leading to the formation of a microgrid (**Figure 33-d**).

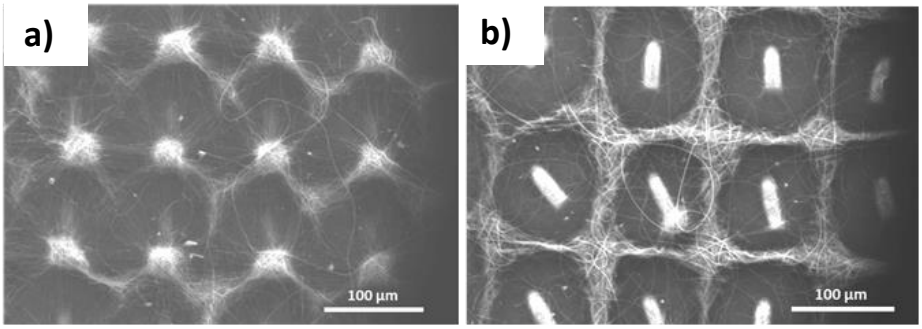


**Figure 34: SEM images of the first moment of the deposition of PCL on micropatterned blocks silicon collectors.**

Unfortunately, the SU-8-based blocks patterns with a diameter of 20 µm were too fragile when they were made on silicon wafers. For example, we noticed that the blocks fall off of the silicon substrate when the membrane was peeled from the collector immersed in ethanol.

Normally, one advantage of using micropatterned collectors is that the collector could be reusable for making many scaffolds for biological applications. Therefore, the micropatterned collector should present a good resistance during immersion to solvents and peeling operations to produce scaffolds in a large number.

To solve this problem of fragility, we elaborated block collectors in poly(dimethyl-siloxane) PDMS by the replication molding technique.

Normally, a micropatterned collector should be reusable several times without affecting the structure of the electrospun membrane. However, with PDMS blocks collectors, after the second use of the collectors, the PCL electrospun scaffolds were losing their grid architecture (**Figure 35-a**and **Figure 35-b**). After the third use of the micropatterned collector during the electrospinning process, the microstructure of the membrane had almost completely disappeared (**Figure 35-c**). The loss of the microstructuration with PDMS collector is due the bad adhesion of the conductive gold layer at the surface of the PDMS

collectors. After the third use, one part of the gold layer was gone from the surface of the collector and many cracks were visible at the surface, breaking the electric contact between the different areas parts of the collector.

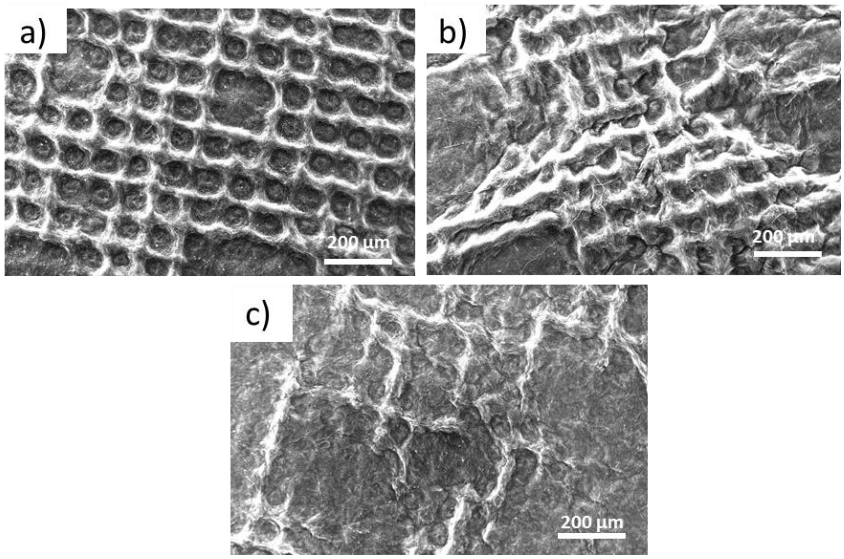


**Figure 35: a) SEM image of a PCL micropatterned electrospun membrane after the first use of the PDMS micropatterned collector during the electrospinning process**
**b) SEM image of a PCL micropatterned electrospun membrane after the second use of the PDMS micropatterned collector during the electrospinning process**
**c): SEM image of a PCL micropatterned after the third use of the PDMS micropatterned collector during the electrospinning process**

Unfortunately, we were not able to elaborate a protocol that can in a repeatable way, produce a large number of grid scaffolds. Thus, even if we proved that we were able to produce electrospun micropatterned grids, we did not study the influence of the grid structure on the osteoblasts cells behaviors.

In the next part, we present the results that were obtained using honeycomb micropatterned collectors. Contrary to block collectors, honeycomb collectors were reusable many times (15 times) after the peeling of the electrospun membrane. Honeycomb micropatterned collectors were less fragile than block collectors because the walls of the honeycomb were forming a network on the silicon wafer, giving a strength and resistance to the micropatterns.

## 4.2 Electrospinning on honeycomb micropatterned collectors

# Electrospun Honeycomb as Nests for Controlled Osteoblast Spatial Organization

***Macromolecular Bioscience*, 2014, Vol. 14, pp. 1580–1589**

**Salima Nedjari, Sandy Eap, Anne Hébraud, Corinne R. Wittmer, Nadia Benkirane-Jessel, Guy Schlatter,**

**Abstract:**

Honeycomb nanofibrous scaffolds with a characteristic pattern size ranging from 40 to 360 µm were prepared. poly(ε-caprolactone) (PCL) and poly(D, L-lactic acid) (PLA) scaffolds were obtained by electrospinning onto honeycomb micropatterned collectors and led to two different types of microstructure. We showed that a unimodal distribution of fiber diameters, observed for PLA, led to relatively flat scaffolds; on the other hand, the bimodal distribution of PCL fiber diameters significantly increased the relief of the scaffolds' patterns due to the preferential deposition of the fiber portions with the larger diameter on the walls of the collector's patterns via preferential electrostatic interaction. Finally, a preliminary biological evaluation demonstrated the effect of the morphology of the scaffolds on the spatial organization of MG63 osteoblast-like cells. It is shown that the localization of MG63 cells depended significantly on the relief of the scaffold. Mimicking hemi-osteons, cell gathering was observed inside PCL honeycomb fibrous nests with a characteristic size ranging from 80 µm to 360 µm.

### 4.2.1 *Introduction*

Scaffolds that mimic the extra-cellular matrix of living tissues are widely used in biomedical applications such as tissue engineering [158]. An ideal construct should mimic the physiological environment, mechanical properties and structure of native tissues from nano- to macroscopic length scales [159]. Indeed, living cells sense their environment and respond to the topography thereof through adhesion, growth and, finally, organization into a multiscale, hierarchical structure that gives tissue its specific functions [160]. At length scales $D$ smaller than the characteristic size of living cells $D_c$ ($D_c$ ~ few tens of µm), it has been shown that the chemistry of the surface and the fluctuations of the scaffold's topography play an important role in cell adhesion [161-163]. At intermediate length scales $D \sim D_C$, this topography exerts stresses on cells and on their spatial organization [164-167]. At these length scales, it has been shown that not only the lateral size $D$ of scaffold patterns but also their height [168] and their curvature [169] affect cell behavior. Finally, at larger length scales $D >> D_C$, a scaffold's topography and the porosity must be sufficiently open to allow for the formation of large cell assemblies with vessels and conduits for nutrients.

Bone regeneration is a good example of a process for which the hierarchical multiscale geometry of scaffolds is of prime importance. At the subcellular length scale, cell support is mainly ensured by submicron-diameter collagen fibers of the extracellular matrix (ECM). Electrospun nanofibrous scaffolds that mimic the dimensions of those fibers have been used as efficient promoters of cell adhesion and proliferation [170]. At length scales $D \sim D_C$, local geometry has proven to play a major role in new tissue formation. During bone remodeling, osteoclasts dig out small cylindrical pores called osteons or semicircular cavities and grooves called hemi-osteons [171] with typical sizes on the order of a few hundreds of microns [172]. Osteoblasts are then recruited in those cavities and start to form new bone tissues. Mimicking those geometries by using concave areas for example, in artificial hydroxyapatite scaffolds *in vitro* and *in vivo* has shown that topography at this length scale can stimulate osteoblasts to enhance bone formation [173]. Indeed, the kinetics of new tissue production by osteoblasts depends on the local surface curvature; this phenomenon is called curvature-controlled tissue growth [174]. Bidan and co-workers [175] designed hydroxyapatite scaffolds with circular and semi-circular pores to mimic osteons and hemi-osteons. The authors showed that, in circular pores, bone formation led to uniform, concentric tissue growth that progressively closed the cylindrical pores, thus increasing the curvature of the surface, whereas in semi-circular channels, the production of new tissue slowed down as the cavity and curvature of the

surface decreased. Moreover, no tissue was formed on convex surfaces. The authors elaborated a "chord model" to explain the curvature-controlled tissue growth and used it to design pore geometries that improve the speed of bone tissue growth in porous scaffolds [176]. Based on these results, honeycomb scaffolds, which exhibit concave pores that mimic hemi-osteons, should be ideal for the rapid formation of new bone tissues. Indeed, George *et al*. have already demonstrated that honeycomb collagen sponges are excellent scaffolds for the differentiation and proliferation of mesenchymal stem cells into osteoblasts [177].

In this paper, we discuss the preparation of honeycomb electrospun scaffolds that mimic the fibrous structure of the natural ECM matrix with hemi-osteon-like cavities and the use of these scaffolds as supports for the adhesion and proliferation of MG-63 osteoblast-like cells. Among the techniques that allow for the elaboration of scaffolds, electrospinning is currently one of the most widely used tools of prime importance for biomedical applications [178-180]. Indeed, electrospinning enables the production of nanofibrous scaffolds from a wide range of materials with large surface-to-volume ratios, tunable porosities and functionalized surfaces. Although electrospinning usually leads to the production of random non-woven mats, several studies have focused on the production of structured fibers assemblies [25, 61, 79, 181, 182]. For example, it is possible to control the spatial organization of the nanofibers formed by electrospinning by using microstructurally patterned collectors [87, 90, 183-186]. The relief of the patterns allows for the modulation of the electric field in the vicinity of the collectors. The deposition of electrospun electrically charged nanofibers is thus guided by electrostatic forces. Therefore, this phenomenon results in an organized nanofibrous structure. In this study, we fabricated honeycomb micropatterned collectors with characteristic sizes ranging from a few tens to a few hundreds of microns by photolithography, thus corresponding to scales ranging from the size of unique cells to the size of small cellular assemblies. poly(ε-caprolactone) (PCL) and poly(D, L-lactic acid) (PLA) were electrospun on these collectors to form honeycomb-like scaffolds with distinct morphologies. Then, for each of these polyesters, the effect of the honeycomb pattern size on the spatial organization of MG-63 osteoblast-like cells was investigated.

### 4.2.2 *Experiments*

#### *4.2.2.1* Fabrication of honeycomb collectors

Honeycomb micropatterns were formed by photolithography on silicon wafers (mask aligner MJB4, SUSS Microtec). The photoresist used was SU-8 2050 (Microchem). A Plassys MEB5505 electron beam evaporator was used to deposit a conductive layer (compose of a 120-nm Al layer and a 30-nm Au layer) on the collectors. The collectors were divided into four zones, for which the internal diameters $D_p$ of the honeycombs were 40, 80, 160 and 360 µm (see Figure 1 for the definition of $D_p$). The width and the height of the honeycomb walls were 20 µm and 60 µm, respectively.

#### *4.2.2.2* Electrospinning

PCL polymer solutions were prepared by dissolving poly(ε-caprolactone) (PCL) (Mw=80 kg.mol$^{-1}$, PDI=1.1, Perstrop, commercial name: CAPA 6806) in dichloromethane (DCM, Sigma-Aldrich)/ N,N-dimethyl-formamide (DMF, ReagentPlus® ≥ 99%, Sigma-Aldrich) (60/40 V/V) at a concentration of 15 wt.%. Then, 5% formic acid (Riedel-de Haën) was added to increase the solution's conductivity. A 8.2 wt.% poly (D, L-lactic acid) (PLA) solution (Mw=180 kg.mol$^{-1}$, Natureworks, commercial name: 7000 D, 7% D) was prepared in a DCM/DMF mixture (50/50 V/V).A homemade vertical electrospinning setup was used. The device was composed of an 18G needle connected to a positive high-voltage power supply (Spellmann SL 10) and a collector connected to a negative high-voltage power supply (Spellmann SL 10). The polymer solution was pushed through the needle via a silicon feedline connected to a 10-mL syringe mounted on a syringe pump.

Electrospinning experiments were performed 24 hours after the polymer solutions were prepared. For the electrospinning of the PCL fibers, the needle-to-collector distance was 13 cm, the high voltage applied at the needle was 25 kV, the collector was electrically grounded and the solution flow rate was 1.1 mL.h$^{-1}$. Additionally, a 3-mm-thick poly(methyl methacrylate) PMMA plate with a circular opening measuring 45 mm in diameter was placed on the collector before electrospinning to concentrate the fiber deposition. The electrospinning time was 10 minutes. The scaffold was retrieved from the collector by immersing the two in ethanol. The scaffold was then carefully peeled off the collector, dried and placed under vacuum overnight to remove any residual solvent. For the electrospinning of the PLA fibers, the needle-to-collector distance was 18 cm, the positive high voltage applied

at the needle was 12 kV, the negative high voltage applied at the collector was -5 kV and the flow rate was 1.2 $mL.h^{-1}$. A 3-mm-thick PMMA plate with a circular opening measuring 55 mm in diameter was used to concentrate the jet on the collector. The fiber collection time was 15 minutes. The collector was then immersed in isopropanol, and the scaffold was carefully peeled off the collector, dried and placed under vacuum overnight to remove any residual solvent. The PCL scaffolds were sterilized by immersion in ethanol for 20 minutes and exposure to UV light for at least 30 minutes. The PLA scaffolds were sterilized by immersion in isopropanol and exposure to UV light for one hour. Then, isopropanol was replaced by water, and the PLA scaffolds were again exposed to UV light for 3 hours. Isopropanol was used instead of ethanol for the PLA scaffolds because of the higher extent of shrinkage of PLA in ethanol.

#### *4.2.2.3* Scanning electron microscopy

The morphology of the honeycomb nanofibers scaffolds was observed by scanning electron microscopy (SEM) (VEGA 3 LMV, TESCAN, Czech Republic) at a voltage of 5 kV. Before observation, the samples were sputter-coated with gold using a Q 150RS sputter coater (Quorum Technologie, United Kingdom). For each scaffold, the diameters of approximately 300 randomly chosen fibers were measured from five SEM images using the image analysis software ImageJ (National Institutes of Health, USA).

The height *H* of the fibrous honeycomb walls was measured by using the defocus function of the scanning electron microscope, which exhibits a reported precision of 1 µm. To this end, the electron beam was first focused with the condenser lenses of the SEM on the top of a honeycomb relief where the vertical *Z* value was reset to 0. Then, the picture was centered on the bottom of the relief pattern and the electron beam was refocused. Thus, the *Z* value provided an estimate of the honeycomb height *H*. The average height was calculated based on 10 values in each case.

#### *4.2.2.4* Cell culture and seeding

MG-63 osteoblast-like cells were cultured in Dulbecco's modified eagle medium (D-MEM®, PAA, Austria) supplemented with 10% fetal bovine serum (FBS), 50 U/mL penicillin, 50µg/mL streptomycin, 5µg/mL Fungizone and 1% sodium pyruvate in 75 $cm^2$ flasks. The MG-63 cells were incubated at 37 °C in a humidified atmosphere of 5% $CO_2$ and fed every 3 days. The cells were detached by trypsin-ethylenediaminetetraacetic (trypsin-

EDTA) . Then the cells were seeded onto honeycomb PCL and PLA scaffolds, placed in a 48-well plate at a density of 10000/cm$^2$ and cultured with supplemented D-MEM®.

#### *4.2.2.5* Osteoblasts proliferation study

The osteoblasts proliferation and activity were monitored after 3, 7 and 14 days by an alamarBlue® (Serotec) assay. The honeycomb scaffolds were incubated with 10 % alamarBlue® reagent in culture medium for 4h. Then, aliquots were pipetted into 96-well plates and their absorbance was measured with a spectrophotometric plate reader at 570 nm and 630 nm. These experiments were performed in triplicates for each pattern size and each polymer. Comparisons were made between patterned and random scaffolds at each time interval using paired t-tests ($p<0.05$).

#### *4.2.2.6* Osteoblasts morphology study

##### 4.2.2.6.1 *Scanning electron microscopy*

After 3 days of culture, cells were fixed using 2.5% glutaraldehyde diluted in phosphate buffered saline (PBS) and then 1% osmium tetroxide diluted in PBS. The samples were then washed several times with PBS and dehydrated gradually with increasing concentrations of ethanol (25%, 50%, 75%, 90%, and 100%). Finally, the cells were chemically dehydrated with hexamethyldisilazane (HMDS) and observed by SEM as previously described.

##### 4.2.2.6.2 *Fluorescence microscocopy*

Cell nuclei were stained with a DAPI (4',6-diamidino-2-phenylindole, Sigma) solution (200 ng/ml) for 5 minutes and washed three times with PBS. The honeycomb scaffolds seeded with MG-63 cells were then incubated for 20 min with Alexa Fluor 546-conjugated phalloidin (Molecular Probes) for F-actin labeling before being washed again three times with PBS. The samples were observed by using an optical microscope (LEICA DM 4000B, Germany) under fluorescent light. Fluorescence images of PCL scaffolds were captured to estimate the cell density relative to the nest area. The number of cell nuclei was counted for at least 20 nests for each honeycomb characteristic diameter *D*.

### 4.2.3 *Results and Discussion*

#### *4.2.3.1* Electrospinning of PCL and PLA honeycomb fibrous structures

In a previous study, we demonstrated that the distribution of fiber diameters affects the internal structure of scaffolds [99]. Therefore, we first optimized the processing conditions for two biopolyester systems to control the fiber morphology and the production stability. The electrospinning of solutions of PLA and PCL in DCM/DMF mixtures was thus investigated in the current study. DCM serves as a good solvent for these polyesters, and DMF causes a decrease in vapor pressure allowing for stable electrospinning over long periods without any clogging of the needle.

In this solvent mixture, PLA fibers showing a unimodal diameter distribution with an average value of 410 nm were obtained, as shown in **Figure 35-a**. In contrast, in the case of PCL, a bimodal diameter distribution was observed (**Figure 35-a**), with thin and thick fiber portions exhibiting average diameters 270 nm and 920 nm, respectively. This bimodal distribution may be due to concentration heterogeneities in the PCL solution resulting from the presence of DMF, a poor solvent of PCL. However, this solvent is necessary to prevent any clogging at the needle exit due to rapid evaporation of DCM. A small amount (5% of the total solvent weight) of formic acid was added to the PCL formulation to increase the solvent's conductivity and the surface charge density of the electrospun jet, thus reducing the diameter and number of thick fibers portions.

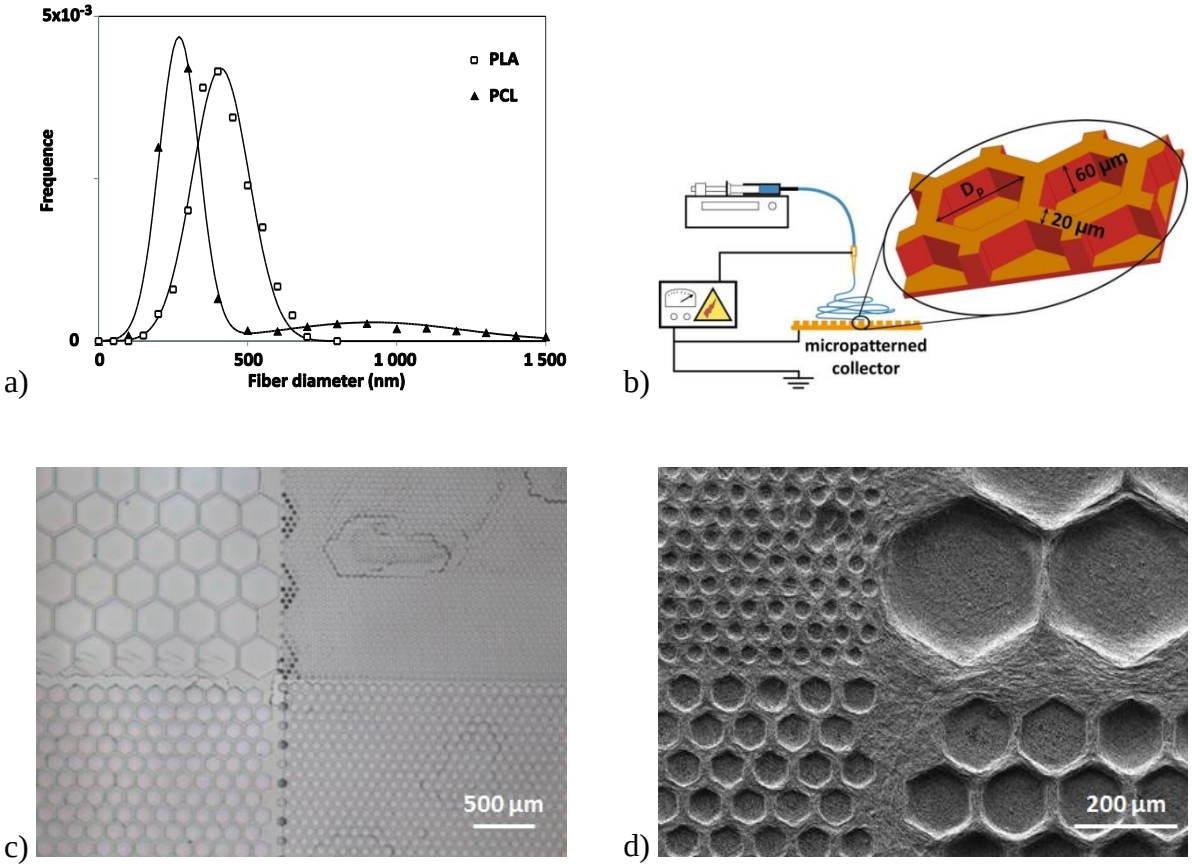


**Figure 36: a) Normalized distributions of PLA and PCL fiber diameters obtained from fibers deposited on a flat aluminum foil. b) Principle of electrospinning on micropatterned honeycomb collectors with $D_p$ = 40, 80, 160 and 360 µm. c) Optical microscopy image showing the central part of a honeycomb collector. d) SEM image of the same area of a PCL electrospun scaffold after being peeled from the collector. The image shows the side that was in contact with the patterned collector (see also Figure S1 in Supp. Info.).**

To construct honeycomb nanofibrous scaffolds, electrospinning was carried out on micropatterned collectors fabricated using photolithographic techniques. The collectors, coated with an Al-Au layer, were divided into four square areas measuring 20x20 mm covered with honeycomb patterns with an internal diameter $D_P$ of 40, 80, 160 or 360 µm (see **Figure 36b-c**). The honeycomb patterns were separated by walls measuring 20 µm in width and 60 µm in height as shown in **Figure 36-b**. The collector served as an electrostatic template, and the replication of the honeycomb structure could be observed on the electrospun membrane (**Figure 36-d**). In the vicinity of the collector, the electrostatic forces were driven by the micro topography of the collector.

Therefore, charged electrospun fibers were preferentially deposited on the honeycomb walls [90], leading to the efficient replication of the microstructure of the collector even for the smallest pattern diameter of $D_p$ = 40 µm (see also **Figure S2** of Supp. Info.).

**Figure 37-a** shows PLA fibers organized on a honeycomb pattern with $D_P$ = 160 µm for the collector after a short period of electrospinning. It can be observed that most of the fibers were aligned along the walls of the honeycomb pattern, whereas few fibers were stretched and suspended above the honeycomb cavity at a depth of 60 µm (see **Figure 37-b**). The density of the fibers inside the patterns is thus lower then on the wall.

Similar observations have been done by Lavielle *et al.* [90] for patterns in the same size range and by Ortega *et al.* [167] for millimeter-sized patterns. This effect can be explained by the fact that during electrospinning, the suspended fibers could not release their electric charges.

Thus, preferential deposition on the walls of the collector's patterns was due both to attraction above these walls where the electric field was more intense and to repulsion by the suspended fibrous and charged net. **Figures 37b-d** show that the peeling of the scaffold from the collector, carried out in isopropanol, caused the entire scaffold to shrink due to fiber retraction. Shrinkage rates ranging from 12 to 25% were measured for all PLA scaffolds. However, the overall morphology of the scaffold was preserved.

One can also observe a rather good alignment of the fibers along the walls of the honeycomb patterns (**Figure 37-d**) and a random orientation inside the patterns (**Figure 37-c**). Similar results have also been obtained for other pattern diameters $D_p$ (**Figure 40** and **Figure S2** of Supp. Info.).

**Figures 37e-g** clearly show that the morphology of the PCL scaffolds differed from that obtained with PLA. Indeed, for the PCL scaffolds, honeycomb fibrous structures with well-defined relief were formed. These structures replicated the collector patterns. With PCL, just as in the case with PLA, the peeling step, carried out in ethanol, led to a low shrinkage rate of 5-10%.

A statistical study of the fiber diameter revealed that in the case of PCL, only the thin fiber fractions with diameters of ~ 270 nm were located inside the honeycomb patterns, whereas a bimodal distribution of thin (~ 270 nm) and thick (~ 920 nm) fiber portions was observed on the walls of the honeycomb patterns (**Figure 37-h**). A similar effect was observed by Rogers *et al.* [186] when electrospinning PLGA onto patterned resins collectors.

A difference in diameters of the fibers was obtained between peak and valley regions of their membranes. Because the linear charge density $\lambda$ of an electrospun jet is proportional

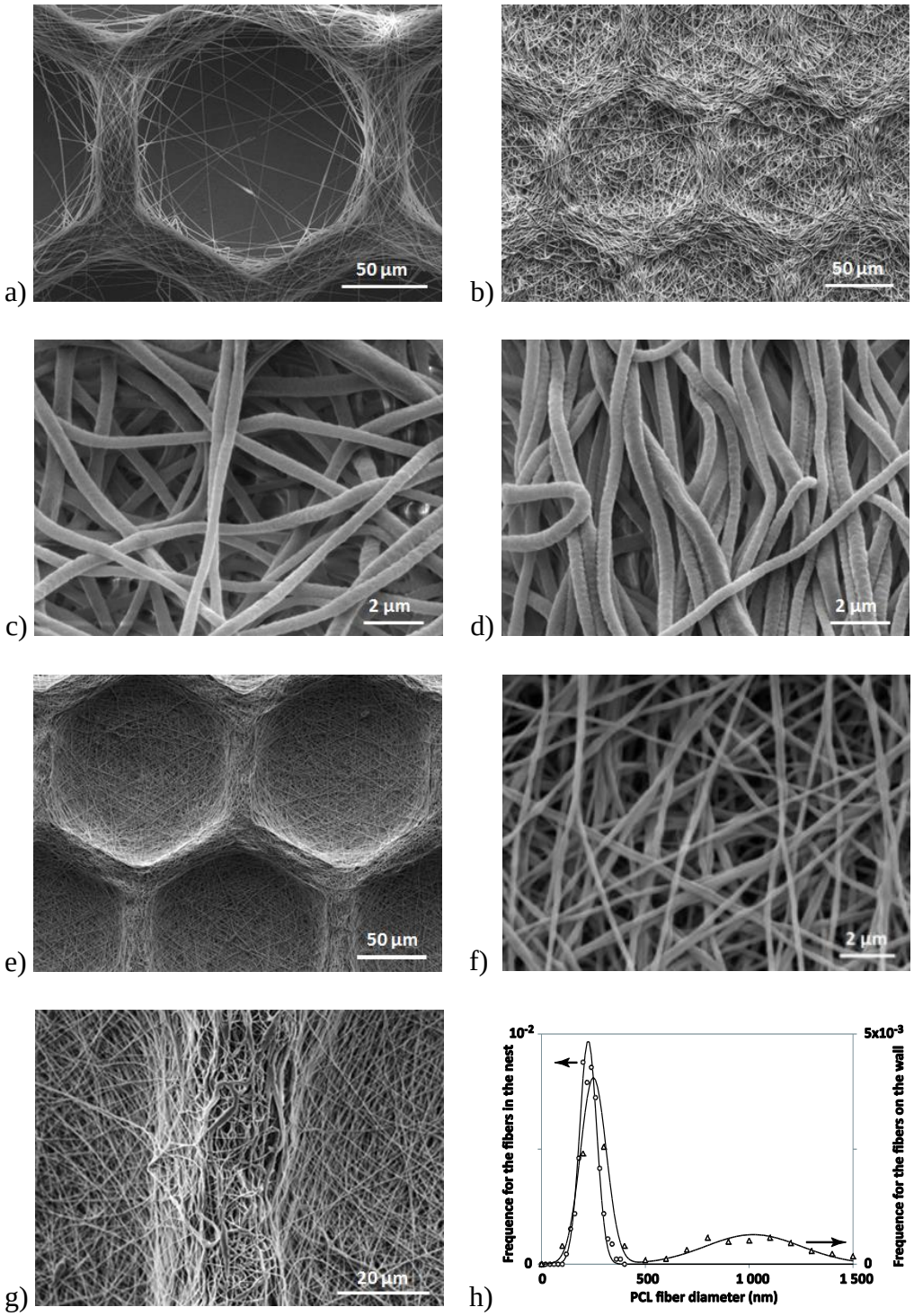


**Figure 37: a) SEM image of PLA fibers deposited on a honeycomb pattern with $D_p$ = 160 µm for the collector after a short deposition period. b) SEM image of PLA honeycomb patterns obtained with $D_p$ = 160 µm after being peeled from the collector in isopropanol. c) SEM image of PLA nanofibers located inside the nest of a honeycomb. d) SEM image of PLA nanofibers located on the wall of a honeycomb. e) SEM image of PCL honeycomb patterns obtained with $D_p$ = 160 µm. f) SEM image of PCL nanofibers located inside the nest of a honeycomb. g) SEM image of PCL nanofibers located on the wall of a honeycomb. h) Normalized distribution of PCL fiber diameters located on the wall and in the nest of honeycombs. Images b to g shows the side that was in contact with the patterned collector after the peeling of the scaffold.**

to the square of its diameter [187],the thick PCL fiber portions exhibited a $\lambda$ roughly ten times greater than that of the thin portions. Thus, the thick fiber portions were more sensitive to fluctuations in the electric field encountered in the vicinity of the collector, resulting in the fibers' deposition on the honeycomb walls of the collector only.

This highly selective deposition induced the well-defined relief of the PCL scaffolds, which was consequently much more pronounced than that of the PLA scaffolds (**Figures 38 a-c**). A maximum height *H* of 10 µm was measured for the PLA scaffolds with a $D_p$ of 360 µm, whereas a height of 40 µm was measured for the PCL scaffolds of the same $D_p$. Furthermore, an increase in the pattern height *H* with the pattern diameter $D_p$ was observed (**Figure 38-c**). This effect can be easily explained by the increase in the electric field with $D_p$ [99], resulting in an enhancement in the deposition of the electrospun fibers on the honeycomb walls. In conclusion, electrospinning on honeycomb collectors allows for an efficient replication of the patterns, with distinct scaffold structures formed depending on the fiber morphology.

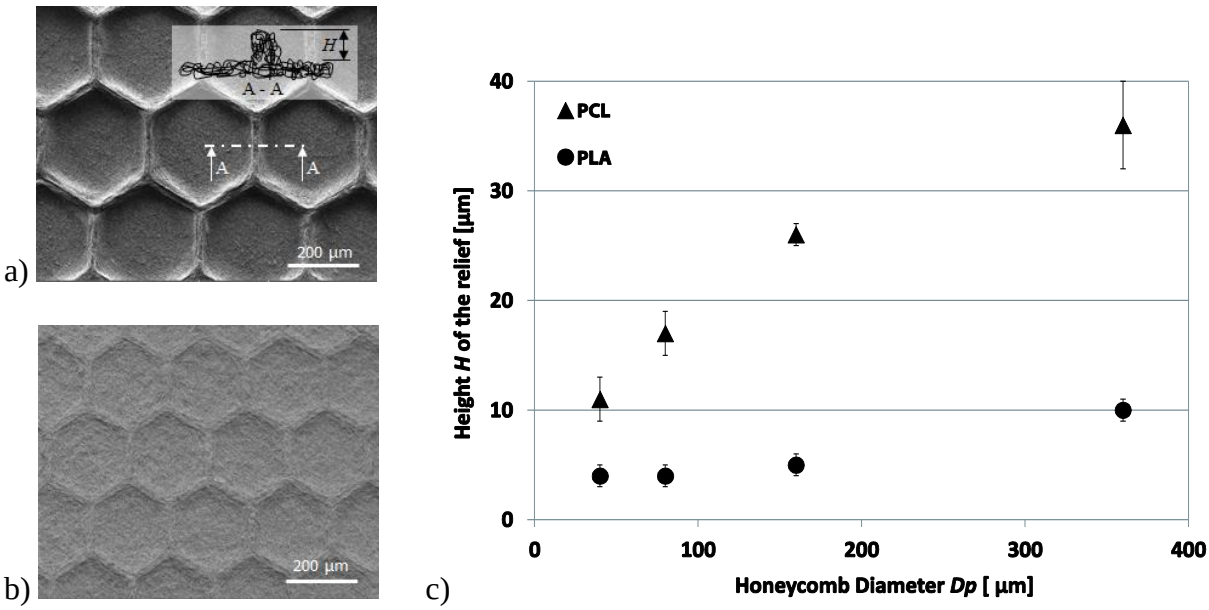


**Figure 38: a) SEM image of a PCL honeycomb scaffold obtained with $D_p$ = 360 µm. b) SEM image of a PLA honeycomb scaffold obtained with $D_p$ = 360 µm. c) Height H of the wall relief as a function of $D_p$.**

#### *4.2.3.2* Effect of scaffold morphology on spatial organization of MG-63 osteoblast-like cells

The adhesion and proliferation of MG-63 cells on the PLA and PCL honeycomb patterned scaffolds was studied for up to 14 days and compared to those properties of cells on random electrospun scaffolds. At day 3, the percentage of alamarBlue reduction was approximately 10% for the PCL and PLA scaffolds, demonstrating the good adhesion of cells on both types of scaffolds. Then, on the PCL scaffolds, MG-63 cells grew rapidly between day 3 and day 7, reaching confluence around day 14 (**Figure 39-a**). No significant difference ($p < 0.05$) was observed between the patterned and random fibrous scaffolds. The same behavior was observed for the PLA scaffolds (see **Figure 39-b**), however, with a slightly lower proliferation rate. This difference in proliferation rate could be explained by the different properties of the two polyesters, such as their elastic modulus and their hydrophobicity.

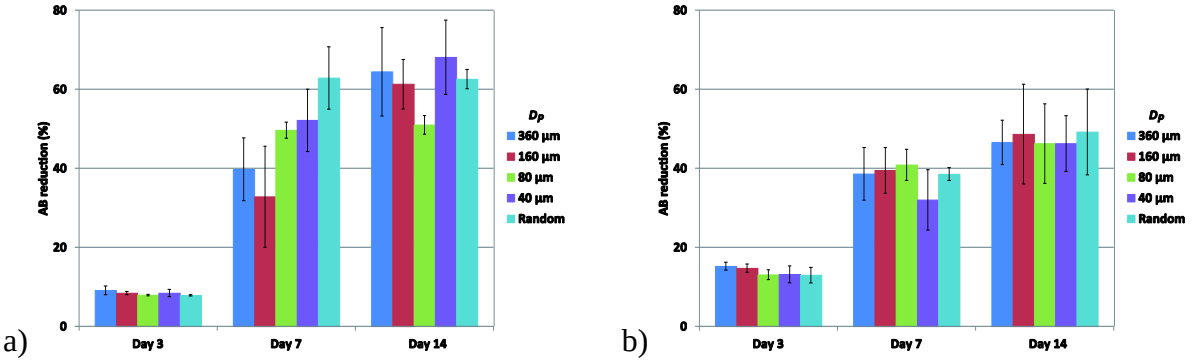


**Figure 39: a) MG-63 cell adhesion and proliferation on honeycomb PCL scaffolds with various diameters $D_P$ and on random scaffolds. b) MG-63 cell adhesion and proliferation on honeycomb PLA scaffolds with various diameters $D_P$ and on random scaffolds (n=3).**

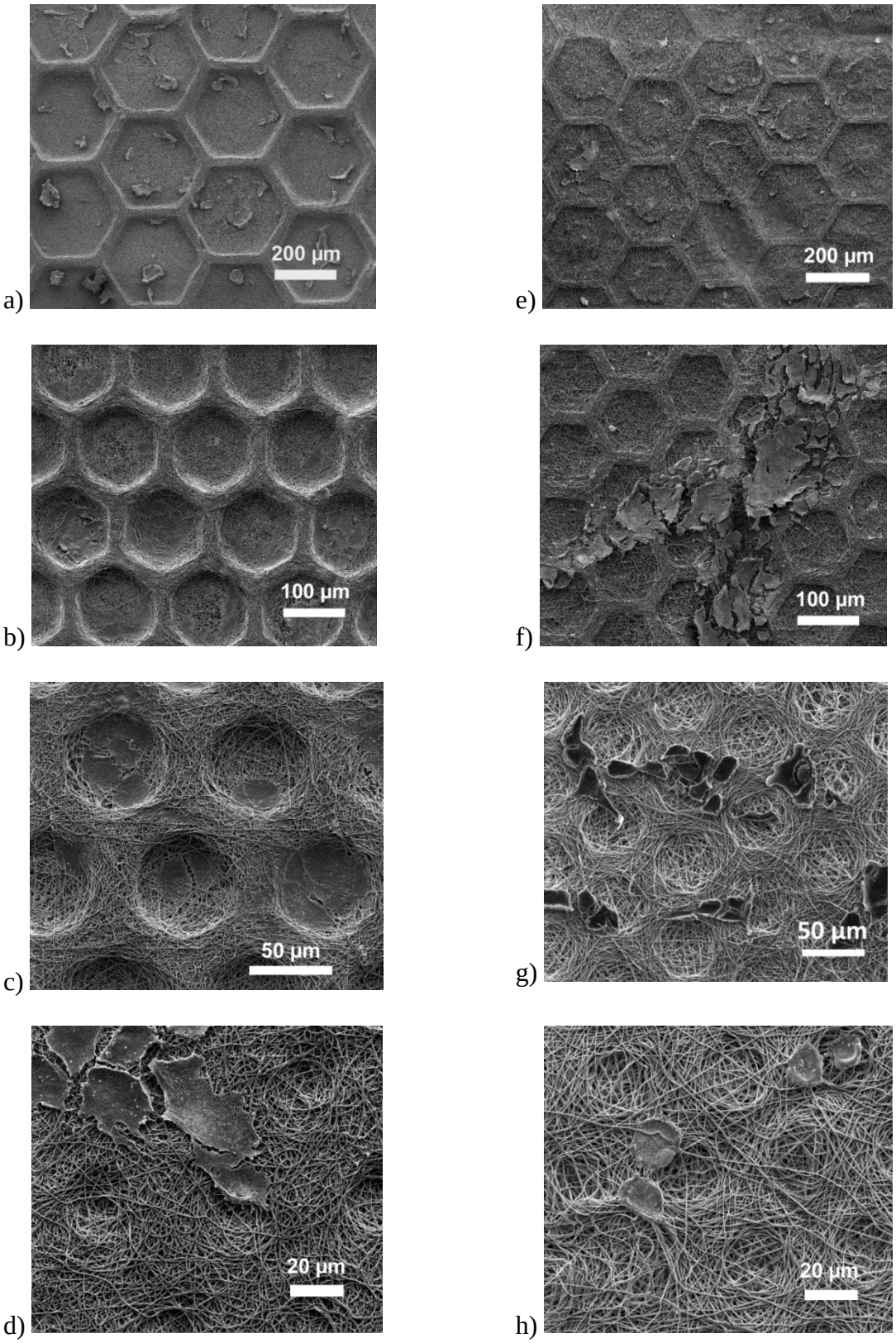


**Figure 40: SEM images of osteoblast cell line MG-63 after 3 days of proliferation. a-d) PCL scaffolds; e-h) PLA scaffolds. a) and e) $D_P$ = 360 µm; b) and f) $D_P$ = 160 µm; c) and g) $D_P$ = 80 µm; d) and h) $D_P$ = 40 µm; more detailed pictures are shown in Figure S3 and S4 in Supp. Info.**

To gain insight into the spatial organization of the cells on the honeycomb scaffolds, samples incubated for 3 days were prepared for SEM observation. It should be noted that the cells' organization on the scaffolds was studied based on the obtained morphologies of the scaffolds only.

A comparison between PCL and PLA could not be carried out because of their different physical properties (e.g., elastic modulus, hydrophobicity).In the case of the PCL scaffolds (**Figures 40a-d**), cells preferentially adhered inside the patterns (concave surfaces) rather than on the walls (convex surfaces). This phenomenon was particularly clear for pattern diameters of 160 and 80 µm, at which cells gathered inside the patterns, as in nests, and began forming microtissues. In contrast, in the case of the PLA scaffolds (**Figures 40e-h**), the cells adhered to the walls as well as to the inside of the patterns, crossing the patterns without being affected by the topography (for magnified views, see **Figure S3** and **S4** of Supp. Info.).

These results are confirmed by fluorescence microscopy images of cells cultured on the scaffolds for 14 days (**Figure 41**). For these experiments, the nuclei of the cells were stained blue with DAPI and their cytoskeletons stained red with phalloidin. One can also observe that the scaffolds, especially the PCL scaffolds, also absorbed some phalloidin and appeared red in the pictures (higher-magnification images showing the cytoskeletons of cells are shown in **Figure S5** of the Supp. Info).

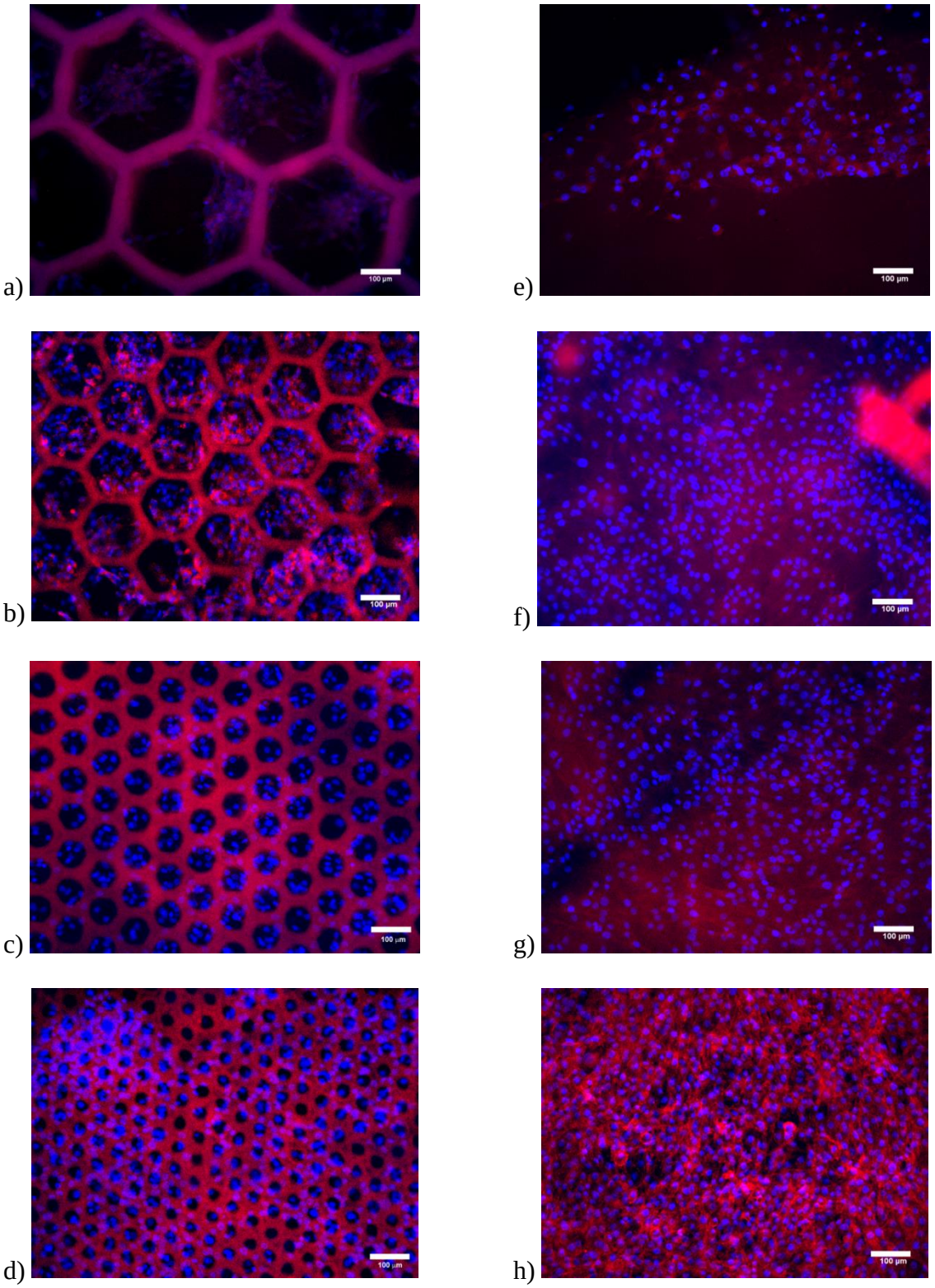


**Figure 41: Fluorescence microscopy images of MG-63 cells on honeycomb nanofibrous scaffolds after 14 days for a) PCL and $D_P$ = 360 µm; b) PCL and $D_P$ = 160 µm; c) PCL and $D_P$ = 80 µm; d) PCL and $D_P$ = 40 µm; e) PLA and $D_P$ = 360 µm; f) PLA and $D_P$ = 160 µm; g) PLA and $D_P$ = 80 µm; h) PLA and $D_P$ = 40 µm. All scale bars = 100 µm.**

After 14 days of incubation, the preferential location of the cells inside the PCL honeycomb nests could be clearly observed for patterns with $D_p$ values ranging from 80 to 360 µm.

As indicated in these images, 98, 90 and 79% of the cell nuclei were located within nests obtained with $D_p$ = 360, 160 and 80 µm, respectively. **Figure 42** plots the ratio of the density of cell nuclei (number of cell nuclei relative to the surface area of the nest) inside the nest $d_{HC}$ to the density of cell nuclei on the walls $d_W$ (number of cell nuclei relative to the surface area of the wall) as a function of the pattern diameter $D$ (i.e., the honeycomb nest diameter measured for the scaffolds, which thus takes into account the shrinkage that occurred during the peeling step). Thus, this plot accounts for the effective surface areas of the walls and nests, which depend significantly on $D$. A random distribution of the cells without any effect due to structure would result in a $d_{HC}/d_W$ ratio of 1. This ratio was observed to be close to 1 for the smallest pattern, which had a diameter close to the cell diameter and a wall height of only approximately 10 µm. The ratio increased with the size and height of the patterns to finally reach a value of ~6, corresponding to a cell density 6 times greater inside the honeycomb nests than on the walls for the largest patterns.

For all PLA scaffolds, in contrast, the cells appeared to have been distributed randomly over the surface of the scaffolds with no preferential location, regardless of pattern size. These scaffolds were nearly flat with a roughness of only a few microns and a uniform fiber diameter over the entire surface. The only parameter that differed between PLA scaffolds and the random scaffolds was the extent of fiber alignment along the walls of the patterns. Therefore, this parameter did not have a strong effect on the MG-63 cells.[167, 186] The above-described results suggest that the structure of the scaffolds at length scales of $D \sim D_C$ to $D > D_C$ (corresponding to small cellular assemblies) affected cell localization as long as the height of the patterns was sufficiently high. Thus, osteoblast-like cells tended to assemble preferentially on concave surfaces as they would in hemi-osteons during bone remodeling.

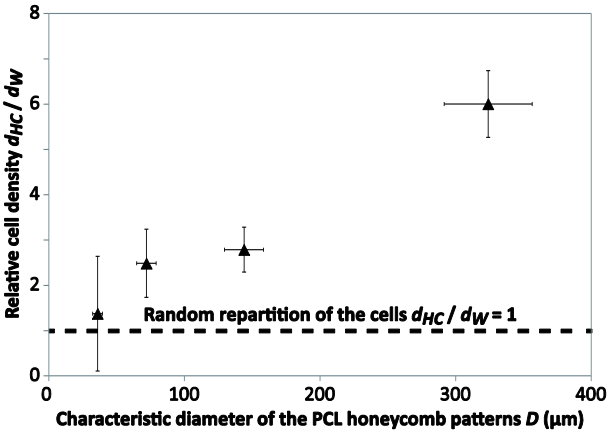


**Figure 42: Ratio of the density of cell nuclei (number of cell nuclei per surface area unit) inside the nest ($d_{HC}$) to the density of cells nuclei on the walls ($d_W$) plotted as a function of the pattern diameter D measured for PCL scaffolds (D is slightly smaller than $D_P$ because it incorporates the shrinkage that occurred during the peeling step). The dashed line at $d_{HC}/d_W = 1$ represents the ratio at which the cells are randomly distributed over the wall and the honeycomb nests are not affected by the scaffold geometry.**

### 4.2.4 *Conclusions*

We developed new types of electrospun honeycomb scaffolds by using honeycomb micropatterned collectors formed by photolithographic processes. By comparing two biopolymers, PCL and PLA, we demonstrated effective control over the morphology of the engineered scaffolds with characteristic pattern sizes ranging from the size of individual cells to the size of small cellular assemblies.

The topography of the honeycomb scaffolds was characterized by the height of the walls *H*, which depends on the diameter of the honeycomb patterns and the morphology of the fibers. A unimodal distribution of fiber diameters, observed for PLA, led to relatively flat scaffolds, whereas the bimodal distribution of PCL fibers significantly increased the *H* value of the scaffolds' patterns due to the preferential deposition of larger fiber portions on the walls of the collector patterns. Furthermore, an increase in *H* with the characteristic size of the honeycomb patterns was observed. This microstructuration was explained by electrostatic effects induced during the electrospinning step.

Finally, a preliminary study of the proliferation and spatial organization of MG-63 cells on these scaffolds was performed. It appears that the structure obtained for the PLA scaffolds does not affect the organization of MG63 cells. However, the formation of

osteoblast-like cell assemblies inside the honeycomb nests of PCL scaffolds was observed, suggesting that the patterns successfully mimicked hemi-osteon structures.

### 4.2.5 *Supporting informations*

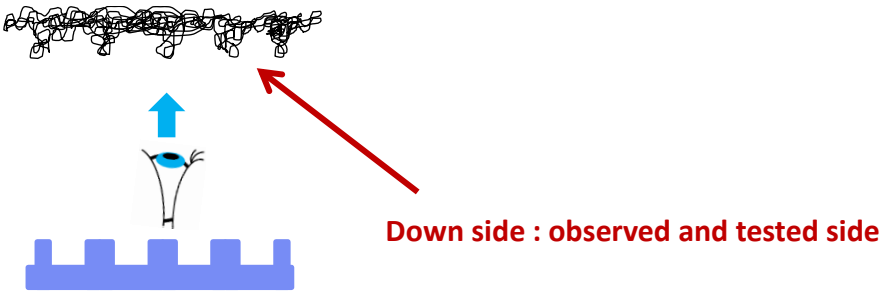


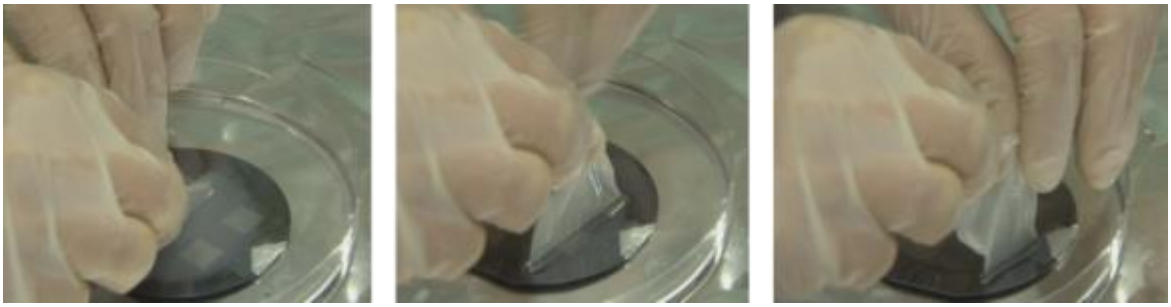

**Figure S1: Peeling operation to remove the membrane from the micropatterned collector**

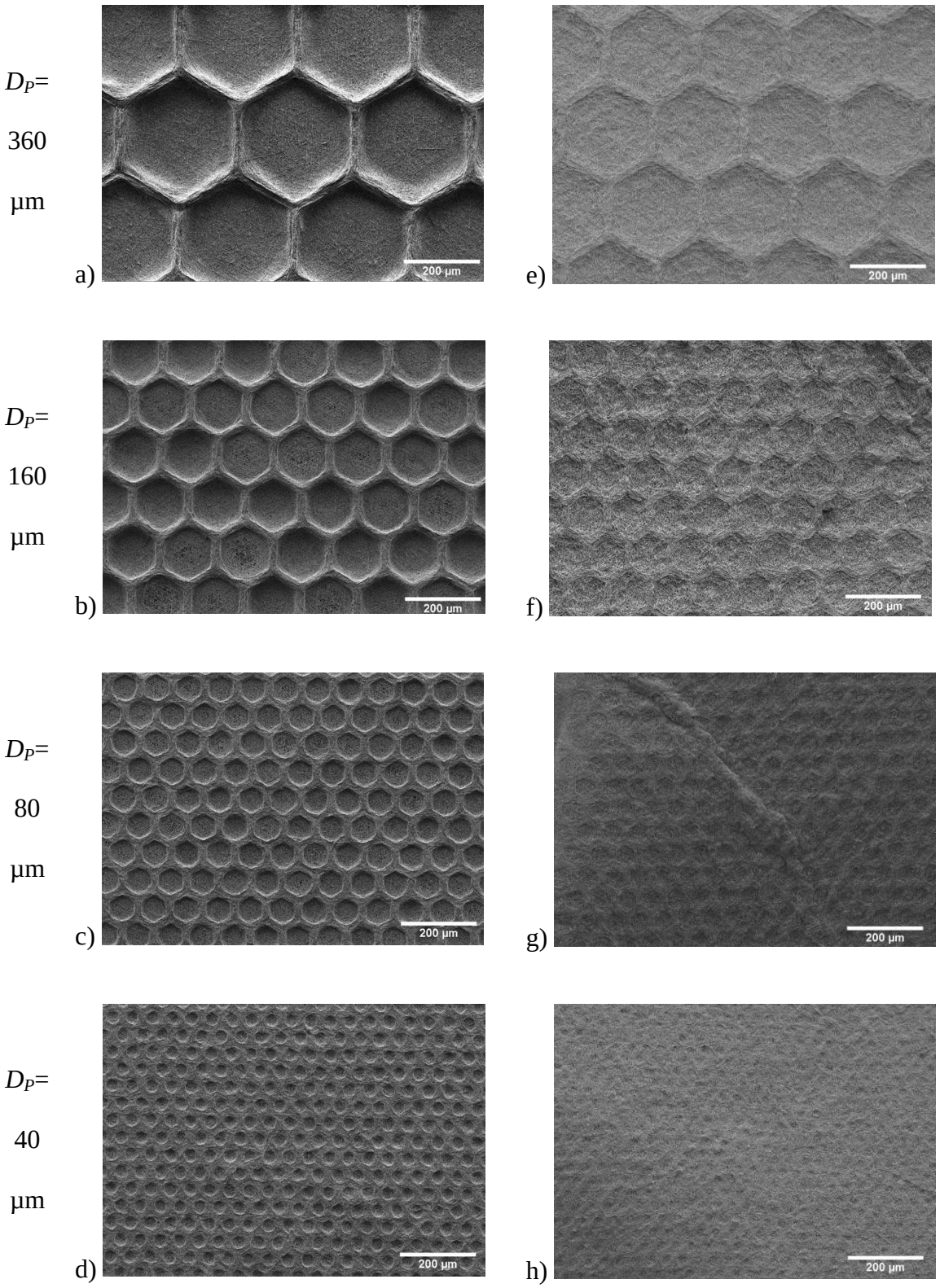


**Figure S2: SEM images of PCL and PLA honeycomb scaffolds. a-d) PCL scaffolds; e-h) PLA scaffolds. a) and e) $D_P$ = 360 µm; b) and f) $D_P$ = 160 µm; c) and g) $D_P$ = 80 µm; d) and h) $D_P$ = 40 µm;**

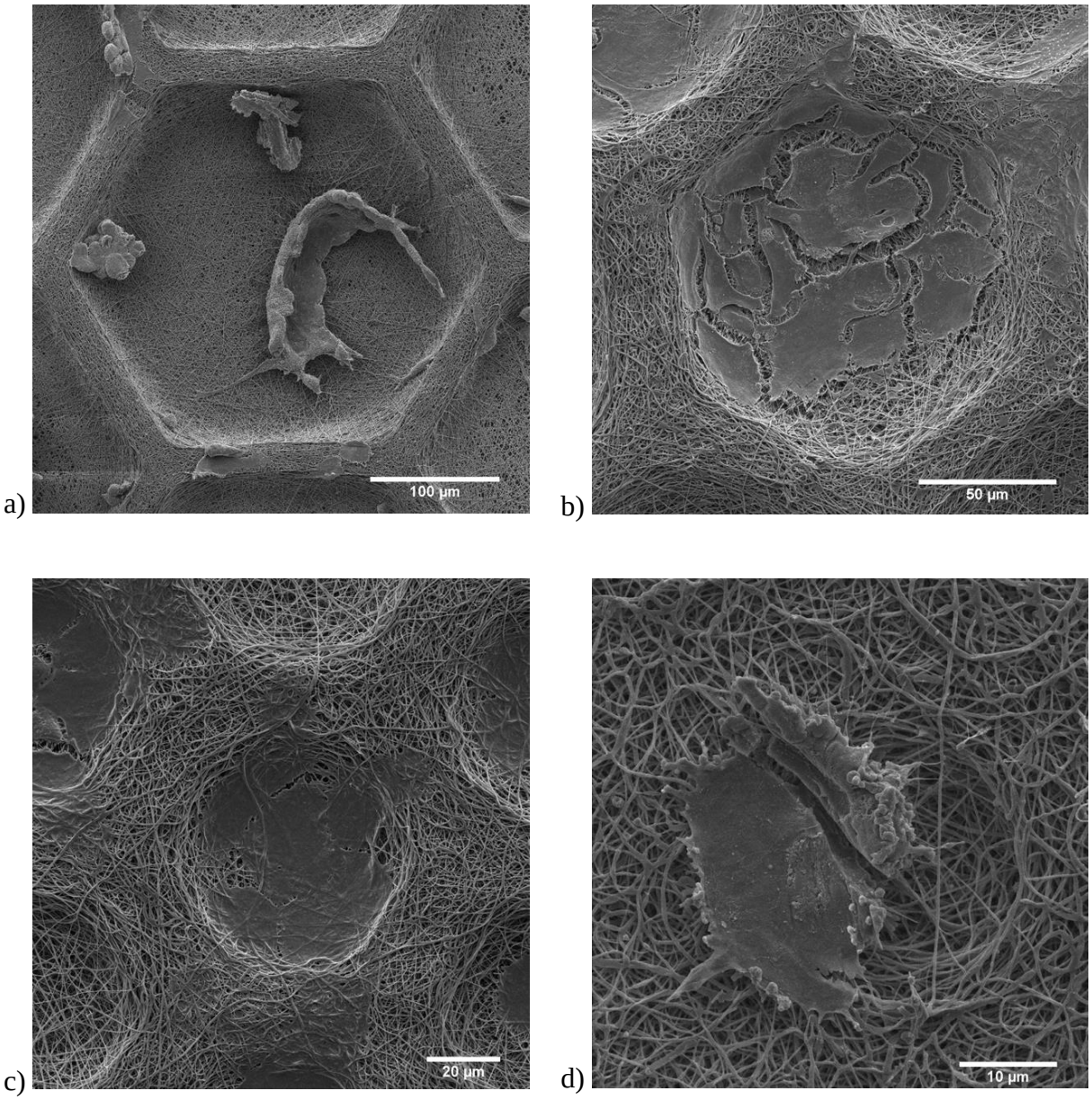


**Figure S3: SEM images of osteoblasts cell line MG63 after 3 days of proliferation on PCL honeycomb scaffolds a) $D_P$ = 360 µm; b) $D_P$ = 160 µm; c) $D_P$ = 80 µm; d) $D_P$ = 40 µm;**

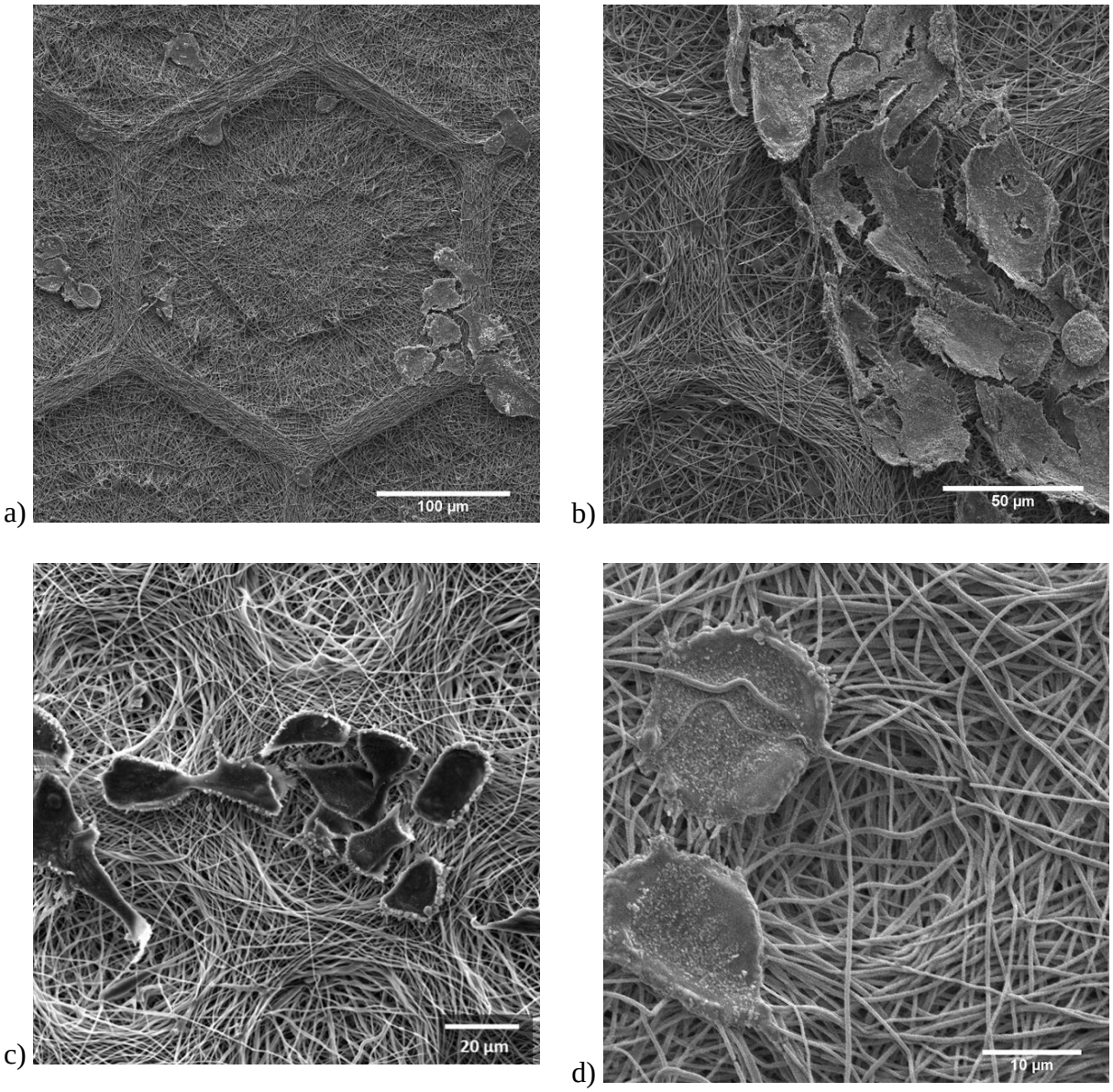


**Figure S4: SEM images of osteoblasts cell line MG63 after 3 days of proliferation on PLA honeycomb scaffolds a) $D_P$ = 360 µm; b) $D_P$ = 160 µm; c) $D_P$ = 80 µm; d) $D_P$ = 40 µm;**

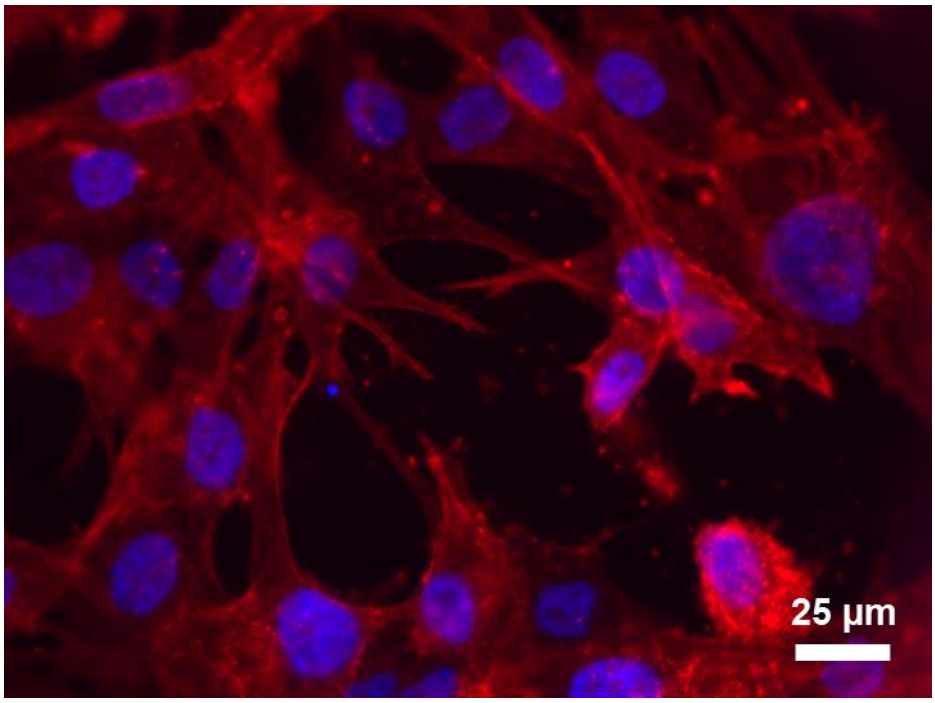


**Figure S5: Fluorescence microscopy image of MG-63 cells located inside a nest of a honeycomb PCL scaffold obtained with $D_P$ = 360 µm after 14 days of proliferation.**

## 5. 3D structuration

In this part, we present how we were able to construct new kind of 3D thick electrospun scaffolds. By combining the self-assembly phenomenon of PCL (bimodal distribution of the fibers) and the use of honeycomb micropatterned collectors, 3D honeycomb scaffolds with controlled pore size and porosity gradient could be obtained. This work was accepted in the journal *Material Letters*.

# Thick Honeycomb Electrospun Scaffold with Controlled Pore Size

**Accepted in *Material Letters*, 2014, DOI:10.1016/j.matlet.2014.11.118,**

**Salima Nedjari, Guy Schlatter, Anne Hébraud**

**Abstract:**

A novel strategy to prepare thick nanofibrous scaffolds with controlled pore size and graded porosity by electrospinning was developed. Taking advantage of the self-assembling properties of bimodal nanofibers, it was possible to grow columns of pores with mm height. The use of a honeycomb microstructured collector allows the control of the pore diameter from 80 to 360 µm. With increasing sample thickness, the columns of pores began to merge creating a gradient in pore diameter of up to several hundreds of microns. These scaffolds should be ideal for tissue engineering applications.

### 5.1 Introduction

Electrospun scaffolds are known to be good candidates for tissue engineering applications because of their ability to mimic the extra cellular matrix (ECM) of living tissues [188, 189] mainly composed of collagen or elastin fibres, ranging from 10 to several hundreds of nanometres. Electrospinning usually produces 2D nonwoven nanofibrous scaffolds with interconnected pores in the range of a few microns. However, such densely packed scaffolds do not allow the migration of cells through the structure and present a barrier to the vascularization of the tissue. An ideal scaffold should be nanofibrous with pore sizes in the range of a few tens to a few hundreds of micrometers and thicknesses up to a few millimeters, depending on the targeted tissue [190, 191].

Recently, different strategies have emerged to approach this goal. Thicker scaffolds have been obtained by stacking 2D membranes [192-194], wet electrospinning [195, 196] or using spherical dish collectors with needles [197, 198]. Moreover, important efforts have also been made to increase the

pore size of electrospun scaffolds. Increase of the nanofibrous diameters [199], addition of porogen agents [195, 200, 201], or cryoelectrospinning [202, 203] leads to pore sizes ranging from tens to hundreds of microns. Bigger pores can also be burned into the scaffold by post-electrospinning femtosecond laser processing [204]. Yet, most of these strategies require special electrospinning set up or post processing operations.

A simpler method has been developed recently to create large pores and thick samples, based on the self-organization of nanofibers into honeycomb-like structures due to modulated electrical interactions [99]. The obtained cm-thick structures presented a gradient in pore sizes increasing from a few microns to a few hundreds of microns and good mechanical properties (compression modulus of 65 kPa with a porosity of 87 %). However, pore sizes were not controlled and depended on nanofibers self-assembly, starting from very small pore sizes that could still prevent cells migration through one side of the scaffolds.

In this study, we have combined this approach with the use of honeycomb microstructured collectors in order to control the size of the honeycomb pattern and construct 3D scaffold with columns of pores of controlled sizes.

## 5.2 Materials and Methods

### 5.2.1 *Fabrication of honeycomb micropatterned collector*

Honeycomb micropatterns of 60 µm height, internal diameter of 80, 160 or 360 µm and wall width of 20 µm (**Fig. 43A**) were obtained by photolithography on silicon wafers (mask aligner MJB3 SUSS Microtec) using SU-8 2050 photoresist (Microchem). A conductive layer (Al-150 nm and Au-20 nm) was then deposited on the collector by electron beam evaporation (Plassys MEB5505).

### 5.2.2 *Electrospinning of 3D Scaffold*

15 wt.% poly(ε-caprolactone) (PCL, Mw=80 kg.mol$^{-1}$, CAPA 6806, Perstorp) solutions in 60/40 V/V dichloromethane/N, N-dimethylformamide (Sigma-Aldrich, predistilled) and 10 wt.% poly(lactic acid) (PLA, Mw=180 kg.mol$^{-1}$, 7000 D, NatureWorks) solution in 50/50 V/V dichloromethane/N, N-dimethylformamide, were prepared 24h prior to electrospinning. The solutions were electrospun during 1 hour using a homemade vertical set-up [99, 205] (**Fig. 43A**, electrospinning conditions: PCL: needle/collector voltage = +15/-15 kV, distance = 15 cm, 1.4 mL/h; PLA: needle/collector voltage = +12/-5 kV, distance = 18 cm, 1.6 mL/h, temperature = 21±1°C, humidity = 44±3 %). Additionally, a 3 mm thick poly(methyl methacrylate) plate with a 25 mm diameter circular hole was placed onto the collector during electrospinning in order to concentrate the fiber deposition.

### 5.2.3 *Scanning electron microscopy (SEM) and X-ray microcomputed tomography*

Samples were peeled off from the collector by immersion in ethanol for PCL or isopropanol for PLA, dried, cut with a rasor blade in liquid nitrogen and characterized by SEM and X-ray microcomputed tomography as described in the Supplementary Data.

## 5.3 Results and Discussions

A PCL solution was first electrospun for 10 minutes onto a flat aluminium collector. As described by Ahirwal *et al.* [99], nanofibers self-assembling occurs, leading to honeycomb-like patterns with a polydispersity in the pattern size (**Fig. 43B**). This phenomenon is due to a heterogeneous dissipation of the electric charges induced by the bimodal size distribution of PCL nanofibers diameter showing thick and thin domains [99] (Supp. Data. Fig. S1 and S2). Aggregates of thick fibers formed in the first seconds of the deposition are in good contact with the collector while thin fibers suspended in-between remain electrically charged, thus forming an electrostatic template of attractive and repulsive domains to the upcoming charged fiber. The electrostatic template mainly affects the thick portions of fibers that carry a higher linear charge density λ [206] (**Fig. 43E**). It results in the construction of a honeycomb-like structure with thick fibers, still slightly wet, merging to form the walls of the patterns and thin fibers crossing them (**Fig. 43C**).

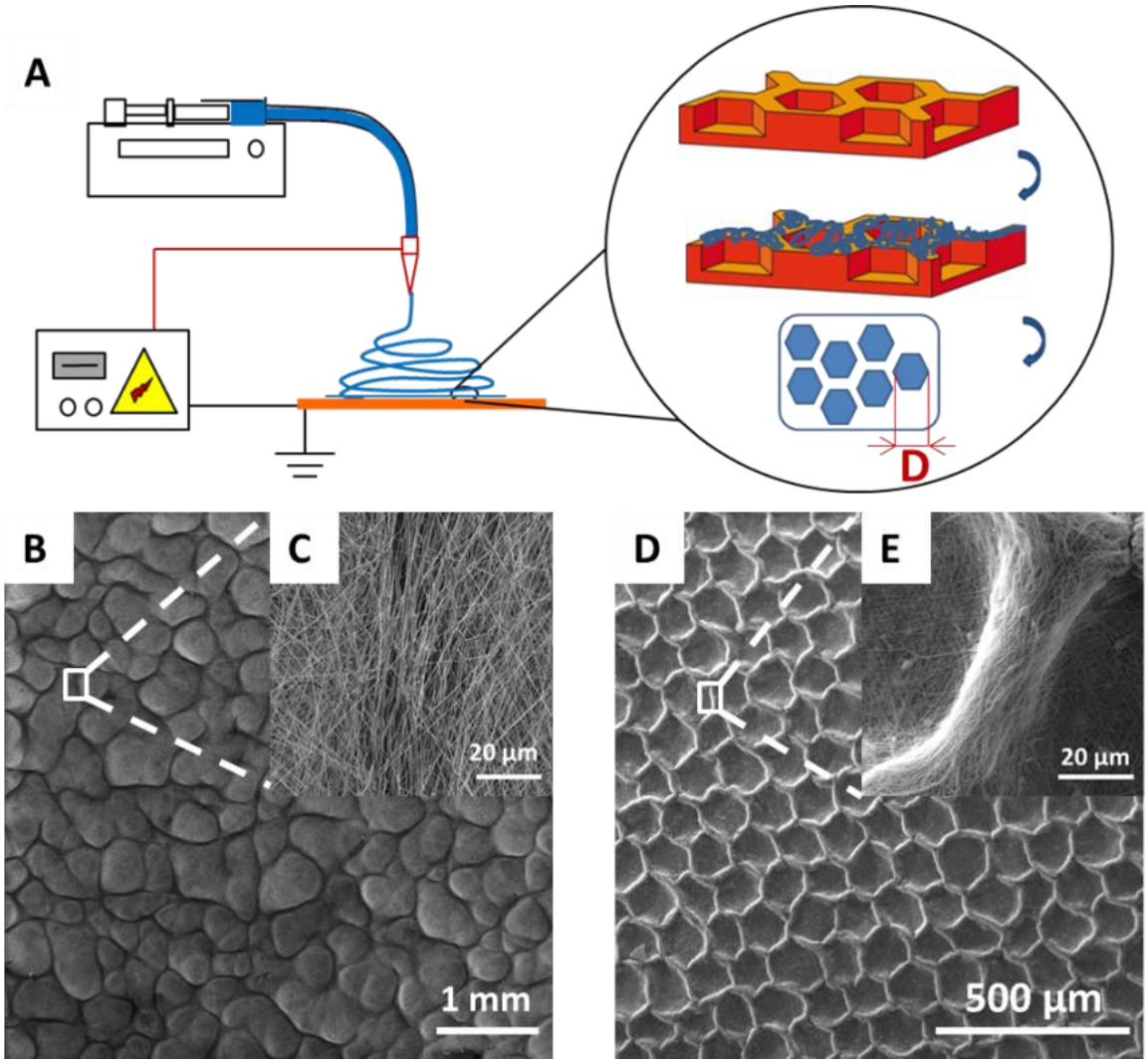


**Figure 43: A) Electrospinning setup using a honeycomb collector. B) SEM image of a PCL honeycomb-like self-assembled structure on a flat collector (10 min). C) SEM image of a wall of the honeycomb-like pattern. D) SEM images of PCL honeycomb structure on a honeycomb microstructured collector (10 min, D=160 µm). E) SEM image of a wall of the honeycomb pattern**.

To control the size and polydispersity of the self-assembled fibers patterns, a honeycomb micropatterned collector was used **(Fig. 43A**) with internal diameter D of the honeycomb patterns of 160 µm. The organization of the fibers and the formation of the patterns are then guided by the collector, leading to a more regular honeycomb structure (**Fig. 43D**). Once again, an electrostatic template is formed at the first deposition times, with attractive domains over the pattern walls and repulsive domains over the pattern nests leading to preferential deposition of the thick fibers over the walls in a self-sustained process. This phenomenon allows for the vertical growth of the patterns walls

leading to the formation of columns of pores with diameters corresponding to the internal diameter D of the honeycomb pattern of the collector (**Fig. 44A** and **44B**).

However, after 200 µm in thickness, pores columns start to merge by pairs, forming larger pores columns. Variations in the nanofibers deposition are responsible for the formation of smaller walls that disappear as soon as a new fiber is able to cross over them without touching them. This fiber remains positively charged and becomes repulsive to the upcoming jet. The electrostatic template is modified and the columns are growing by increment (**Fig. 44C-D**). Thus, after 1 hour electrospinning, mm-thick scaffolds, with a porosity of 91±3 % measured by gravimetry, are obtained and a gradient of pore size is observed in the thickness of the material, starting from a chosen pore diameter, controlled by the pattern size of the microstructured collector (**Fig 44E**). In contrast, when the distribution of diameters of the electrospun fibers is monodisperse, as for PLA nanofibers (Supp. Data Fig. S1 and S3), the electrostatic template effect is lost rapidly and a dense and flat sample is obtained in the same conditions even after 1 hour (**Fig. 44F**). Nanofibers with bimodal distribution of diameters, capable of self-organization are necessary to grow thick porous samples [99]. Indeed, thick portions of fibers, still slightly wet when landing, tend to merge in the wall, allowing a good dissipation of electric charges, which is not possible in the case of regular PLA fibers. The role of the microstructured collector is only to guide the fibers self-organization into a more regular structure. Thus pore size can be precisely tuned by changing the collector pattern size respectively to 360 and 80 µm (**Fig.45A** and **45B**). In these cases, the same mechanisms of 3D construction occur leading to mm-thick scaffolds with an increasing gradient in pore size, starting from 80 and 360 microns.

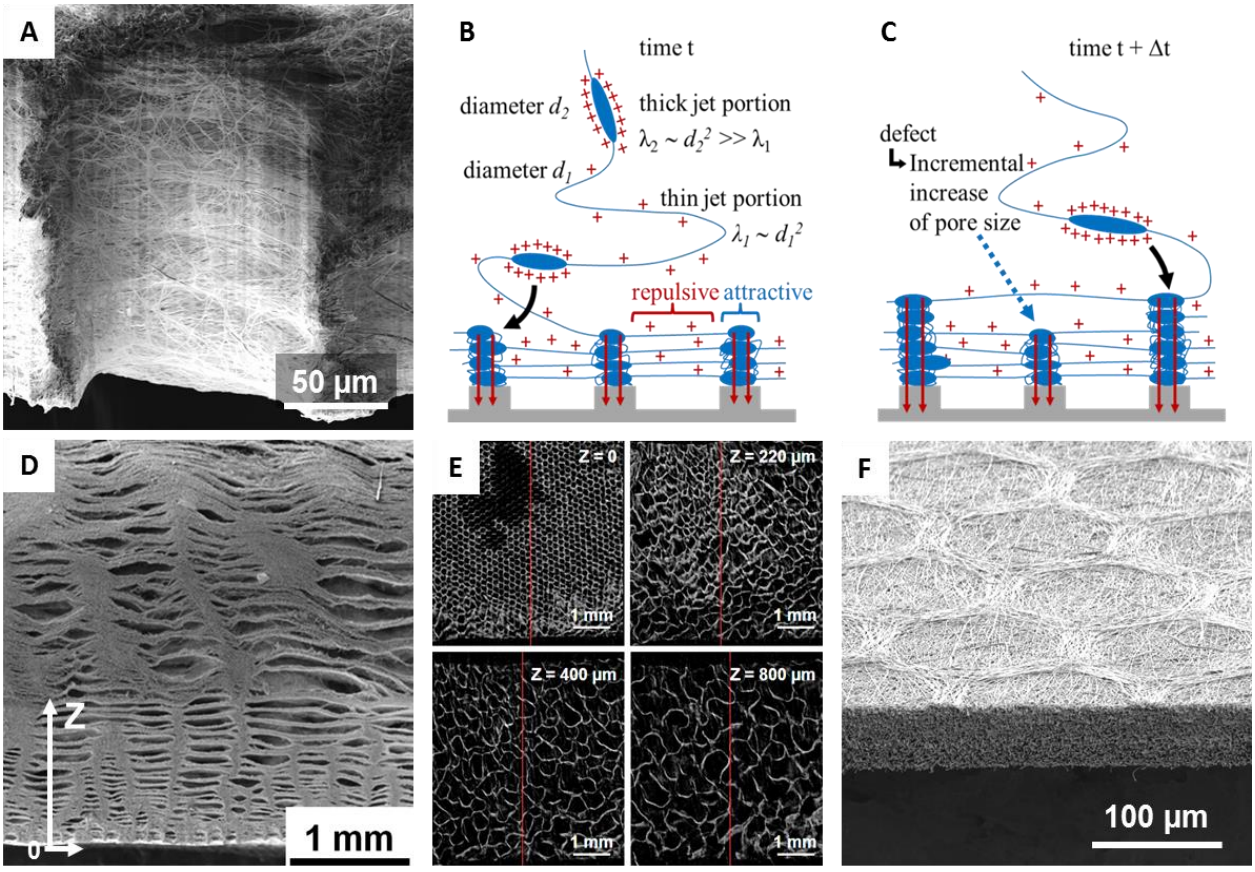


**Figure 44: A) SEM image of a porous column with controlled pore size (D= 160 µm) in a PCL scaffold. B) Proposed mechanism for the construction of porous columns with controlled pores size C) Proposed mechanism for the merging of two columns. D) SEM image of the cross-section of a PCL scaffold (1 hour, D= 160 µm). E) MicroCT images showing 4 slices at different Z values of a thick PCL honeycomb structure. F) SEM image of a thin PLA honeycomb structure (1 hour, D= 160 µm). Videos of 3D micro-CT pictures can also be viewed in the Supplementary Data.**

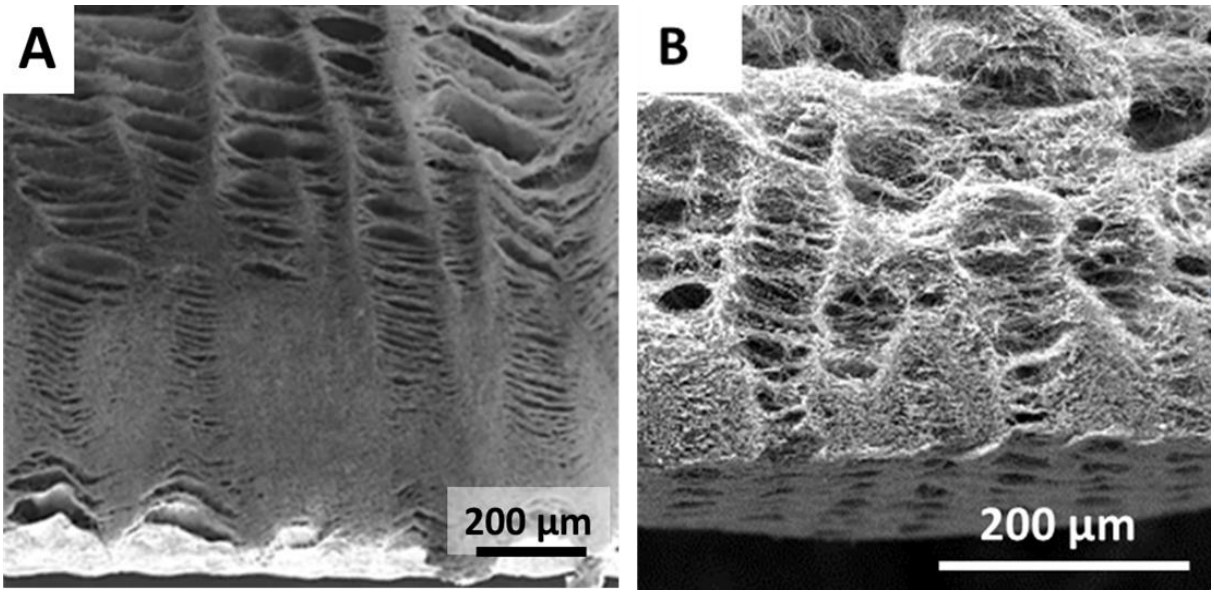


**Figure 45: SEM images of the cross-section of thick electrospun PCL scaffolds with regular porous columns of controlled pore sizes of A) D=360 µm B) D = 80 µm.**

## 5.4 Conclusions

In summary, 3D nanofibrous honeycomb micropatterned scaffolds were obtained by simultaneously using a honeycomb micropatterned collector during the electrospinning process and the self-assembling properties of the PCL nanofibers. These scaffolds present a pore size gradient from tens of microns to the millimeter scale with a controlled minimum size depending on the honeycomb pattern size of the collector. Such scaffold should be adaptable for the regeneration of various targeted tissues such as bone [191] or cardiac tissues [190]. Their porosity gradient make them particularly interesting at interfaces between two tissues [207].

## 5.5 Supporting informations

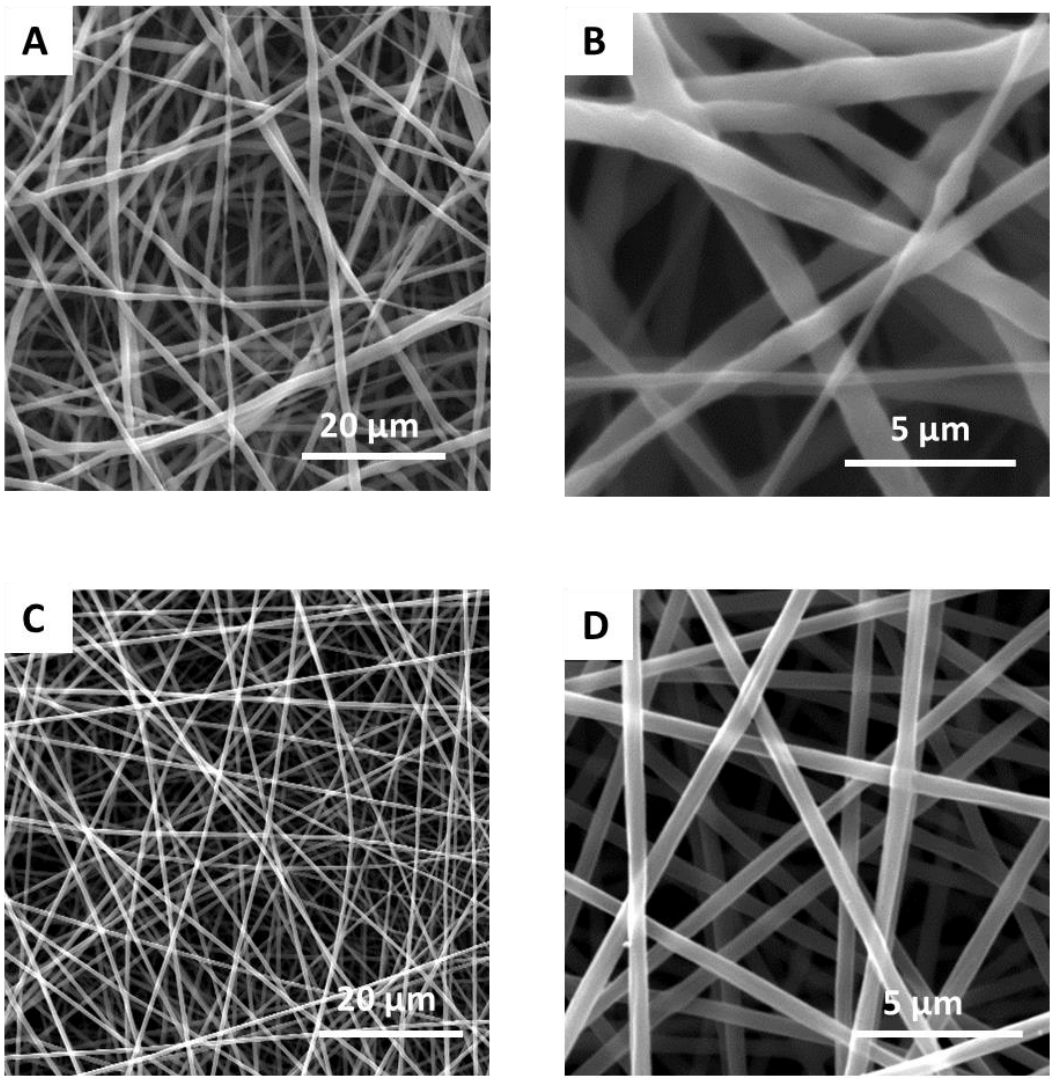


**S1: A and B) SEM images of PCL nanofibers; C and D) SEM images of PLA nanofibers**

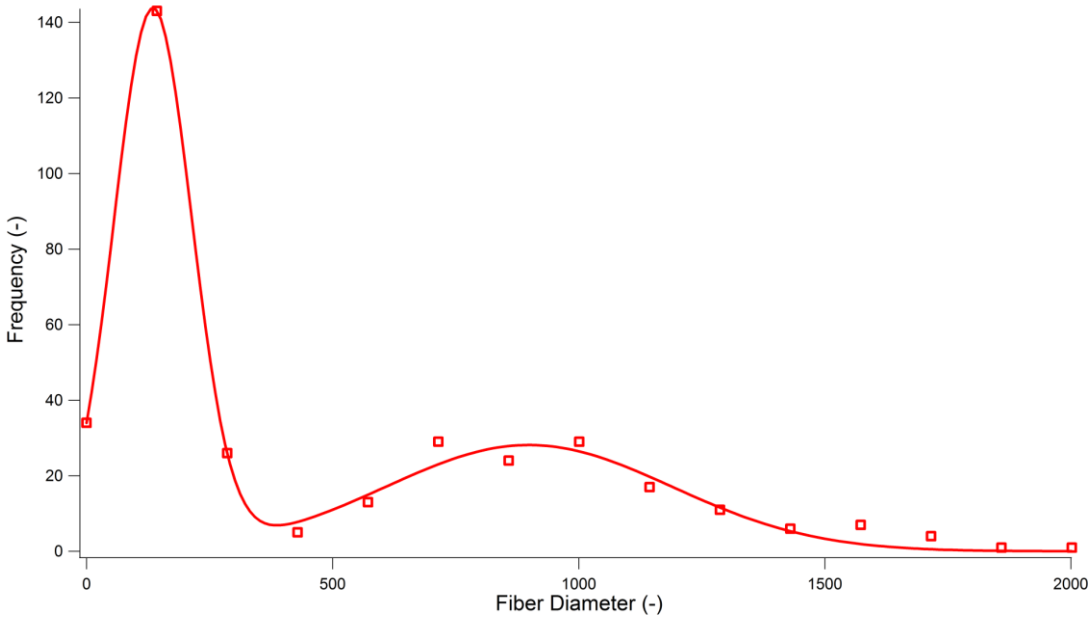


**S2: Bimodal Distribution of the diameter of PCL nanofibers**

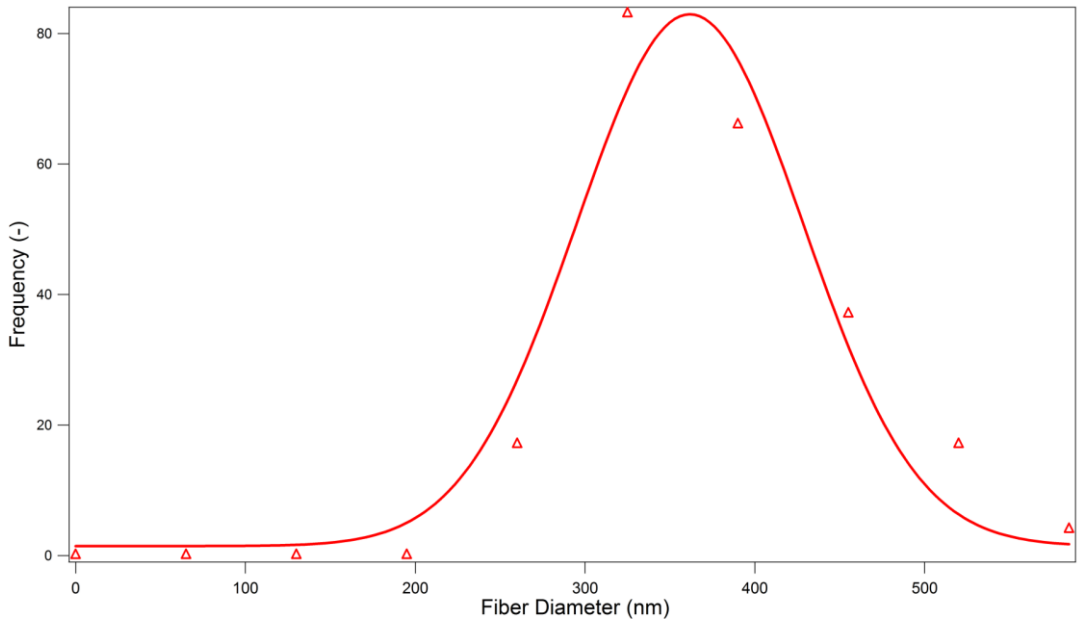


**S3: Unimodal Distribution of the diameter of PLA nanofibers**

## 6. Conclusions of the Chapter two

In this chapter, we presented the elaboration of monocomponent micropatterned electrospun membranes by making electrospinning on micropatterned collectors.

On the first hand, we presented the elaboration of 2D micropatterned electrospun membranes. Different kinds of micropatterned collectors (block collector, honeycomb collector) were fabricated thanks to lithographic processes (which were also presented). Then, two biopolymers, PCL and PLA were used for the electrospinning process. Optimization of the electrospinning conditions of the two biopolymers was done. Then, with the optimal electrospinning conditions, electrospun PCL and PLA honeycomb micropatterned electrospun membranes were elaborated. The honeycomb patterns had an internal diameter going from 40 µm to 360 µm. We showed that unimodal distribution of the diameter of PLA leads to flat honeycomb scaffold. Despite, the bimodal distribution of the diameter of PCL fibers and the preferential deposition of thick fibers over the walls of the honeycomb increase the relief of the scaffold. Then we studied the influence of the honeycomb structure on MG-63 osteoblasts. We demonstrated that we were able to create osteoblasts niches inside the PCL honeycomb nests for honeycomb diameter going from 80 µm to 360 µm.

On the second hand, we showed that by using honeycomb micropatterned collector during electrospinning process and the self-assembling properties of PCL, we were able to make growth 3D scaffold with very interesting morphology. Indeed, these scaffolds presented a controlled pore size, directly depending on the honeycomb internal diameter on which they electrospun. We noticed that porous columns of the 3D scaffolds were gathering together and made a porosity gradient in the thickness of the scaffold. This very special 3D scaffold with controlled pore size could be very useful for different field of tissue engineering.

Now, we will interest to the elaboration of composites electrospun scaffolds by electrospinning and electrospraying techniques. By coupling these techniques, we want to elaborate complex 2D and 3D composite scaffolds with different architectures. The 2D composite membrane will be elaborated for one dedicated application: the screening of different electrospun micropatterns in order to find quickly which kind of architecture could enhance the bone regeneration. On the other hand, we want to elaborate 3D scaffold with controlled pore size with another strategy than the self-assembly of polymers coupled to honeycomb micropatterned collector. These two main subjects are the main topics of the next chapter.

# Chapter 3: Composite 2D and 3D architectured nanofibrous scaffolds

## 1. Introduction

Monocomponent micropatterned scaffolds are very interesting for bone applications. Because hydroxyapatite is one of the major components of the extracellular matrix in bones tissues, composite scaffold made of electrospun nanofibers and electrosprayed hydroxyapatite have been developed by coupling electrospinning of biopolymers and electrospraying of hydroxyapatite.

In a first part, bilayers composed of fibers and particles were elaborated on micropatterned collectors. Alginate and PCL fibers in combination with hydroxyapatite particles were produced and the effect of the nature of the fibers on the final structure of the scaffold was studied. This novel technique allowed the electrostatic-assisted template deposition particles at precise locations on the scaffold. Bilayer membranes of PCL and hydroxyapatite composed of 21 different micropatterned structures were elaborated and incorporated into a PMMA plate containing 21 wells. The all formed a biochip dedicated to the screening of microstructured fibrous structures. As a proof of concept of the use of such biochips, the proliferation of MG-63 osteoblasts like cells as well as their mineralization was followed as a function of the scaffold structure.

In the second part of this chapter, a new kind of 3D composite electrospun construct elaborated by alternately electrospinning nanofibers and electrospraying particles are presented. This 3D construct presents cylindrical pores which could be tuned from tens to hundreds microns. Finally, tensile tests on these 3D composite electrospun scaffolds have been performed proving their suitability for biomedical applications. This work has been published in the journal *Polymer*.

# 2. Electrostatic template-assisted deposition of microparticles on electrospun nanofibers: Application to the fabrication of biochips for the screening of composite microstructured materials for bone regeneration

## 2.1 Introduction

Today, one main objective of cell biology and biotechnology is to find the optimal *in vitro* micro-environment for cells that can mimic the one existing *in vivo*. Indeed, cell behaviors such as proliferation, migration and differentiation are deeply depending on their micro-environment, which could be defined by different parameters such as the substrate topography, surface chemistry, substrate stiffness and mechanical deformation, shear stress, cell culture media composition, and physiochemical conditions (temperature, pH, $O_2$, $CO_2$) [208]. Cell substrate or topography is particularly one of the most impacting parameter of the cell fate, especially for stem cells or bone cells.

High throughput screening has been developed in order to test a large number of micro-environment conditions. Thanks to microfabrication and microfluidics techniques (photolithography, etching, and molding), new lab-on-chip have emerged, offering the possibility to test different libraries (molecules, topography, etc) in order to find the best cellular micro-environment. Repeatability and rapidity provided by these lab-on-chip make them very attractive for biologists [209].

Concerning the topography, lab-on-chips could allow the screening of hundreds different patterns to thousands different patterns. For example, the BSSA is a lab-on-chip made by photolithographic processes and proposing 160 different patterns which is a combination of micro-pillars of different shapes and different spacing [210]. The Topochip housing 2176 distinct topographical units was developed by Unadkat *et al.* [211]. They used mathematical algorithms to design arrays of patterns onto a single chip with distinct combinations on each field. Due to the limitation of the lithographic processes, the size of the topographical features was in the micron range and the height of the topographical features was the same on the same chip [211]. However, by combining, different methods of microfabrication techniques, more complex topographical patterns (curved structures or 3 dimensional structures for example) could be designed. For instance, Multiarchitecture (MARC) chip has different complex hierarchical structures and topographies [212, 213].

Today, while a large number of lab-on-chip are made from hydrogels, they have the disadvantage to not mimic well the *in vivo* conditions of cells. Indeed, *in vivo,* cells are naturally growing on the extracellular matrix (ECM) which is mainly made by collagen nanofibers. Effective high throughput screening should be done on fibrous structures, in order to be closer to cell micro-environment *in vivo*.

During the last few decades, electrospinning has emerged as a simple fabrication technique to obtain fibers with sub-micron diameter. Electrospun fibers have a wide range of applications, especially in biomedical area, where they have proved to be excellent candidates as substrates for cell growth *in vivo* and *in vitro*. The electrospun nanofibers appear really attractive due to their ability to structurally mimic the extracellular matrix ECM. Besides, electrospun mats have the advantage to present large surface area to volume ratio favoring cell adhesion which can be tailored to have different structures or pores size allowing cell colonization and migration [188, 189, 214-216].

For high throughput testing applications, new platforms incorporating nanofibrous electrospun membrane have emerged. Galago-Perez *et al.* designed a new micro-well platform in which the well bottom is made entirely of nano-microscale polymer fibers. Thanks to soft-lithographic processes, different size and shape of micro-wells in polydimethylsiloxane (PDMS) platforms were designed. Their results showed that the fibrous well bottom enhanced cell retention and allowed spatially controlled assembly of cell hepatocyte clusters [217]. The geometrical properties of the wells can be easily modified to obtain cell clusters with numerous sizes and shapes. However, they were only able to change the size and shape of the wells; the fibers located inside the wells were randomly deposited and did not present any special architecture.

Another kind of platform with multi-wells were developed by Lee *et al.* [218]. They developed micropatterned scaffolds by fabricating poly(ethylene glycol) (PEG) hydrogel micropatterned wells on electrospun poly(styrene) (PS) fiber matrices, resulting in a free-standing bidirectional porous sheets. Hydrogels micropatterns were prepared by using photolithography without any residual hydrogel precursor remaining in the PS fiber region. PS fibers were inserted through the side walls of the hydrogel microstructures. Cells selectively adhered and remained viable within the PS fiber region, thereby creating cellular micropatterns [218].

Micropatterned electrospun structures (aligned fibers, micropatterned structures) could greatly affect cells behaviors. For example, it was found that for PCL honeycomb micropatterned scaffolds, osteoblasts MG-63 grew preferentially inside the nests of the

honeycomb, creating niches of osteoblasts cells [219]. To our knowledge, testing different structures of electrospun membranes on the same chip has been made only once by Wallin *et al.* [220]. Spatially defined regions of electrospun fibers of both aligned and random orientation were patterned on glass substrates that were irreversibly bonded to microfluidic networks produced in PDMS. Their device was then tested with neural stem cells and the effect of the alignment of the fibers on the neural stem cell alignment was showed. The topology of the electrospun fiber mat changed in term of fiber morphology, fiber patterns and orientation, and was found to closely mimic the *in vivo* conditions of neural stem cells [220].

In bone tissue engineering, new composite scaffolds composed of nanofibers and hydroxyapatite, a component present in bone tissue, have emerged in order create a better osteophilic environment for the growth and mineralization of the osteoblasts. Such kind of composites can be elaborated by different strategies [195, 221, 222] . For example Gupta *et al.* [223] showed that simultaneous electrospinning of polymers (gelatin or poly(L-lactic acid)-*co*-poly(ε-caprolactone) and electrospraying of HA could lead to a composite structure that can enhance the cell proliferation and the cell mineralization [223] .

In this work, we propose a new strategy allowing the controlled deposition of electrosprayed microparticles on electrospun fibers which will then be applied for the elaboration of a biochip allowing the screening of composite fibrous structure for bone regeneration. In the first part, we will introduce the concept of electrostatic-assisted template deposition of microparticles on electrospun fibers. Then, the development of a multi-wells plate device called a biochip incorporating different kinds of electrospun fibers and electrosprayed particles structures for screening application with bone cells will be shown. To mimic the ECM of bone tissues, the composite biochip membrane was a bi-layer membrane made of electrospun PCL nanofibers and electrosprayed hydroxyapatite microparticles. The biochip was composed of 21 different micropatterned structures such as hexagon, block, bar, maze and random. Finally, MG-63 osteoblasts were cultured in this biochip device. Immunochemistry and alizarin red staining were performed on these biochips to evaluate the influence of the micropatterned structures on the mineralization process.

## 2.2 Electrostatic template-assisted deposition of microparticles on electrospun nanofibers

Before showing the concept of the electrostatic template effect, we will present the results regarding the optimization of electrospraying of hydroxyapatite and electrospinning of alginate, the two novel components tested for this part of the work.

### 2.2.1 *Electrospraying of hydroxyapatite*

Hydroxyapatite (HA) is a ceramic with chemical composition similar to the mineral component of bone. Synthetic HA ($Ca_{10}(PO_4)_6(OH)_2$) has been extensively used as an implant material for bone substitute due to its excellent ostoinductive properties [224]. HA has been used in dental and orthopaedic surgery as bone defect fillers and as coatings on metallic implant surfaces, to enhance bone regeneration [225]. HA could be synthesized via a wet precipitation reaction between calcium hydroxide [$Ca(OH)_2$] and orthophosphoric acid ($H_3PO_4$) solutions [226].

It has been found that HA could be electrosprayed from suspensions into ethanol [227-229] or methanol [230] leading to microparticles. In others case, hydroxyapatite could be blended with gelatin in solvents such as TFE or distilled water [222, 231] for bone tissue regeneration.

We conducted different experiments to optimize the electrospraying of HA. Synthetic HA (Sigma-Aldrich) was suspended into ethanol at different concentration: 4 wt % and 6 wt %. Microparticles were obtained with both concentrations. Solution of 6 wt % of HA was preferred to the solution of 4 wt % because the Taylor cone was more stable with the solution of 6 wt%. SEM pictures of obtained samples are proposed on **Figure 46**.

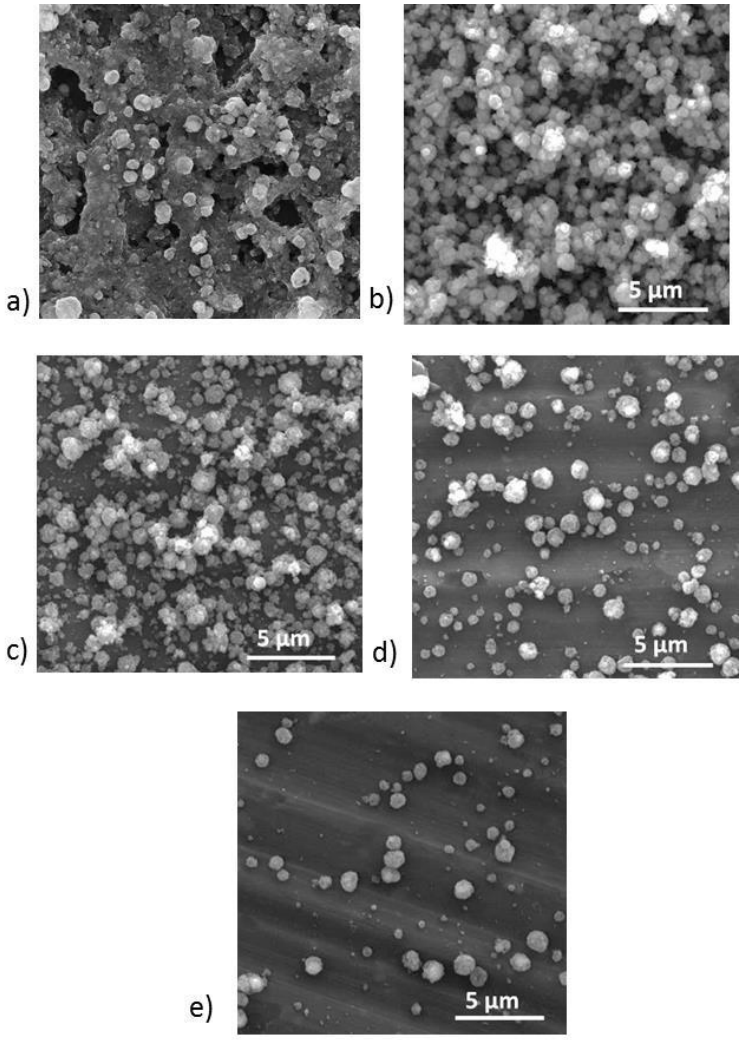


**Figure 46: Different SEM images of electrospun HA microparticles obtained from a 6% wt/ HA suspension electrosprayed with a flow rate of 0.612 ml/h, a voltage of 13/0 and a varying needle-collector distance D: a) with D= 1 cm with; b) D= 5 cm; c) with D =7 cm; d) with D= 10 cm; e) with D= 13.5 cm**

By changing only the distance (keeping the flow rate constant and the voltage constant) during the electrospraying of hydroxyapatite (**Figure 46**), the morphology of the particles was greatly affected, going from aggregates of particles to particles. In fact, at a short distance (1cm, 5cm or 7cm), the density of deposited particles is higher than the density of particles deposited at higher distance (10 or 13 cm). Moreover, at shorter distance, the deposit was still wet after the electrospraying, proving that the ethanol did not well evaporate during the process, thus leading to aggregated particles. Distances like 10 cm or 13 cm, leading to isolated microparticles, were privileged for the next experiments.

### 2.2.2 *Electrospinning and cross-linking of Alginate nanofibers*

"Alginate" is a collective term for a family of polysaccharides produced by brown algae and bacteria. Alginic acid was first discovered, extracted, and patented by Stanford [232]. Alginates with algae's source show different structural and chemical properties with respect to their seasonal and growth conditions. Alginates could be described as a linear binary copolymers with homopolymeric regions of (1-4)-linked β-D-mannuronic acid sequences (M-blocks) arranged with homopolymeric region of α-L-guluronic acid residues (G-blocks) interspersed by regions in which the two groups coexist in a strictly alternating sequences (MG-blocks) [233] (**Figure 47**). Due to the presence of carboxylic acid COONa on its chaine, alginate is a polyanion at neutral pH and could be cross-linked by calcium chloride solution ($CaCl_2$).

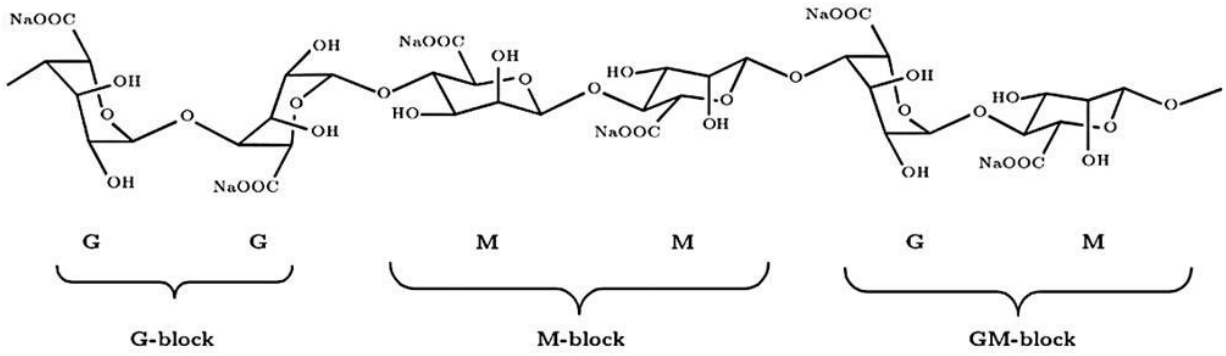


**Figure 47: a) Chemical structure of sodium alginate [233]** .

The main industrial applications of alginate as a natural polymeric material are linked to its stabilizing, viscosifying, and gelling properties and its ability to retain water [232]. Due to its properties of biocompatibility, biodegradability, and non-toxicity, alginates meet well all the requirements for their use in pharmaceutical and biomedical applications. They have been largely used in wound dressings, dental impression, and formulations for preventing gastric reflux. In tissue engineering applications, alginate has attracted the attention due to its hydrophilicity which could facilitate uniform cell growth during a regeneration process [234, 235].

In electrospinning, the major issue in fabrication of alginate-based nanofibers is its high viscosity in aqueous solutions. Researchers did not succeed for the electrospinning of alginate solution alone. To get alginate nanofibers, it must be blended with a template polymer such as

poly(ethylene oxide) (PEO) [236-238]. Saquing *et al.* showed that by changing the molar mass of the PEO from 100 kDa to 2000 kDa, the morphology of alginate fibers could be changed from beaded to non-beaded fibers. Based on these studies, we decided to use a PEO with a molar mass of 1000 kDa in a 50/50 blend alginate/PEO, which normally leads to non-beaded fibers [238].

Different kinds of alginate are synthetically prepared and available on the market: alginate with low, medium and high viscosity. As it was reported on literature, we decided to work with two different kinds of alginate:

- Alginate low viscosity ( 4-12 mPa.s at 1% in water at 25°C)
- Alginate medium viscosity ( ≥ 2000 mPa.s at 2% in water at 25 °C)

Alginate and PEO were dissolved in water during 24 hours. Then, the solutions were mixed together in a 50/50 wt/wt ratio. Different solutions of alginate medium viscosity/PEO (1000 kDa) were prepared and tested in order to find possible electrospinning conditions. However, it was very difficult to find electrospinning conditions allowing production of alginate fibers with alginate medium viscosity (**Table 9)**. The only fibers that were obtained are presented of **Figure 48-a** and **Figure 48-b**. As shown, only a beaded morphology was achieved and gellification rapidly occurred at the needle due to the very high viscosity of the solution. Therefore, it was not possible to increase the PEO amount in the solution to obtain uniform fibers.

| System Alginate/PEO | Voltage (kV) | Distance (cm) | Flow rate (ml/h) | Presence nanofibers | Presence of beads |
|---|---|---|---|---|---|
| Alginate 1.5%/PEO1.5% | 13.5/0 | 15 | 0.3 | Yes | Lots of beads |
| Alginate 1.5%/PEO1.5% | 16/0 | 15 | 0.5 | No | No |
| Alginate 1.5%/PEO1.5% | Various tested voltages | 18 | 1 | No | No |
| Alginate 1.5%/PEO1.5% | Various tested voltages | 13 | 0.3 | No | No |
| Alginate 1.5%/PEO1.5% | Various tested voltages | 10 | 0.5 | No | No |
| Alginate 1.5%/PEO1.5% | Various tested voltages | 7 | 0.5 | No | No |

**Table 9: Different electrospinning conditions of Alginate (medium viscosity)/PEO (1000 kDa) solution**

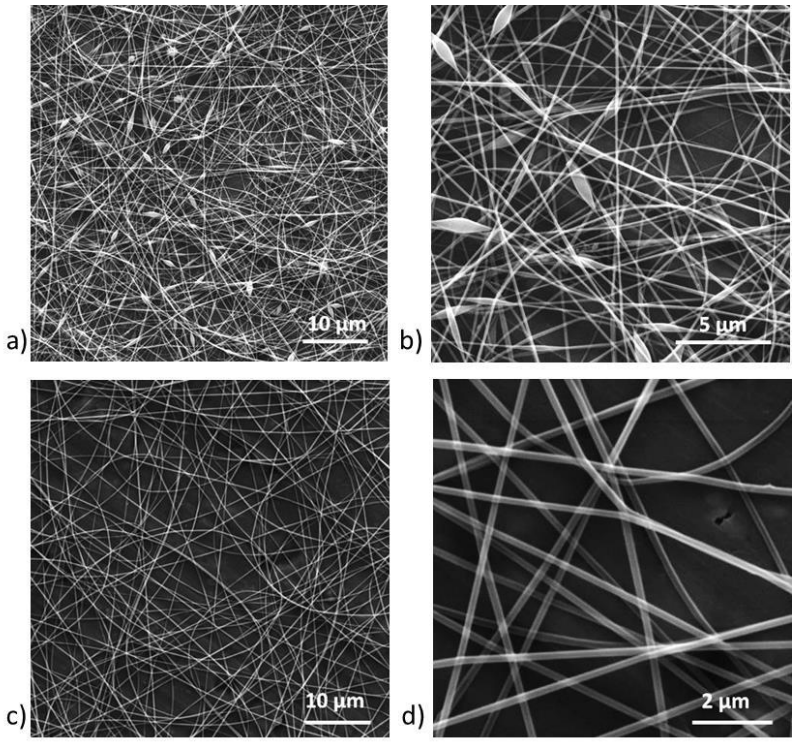


**Figure 48: SEM images of electrospun alginate nanofibers: a and b) alginate nanofibers obtained from a solution of alginate medium viscosity; c and d) alginate nanofibers obtained c 'from a solution of alginate low viscosity.**

The **Table 10** presents the different conditions of electrospinning of alginate fibers from solutions made of alginate low viscosity and PEO (1000 kDa). These solutions were

more easily electrospun and stable processing conditions were found. Beaded electrospun alginate fibers were first electrospun (with many droplets at the surface of the alginate mat) but after optimization of the conditions, uniform alginate fibers could be obtained (see **Table 10)**. Alginate fibers are presented on **Figure 48-c** and **Figure 48-d**: they present a unimodal distribution of the fiber diameter with an average diameter of 182 nm (+/-10 nm).

| System Alginate/PEO | Voltage (kV) | Distance (cm) | Flow rate (ml/h) | Presence of nanofibers | Presence of beads |
|---|---|---|---|---|---|
| Alginate 1.5%/PEO 2% | 9.5/0 | 15 | 0,6 | Yes | Yes |
| Alginate 1.5%/PEO 2% | 8.5/0 | 15 | 0,5 | Yes | No |
| Alginate 1.5%/PEO 2% | 8.5/0 | 15 | 0,3 | Yes | Yes |
| Alginate 1.5%/PEO 2% | 7.5/0 | 12,5 | 0,4 | Yes | No |
| Alginate 1.5%/PEO 2% | 7.5/0 | 12,5 | 0,4 | Yes | Yes (droplets also) |
| Alginate 1.5%/PEO 2% | 6/0 | 10 | 0,3 | Yes | Yes |

**Table 10: Different electrospinning conditions of Alginate (low viscosity)/PEO (1000kDa) solution**

### Cross-linking of alginate fibers:

Alginate electrospun fibers are soluble in water. To be able to use them as scaffolds for biological applications, alginate electrospun nanofibers should be cross-linked. As mentioned previously, alginate could be cross-linked by calcium chloride ($CaCl_2$). The ions $Ca^{2+}$ take the place on the ion $Na^+$ on the chain and interact with the ions $CO_2^-$. Because the ions $Ca^{2+}$ have double positive charges, they can interact with two $CO_2^-$ groups, thus forming a link between two alginate chains, creating a cross-linked network.

Thus, alginate nanofibrous membranes were immersed during one night into $CaCl_2$ solutions with different molar concentrations. The different tested $CaCl_2$ solutions are listed on the **Table 11**. Then, the samples were washed three times with distilled water and observed with the SEM. Results are presented on the **Figure 49**.

As seen on the images, after cross-linking in $CaCl_2$ solutions of 0.1 mol/L concentration or less, the alginate fibers were in majority redissolved in deionized water. At a

concentration of $Cacl_2$ of 0.5 mol/L, important swelling of the fibers occurred. Good cross-linking of alginate nanofibers could be reached with a solution of $CaCl_2$ with a molar concentration of 1 mol/L. In this case, fibers were nearly unchanged when immersed in water.

| **Concentration in $CaCl_2$ (wt/wt)** | **Solution** | **Molar Concentration (mol/L)** |
|---|---|---|
| 0.3 | Deionized water | 0.05 |
| 0.6 | Deionized water | 0.1 |
| 1 | Deionized water | 0.2 |
| 2.5 | Deionized water | 0.5 |
| 5 | Deionized water | 1 |

**Table 11: Different Solutions of $CaCl_2$ used for the cross-linking of alginate nanofibers**

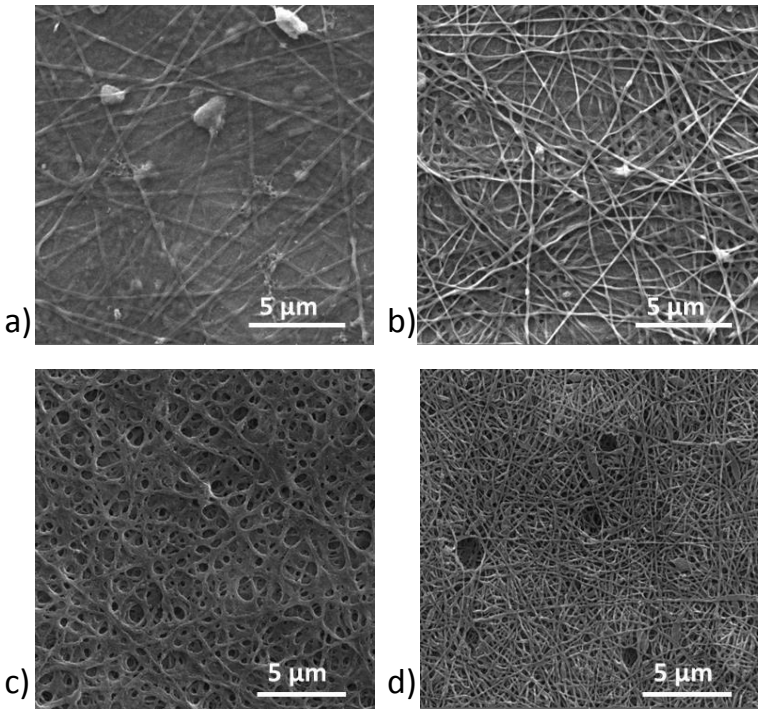


**Figure 49: SEM images of electrospun alginate nanofibers cross-linked into different $CaCl_2$ solutions: a) cross-linking in a solution of 0.05 mol/L; b) cross-linking in a solution of 0.1 mol/L; c) cross-linking in a solution of 0.5 mol/L; d) cross-linking in a solution of 1 mol/L**

Once good electrospinning conditions of alginate and electrospraying of hydroxyapatite were found, we tried to develop new kind of bi-layer alginate-hydroxyapatite electrospun membrane with honeycomb micropatterned collector.

### 2.2.3 *Selected experimental conditions*

Here, we present the conditions of electrospraying of HA and electrospinning of PCL which were used in all the following results shown in parts 2.2.4 and 2.2.5. The vertical homemade electrospinning setup was composed of 18G needle connected to a positive high voltage power supply (Spellmann SL 10) and a rotative collector (rotating in the horizontal plan with a speed of 100 rpm) connected to the ground (high voltage power supply Spellmann SL 10) in order to homogenize the deposition of the fibers. The polymer solution was pushed through the needle via a silicon feedline connected to a 10 mL-syringe installed on a syringe pump.

**Electrospinning of PCL**

PCL polymer solutions were prepared 24 h before by dissolving poly(ε-caprolactone) (PCL) (Mw=80 kg.mol$^{-1}$, PDI=1.1, Perstrop, commercial name: CAPA 6806) into dichloromethane (DCM, Sigma-Aldrich)/ *N*,*N*-dimethylformamide (DMF, ReagentPlus® ≥ 99%, Sigma-Aldrich) (60/40 V/V) at a concentration of 15 wt.%. The PCL solution was delivered with a flow rate of 1mL.h$^{-1}$. The potential at the needle was $V_{needle}$= 25 kV and the distance was 13.5 cm.

**Electrospraying of hydroxyapatite**

After the step of electrospinning, a layer of electrosprayed HA microparticles was deposited. A 6 wt % hydroxyapatite (HA, Sigma-Aldrich, nanopowder ≤ 200 nm particles size (BET), ≥ 97 % synthetic) solution was prepared in ethanol (Sigma-Aldrich) 48 h prior to electrospraying. The potential at the needle was $V_{needle}$ =18 kV. The solution was delivered at a flow rate of 0.62 mL.h$^{-1}$.

### 2.2.4 *Controlled deposition of hydroxyapatite particles on electrospun fibers*

Bi-layer composite membranes containing hydroxyapatite (HA) were made in a two steps process. The first layer was elaborated by the electrospinning of a polymer (alginate or PCL) (**Figure 50-a**), and the second layer was elaborated by the electrospraying of HA (**Figure 50-b**).

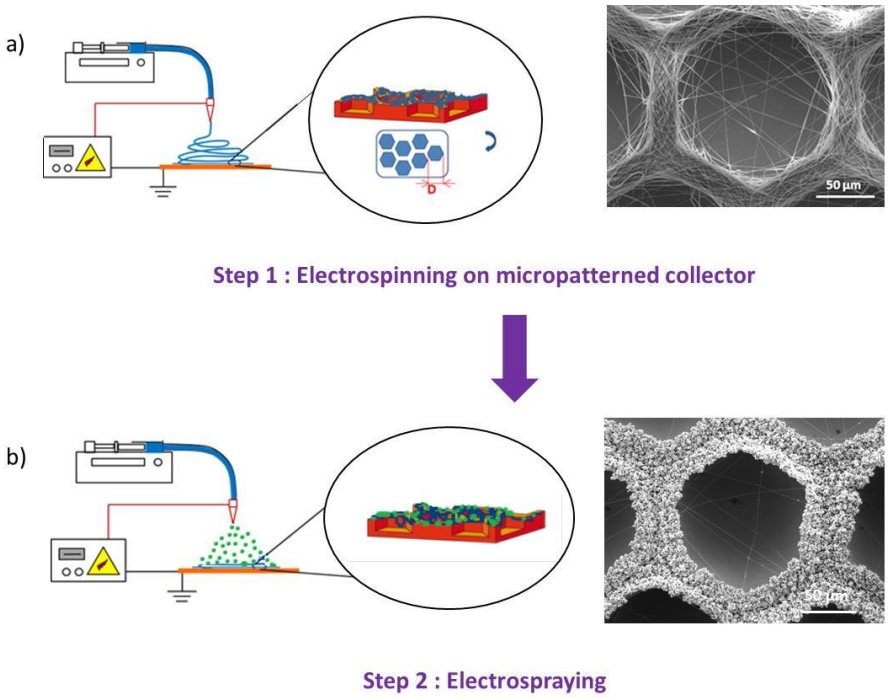


**Figure 50: The two step processes: a) Electrospinning onto a micropatterned collector; b) Electrospraying onto the thin layer of nanofibers deposited onto a micropatterned collector**

In this part, the micropatterned collectors are the same as the ones presented in the previous chapter 2. As we can see on the **Figure 51-a,** when HA is electrosprayed over a honeycomb collector (i.e.without the first layer of electrospun fiber). HA particles are deposited everywhere on the honeycomb micropatterns, inside the nests of the honeycomb as well as over the walls of the honeycombs. However, when PCL is first electrospun onto the honeycomb collector and followed by electrospraying of HA, the particles are selectively deposited over the walls of the honeycomb micropatterns with characteristic sizes ranging from 40 to 360 µm (**Figure 51-b-c**). As described in Chapter 2, when electrospinning of PCL is made onto a honeycomb collector, thin fibers are crossing the patterns remaining suspended in air. As PCL is not conductive, the suspended fibers cannot discharge. The areas inside the nests become positively charged and repulsive for the electrosprayed particles, forming an electrostatic template. Therefore the HA particles are driven toward the walls and exclusively deposit over them. It is then possible to spatially control the deposition of HA particles (**Figure 51-f)**.

When the first layer of electrospun fibers was made of alginate, there was not selective deposition of hydroxyapatite microparticles on the walls of the honeycomb patterns. This may be explained by the fact that alginate electrospun fibers are conductive. Thus, the electric charges can dissipate along the fibers towards the walls of the micropatterns. In this case, the

electrostatic template effect is not insured and the whole surface remains attractive for the particles **(Figure 51-d and Figure 51-e),** even if a slight selective deposition could be observed.

Because we were able to spatially control the deposition of hydroxyapatite onto a micropatterned honeycomb collector covered by a thin layer of PCL, we elaborated bi-layer PCL/HA electrospun-electrosprayed membranes. Such kinds of membranes were used to elaborate an biochip device dedicated to the screening of different micropatterns structures in order to find the best architecture for bone regeneration.

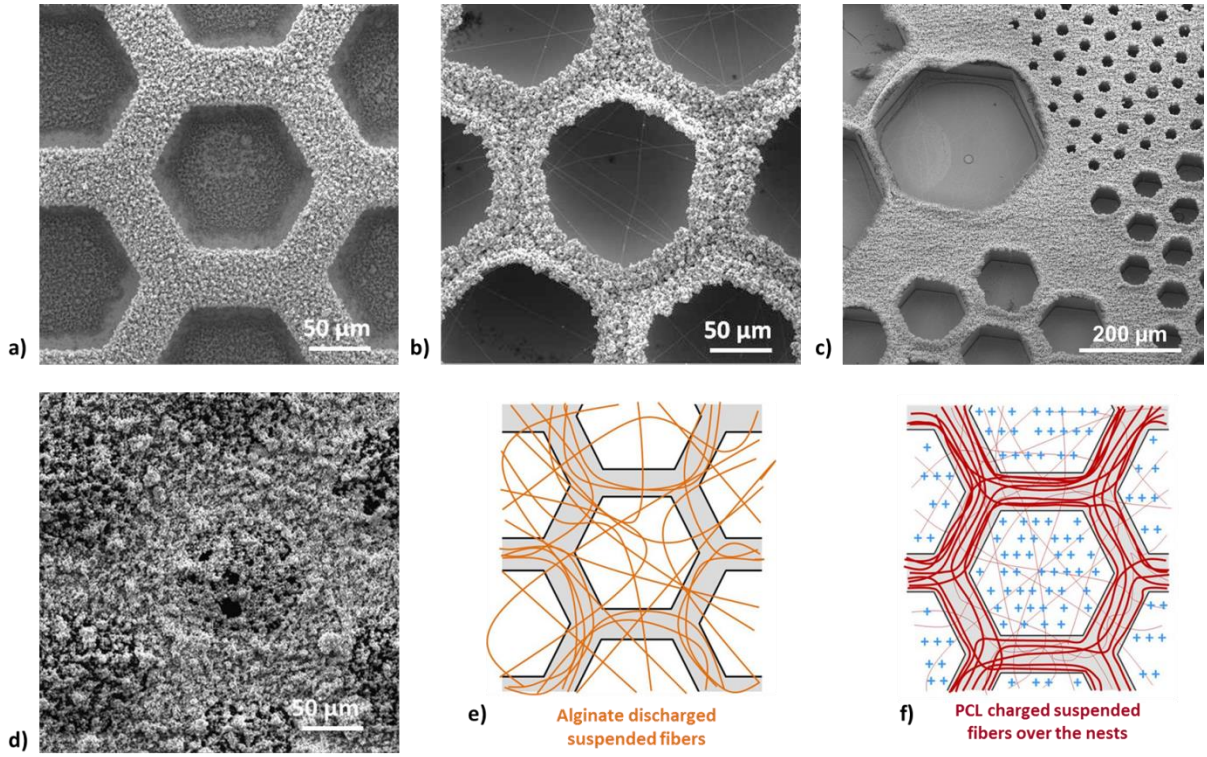


**Figure 51: a) SEM image of a hydroxyapatite electrospray deposition onto a honeycomb micropatterned collector without electrospun fibers; b) SEM images of bi-layer electrospun/electrospray PCL/HA membrane onto honeycomb micropatterned collector; c) Same conditions as c) but at another scale showing different honeycomb pattern sizes; d) SEM images of a bi-layer electrospun/electrospray Al/HA membrane onto a honeycomb micropatterned collector**

**e) Scheme of the deposition of alginate fibers onto a honeycomb micropatterned collector showing the electric charges dissipated along the fibers towards the honeycomb walls; f) Scheme of the deposition of PCL fibers onto a honeycomb micropatterned collector with undischarged fibers showing the electrostatic template.**

## 2.3 Biochip by electrospinning and electrospraying: application for the screening of PCL/HA microstructured composites for bone regeneration

To fabricate the biochip device for the screening of composite fibrous structures, we designed a micropatterned collector with 21 circular areas having their own micropatterned structures; where each area of 5 mm in diameter corresponds to a milli-culture dish (or well) of the biochip (see **Figure 52-a**). Each area of the collector is composed of honeycomb, block, bar, maze or flat micropatterns with their own characteristic sizes D, L and H as shown in **Table 12** and **Figure 52-b,52-c, 52-d and 52-e**. After the electrospinning and electrospraying steps (**Figure 52-f and 52-g**), the structured membrane (**Figure 52-h**) is peeled from the collector and integrated in the biochip for cell culture and biological characterization as shown in **Figure 52-i**.

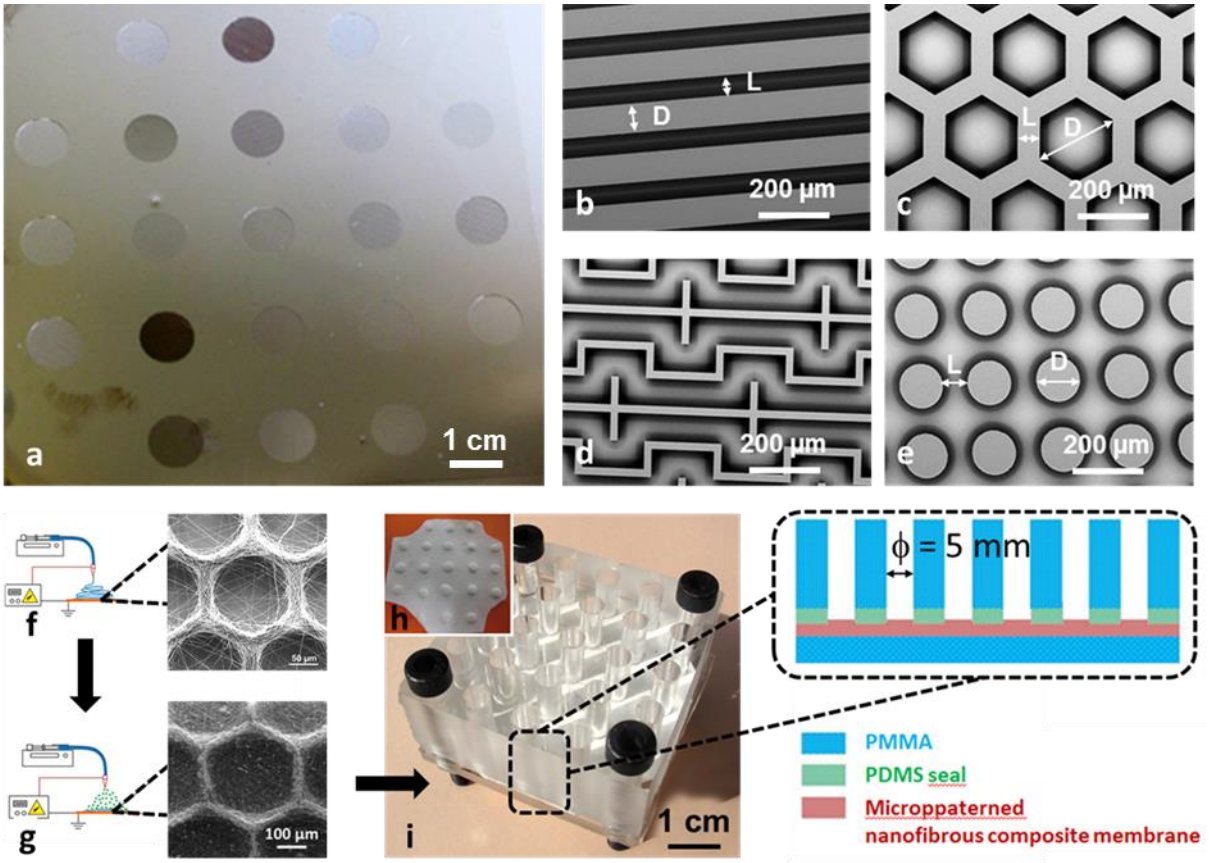


**Figure 52: The main steps for the elaboration of a biochip. a) A micropatterned collector elaborated from photolithographic processes. b) $Bar_{20,80}$ structures. c) $Block_{60,80}$ structures. d) Maze structures. e) $Hex_{240,20}$ structures. f) Electrospinning on the micropatterned collector. g) Electrospraying on the electrospun fibers. h) A microstructured composite membrane with the 21 microstructured areas. i) The membrane integrated in the biochip and its design.**

| Structure | Name | D (µm) | L (µm) | H (µm) | L / H |
|---|---|---|---|---|---|
| Bar | $Bar_{20,20}$ | 20 | 20 | 60 | 0,3 |
| | $Bar_{80,20}$ | 80 | 20 | 60 | 0,3 |
| | $Bar_{20,60}$ | 20 | 60 | 60 | 1,0 |
| | $Bar_{80,60}$ | 80 | 60 | 60 | 1,0 |
| | $Bar_{20,80}$ | 20 | 80 | 60 | 1,3 |
| | $Bar_{80,80}$ | 80 | 80 | 60 | 1,3 |
| Block | $Block_{60,80}$ | 60 | 80 | 60 | 1,3 |
| | $Block_{120,80}$ | 120 | 80 | 60 | 1,3 |
| | $Block_{60,40}$ | 60 | 40 | 60 | 0,7 |
| | $Block_{120,40}$ | 120 | 40 | 60 | 0,7 |
| Hexagon | $Hex_{240,20}$ | 240 | 20 | 60 | 0,3 |
| | $Hex_{120,20}$ | 120 | 20 | 60 | 0,3 |
| | $Hex_{60,20}$ | 60 | 20 | 60 | 0,3 |
| | $Hex_{240,60}$ | 240 | 60 | 60 | 1,0 |
| | $Hex_{120,60}$ | 120 | 60 | 60 | 1,0 |
| | $Hex_{60,60}$ | 60 | 60 | 60 | 1,0 |
| | $Hex_{240,100}$ | 240 | 100 | 60 | 1,7 |
| | $Hex_{120,100}$ | 120 | 100 | 60 | 1,7 |
| | $Hex_{60,100}$ | 60 | 100 | 60 | 1,7 |
| Maze | Maze | 80 | 20 | 60 | 0,3 |
| Flat | Random | - | - | 0 | - |

**Table 12: Description of the 21 different micropatterns of the collector.**

**Table 12** shows in detail the characteristic sizes of the 21 micropatterns. The height H as well as the distance L between two patterns and the size D were chosen according to the work of Lavielle *et al.* explaining that structuration of electrospun nanofibers occurs efficiently when the ratio $L/H \leq 1.5$ [90]. In our case, H was fixed to 60 µm by the choice of the photoresist and the spin-coating conditions for its deposition and L values lower than 100 µm were chosen. Using such a collector, sequential electrospinning/electrospraying was carried out in order to elaborate a bi-layer of PCL nanofibers covered by a microstructured layer of HA microparticles.

### 2.3.1 *Protocols*

**Fabrication of the biochip collector**

Micropatterns of biochip collectors were obtained applying photolithographic processes on silicon wafers (mask aligner MJB4, SUSS Microtec). The photoresist used was the SU-8 2050 (Microchem). Electron beam evaporator Plassys MEB5505 was used to deposit a conductive layer (Al-160 nm and Au-40 nm) on the collectors to make them conductive.
On each biochip collector, 21 wells were fabricated with 21 different structures. Each well had a diameter of 5 mm and they were spaced from each other by 5 mm. 5 different kinds of structures were studied: hexagon, bar, block, maze and random structure. The width L between the patterns and the internal diameter D of the pattern varied for each structure (see **Table 12** for the definition of L and D for each structure).

**Elaboration of the biochip**

As shown in **Figure 52-i**, the biochip was a homemade device. It was composed of different elements:

- a 50x50 x20 mm PMMA plate drilled with 21 holes to form the wells, corresponding to the 21 different electrospun structures
- a 50x50 mm PDMS seal with a height of 4 mm with 21 holes corresponding to the ones of the PMMA plate.
- a PCL/hydroxyapatite membrane obtained with the biochip collector
- a 50x50 mm PMMA plate with a height of 5 mm

Before assembling, each part was sterilized in ethanol (except the PCL/HA membrane). The four parts were assembled together with four screws (see **Figure 52-i**). The assembled biochip was then exposed to UV light during 30 minutes to insure good sterilization.
The PDMS seal was homemade. A 10/1 ( wt/wt) mixture of PDMS-Sylgard Silicone Elastomer and Sylgard Curing Agent 184 ( Dow Corning Corp., Seneffe, Belgique) was poured into a petri dish.
Then the mixture of PDMS-elastomer and curing agent was cured at 65°C during 1 hour until the polymer became rigid. After cooling at room temperature, the PDMS seal was carefully peeled from the petri dish and perforated with a punch to make 21 holes with a diameter of 5 mm.

### 2.3.2 *Results and discussions*

With the different structures of the biochip collector, we showed that we were able to spatially control the HA deposition on the different type of patterns: hexagons, blocks, bars, and maze. Indeed, as presented on **Figures 53 a-b and Figure 54 a-c,** the "*electrostatic template effect*" induced by the thin electrospun layer of PCL firstly deposited on the collector led to a precise structuration of the HA microparticles on the collector patterns.

As shown in **Figure 53 a-b**, the thin fiber segments which are suspended over the hexagon cavities of the collector could not release their electrical charges, allowing the formation of repulsive areas inside the nests that prevent the deposition of the incoming particles. Conversely, the fibers which are in good contact with the walls of the honeycomb are able to discharge their electrical charges, allowing the deposition of HA particles especially on the walls. By increasing the width of the honeycomb walls, the HA particles deposited over all the wall surface, forming thicker HA walls **(Figure 53-b**).

Regarding the block pattern areas, the suspended fibers between the blocks could not discharge while the fibers deposited on the top of the blocks, which are perfectly in contact with collector, are able to dissipate the electric charges. In this case also, the jet of hydroxyapatite undergoes the repulsive effect of the charged areas leading to the preferential deposition on the top of the blocks forming small HA islands **(Figure 54-a**). Similarly, the selective deposition of HA was observed over bar and maze micropatterns (**Figure 54-b and 54-c)**.

In our device screening, we wanted to use PCL/HA electrospun-electrospray composite membrane that could be manipulated and integrated into a biochip. Our first strategy was to electrospin the PCL fibers for a short time in order to insure an efficient electrostatic template effect allowing a perfect controlled microstructuration of HA microparticles. In this case, we should have let the membrane on the collector and integrate both the membrane and the collector in the biochip to limit any manipulation of the membrane leading to its destruction. However, our choice was to use each collector for several times to elaborate a large number of membranes. Then, a thick bi-layer PCL/HA, showing better mechanical properties due to the long time deposition of PCL, would make this bi-layer easy to manipulate for further applications. Thus, we elaborated membranes having a fibrous layer enough thick in order to facilitate their peeling from the collector, their integration in the biochip device and finally their manipulation during several biological characterizations. An

optimal time of electrospinning of 13 min was thus necessary to fill this criterion while keeping at best the electrostatic template effect (**Figures 53 a'-b', 54 a'-c'**).

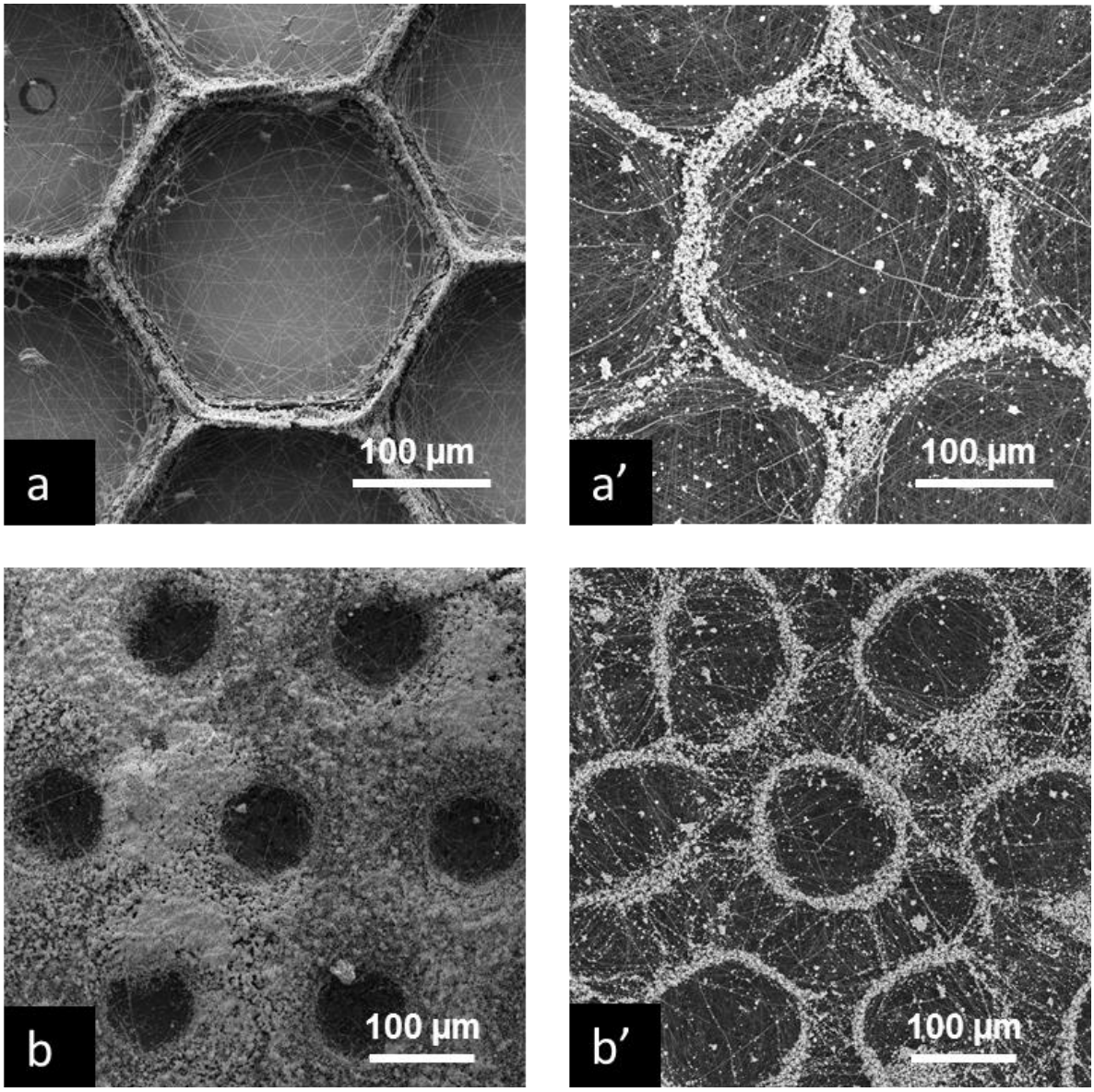


**Figure 53: SEM of structured bi-layers obtained after PCL electrospinning and 14min of HA electrospraying. a, b) Thin layer of nanofibers (1 min 30 of PCL electrospinning); a',b') Thick layer of nanofibers (13 min of PCL electrospinning); a,a') $Hex_{240,20}$; b,b') $Hex_{120,100}$.**

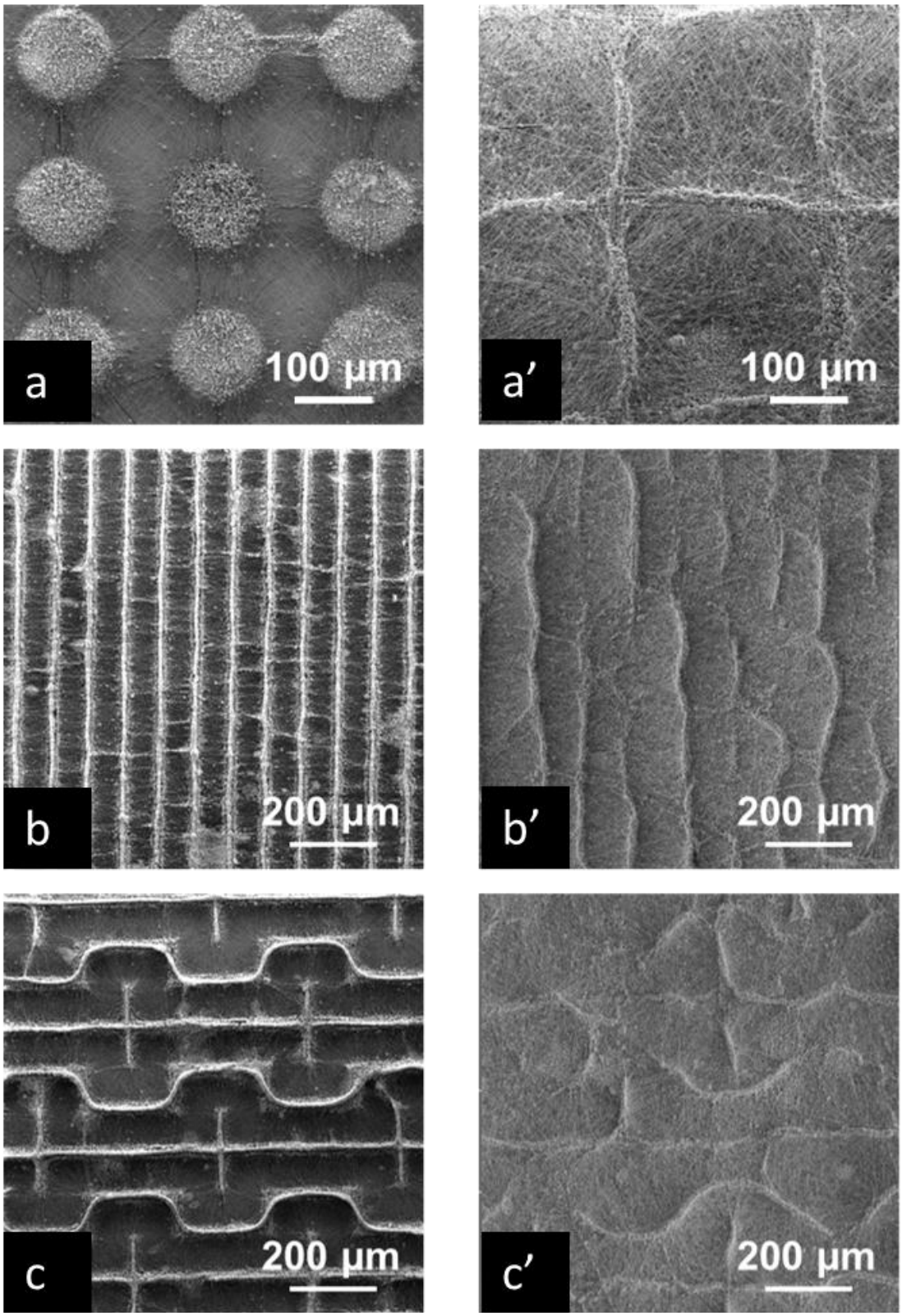


**Figure 54: SEM of structured bi-layers obtained after PCL electrospinning and 14min of HA electrospraying. a,b,c) Thin layer of nanofibers (1 min 30 of PCL electrospinning); a',b',c') Thick layer of nanofibers (13 min of PCL electrospinning); a,a') $Block_{120,80}$; b,b') $Bar_{20,80}$ ; c, c') Maze.**

Indeed, **Figures 53 a'-b'** and **54 a'-c'** shows that HA microstructuration and thus the electrostatic template effect can still occur even for a thick deposited PCL membrane. However, the structuration shows some differences compared to shorter time of PCL deposition.

First of all, we noticed that for all the composite micropatterns, the width of the HA patterns walls was not varying; its value $L_{HA}$ was ranged from 15 and 20 µm for each type of composite structure (See **Table 13**).

Regarding the honeycomb patterns, by changing the width of the honeycomb walls on the collector, we managed to tune the diameter and the shape of the honeycomb composite structure. For example, as seen on **Figure 53-a'**, for $Hex_{240,20}$, HA microparticles had covered almost all the wall, forming well controlled hexagonal structure. However, for $Hex_{120,100}$, the morphology of the honeycomb patterns changed from a honeycomb shape to a circular shape in the composite structure (**Figure 53-b').** In this case, HA microparticles seem to particularly deposit only on the edges of the honeycomb walls. Sometimes, we observed that HA preferentially deposit at the center of the walls without recovering all the width of the wall (**Figure 55 g-g', d-d', e-e'**). Thus, as shown in **Table 13** the internal diameter of the honeycomb composite structure increased. Its value seems to correspond to the median internal diameter $D_m$ defined by $D_m = D + (L-L_{HA})$.

For two hexagon patterns $Hex_{120,20}$, $Hex_{60,20}$, (**Figure 55 b-b', c-c'**), the microstructuration of the nanofibers appears to be in competition with the self-assembling properties of the PCL nanofibers, leading a heterogeneity on the honeycomb pattern size (**Table 13**).

Finally, hexagon patterns are the ones which are capable to impose their morphology the most efficiently (**Figure 55 and Figure 53-a'**). Only two hexagonal patterns did not lead to well-organized HA microparticles ( **Figure 55 f-f', i-i'**).

In the case of bar patterns (**Figure 56**), the structuration after 13 min of electrospinning was only possible for the largest gap L corresponding to the imposed length of the fiber portion suspended in the air and participating to the electrostatic template effect. For the lowest L values, the slightest defect induced on the electrostatic template led to the loss of the structuration by electrospraying. Due to the propensity of the PCL fibers to self-assemble after a long time of electrospinning [99], the formation of bundles of fibers crossing the bar gap was observed. These bundles induced a roughness and may also allow the electric charges dissipation along their axes favoring thus their coverage by HA electrosprayed microparticles. Moreover, the electric contact between the top surface of the fibers and the top

surface of the patterns was also partially lost as shown in **Figure 54-b',** leading to interrupted HA bars patterns with a width narrower than the bar collector (**Table 13**).

In the case of block patterns, similar phenomena were observed and led to the loss of the block structures at the expense of grid structures (**Figure 54-c'**). Indeed, with an increase of electrospinning time, PCL formed bundles of aligned fibers between the different block patterns, forming an electrospun grid. Consequently, HA preferentially deposited on the PCL bundles, leading to the formation of a hydroxyapatite grid (**Figure 57**).

In conclusion, among the 21 areas, 15 of them had a well-controlled structuration which is detailed in **Table 13** and were thus used to study the effect of the structure of the membrane on the biological properties. For the 6 other areas, the patterning was unfortunately lost.

| **Structure** | **Name** | **Controlled electrospraying after 1 min of electrospinning** | **Controlled electrospraying after 13 min of electrospinning** | **Width of HA patterns (µm)** | **Gap between HA patterns (µm)** |
|---|---|---|---|---|---|
| Bar | $Bar_{20,20}$ | Yes | No | - | - |
| | $Bar_{80,20}$ | Yes | No | - | - |
| | $Bar_{20,60}$ | Yes | Yes | 18 ± 4 | 110 ± 30 |
| | $Bar_{80,60}$ | Yes | Yes | 18 ± 5 | 123 ± 9 |
| | $Bar_{20,80}$ | Yes | Yes | 15 ± 3 | 94 ± 30 |
| | $Bar_{80,80}$ | Yes | No | - | - |
| Block | $Block_{60,80}$ | Yes | Yes | 17 ± 3 | 118 ± 16 |
| | $Block_{120,80}$ | Yes | Yes | 17 ± 4 | 174 ± 12 |
| | $Block_{60,40}$ | Yes | No | - | - |
| | $Block_{120,40}$ | Yes | Yes | 16 ± 2 | 143 ± 15 |
| Hexagon | $Hex_{240,20}$ | Yes | Yes | 19 ± 3 | 239 ± 11 |
| | $Hex_{120,20}$ | Yes | Yes | 18 ± 3 | 121 ± 32 |
| | $Hex_{60,20}$ | Yes | Yes | 17 ± 3 | 139 ± 49 |
| | $Hex_{240,60}$ | Yes | Yes | 16 ± 3 | 292 ± 21 |
| | $Hex_{120,60}$ | Yes | Yes | 17 ± 2 | 152 ± 15 |
| | $Hex_{60,60}$ | Yes | No | - | - |
| | $Hex_{240,100}$ | Yes | Yes | 18 ± 2 | 301 ± 16 |
| | $Hex_{120,100}$ | Yes | Yes | 17 ± 3 | 118 ± 10 |
| | $Hex_{60,100}$ | Yes | No | - | - |
| Maze | Maze | Yes | Yes | 15 ± 3 | - |
| Flat | Random | Random, homogeneous deposition | Random, homogeneous deposition | HA covering all the surface | - |

**Table 13: Summary of the 21 micropatterned structures obtained after electrospinning/electrospraying**

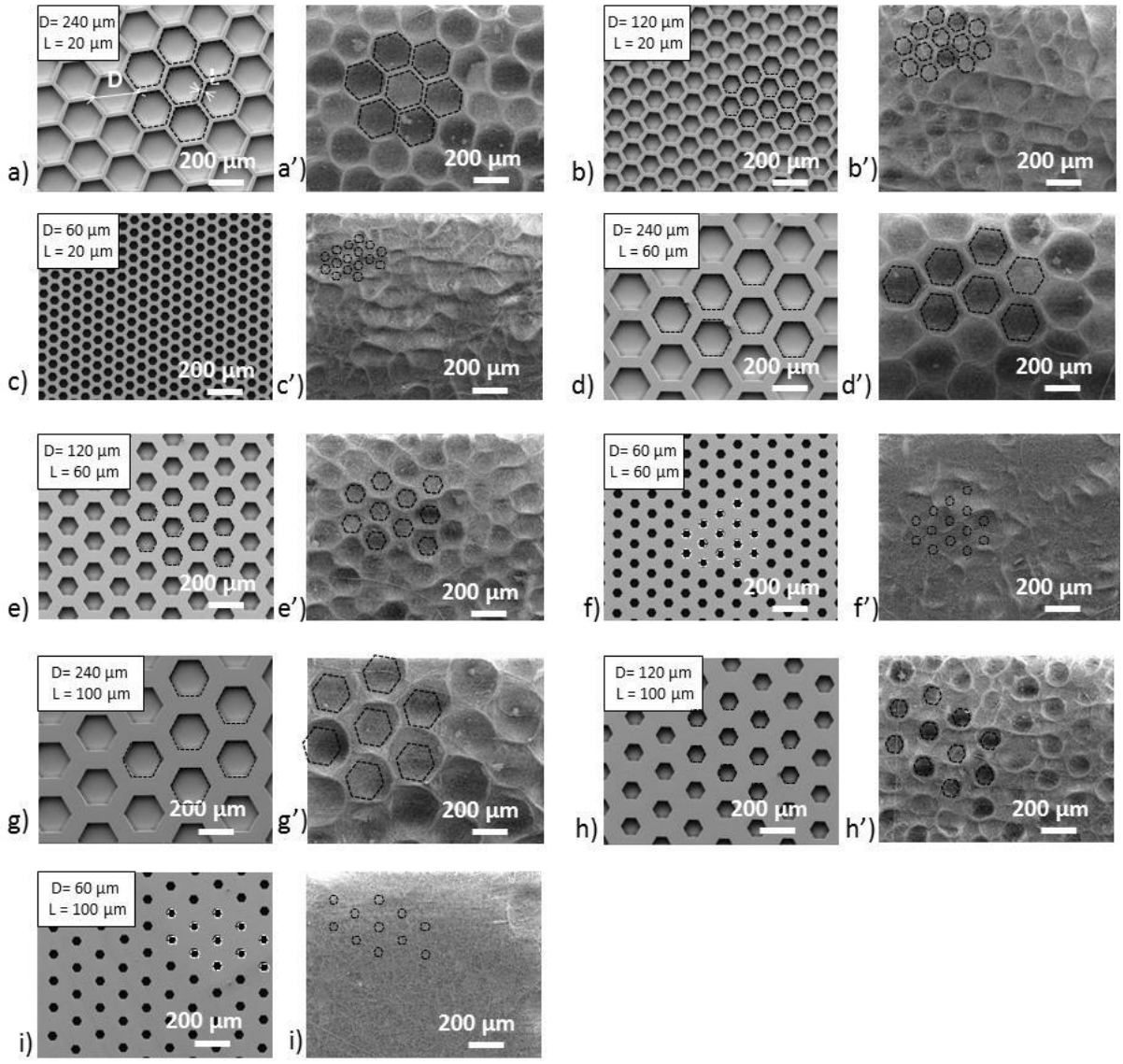


**Figure 55: a, b, c, d, e, and f: SEM images of the different micropatterned hexagons of the biochip collector; a', b', c', d', e', and f': SEM images of the PCL/HA membrane obtained with the corresponding micropatterned honeycomb collector; a and a') $Hex_{240,20}$; b and b') $Hex_{120,20}$; c and c') $Hex_{60,20,}$; d and d') $Hex_{240,60}$; e and e') $Hex_{120,60}$; f and f') $Hex_{60,60}$; g and g') $Hex_{240,100}$; h and h') $Hex_{120,100}$; i and i') $Hex_{60,100}$.**

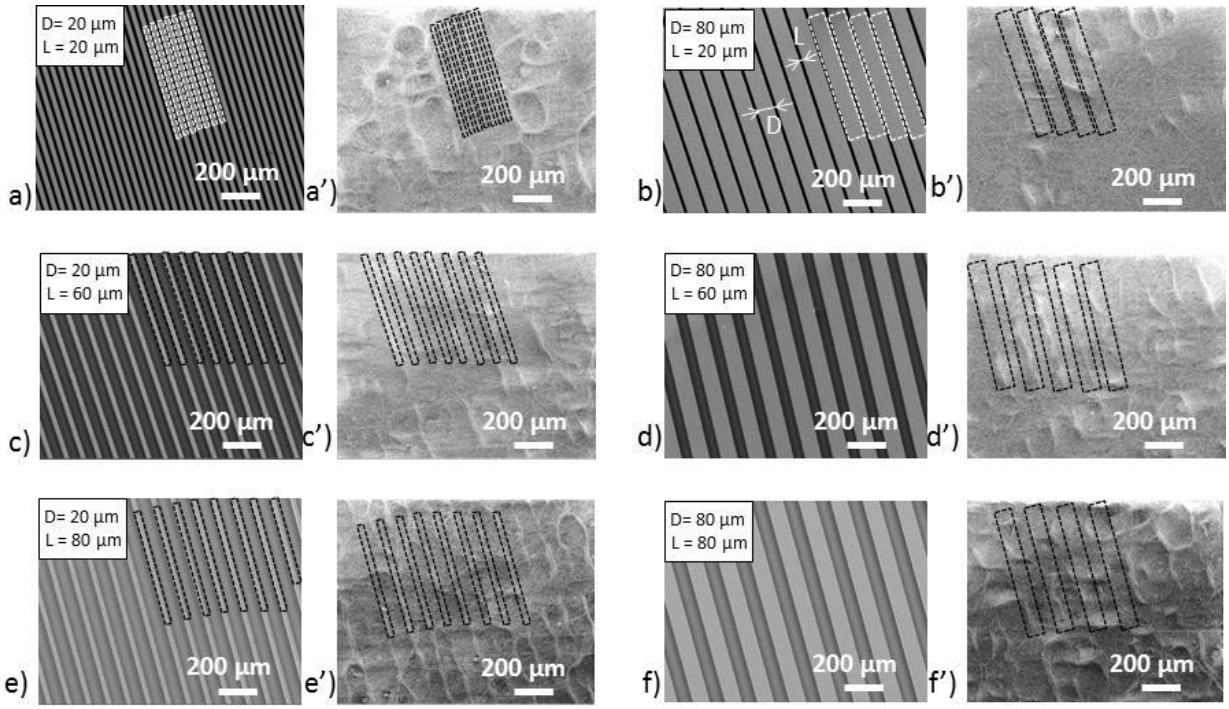


**Figure 56: a, b, c, d, e, and f: SEM images of the different micropatterned bar structures; a', b', c', d', e', f': SEM images of the PCL/HA membrane obtained with the corresponding micropatterned bar areas; a and a') $Bar_{20,20}$; b and b') $Bar_{80,20}$; c and c') $Bar_{20,60}$; d and d') $Bar_{80,60}$; e and e') $Bar_{20,80}$; f and f') $Bar_{80,80}$.**

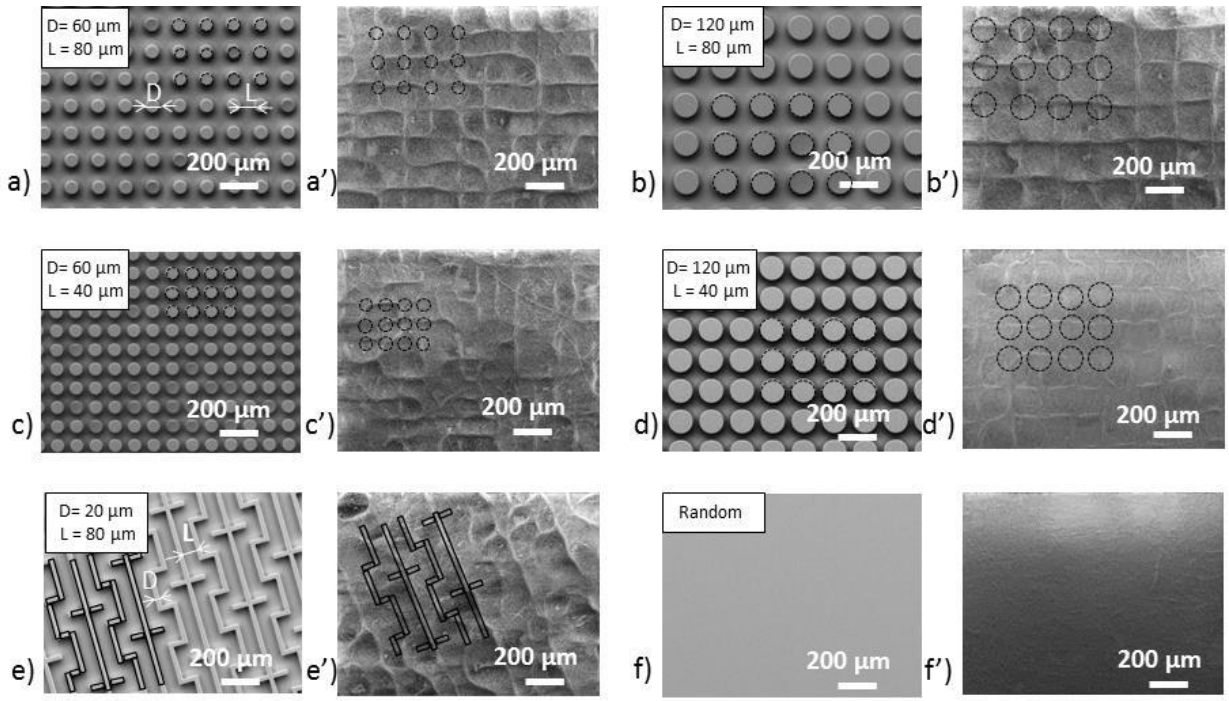


**Figure 57: a, b, c, d, e, and f: SEM images of the different micropatterned structure (block, maze, random) of the biochip collector; a', b', c', d', e', and f': SEM images of the PCL/HA membrane obtained with the corresponding micropatterned structure collector; a and a') Block $_{60,80}$; b and b') Block$_{120,80}$; c and c') Block$_{60,40}$; d and d') Block$_{120,40}$; e and e') Maze structure; f and f') Random well**

## 2.4 Screening of composite fibrous structured materials for bone regeneration: preliminary results

In this part, we show the preliminary results concerning the use of our composite hydroxyapatite/PCL biochip to screen in parallel the effect of the different fibrous architecture on the proliferation and activity of osteoblast-like MG63 cells. The main role of osteoblasts is to produce and secrete organic and inorganic bone ECM, called ostoid [239]. The organic bone matrix is constituted of various proteins, such as collagen, osteonectin, osteocalcin, and sialoproteins such as osteopontin and BSPII (Bone SialoProtein II). The inorganic bone matrix is constituted of calcium-phosphate salts. Osteoconductivity of the various scaffold architecture was investigated by monitoring the proliferation and ECM forming activity of osteoblasts cultured in the biochip wells.

We chose different biological characterization to evaluate the production of the extracellular matrix by the MG-63 osteoblasts-like cells and the mineralization process.After 21 days, the cells nuclei were stained with DAPI in order to evaluate cells proliferation and localization on the structured scaffold. Then the production of ECM by MG63 cells was estimated by immunofluorescence assays. First, after 14 days and 21 days, the expression of BSPII, an RGD-type protein synthetized by osteoblasts and recognized by integrin receptors, was observed. Then, after 21 days, immunofluorescence assay of osteocalcin, a protein synthesized solely by osteoblasts, was performed. Finally, the presence of calcium rich deposits by osteoblasts was revealed by a biochemical assay using Alizarin Red Staining after 21 days of cell culture.

### 2.4.1 *Protocols for biological characterization*

**Cell culture and seeding**

Human osteoblast cells were obtained from the cell line MG-63 coming from human osteosarcosis. MG-63 osteoblasts were cultured in DMEM® (BioWhittaker® Lonza, France) completed with 10% FBS (Gibco® Life Technologies™, France) , 50 $U.mL^{-1}$ penicillin, 50 $\mu g.mL^{-1}$ streptomycin, 2,5 $\mu g.mL^{-1}$ amphotericin B (BioWhittaker® Lonza, France), 200mM sodium pyruvate (Gibco® Life technologies™, France), and 200mM of glutamine (PAA, France) in 75 $cm^2$ flasks. The cells were incubated at 37°C in a humidified atmosphere of 5% $CO_2$ and fed every 3

days. When cells reached sub-confluence, they were harvested by trypsin-EDTA treatment and viable cells were counted by trypan blue assay. The MG-63 osteoblasts were then seeded into the biochip 21-well plate at a density of 3000 cells per well and cultured with DMEM®. The seeded biochip were incubated at 37°C in a humidified atmosphere of 5% $CO_2$ and fed every 3 days.

**Immunocytochemistry staining and observation**

Biochip seeded with MG-63 osteoblasts were cultivated for 21 days in Dulbecco's modified eagle medium (D-MEM®, PAA, Austria) supplemented with 10% fetal bovine serum (FBS), 50 U/mL penicillin, 50µg/mL streptomycin, 5µg/mL Fungizone and 1% sodium pyruvate. Then, they were fixed with 4% paraformaldehyde for 1 h at 37°C, permeabilized and saturated with a solution of 0.1% Triton X-100 and 1% BSA diluted in PBS for 1 h. After washing with PBS, the biochips were then incubated for 30 min with Alexa Fluor 546–conjugated phalloidin (1/200, Molecular Probes) for F-actin labelling and 5 min with 200 nM DAPI (Sigma) for nuclear staining. Bone growth induction and extracellular matrix synthesis were measured by assaying expression of osteocalcin and BSPII, using polyclonal goat anti-oscteocalcin (1/200; Santa Cruz Biotechnology) and monoclonal mouse anti-BSPII (1/200; Santa Cruz Biotechnology) overnight at 4 °C.After washing with PBS three times for 10 min, the seeded biochip were incubated with secondary anti-goat or anti-mouse antibodies conjugated to Alexa Fluor 488 (1/200, Invitrogen). The biochips were observed under an epifluorescence microscope (LEICA DM 4000 B). Image treatment was carried out with Image J software.The gain exposition was 3 for the DAPI, osteocalcin or BSPII. The time exposition for DAPI was 350 milliseconds and the time exposition for osteocalcin was 920 milliseconds. The time exposition for BSPII expression was 500 milliseconds. BSPII expression was measured after 14 and 21 days of cell culture in two different biochips devices while osteocalcin expression was observed after 21 days of cell culture in one biochip device.

**In vitro examination of mineralization using Alizarin Red S staining after 21 days of cell culture**

Alizarin Red S powder was dissolved in distilled water in a concentration of 2 g for 100 mL. The pH of the Alizarin Red S solution was adjusted between 4.1 and 4.3. After washing the scaffolds with PBS twice, the cells were fixed by adding 75% ethanol in each well of the biochips. The biochips were incubated in the Alizarin Red solution for 20 min and then thoroughly rinsed with distilled water. The biochips were then observed under an optical microscope. Image treatment was carried out with Image J software. Three biochips were incubated with the Alizarin Red solution: two biochips seeded with MG-63 cells and one biochip without cells (the control).

For each well, the mean grey value was measured (between 0 and 255). We define the Alizarin Red Intensity: *Alizarin Red Intensity = 255-mean grey value.*

### 2.4.2 *Results and discussion*

**Observation of MG63 osteoblasts on the various micropatterned structures**

The proliferation and localization of MG63 osteoblasts on the micropatterned scaffold was observed by staining the cells nuclei with DAPI after 21 days of culture (**Figure 58**).

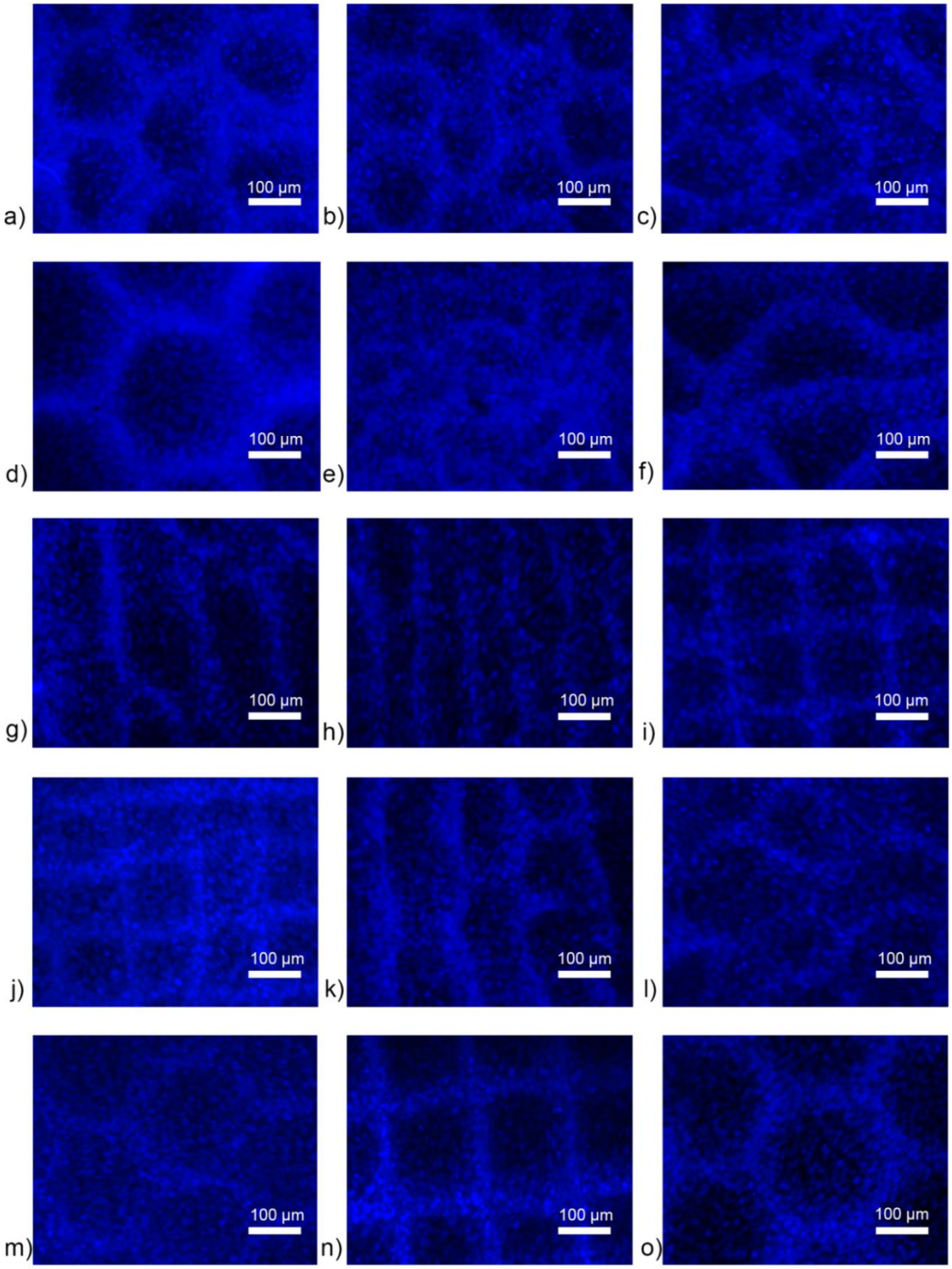


**Figure 58 : Observation of MG-63 osteoblasts adhesion within the micropattern composite electrospun wells of the biochip after 21 days (nucleus stained with DAPI in blue) : a) $Hex_{120,100}$; b) $Hex_{120,60}$; c) $Hex_{60,20}$; d) $Hex_{240,100}$; e) Random; f) Maze; g) $Bar_{20,60}$; h) $Bar_{20,80}$; i) $Block_{120,40}$; j) $Block_{60,80}$; k) $Bar_{80,20}$; l) $Hex_{120,20}$ ; m) $Hex_{240,20}$; n) $Block_{120,80}$; o) $Hex_{240,60}$.**

A large amount of cells is present in all wells, covering each time the whole micropatterned structure. However, a stronger blue intensity can be observed over the wall of the structures. In particular for hexagonal patterns, this result seems to be in contradiction with our previous study [219] (Chapter 2, §4.2), in which a preferential location of MG-63 cells inside the nests of the honeycomb was observed. This difference could be explained by the presence of hydroxyapatite particles located onto the structure walls in our composite PCL/HA biochip. MG-63 cells seem to have a higher affinity for hydroxyapatite then PCL fibers which are hydrophobic.

**Expression of bone ECM proteins by immunofluorescence assays**

After 14 days and 21 days of cell culture, BSPII expression was observed for the different composite fibrous structures. The fluorescence intensity was similar at 14 and 21 days and for all microstructures of the biochip. **Figure 59** shows the fluorescence image obtained for the random well and a hexagon well, showing a significant expression of BSPII by the MG-63 cells.
This result also demonstrates that the home-made biochip device allows cell proliferation and extra-cellular matrix synthesis *in vitro*.

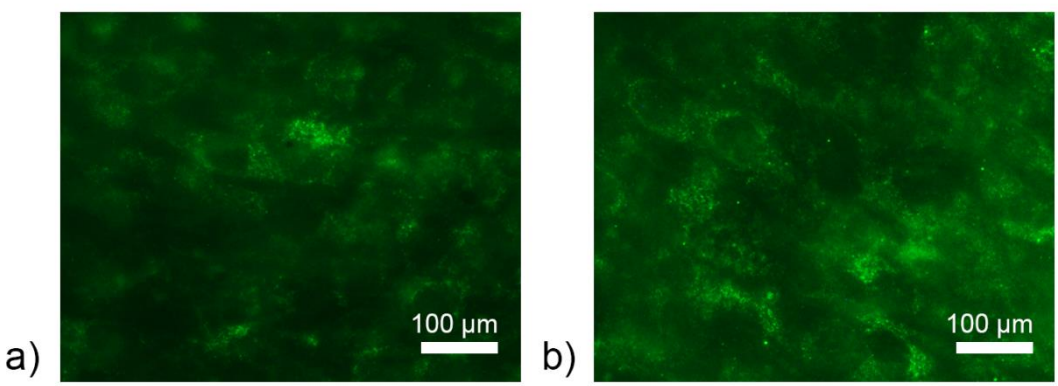


**Figure 59: Observation of BSPII expression after 14 days of MG-63 osteoblast cell culture: a) on the membrane without structure; b) on a honeycomb pattern ($Hex_{120,60}$)**

In contrast with BSPII, important differences are observed in the expression of osteocalcin by the cells as a function of the scaffold microstructures (**Figure 60**).

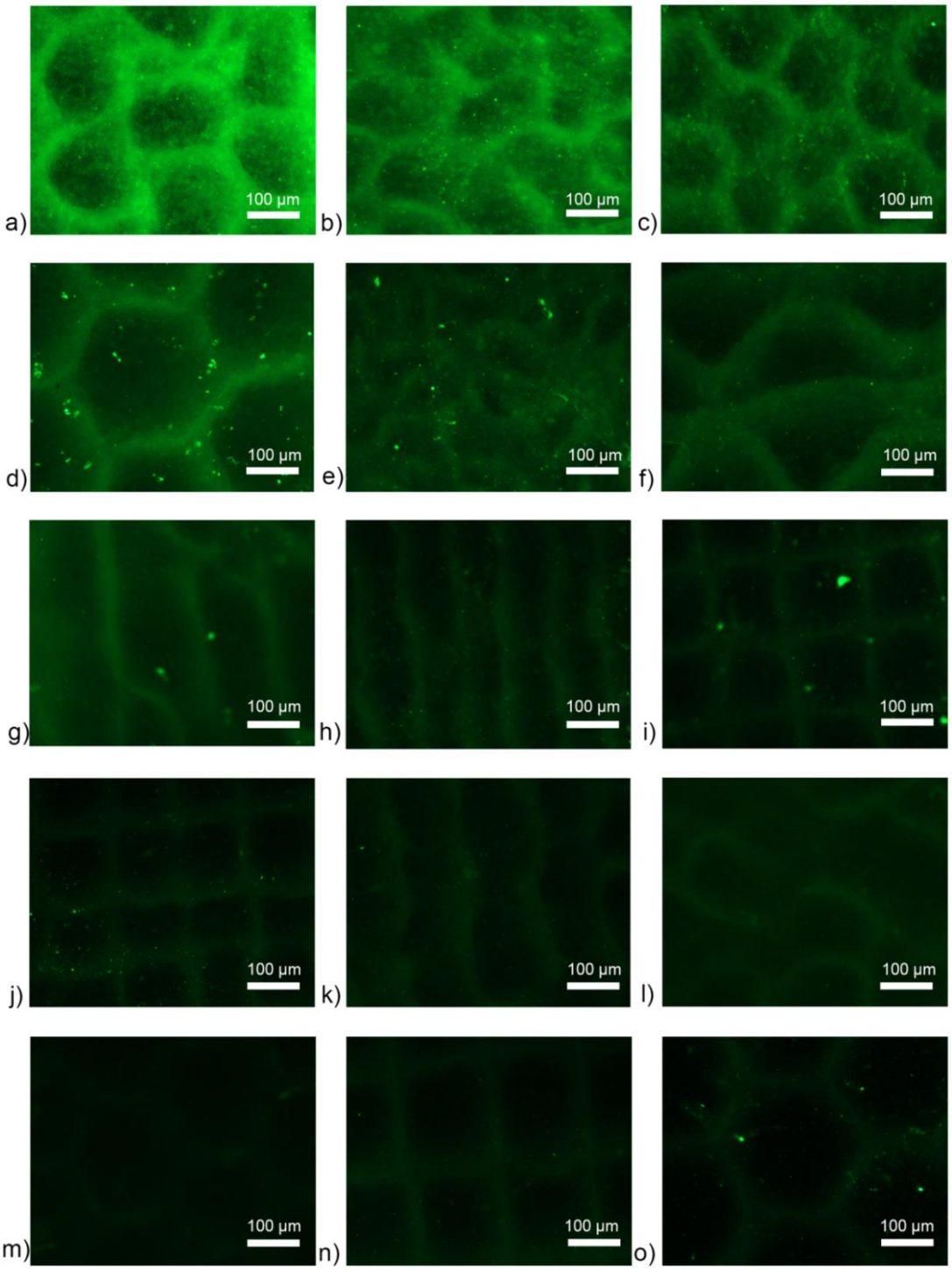


**Figure 60 : Observation of osteocalcin (OCN in green) expression of MG-63 osteoblasts after 21 days of culture : a) $Hex_{120,100}$; b) $Hex_{120,60}$; c) $Hex_{60,20}$; d) $Hex_{240,100}$; e)Random; f) Maze; g) $Bar_{20,60}$; h) $Bar_{20,80}$; i) $Block_{120,40}$; j) $Block_{60,80}$; k) $Bar_{80,20}$; i) $Hex_{120,20}$; m) $Hexa_{240,20}$; n) $Block_{120,80}$; o) $Hex_{240,60}$.**

In **Figure 60**, the fluorescence images are presented by decreasing fluorescence intensity. It is then obvious that some hexagonal patterns (**$Hex_{120,100}$**; **$Hex_{120,60}$**, **$Hex_{60,20}$** and **$Hex_{240,100}$**) showed higher fluorescence intensity than other types of patterns.

A comparison between the structured and the random scaffolds was performed by calculating the ratio of the intensity of OCN expression within the micropatterned well (I-OCN Structure) over the intensity of OCN expression within the random well (I-OCN Rd). Because general tendencies have been observed as a function of the pattern family, average values were given for each family (**Figure 61**).

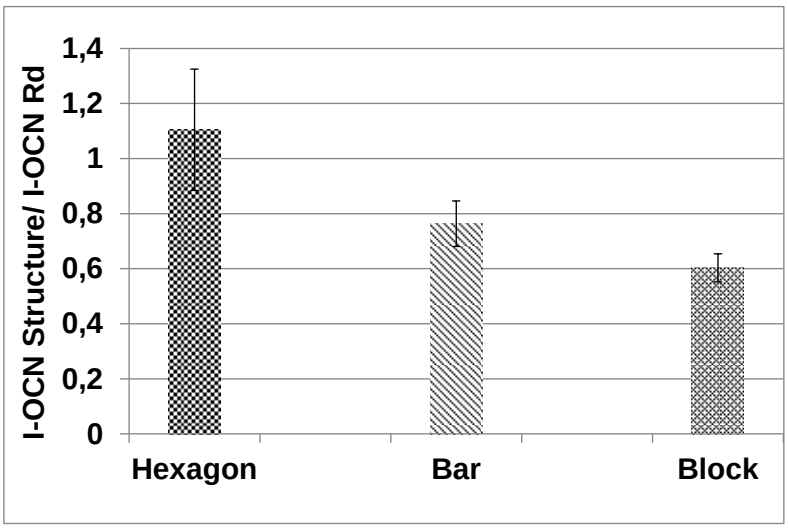


**Figure 61: Relative intensity of OCN expression of MG-63 osteoblasts onto hexagon, bar, and block patterns (I-OCN Structure) in regard to the intensity of OCN expression within the random well (I-OCN Rd) after 21 days of culture.**

A slight improvement of osteocalcin expression by cells cultured on hexagon structured scaffolds as compared to the random scaffold was oberved. However, for bars and blocks a lower osteocalcin production seems to be obtained. More immunoassays experiments should be done to confirm these tendencies.

### Mineralization of the scaffold by MG63-cells

In order to evaluate the mineralization of the scaffolds by the MG-63 osteoblast-like cells, Alizarin Red coloration of the membrane after 21 days of cell culture was performed. In this assay, calcium salts are stained in red and a stronger red intensity indicates the presence of higher amount of calcium salts. Because our membrane already contains a certain amount of hydroxyapatite, a negative control test has been carried out by Alizarin Red coloration of a biochip membrane containing hydroxyapatite without cells (data not shown).

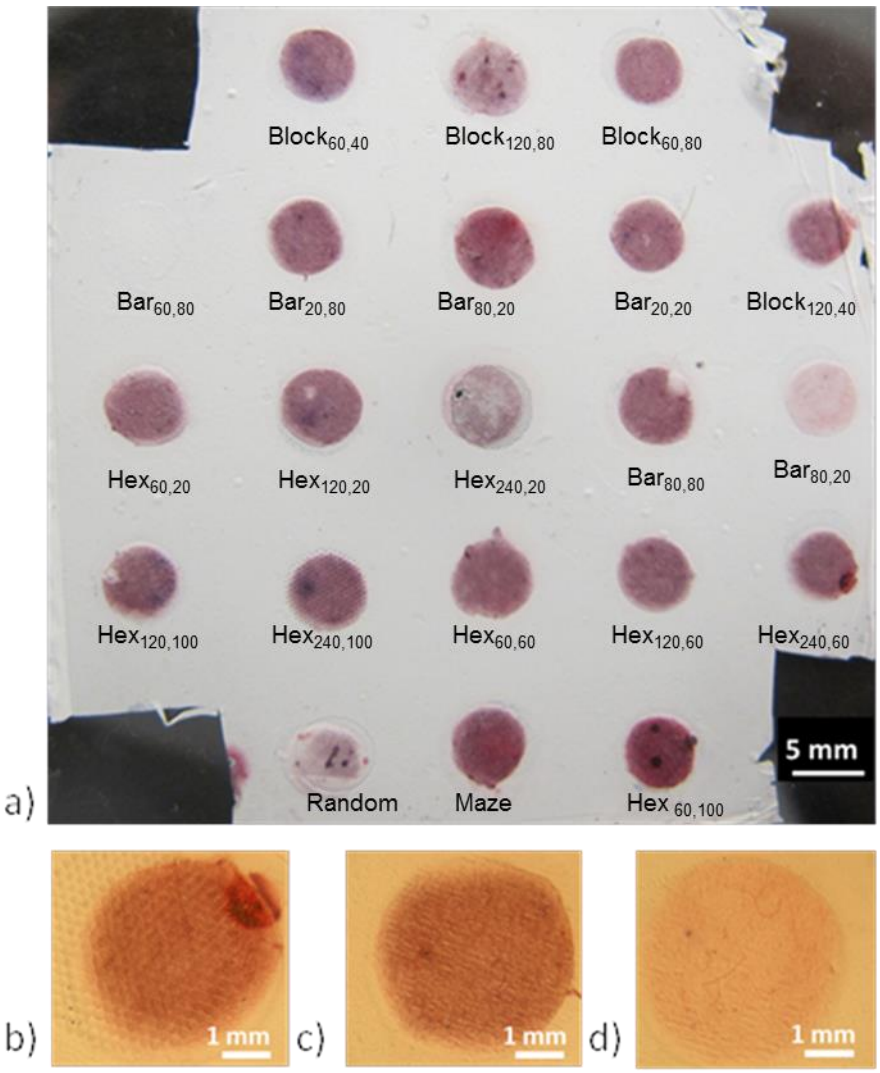


**Figure 62: a) Photograph of a biochip membrane after Alizarin Red coloration after 21 days of *in vitro* culture; b); Stereomicroscope image of an hexagon well ( $Hex_{240,60}$); c) Stereomicroscope image of a bar well ($Bar_{20,80}$); d) Stereomicroscope image of a bar well ($Bar_{80,20}$)**

**Figure 62** shows the membrane after removing from the microchip and coloration by Alizarin red. Differences in Alizarin Red intensity are observed depending on the micropattern structures ranging from dark red (**$Hex_{240,60}$: Figure 62-b**) to light pink (**$Bar_{80,20}$: Figure 62-e**) .

Depending on the micropattern structure onto which the cells were in contact, *in vitro* mineralization has been more or less fast or has not even occurred at all (**$Bar_{80,20}$: Figure 62-e**). Finally, determination of the Alizarin Red intensity, defined as Alizarin Red intensity=255-mean gray value, was performed using image J.

In order to compare the different type of structures with the random scaffold, we present in **Figure 63** the ratio of the mean Alizarin Red intensity of the structure family over the Alizarin Red intensity of the random scaffold.

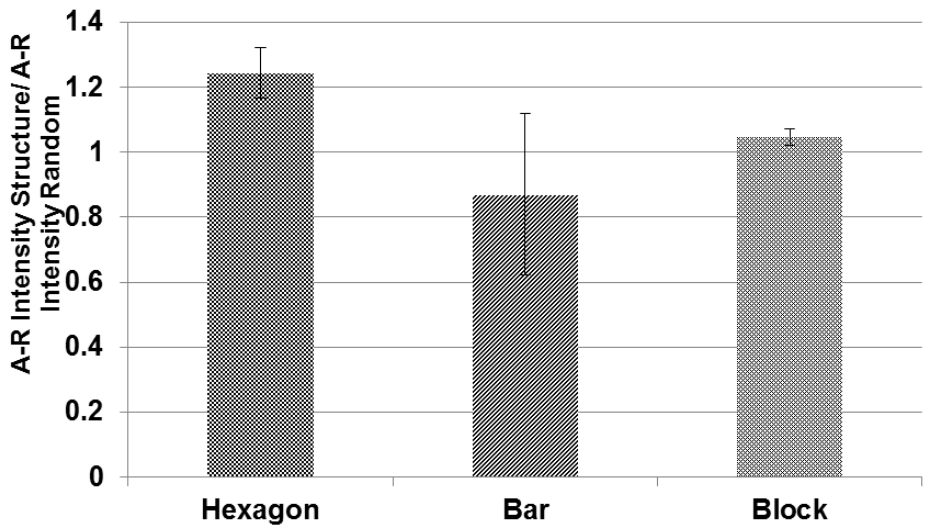


**Figure 63: Relative Alizarin Red Intensity of micropatterned wells after the Alizarin Red coloration (A-R Intensity structure) in regard to the Alizarin Red intensity of random well (A-R Intensity Random).**

As for the osteocalcin expression, the mineralization on hexagonal structures seem to be the more important, it is particularly true for **$Hex_{240,100}$, $Hex_{120,100}$, $Hex_{240,60}$** and **$Hex_{120,60}$,** which were the structures with the higher osteocalcin expression. It seems that the honeycomb patterns with an average diameter of 300 µm ($Hex_{240,10}$, $Hex_{240,60}$) and the circular patterns with a diameter of 150 µm ($Hex_{120,100}$) are structures that allow an improvement of the mineralization process compared to the

random structure. Bars and blocks, on the contrary, do not seem to improve mineralization of the scaffold by the cells.

## 2.5 Conclusions

In the first part of this chapter, we explained the spatially controlled deposition of microparticles on a thin electrospun micropatterned membrane, which played the role of an "electrostatic template" for the particles. Then, we demonstrated the elaboration of a new kind of biochip dedicated to the screening of fibrous composite structure for bone regeneration applications. Electrospun-electrosprayed PCL/HA membrane was elaborated by successive electrospinning PCL and electrospraying hydroxyapatite on a micropatterned collector containing 21 micropatterns such as hexagon, bar, block, and maze. We showed the effect of the thickness of the PCL electrospun layer on the HA structuration. For short time of electrospinning (i.e. very thin layer of fibers), the HA particles precisely covered all the top surface of the walls of the patterns. For longer time of electrospinning, the mechanism of HA structuration was more complex in the case of pattern walls much larger than 20 µm. However, a thick electrospun layer was necessary to achieve good mechanical properties allowing the manipulation of the membrane. Finally, this membrane was integrated into a small PMMA plate for the fabrication of a biochip dedicated to the screening of composite electrospun-electrosprayed structures.

MG-63 osteoblasts-like cells were then successfully cultured into the different wells of the biochip and immunochemistry as well as biochemistry assays were performed in order to evaluate the production of specific proteins and calcium salts of the bone ECM by the MG-63 cells. The biochip device was then successfully tested with MG-63 cells. General trends could be observed from these experiments suggesting that hexagonal patterns are more adapted to the culture of osteoblasts than blocs or bars. These results show that our biochip could be a good device to screen in parallel different scaffold structures for various tissue engineering applications. However, repetitions of the biological experiments have to be performed to confirm the preliminary results obtained in the case of osteoblasts. Adjustment of the design of the microchip in order to use a microplate delivery system and a microplate reader would render the multiplication of assays easier.

In the second part of this chapter, we present another strategy using electrospinning of nanofibers and electrospraying of microparticles on micropatterned collector in order to elaborate new kind of 3D scaffolds with controlled pore size. This work is published in the journal *Polymer*.

## 3. 3D composite electrospun scaffold with controlled pore size

## Well-Organized 3D Nanofibrous Composite Constructs using Cooperative Effects between Electrospinning and Electrospraying

***Polymer*, 2014, Vol. 55, pp. 5781-5787**

**Corinne R. Wittmer, Anne Hébraud, Salima Nedjari, Guy Schlatter**

**Abstract:**

A new strategy to generate nanofibrous composite constructs with a controlled internal 3D microstructure is proposed. The process exploits the cooperative effect of electric field and charges occurring when electrospinning and electrospraying are carried out alternately on a micropatterned collector. Experiments and numerical simulations show that the nanofibers form a perfect electrostatic template capable of controlling the deposition of the microparticles, which in turn help the electric charge release and the building of the construct. As an example, we show that 3D nanofibrous constructs having cylindrical pores that internal diameter could be precisely tuned from tens to hundreds of microns can be obtained. Furthermore, tensile measurements showed good mechanical properties allowing the facile manipulation and handling of these 3D composite constructs. Furthermore, this process has the advantage to enable the design of composite materials made of particles and fibers of different nature and properties that can be chosen depending on the intended application.

### 3.1 Introduction

Significant efforts have been invested in the developments of methods able to generate 3D nanofibrous structures. Compared to their 2D counterparts, 3D structures with a significant thickness are showing substantial improvements in areas of applications requiring a third dimension such as tissue engineering [240], filtration [241], or solar cells [242], Among the techniques used to produce nanofibrous assemblies, electrospinning is regarded as a powerful and versatile approach. In addition to its capability to produce 2D nanofibrous structures with nanofibers of extremely long length and high specific surface area, electrospinning is becoming a prevailing technique in the fabrication of 3D constructs due to recent developments and modifications of the electrospinning process such as multilayering electrospinning [243], low-temperature electrospinning [244], post-

processing after electrospinning [245], template assisted collection [246] , liquid assisted collection [247], porogen added electrospinning [195], or self-assembly [99, 248]. Although these techniques are able to produce 3D constructs in a reproducible way, they do not allow for the control of the fibrous assembly inside the 3D construct mainly because of the whipping movements undergone by the electrospun jet [11].

To avoid this issue, near-field electrospinning (NFE) was developed by bringing the collector at only few mm away from the emitter, in the straight jet region, before the onset of the bending instability. NFE allows either to write with the electrospun jet by imposing a controlled displacement of the collector at very high speed [249, 250] either to build tubular microstructures using sharp collectors [251]. Although a sub-micron diameter fiber can be easily produced, the poor production rate and the charge repulsion between the landing jet and the already deposited layer do not allow the fabrication of thick constructs (i.e. constructs with a thickness of tens to hundreds of microns) by NFE. Electrostatic field-assisted 3D printing has thus been proposed to build well organized 3D constructs. This technique, similar to NFE, is carried out with a polymer melt instead of a polymer solution. It has the advantages to insure a better control of the jet deposition and to allow the building of thick constructs because:

- (i) the jet is almost not subjected to the whipping movements
- (ii) the jet velocity is much lower than for NFE
- (iii) the charge repulsion effect is negligible [252].

Electrostatic field-assisted 3D printing allows the deposition of a jet with a diameter 10 times smaller than with standard 3D printing but nevertheless 10 times bigger than with solution electrospinning. Thus, although many advances have been achieved, the control of the deposition of a sub-micron diameter electrospun fiber allowing the building of 3D constructs still requires further improvements and refinements. It is particularly critical in tissue engineering where there is a need for bigger and better controlled pore size and architecture to improve cell migration and nutrient transport through 3D nanofibrous scaffolds.

In this paper, we propose a new strategy to generate 3D nanofibrous constructs with controlled internal fiber organization and pore size. We have recently shown that it was possible to produce 3D thick fibrous materials by taking advantage of the honeycomb-like self-assembly of either electrospun bimodal nanofibers [99] either uniform electrospun fibers and electrosprayed microparticles combined together [90]. In both cases, the obtained 3D construct showed high porosity with a gradient in pore sizes in the thickness of the sample. However the localization of the

nanofibers, as well as the size of the pores could not be tuned by these two approaches. To reach this goal, we have decided to associate the combination of electrospinning and electrospraying with the use of honeycomb patterned collectors [57, 184]. Indeed, patterned collectors already showed their ability to guide the deposition of electrospun nanofibers on a 2D surface [90]. We will show here that it is possible to extend this ability to control the deposition in 3D (i.e. laterally and even in the thickness of the construct) when both electrospinning and electrospraying are used. Our method thus allows the control of the self-assembly mechanism to produce 3D composite materials with controlled pores shape, location and size, in the range of a few tens to a few hundreds of microns. This method has moreover the advantage to enable the design of composite materials made of particles and fibers of different nature and properties that can be chosen depending on the intended application.

## 3.2 Experimental Section

### 3.2.1 *Materials*

Poly(D,L-lactide) (PLA) (MW 180kDa, NatureWorks), poly(ethylene oxide) (PEO) (Mw 20kDa, SERVA electrophoresis GmbH) and poly(ε-caprolactone) (PCL)(MW 14kDa, Sigma-Aldrich) were used as received. Solutions of 10% PLA in dichloromethane-dimethylformamide (50:50 V/V), 40 wt/wt % PEO in distilled water and 40 wt/wt % PCL in dichloromethane-dimethylformamide (50:50 V/V) were prepared 24 hours prior to electrospinning / electrospraying.

### 3.2.2 *Fabrication of the collectors*

Honeycomb micropatterns were obtained applying photolithographic processes on silicon wafers of 3 inches diameter (mask aligner MJB4, SUSS Microtec). The photoresist used was the SU-8 2050 (Michrochem). After the step of photolithography, an electron beam evaporator Plassys MEB5505 was used to deposit a conductive layer (Al-120 nm and Au-30 nm) on the patterns to make them conductive. The patterned surface was divided in four zones A, B, C, D of 25mm×25mm wide. Each zone was patterned with one characteristic honeycomb internal diameter *D* (360 µm for A, 160 µm for B, 80 µm for C and 40 µm for

D). The width and the height of honeycomb walls were respectively 20 µm and 60 µm. The geometry of the honeycomb is shown in **Figure 64**. The wafer was finally cut in order to obtain 4 collectors of 25mm×25mm wide containing one honeycomb size.

### 3.2.3 *Electrospinning / electrospraying*

A patterned collector of 25x25 mm wide was fixed on a rotating mandrel to collect the fibers and particles. A rotation speed of 60 rpm of the mandrel was applied, allowing alternating exposures of the collector in front of the electrospraying and electrospinning capillaries.

For electrospinning, the PLA solution was delivered with a constant flow rate of 1.6 $ml.h^{-1}$ using a syringe pump (Fischer scientific). The distance between the 18 gauge needle and the micropatterned collector was 18 cm. A positive potential $V_{PLAneedle}$ = 12kV was applied on the needle and a negative potential $V_{collector}$ = -5kV was applied on the collector using power supplies (Spellman SL10).

The PEO solution for electrospraying was delivered with a flow rate of 0.2 ml.h-1. The distance between the needle and the micropatterned collector was 15 cm. Experiment were performed with $V_{PEOneedle}$ = 18kV and $V_{collector}$ = -5kV. For the electrospraying of PCL, the solution was delivered at a flow rate of 1.4 $ml.h^{-1}$. The needle was at 18 cm from the collector under a positive applied potential $V_{PCLneedle}$ = 15kV using a power supply (Spellman SL10). In order to verify the reproducibility of the proposed methodology, ten samples at least were produced for each honeycomb diameter *D*.

### 3.2.4 *SEM analysis*

The scaffold morphology was observed by scanning electron microscopy (SEM, TECSAN Vega 3 LMU). Thin samples of **Figure 65** were not sputter coated. 3D electrospun samples were sputter coated with gold prior to observation (Q150RS, Quorum technologies). Samples showing an image of a transversal cut were peeled off from the collector, dipped in liquid nitrogen for 10 minutes and cut with a blade before sputter coating.

At least 100 measurements were done using Image J to characterize the diameter of the PLA fibers, the PEO or PCL particles.

At least 6 measurements were done using Image J to estimate the height reached by the columnar structures of the 3D constructs.

### 3.2.5 *Mechanical characterization*

The tensile stress-strain behavior of the scaffolds was obtained with a MCR301 rheometer from Anton-Paar. The rheometer was equipped with the Universal Extensional Fixture (UXF). The UXF system incorporates two drums allowing the fixation of a rectangular film sample. The rotating wind-up drum and the eccentrically positioned drum allowed uniaxial extensional measurements (see **Figure 67**). Simple PLA electrospun scaffolds as well as structured composite constructs of thickness $h = 60 \pm 25$ µm obtained from electrospinning/electrospraying of PLA/PEO with a patterned collector having a honeycomb internal characteristic size $D = 160$ µm were characterized. The scaffolds were carefully cut with a razor blade in order to obtain rectangular specimens 7 mm wide and 35 mm long. The width of each sample was precisely measured after they have been cut. The thickness of the cross-section of each sample was measured under the SEM. The weight of the samples was also measured in order to obtain their porosity and apparent density. The effective sample tested length corresponding to the distance between the axis of the two drums was 18 mm. Five samples per membrane type were characterized at $T = 23 \pm 0.5$ °C and at constant angular rotation of the rotating wind-up drum of $10^{-2}$ rad/s which corresponded to an engineering strain rate of $3.33 \times 10^{-3}$ $s^{-1}$.

## 3.3 Results and discussion

To demonstrate the ability of the process to produce 3D organized constructs, electrospinning of PLA nanofibers and electrospraying of PEO particles were performed simultaneously using two capillaries situated on opposite sides of a rotating mandrel. Collectors with honeycomb patterns of diameters 160 µm were fixed on the rotating mandrel allowing alternating exposures in front of the electrospraying and electrospinning capillaries (**Fig. 64-a**). Under these processing conditions, PLA nanofibers with diameters of 520 ± 80 nm and PEO microparticles with diameters of 1.9 ± 0.4 µm were collected in a well-controlled fashion on the honeycomb collector and generated 3D nanofibrous composite structures (**Fig. 64b-c** ).

On the surface of those structures, the replication of the honeycomb patterns of the collector can be observed. In the thickness of the construct, a 3D architecture is clearly appearing through columnar structures of pore diameters of 160 µm (**Fig. 64-c**). The walls of these columns, composed of nanofibers and microparticles, are building up exactly on top of the honeycomb patterns confirming that the collector efficiently directs the internal microstructuration of the composite nanofibrous materials. This structuration is stable for about 100 µm in height. Beyond this height the porous structure gradually disappears, as can be observed in thicker samples (**Fig. 64-b**) for which the thickness is greater than 220 µm. Moreover, it must be mentioned that when electrospinning was carried out alone (i.e. for the same production time but without electrospraying), a thickness of only 45 µm was obtained and no internal pores and structures were formed (**Fig. 64-d**). Thus, both electrospinning and electrospraying seem to be necessary for the construction of microstructured 3D samples.

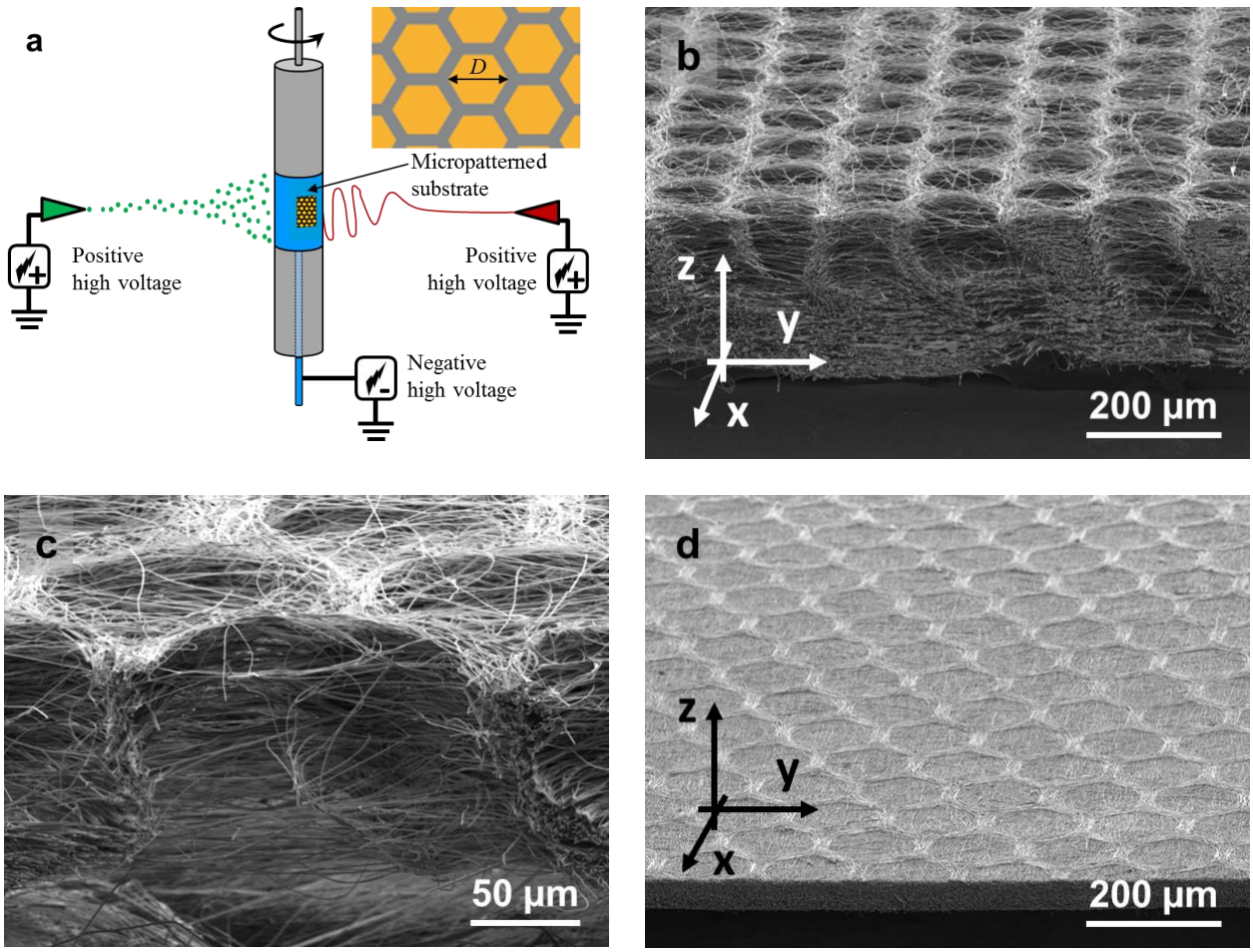


**Figure 64: (a) Schematic of the process. The diameter *D* of the honeycombs was 40 µm, 80 µm, 160 µm or 360 µm. The width and the height of honeycomb walls were respectively 20 µm and 60 µm. (b) 3D columnar structures obtained for *D* = 160 µm after 1 hour of production. (c) 3D columnar structure obtained after 15 minutes of production. (d) Fibrous structure obtained with the same operating conditions and time of production than for (b) but without electrospraying. No internal 3D microstructure can be achieved in this case.**

To understand the build-up process, the construction of this structure has been observed after only 3 minutes of exposure in front of the electrospinning and electrospraying devices. In this condition, most of the fibers were aligned along the walls of the honeycomb patterns in dense bundles and only a few of them were suspended across those patterns (**Fig. 65-a**). No particles could be observed inside the patterns. A closer look to the top of the pattern walls shows that the bundles are formed of fibers and particle clusters (**Fig. 65-b** and **Fig. 66-a**). The bundles made of microparticles and nanofibers on top of the walls were higher

than the thin structure made of few fibers crossing the patterns, already showing the premises of a 3D structure on top of the honeycomb patterns. To prove the necessity to have both electrospinning and electrospraying to achieve this result, control experiments with electrospinning or electrospraying alone were performed. After 3 minutes, when the electrospinning of the fibers was performed alone, a small number of suspended fibers crossing the patterns could still be found. However, on the walls of the patterns, no fibrous bundles could be observed. In their place, there was only a flat mat of fibers (**Fig. 65-c** and **Fig.65-e**).

When the electrospraying of particles was performed alone, microparticles could be observed on the walls as well as inside of the patterns (**Fig. 65-f**). The density of the particles was slightly higher on the walls than on the center of the pattern but no particle aggregation able to initiate a 3D structure could be found. Those experiments show that interactions between electrospraying and electrospinning are necessary to build 3D structures. The mechanism seems to result from the very first deposited layer of electrospun nanofibers and its subsequent capability to induce the selective deposition of the electrosprayed particles onto the walls. Indeed, the few fiber segments which are suspended over the honeycomb cavities of the collector cannot release efficiently their electric charges forming thus repulsive areas that prevent the deposition of the incoming particles whereas the fiber segments which are in contact with the wall of the honeycomb patterns can dissipate their charges allowing the deposition of the particles.

To get more insight into the structuration mechanism, we modeled the electric field resulting from the suspended fibers and the processing conditions. Considering that a nanofiber carries a linear charge density $\lambda$, $N$ fiber segments suspended over a honeycomb cavity of characteristic diameter $D$ and area $A$ can be modeled by a repulsive surface having a surface charge density:

(1)

with  being the average length of the fiber segments. Thus, $\sigma$ scales as:

(2)

Knowing that $\lambda$ results from the flux of electric charges and can be expressed as $\lambda = I / v$ with $I$ being the electric current during electrospinning and $v$ the velocity of the landing nanofiber which could be easily estimated from the mass balance:

(3)

Where $Q_{sol}$ is the flow rate of the polymer solution, $C_{pol}$ the weight polymer fraction in the solution, $\rho_{pol}$ the polymer density and the fiber diameter. Thus, the linear charge density is:

(4)

Finally, from (2) and (4), the surface charge density over $N$ suspended nanofibers is estimated by:

(6)

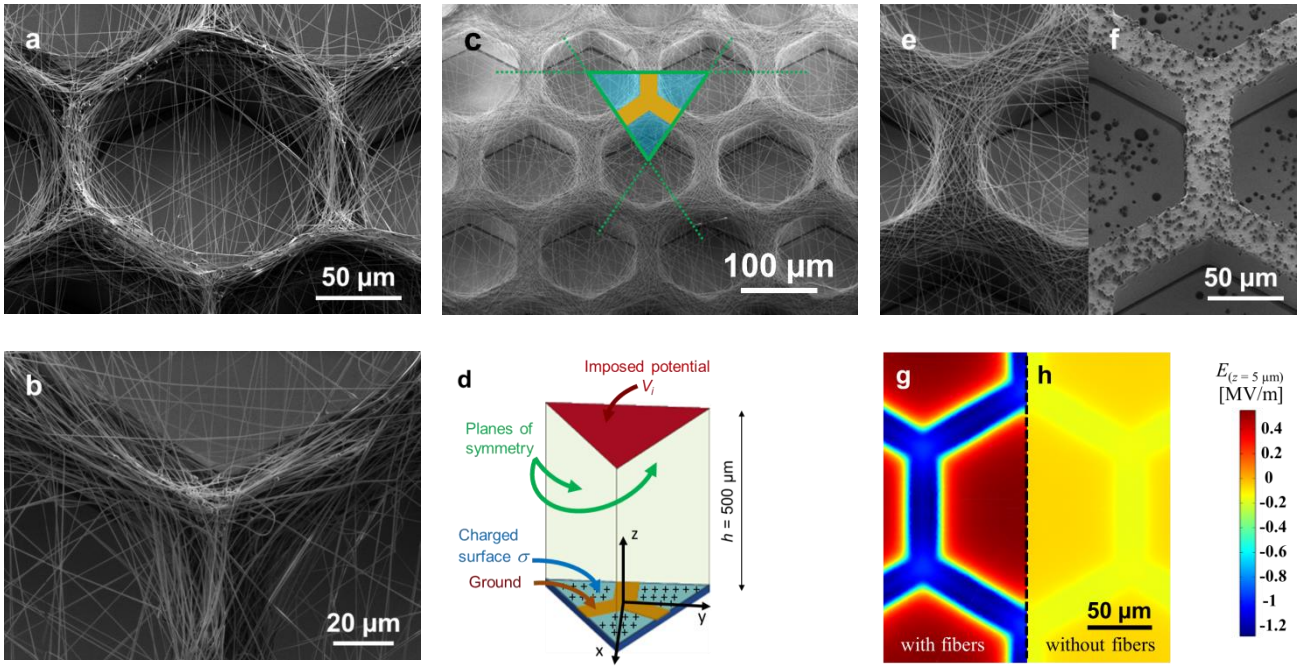


**Figure 65: (a) SEM picture obtained after 3 minutes of electrospinning and electrospraying on a honeycomb collector with $D$ = 160 µm. (b) Detail of (a) at an intersection of 3 honeycombs showing a bundle of fibers containing aggregated particles. (c) Nanofibers deposited on a honeycomb collector after 3 minutes of electrospinning alone. The 3 green dotted lines represent the planes of symmetry. (d) 3D domain for the computation and imposed boundary conditions. For the calculations we choose $h$ = 500 µm. Furthermore, knowing that the distance from needle to collector is $H$ = 18 cm and that $V_{needle}$ - $V_{collector}$ = 17 kV, the imposed potential at $z = h$ was $V_i = (V_{needle} - V_{collector})h/H$ = 47.2V. (e) Half of a honeycomb pattern showing the result of 3 minutes of electrospinning only. (f) Half of a honeycomb pattern showing the result of 3 minutes of electrospraying only. (g) Simulation of the vertical component of the electric field 5 µm above a charged fibrous layer deposited on the top of a honeycomb pattern of $D$ = 160 µm. (h) Simulation of the vertical component of the electric field 5 µm above a honeycomb pattern of $D$ = 160 µm and without the presence of fibers. The same scale of colors is used for (g) and (h).**

$\sigma$ and its corresponding electric field can thus be estimated using typical experimental values ($I$ = 10 nA, $v$ = 174 m/s and $\varepsilon_0$ = 8.854 × $10^{-12}$ F/m, the permittivity of free space) [253].

In the case where $D$ = 160 µm and $N$ = 10, one obtains $\sigma \sim 5.5\ 10^{-6}$ C/$m^2$ which leads to a repulsive electric field of roughly $\sigma / \varepsilon_0 \sim 0.6$ MV/m. In order to get more insight, numerical simulations (see **Fig. 65c-d** for the boundary conditions) of the vertical component $E$ of the electric field in the vicinity (i.e. $z$ = 5 µm) of the collector's top surface were performed by the finite elements method using Comsol® software for the two conditions of interest: with (**Fig. 65-g**) and without (**Fig. 65-h**) the presence of the thin layer of fibers.

When the thin fibrous layer is deposited on the honeycomb patterns (**Fig. 65-g**), $E$ varies from -1.3 MV/m over the attractive honeycomb walls to +0.55 MV/m over the repulsive area corresponding to the suspended fibers. When no fibers are deposited (**Fig. 65-h**) the gradient of $E$ is only due to the topographic effect of the collector and no repulsive effect is obviously observed.

Moreover, although the walls are more attractive ($E \sim$ -0.17 MV/m) than the bottoms ($E \sim$ -0.07 MV/m) of the honeycomb, the gradient of $E$ is low and does not allow a selective deposition of particles when electrospraying alone as it was experimentally observed. Thus, the selective deposition of electrosprayed particles over the honeycomb walls is clearly due to an electrostatic template effect occurring as soon as few electrospun charged fibers are deposited across the patterned collector. Furthermore, the electric contact is insured through the fibrous bundles forming the honeycomb walls due to the presence of the particles that bridge the fibers (see **Fig. 66**). This allows the conservation of the electrostatic template effect during the production. This process results finally in the building of a 3D composite material with controlled microstructure over a thickness of ~ 100 µm.

Finally, after longer times of production, the control of the 3D structure is lost, probably because the electric contact between the conductive patterns of the collector and the dense walls formed by the particles and the fibers can no longer be efficiently insured (**Fig 64-b**).

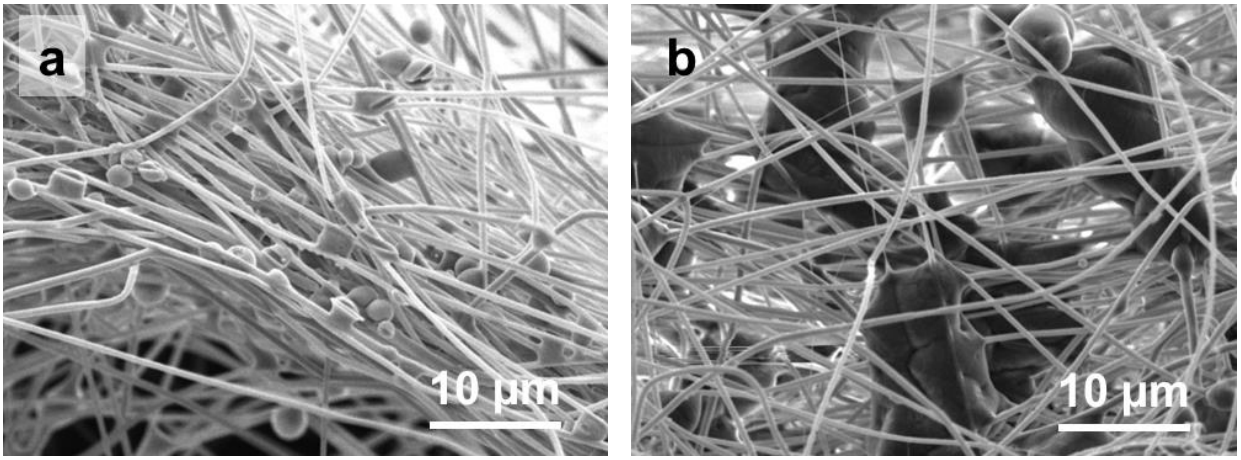


**Figure 66: SEM pictures showing the bundles of fibers and aggregated microparticles located over a honeycomb wall with *D* = 160 µm. (a) PLA fibers and PEO microparticles. (b) PLA fibers and PCL microparticles.**

As expected, the 3D structured composite constructs (**Figure 64-b**) had higher porosity than the PLA scaffolds (**Figure 64-d**) obtained by simple electrospinning. Indeed, gravimetric measurement gave a porosity of ~ 92 % for the simple PLA scaffolds whereas a porosity of ~ 95 % was achieved in the case of the 3D composite constructs obtained with the pattern characteristic diameter *D* = 160 µm. The higher porosity observed for the 3D constructs corresponds to a decrease of ~ 35 % of the apparent density as compared to simple PLA scaffolds.

To get more insight into the effect of the 3D honeycomb fibrous structure on the mechanical properties, tensile measurements were carried out on structured constructs as well as on simple PLA scaffolds (**Figure 67**). Representative stress-strain behaviors are shown in **Figure 67-d** and the mechanical properties are summarized in **Table 14**. The Young moduli found for the two types of fibrous mats are in agreement with those obtained by Simonet *et al.* [244] who studied highly porous scaffolds obtained by low temperature electrospinning. The high porosity of the 3D composite constructs led to a substantial decrease of the Young modulus by a factor 8.5 as compared to simple PLA scaffolds. However, as opposed to Simonet *et al.* [244], all tested mats showed an elastoplastic behavior with significant post-yield hardening and transverse contraction as shown in **Figures 67b-d**. In the case of the simple PLA scaffolds, the hardening appeared immediately after the elastic deformation and occurred up to the breaking of the sample. As

demonstrated by Silberstein *et al.* [254], such typical behavior arise from consolidation and alignment of the fibers that occur due to the bending of fibers that are transverse with respect to the tensile axis. Furthermore, the post-yield hardening may also be due to the transverse contraction that in turn increases the contact area between the fibers. For all tested 3D composite constructs, the post-yield hardening was however restricted into a certain range of strains. Indeed, as shown in **Figure 67-d**, after $\varepsilon_2$, a strain softening behavior appeared. This behavior may be due to the fact that the bending of the transverse fibers is rapidly limited since most of the fibers possess a small radius of curvature corresponding to the honeycomb radius (i.e. ~ 80 µm). Furthermore, the bundles of fibers and particles (**Figure 66-a**) may also limit the bending of the transverse fibers. In conclusion, the 3D composite constructs showed good mechanical properties that enable a facile manipulation and handling.

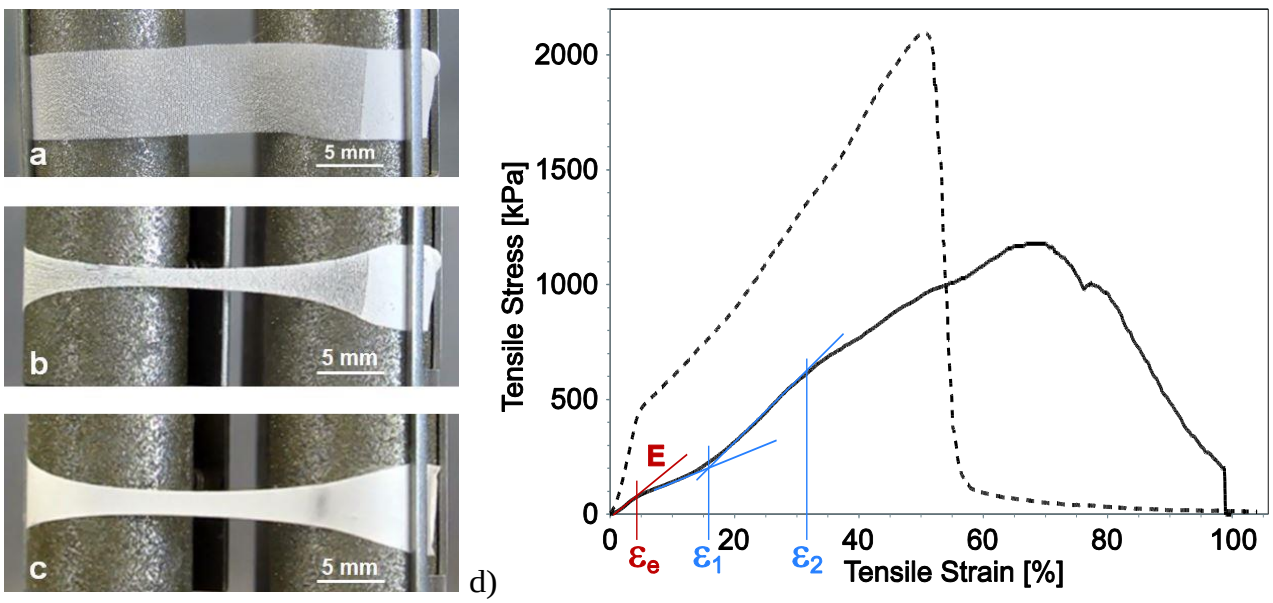


**Figure 67: Mechanical tests. (a) A 3D structured PLA/PEO nanofibers / microparticles construct obtained with honeycomb patterns of *D* = 160 µm and fixed on the drums of the rheometer. The honeycomb structure of the scaffold clearly appears on the picture. (b) The 3D composite construct just before its breaking. (c) A simple PLA scaffold just before its breaking. (d) Typical stress-strain behaviors of a PLA sample obtained by simple electrospinning (dashed line) and of a 3D structured PLA/PEO sample obtained by electrospinning/electrospraying on patterned collector with *D* = 160 µm (solid line).**

| | Young modulus E (MPa) | Elastic yield strain $\varepsilon_e$ (%) | Strain at break $\varepsilon_b$ (%) | Stress at break $\sigma_b$ (MPa) |
|---|---|---|---|---|
| Simple PLA scaffolds | 17 ± 5 | 4 ± 1 | 50 ± 3 | 2.2 ± 0.2 |
| 3D composite constructs obtained with *D* = 160 µm | 2 ± 0.7 | 6 ± 2 | 61 ± 13 | 1.1 ± 0.1 |

**Table 14: Mechanical properties of 3D structured PLA/PEO nanofibers / microparticles constructs obtained with honeycomb patterns of *D* = 160 µm and of simple PLA scaffolds.**

To investigate the possibility to control the pore size, collectors with honeycomb micropatterns of diameters of 40, 80 and 360 µm were used. For all those pattern diameters, it was possible to obtain columns and their morphologies are shown on **Figure 68**. Columnar structures with height up to around 25 µm, 50 µm and 180 µm were observed with patterns of respectively 40, 80 and 360 µm of diameter. The height of the column was found to increase with the diameter of the honeycomb pattern. So, most likely, the size of the pattern impacted to height up to which the micropatterned collector can guide the 3D microarchitecture of the composite material. A possible explanation could be a lower density of particles inside the fibrous walls for smaller patterns. Indeed, the total surface of the collector walls is larger in this case. Thus, the electric contact in the wall of the columnar structure is lost faster for smaller patterns.

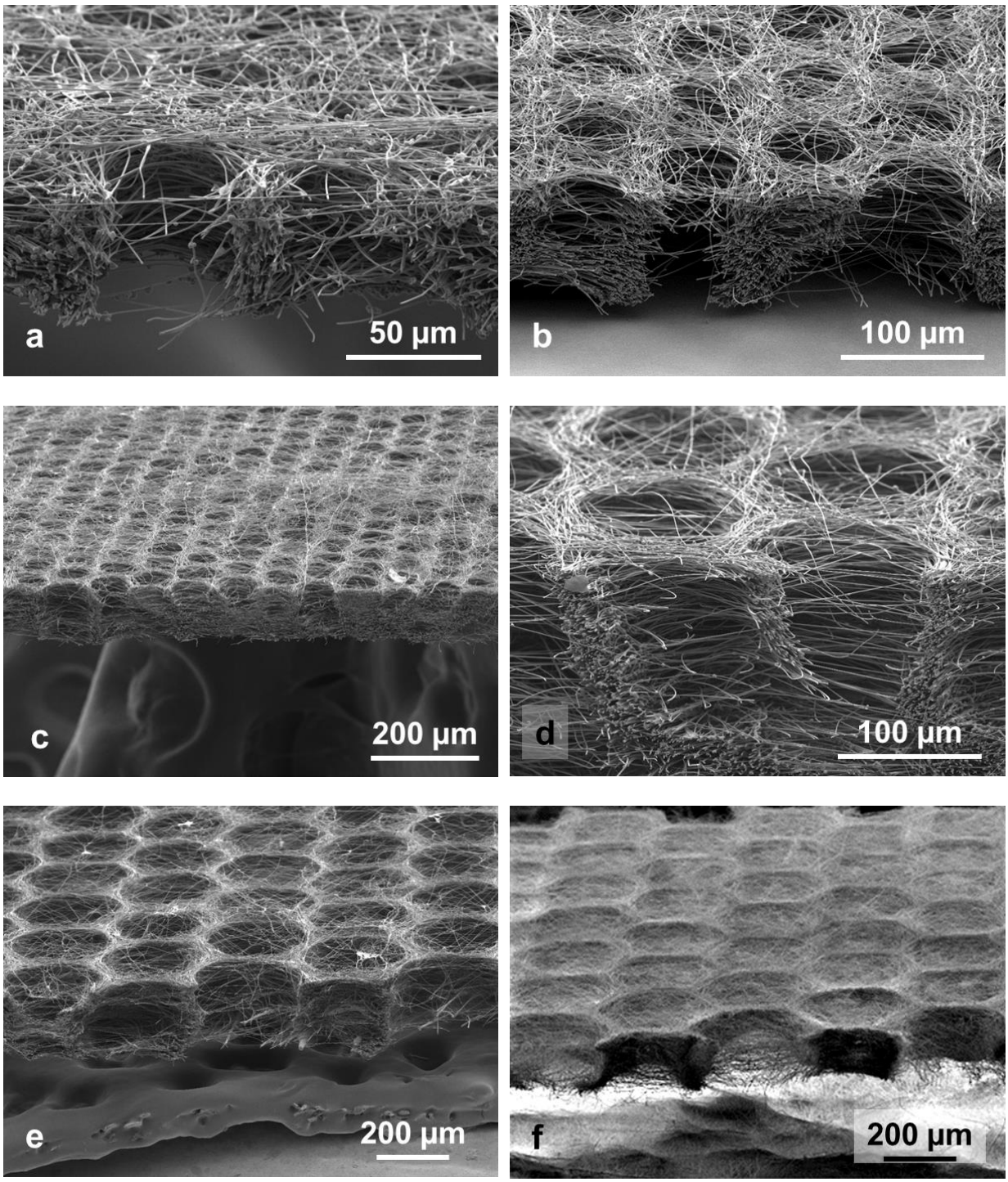


**Figure 68: SEM pictures of various 3D constructs with electrospun PLA nanofibers and electrosprayed PEO microparticles showing their cross-section and the surface which was in contact with the collector. (a) *D* = 40 µm, (b and c) *D* = 80 µm and (d) *D* = 160 µm. (e and f) *D* = 360 µm.**

In order to demonstrate that our technique can be applied with other kinds of microparticles, PCL was electrosprayed as a substitute to PEO. Contrarily to PEO, PCL is not soluble in water. Therefore, obtaining 3D structures with PCL instead of PEO microparticles change drastically the properties of the final composite. As shown in Figure 6, it was possible to generate columnar structure with PCL microparticles and PLA nanofibers. Under our processing conditions, PLA nanofibers with diameters of 500 ± 70 nm and PCL microparticles with diameters of 7.8 ± 1.8 µm were produced and columnar structure with a height of around 260 µm were obtained using honeycomb patterns of 360 µm of diameter. The height of those columns was significantly taller than the ones obtained with PEO particles while keeping the control of the internal structure.

This result shows that the electrostatic template is maintained for larger thickness in the case of PCL particles which means that electric charge dissipation through the bundles of fibers and particles located at the vertical of the collector pattern walls is efficiently insured (see Figures 3 and 6a). Two factors can explain this efficient charge release through the bundles: the quality and the number of contacts between the fibers and PCL particles. Regarding the contact quality, Figure 3b shows fibers embedded in PCL particles which is probably due to the low rate of evaporation of the DMF present in the solvent mixture. On the other hand, the big size of PCL particles could explain a large number of electric contacts. Indeed, compared to a small PEO particle, a big PCL particle alone allows electric interconnections with a larger number of fibers (see Figure 3b).

Finally, having different materials in the fibers and in the particles is highly interesting in terms of additional options for many applications. In particular, inorganic particles may also be envisaged. As an example, among the wide range of potential applications, constructs with pores in the range of few tens to few hundreds of microns and made of biopolymer fibers and hydroxyapatite microparticles could mimic the extracellular matrix of bone. Moreover, particles may also include drugs for their controlled release in the body. Another application may concern the modulation of the inflammatory response that occurred after the implantation of a biomaterial. Indeed, it was shown that tissue engineered biomaterials often induce an inflammatory by the macrophages that are recruited on the site of implantation [255]. This so-called foreign body reaction (FBR) could however be modulated by the optimization of the pore size

that can direct the macrophages toward an M2 state which is known to facilitate proper tissue regeneration [256]. Thus, our technique would allow the elaboration of nanofibrous scaffolds with adjusted pore size leading to the best inflammatory reaction.

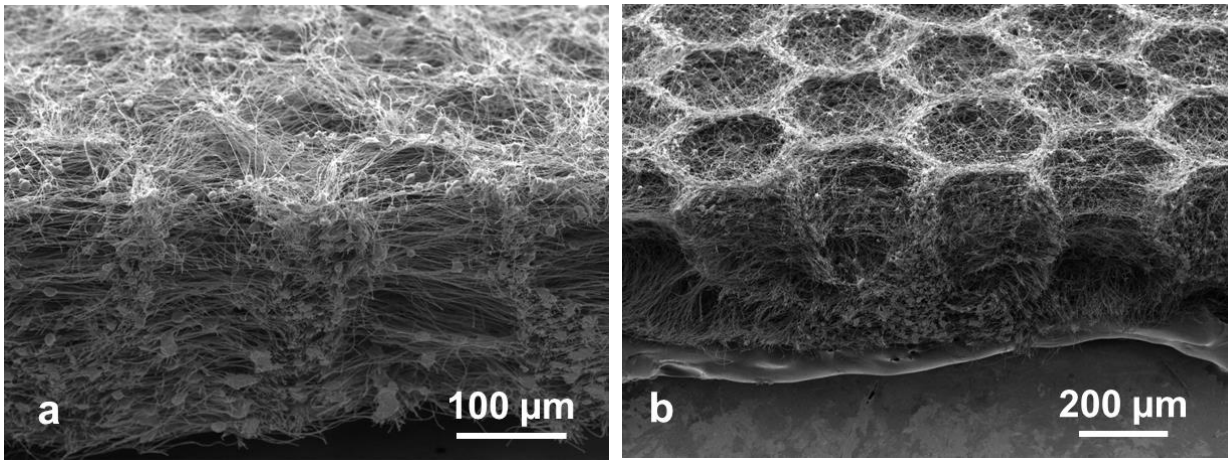


**Figure 69: SEM pictures of 3D constructs with electrospun PLA nanofibers and electrosprayed PCL microparticles showing their cross-section and the surface which was in contact with the collector. (a) *D* = 160 µm, (b) *D* = 360 µm.**

## 3.4 Conclusion

The proposed method allows the production of new 3D nanofibrous composite materials as a platform for many applications. Composed of submicron fibers and microparticles highly organized in 3D, it allows the formation of pores of diameter ranging between a few tens and a few hundreds of microns that can be tuned in accordance with the intended application. Tensile tests demonstrated the good mechanical properties of these materials allowing their simple manipulation and handling. The fibers and the particles can also be chosen independently to cover each partially but complementarily all the requirements of the material to be created. This method is applicable to numerous materials and pattern sizes and shapes, multiplying this way its potential areas of applications. It should be easily transferable to many kinds of polymers as long as the resulting fibers are not conductive enough to discharge when suspended across the pattern walls.

Furthermore, compared to electrostatic field-assisted 3D printing, the proposed strategy allows the building of 3D microstructured constructs with fiber diameter one order smaller and with polymer that could not be processed at the molten state. It is expected that this novel

simultaneous electrospinning and electrospraying method on patterned collectors has a great potential for the fabrication of 3D scaffolds for biomedical or other industrial applications.

## 4. Conclusions of the chapter three

In this chapter, we proved that by using differently the electrospinning of nanofibers and the electrospraying of microparticles, we were able to develop new kinds of composites for various applications in tissue engineering.

First, we elaborated a tool for the screening of different micropatterned electrospun composite structures for the bone regeneration. We successfully designed a new kind of micropatterned collector called a biochip collector with 21 different architectures. We managed to elaborate a 2D biochip composite membrane on this biochip collector by successively electrospinning PCL nanofibres and electrospraying hydroxyapatite. The multi-micropatterned membrane containing 21 different architectures in 21 different circles was then integrated into a small PMMA plate, pierced by 21 wells. In each well, one of the 21 different microarchitecture of the membrane could be found and was separated from the other wells. This small culture plate integrating a composite electrospun membrane was the first device allowing the screening of different micropatterned electrospun composite structure. This device was called a biochip. On the biochip, MG-63 cells were seeded during 21 days. We proved that the biochip was an effective device for the screening of different micropatterned electrospun structures. Indeed, thanks to alizarin red and immunochemistry, we proved that hexagonal rounded micropatterned structures with an internal diameter of 300 µm or circular micropatterned structures with internal diameter of approximatively 150 µm were the best electrospun structures for improving the bone regeneration process (mineralization) *in vitro*.

In the second part of this chapter, we proved that by using simultaneously electrospinning of nanofibers and electrospraying of particles on honeycomb micropatterned collector, we were able to construct 3D composite membranes with controlled pore size. We also showed that we were able to tune the size of the circular pores from tens to hundreds microns. The versatility in the process allowed the elaboration of different kinds of 3D constructs that can be used for various applications. The tensile tests proved that these kinds of scaffold are suitable for different kinds of manipulations.

Finally, the general conclusions and perspectives of this work will be presented on the next part.

# General conclusion and perspectives

## Conclusions and Perspectives

The aim of this thesis was to elaborate and to study new kind of micropatterned scaffolds (2D and 3D) obtained by electrospinning process. The developed structured scaffolds were then be used for bone regeneration applications.

After a detailed presentation of all techniques available in electrospinning to structure the nanofibers, we chose to use micropatterned collector fabricated by photolithographic processes in order to obtain microstructured electrospun scaffolds for bone regeneration.

We first developed monocomponent poly(ε-caprolactone) (PCL) and or poly(lactic acid)( PLA) honeycomb micropatterned scaffolds with a characteristic pattern size ranging from 40 to 360 µm. Two different kinds of structures were obtained: in the case of PLA, the unimodal distribution of the fiber diameters led to flat scaffolds whereas the bimodal distribution of fiber diameters (showing thick and thin fiber portions), observed in the case of PCL, increased the relief of the scaffold patterns due to the higher surface charge density of thicker PCL fiber portions leading to their preferential deposition on the walls of the collector patterns. Then, we studied the impact of the honeycomb architecture on osteoblasts spatial organization. We showed that MG-63 osteoblasts cells are sensitive to the topography of the scaffolds. Cells gathered inside the PCL honeycomb fibrous nests, creating osteoblasts niches inside the fibrous nests. Then, a novel strategy was proposed in order to develop mm-thick 3D electrospun scaffold with controlled internal structure. We demonstrated that electrospinning on honeycomb micropatterned collectors of PCL bimodal fibers showing self-assembling properties, mm-thick 3D honeycomb electrospun scaffold with controlled pore size and porosity gradient can be developed. In the first deposited layers of few hundreds of microns thick, it was possible to control the pore size from 80 µm to 360 µm. Then, columns of pores began to merge together, creating a porosity gradient in the thickness of the scaffold.

In the second part of the work, we focused on the development of 2D and 3D micropatterned composite membranes made of electrospun nanofibers and electrosprayed microparticles. First, we developed bi-layer composite and microstructured electrospun membranes elaborated from electrospun of PCL fibers followed by the deposition of electrosprayed hydroxyapatite particles on micropatterned collectors. The home-made

micropatterned collector presented 21 different kinds of micropatterns (hexagons, blocks, maze, bars, and random). Selective controlled deposition of hydroxyapatite particles was demonstrated thanks to the PCL nanofibrous layer that acted as an electrostatic template due to the residual electric charges covering the fiber portions suspended over the collector patterns. This composite bi-layer structured membrane was then used for the elaboration of biochips for the screening of fibrous composite materials for bone regeneration applications. We demonstrated that we were able to screen the different electrospun structures. Mineralization and bone regeneration process *in vitro* was improved with hexagonal electrospun composite microstructures rather than the other type of structures. Finally, 3D composite electrospun scaffolds were fabricated by the alternate electrospraying and electrospinning on honeycomb micropatterned collector. The electrostatic template role of the nanofibers controlling the deposition of microparticles was demonstrated by experiments and numerical simulations. 3D nanofibrous scaffolds showed controlled cylindrical pores in the thickness of the scaffold. The internal diameter was varying form tens to hundreds of microns. Tensile measurements carried out on such scaffolds demonstrated the good mechanical properties allowing the facile manipulation and handling of these 3D composite scaffolds for tissue regeneration applications. Finally, due to the large range of materials that could be used for the microparticles and the nanofibers, this strategy paves the way for the elaboration of different kinds of composite 3D fibrous constructs for a wide range of applications.

Honeycomb fibrous structures appeared as an interesting structure to develop new kind of 2D and 3D electrospun scaffolds for bone regeneration process and screening applications. In a future work, it could be very interesting to study the effect of the 2D PCL honeycomb electrospun scaffolds on the spatial organization of hematopoietic cells. Hematopoietic cells are cells existing in the bone marrow. They are used to remain in the cavities of the spongious bones and they need to gather in the cavities, creating niches inside the spongious bone. This phenomenon called “homing” could be enhanced by the specific structure of the honeycomb PCL scaffold. Furthermore, the biochip could be considered as the first model of a screening device incorporating a composite structured electrospun membrane. Culturing mesenchymal stem cells on such biochips may give interesting results since differentiation of stem cells is affected by the topography of the substrate on which they are cultured. Regarding the 3D honeycomb scaffolds with controlled pore size, it could be interesting to develop 3D composite scaffold of PCL fibers / hydroxyapatite particles for bone tissue regeneration.

While during this thesis, no *in vivo* study has been made, it would very interesting to evaluate the cell infiltration and the *in vivo* bone regeneration processes.

Furthermore, electrospun/electrosprayed multi-layers could be envisaged and elaborated thanks to different strategies. A first strategy would be to alternately electrospun/electrosprayed different kinds of layers of the composites structures and thus forming a multi-layer composite. Another strategy could be to use a more complex set up with four needles for example, allowing a double electrospinning and double electrospraying. More complex materials could also be considered for screening applications; indeed, while we showed that we were able to fabricate scaffolds with porosity gradient, we never succeed to elaborate membranes with composition gradient (with controlled variation of the amount of microparticles in the membrane). Such membrane could be very interesting for screening applications because we would be able to screen in the same time different micropatterned structures with different composition of the membrane and thus testing more complex micro-environments with the cells. Regarding the structuration process, we presented in detail the electrostatic template effect of a thin layer of electrospun nanofibers on the controlled microparticles deposition. However, spatially controlled deposition of microparticles with some polymers like polysaccharides remains a challenge. One can imagine another strategy to deposit locally the microparticles with a polysaccharide playing the role of the electrostatic template. For example, an idea could be to electrospun core-shell polyanion/polycation polysaccharides on the micropatterned collector. Another strategy could be to study new kinds of solvent systems leading to the decrease of its conductivity.

While we developed all this strategies to structure the electrospun fibers for tissue engineering applications, all the techniques presented in this work for the elaboration of complex nanofibrous materials could be applied with other polymers and particles for other research areas such energy or sensing for example, proving once again that electrospinning/electrospraying processes are very versatile techniques, ensuring them a bright future in the field of materials.

## Conclusions et Perspectives

L'objectif de cette thèse était d'élaborer et d'étudier un nouveau type de scaffolds micro-structurés (2D et 3D) obtenus par le procédé d'électrospinning ou électrofilage. Les scaffolds structurés développés ont été ensuite utilisés pour des applications en régénération osseuse.

Après une présentation détaillée de toutes les techniques disponibles en électrospinning pour structurer les nanofibres, nous avons choisi d'utiliser des collecteurs micro-structurés par des procédés de photolithographie pour obtenir des scaffolds nanofibreux micro-structurés pour la régénération osseuse.

Nous avons d'abord développé des scaffolds monocomposant en poly (ε-caprolactone) (PCL) ou en poly (acide lactique) (PLA) en forme de nid d'abeilles avec une taille de motif caractéristique allant de 40 à 360 µm. Deux différentes types de structures ont été obtenus: dans le cas du PLA, la distribution unimodale du diamètre de fibres a conduit à l'obtention de scaffolds plats, tandis que la distribution bimodale du diamètre des fibres observée dans le cas du PCL (montrant des parties de fibres épaisses et fines), a permis d'augmenter le relief des scaffolds. En effet, dans le cas du PCL, la densité surfacique de charges des fibres épaisses étant supérieure à la densité surfacique de charges des fibres fines, il y a un dépôt préférentiel des fibres épaisses sur les murs des collecteurs en nid d'abeilles, permettant ainsi l'augmentation du relief du scaffold. Ensuite, nous avons étudié l'impact de l'architecture en nid d'abeilles sur l'organisation spatiale des ostéoblastes. Nous avons montré que les ostéoblastes MG-63 sont sensibles à la topographie des scaffolds. Dans le cas des scaffolds en PCL, les cellules se sont rassemblées au cœur des nids d'abeilles, formant ainsi des niches d'ostéoblastes au sein des nids nanofibreux.

Ensuite, une nouvelle stratégie a été proposée afin de développer de nouveaux scaffolds 3D présentant une épaisseur millimétrique ainsi qu'une structure interne contrôlée. Nous avons démontré qu'en réalisant l'électrospinning de fibres bimodales de PCL (qui présentent des propriétés d'auto-assemblage) sur des collecteurs micro-structurés en nid d'abeilles, de nouveaux scaffolds nanofibreux 3D d'épaisseur millimétrique ont pu être élaborés. Ils ont la particularité de présenter des pores de taille contrôlée ainsi qu'un gradient de porosité dans l'épaisseur du scaffold.

En effet, dans les premières couches déposées de quelques centaines de microns d'épaisseur, il est possible de contrôler la taille de pore de 80 µm à 360 µm. Puis, des colonnes de pores ont commencé à fusionner ensemble, créant un gradient de porosité dans l'épaisseur du scaffold.

Dans la deuxième partie du travail, nous nous sommes concentrés sur le développement de membranes composites micro-structurées 2D et 3D réalisées à partir de nanofibres électrospinnées et de microparticules électrosprayées. Dans un premier temps, nous avons développé une membrane composite bicouche micro-structurée élaborée à partir de nanofibres de PCL et de particules d'hydroxyapatite déposées sur des collecteurs micro-architecturés. Le collecteur micro-architecturé présentait 21 types de structures différentes (hexagones, blocs, labyrinthe, barres, et non structuré). Le dépôt sélectif contrôlé des particules d'hydroxyapatite a été démontré grâce à la présence d'une fine couche de nanofibres de PCL préalablement électrospinnée sur le collecteur. En effet, cette fine couche de PCL joua le rôle de « template » électrostatique pour le dépôt de particules en raison des charges électriques résiduelles présentes sur les nanofibres suspendues au-dessus des motifs du collecteur. Cette membrane bicouche structurée composite a ensuite été utilisée pour l'élaboration de biopuces pour réaliser le screening d'architectures nanofibreuses pour des applications en régénération osseuse. Nous avons démontré que ces biopuces appelés biochip permettaient de réaliser le screening de micro-architectures nanofibreuses composites afin d'identifier la structure la plus pertinente pour la régénération osseuse. La minéralisation ainsi que le processus de régénération osseuse *in vitro* ont été améliorés avec les structures composites nanofibreuses hexagonales plutôt que les autres types de structures.

Enfin, des scaffolds composite 3D ont été fabriqués en utilisant alternativement le procédé d'électrospinning et d'électrospraying sur des collecteurs micro-structurés en nids d'abeilles. Le rôle de « template » électrostatique de la fine couche de fibres déposée sur le collecteur contrôlant le dépôt des particules a été démontré par différentes expériences et par des simulations numériques. Les scaffolds 3D nanofibreux présentaient des pores cylindriques de tailles contrôlées dans l'épaisseur du scaffold. Le diamètre intérieur variait de quelques dizaines à centaines de microns. Des tests en traction ont démontré que ces scaffolds présentaient de bonnes propriétés mécaniques, permettant ainsi une manipulation aisée et leur utilisation dans le domaine de la régénération osseuse. Enfin, en raison de la large gamme de matériaux qui peuvent être utilisés pour les microparticules et les nanofibres, cette stratégie

ouvre la voie à l'élaboration de différents types de composites 3D fibreux qui pourraient être utilisé pour une large gamme d'applications.

Les structures en nids d'abeilles sont apparues comme des structures intéressantes pour développer des nouveaux scaffolds 2D et 3D nanofibreux pour des applications en régénération osseuse et dans le domaine du screening. Dans un travail futur, il serait très intéressant d'étudier l'effet des scaffolds 2D nanofibreux en PCL en nids d'abeilles sur l'organisation spatiale des cellules hématopoïétiques. Les cellules hématopoïétiques sont des cellules présentent dans la moelle osseuse. Elles ont l'habitude de se trouver dans les cavités des os spongieux : elles ont besoin de se regrouper ensemble à l'intérieur de ces cavités créant ainsi des niches à l'intérieur des os spongieux. Ce phénomène qui est appelé le «homing » pourrait être encouragé par la structure spécifique des scaffolds PCL en nid d'abeilles.

De plus, le biochip peut être considéré comme la premier model d'un dispositif dédié au screening et incorporant une membrane composite micro-structurée réalisée par électrospinning. Il serait intéressant de cultiver des cellules mésenchymateuses sur ce type de biochip étant donné que le processus de différenciation des cellules mésenchymateuses est grandement affecté par la topographie du substrat sur lequel elles sont cultivées.

En ce qui concerne les scaffolds en nid d'abeilles 3D avec une taille de pores contrôlée, il pourrait être intéressant de développer des scaffolds composite 3D à partir de nanofibres de PCL et de particules d'hydroxyapatite pour la régénération du tissu osseux. Bien que durant cette thèse, aucune étude *in vivo* n'a été faite, il serait très intéressant d'évaluer l'infiltration de cellules *in vivo* et les processus régénération osseuse au sein de ces scaffolds 3D.

D'autre part, des multi-couches électrospinnés/ électrosprayés pourraient être envisagés et développés grâce à différentes stratégies. Une première stratégie consisterait à alternativement électrospinner / électrosprayer différents types de couches sur un collecteur formant ainsi un composite multicouche. Une autre stratégie pourrait consister à utiliser un montage d'électrospinning plus complexe avec quatre aiguilles par exemple, permettant un double électrospinning et un double électrospraying. Des matériaux plus complexes pourraient également être envisagés pour les applications en screening. En effet, alors que nous avons montré que nous étions capables de fabriquer des scaffolds présentant un gradient de porosité, nous n'avons pas réussi jusqu'à présent à élaborer des membranes avec un

gradient de composition (avec une variation contrôlée de la quantité de microparticules dans la membrane par exemple). Une telle membrane pourrait être très intéressante pour les applications dans le domaine du screening car nous serions alors capables de tester en même temps différentes architectures nanofibreuses présentant différentes compositions. Nous testerions ainsi avec les cellules des micro-environnements plus complexes.

En ce qui concerne le processus de structuration, nous avons présenté en détail l'effet de «template » électrostatique de la fine couche de nanofibres déposée sur le collecteur sur le dépôt contrôlé des microparticules. Cependant, le dépôt contrôlé des microparticules avec certains polymères comme les polysaccharides reste encore un défi. On pourrait imaginer une autre stratégie pour déposer localement les microparticules avec un polysaccharide jouant le rôle de « template ». Par exemple, une idée serait d'électrofiler en structure cœur –peau des polysacharrides polyanion / polycation sur un collecteur micro-structuré. Une autre stratégie pourrait consister à étudier de nouveaux types de systèmes de solvants afin de diminuer la conductivité de la solution.

Bien que nous ayons développés toutes ces stratégies de structuration des nanofibres pour des applications en ingénierie tissulaire, toutes les techniques présentées dans cet ouvrage pour l'élaboration de matériaux complexes nanofibreux pourraient être appliquées à d'autres polymères et particules pour d'autres domaines de recherche tels que l'énergie ou les capteurs par exemple, prouvant une fois de plus que les procédés d' électrospinning/ électrospraying sont des techniques très polyvalentes, leur assurant ainsi un brillant avenir dans le domaine des matériaux.

# References

[1] Dobriansky PJ, Suzman RM, Hodes RJ. Why population aging matters: A global perspective. *National Institute on Aging, National Institutes of Health, US Department of Health and Human Services, US Department of State* **2007**.
[2] Lanza R, Langer R, Vacanti JP. Principles of tissue engineering: Academic press; **2011**.
[3] Skalak R, Fox CF. Tissue engineering: proceedings of a workshop, held at Granlibakken, Lake Tahoe, California, February 26-29, 1988: Alan R. Liss; **1988**.
[4] Langer R, Vacanti JP. Tissue engineering. *Science* **1993**;260:920-6.
[5] Daher RJ, Chahine NO, Greenberg AS, Sgaglione NA, Grande DA. New methods to diagnose and treat cartilage degeneration. *Nature Reviews Rheumatology* **2009**;5:599-607.
[6] Carvalho JL, de Carvalho PH, Gomes DA, de Goes AM. Innovative Strategies for Tissue Engineering. *Rosario Pignatello Advances in biomaterials science and biomedical applications INTECH* **2013**:295-313.
[7] Cooley J. Apparatus for electrically dispersing fluids 1902. *US Patent*;US 692631.
[8] Morton W. Method of Dispersing Fluids, 1902. *US Patent Specification*;705691.
[9] Formhals A. Process and apparatus for preparing artificial threads US Patent Specification, 1975504. **1934**.
[10] Process E. Applications of Electrospun Fibers, Doshi et al. *Journal of Electrostatics* **1995**;35:151-60.
[11] Reneker DH, Yarin AL, Fong H, Koombhongse S. Bending instability of electrically charged liquid jets of polymer solutions in electrospinning. *Journal of Applied physics* **2000**;87:4531-47.
[12] Graham K, Ouyang M, Raether T, Grafe T, McDonald B, Knauf P. Polymeric nanofibers in air filtration applications. Fifteenth Annual Technical Conference & Expo of the American Filtration & Separations Society, Galveston, Texas**2002**. p. 9-12.
[13] Yun KM, Suryamas AB, Iskandar F, Bao L, Niinuma H, Okuyama K. Morphology optimization of polymer nanofiber for applications in aerosol particle filtration. *Separation and purification technology* **2010**;75:340-5.
[14] Lee S, Obendorf SK. Use of electrospun nanofiber web for protective textile materials as barriers to liquid penetration. *Textile Research Journal* **2007**;77:696-702.
[15] Lee S, Kay Obendorf S. Developing protective textile materials as barriers to liquid penetration using melt-electrospinning. *Journal of Applied Polymer Science* **2006**;102:3430-7.
[16] Ding B, Wang M, Yu J, Sun G. Gas sensors based on electrospun nanofibers. *Sensors* **2009**;9:1609-24.
[17] Ramakrishna S, Fujihara K, Teo W-E, Yong T, Ma Z, Ramaseshan R. Electrospun nanofibers: solving global issues. *Materials Today* **2006**;9:40-50.
[18] Miao J, Miyauchi M, Simmons TJ, Dordick JS, Linhardt RJ. Electrospinning of nanomaterials and applications in electronic components and devices. *Journal of nanoscience and nanotechnology* **2010**;10:5507-19.
[19] Chronakis IS. Novel nanocomposites and nanoceramics based on polymer nanofibers using electrospinning process—a review. *Journal of Materials Processing Technology* **2005**;167:283-93.
[20] Shalumon K, Anulekha K, Nair SV, Nair S, Chennazhi K, Jayakumar R. Sodium alginate/poly (vinyl alcohol)/nano ZnO composite nanofibers for antibacterial wound dressings. *International journal of biological macromolecules* **2011**;49:247-54.
[21] Liang D, Hsiao BS, Chu B. Functional electrospun nanofibrous scaffolds for biomedical applications. *Advanced Drug Delivery Reviews* **2007**;59:1392-412.
[22] Agarwal S, Wendorff JH, Greiner A. Use of electrospinning technique for biomedical applications. *Polymer* **2008**;49:5603-21.
[23] Lee KY, Jeong L, Kang YO, Lee SJ, Park WH. Electrospinning of polysaccharides for regenerative medicine. *Advanced Drug Delivery Reviews* **2009**;61:1020-32.

[24] Li M, Mondrinos MJ, Gandhi MR, Ko FK, Weiss AS, Lelkes PI. Electrospun protein fibers as matrices for tissue engineering. *Biomaterials* **2005**;26:5999-6008.
[25] Teo WE, Ramakrishna S. A review on electrospinning design and nanofibre assemblies. *Nanotechnology* **2006**;17:R89.
[26] Taylor G. Electrically driven jets. *Proceedings of the Royal Society of London A Mathematical and Physical Sciences* **1969**;313:453-75.
[27] Li F, Zhao Y, Song Y. Core-Shell nanofibers: Nano channel and capsule by coaxial electrospinning. *Nanofibers* **2010**:419-38.
[28] Theron S, Yarin A, Zussman E, Kroll E. Multiple jets in electrospinning: experiment and modeling. *Polymer* **2005**;46:2889-99.
[29] Yeo LY, Friend JR. Electrospinning carbon nanotube polymer composite nanofibers. *Journal of experimental nanoscience* **2006**;1:177-209.
[30] Reneker DH, Chun I. Nanometre diameter fibres of polymer, produced by electrospinning. *Nanotechnology* **1996**;7:216.
[31] Li D, Xia Y. Electrospinning of nanofibers: reinventing the wheel? *Advanced Materials* **2004**;16:1151-70.
[32] Beachley V, Wen X. Effect of electrospinning parameters on the nanofiber diameter and length. *Materials Science and Engineering: C* **2009**;29:663-8.
[33] Touny AH, Lawrence JG, Jones AD, Bhaduri SB. Effect of electrospinning parameters on the characterization of PLA/HNT nanocomposite fibers. *Journal of Materials Research* **2010**;25:857-65.
[34] Huang L, Nagapudi K, P. Apkarian R, Chaikof EL. Engineered collagen–PEO nanofibers and fabrics. *Journal of Biomaterials Science, Polymer Edition* **2001**;12:979-93.
[35] Mit-uppatham C, Nithitanakul M, Supaphol P. Ultrafine Electrospun Polyamide-6 Fibers: Effect of Solution Conditions on Morphology and Average Fiber Diameter. *Macromolecular Chemistry and Physics* **2004**;205:2327-38.
[36] Amiraliyan N, Nouri M, Kish MH. Effects of some electrospinning parameters on morphology of natural silk-based nanofibers. *Journal of Applied Polymer Science* **2009**;113:226-34.
[37] Carrizales C, Pelfrey S, Rincon R, Eubanks TM, Kuang A, McClure MJ, et al. Thermal and mechanical properties of electrospun PMMA, PVC, Nylon 6, and Nylon 6, 6. *Polymers for Advanced Technologies* **2008**;19:124-30.
[38] Zong X, Kim K, Fang D, Ran S, Hsiao BS, Chu B. Structure and process relationship of electrospun bioabsorbable nanofiber membranes. *Polymer* **2002**;43:4403-12.
[39] Jacobs V, Anandjiwala RD, Maaza M. The influence of electrospinning parameters on the structural morphology and diameter of electrospun nanofibers. *Journal of Applied Polymer Science* **2010**;115:3130-6.
[40] Lavielle N, Popa A-M, de Geus M, Hébraud A, Schlatter G, Thöny-Meyer L, et al. Controlled formation of poly (ε-caprolactone) ultrathin electrospun nanofibers in a hydrolytic degradation-assisted process. *European Polymer Journal* **2013**;49:1331-6.
[41] Gupta P, Elkins C, Long TE, Wilkes GL. Electrospinning of linear homopolymers of poly (methyl methacrylate): exploring relationships between fiber formation, viscosity, molecular weight and concentration in a good solvent. *Polymer* **2005**;46:4799-810.
[42] McKee MG, Wilkes GL, Colby RH, Long TE. Correlations of solution rheology with electrospun fiber formation of linear and branched polyesters. *Macromolecules* **2004**;37:1760-7.
[43] Deitzel JM, Kleinemeyer J, Harris D, Beck Tan NC. The effect of processing variables on the morphology of electrospun nanofiber and textiles. *Polymer* **2001**;42:261-72.
[44] Ramakrishna S, Fujihara K, Teo W-E, Lim T-C, Ma Z. An introduction to electrospinning and nanofibers: World Scientific; **2005**.

[45] Subbiah T, Bhat G, Tock R, Parameswaran S, Ramkumar S. Electrospinning of nanofibers. *Journal of Applied Polymer Science* **2005**;96:557-69.
[46] Pham QP, Sharma U, Mikos AG. Electrospinning of polymeric nanofibers for tissue engineering applications: a review. *Tissue Engineering* **2006**;12:1197-211.
[47] Buchko CJ, Chen LC, Shen Y, Martin DC. Processing and microstructural characterization of porous biocompatible protein polymer thin films. *Polymer* **1999**;40:7397-407.
[48] Tripatanasuwan S, Zhong Z, Reneker DH. Effect of evaporation and solidification of the charged jet in electrospinning of poly (ethylene oxide) aqueous solution. *Polymer* **2007**;48:5742-6.
[49] Casper CL, Stephens JS, Tassi NG, Chase DB, Rabolt JF. Controlling surface morphology of electrospun polystyrene fibers: effect of humidity and molecular weight in the electrospinning process. *Macromolecules* **2004**;37:573-8.
[50] Dersch R, Liu T, Schaper AK, Greiner A, Wendorff JH. Electrospun nanofibers : internal structure and intrinsic orientation. *Journal of Polymer Science Part A: Polymer Chemistry* **2003**;41:545-53.
[51] Kuo C-C, Wang C-T, Chen W-C. Highly-aligned electropsun luminescent nanofibers prepared from Polyfluorene/PMMA Blends : fabrication, morphology, photophysical, properties and sensory applications. *Macromolecular Materials and Engineering* **2008**;293:999-1008.
[52] Li D, Wang Y, Xia Y. Electrospinning of polymeric and ceramic nanofibers as uniaxially aligned arrays. *Nano Letters* **2003**;3:1167-71.
[53] Yan H, Liu L, Zhang Z. Alignment of electrospun nanofibers using dielectric materials. *Applied Physics Letters* **2009**;95:143114.
[54] Chaurey V, Chiang PC, Polanco C, Su Y-H, Chia F-C, Swami NS. Interplay of electrical forces for alignment of sub-100 nm electrospun nanofibers on insulator gap collectors. *Langmuir* **2010**;26:19022-6.
[55] Li D, Wang Y, Xia Y. Electrospinning nanofibers as uniaxially aligned arrrays and layer-by-layer stacked films. *Advanced Materials* **2004**;16:361-6.
[56] Jalili R, Morshed M, Ravandi SAH. Fundamental paramaters affecting electrospinning of PAN nanofbers as uniaxially aligned fibers. *Journal of Applied Polymer Science* **2006**;101:4350-7.
[57] Li D, Ouyang G, McCann JT, Xia Y. Collecting electrospun nanofibers with patterned electrodes. *Nano Letters* **2005**;5:913-6.
[58] Zuchelli A, Fabiani D, Gualandi C, Focarete ML. An innovative and versatile approach to design highly porous, patterned, nanofibrous polymeric materials. *Journal of Materials Science* **2009**;44:4969-75.
[59] Zhang D, Chang J. Electrospinning of three-dmensional nanofibrous tubes with controllable architectures. *Nano Letters* **2008**;8:3283-7.
[60] Rafique J, Yu J, Yu J, Fang G, Wong KW. Electrospinning highly aligned long polymer nanofibers on large scale by using a tip collector. *Applied Physics Letters* **2007**;91.
[61] Katta P, Alessandro M, Ramsier RD, Chase GG. Continuous electrospinning of aligned nanofibers onto a wire drum collector. *Nano Letters* **2004**;4:2215-8.
[62] Kakade MV, Givens S, Gardner K, Lee KH, Chase DB, Rabolt JF. Electric field induced orientation of polymer chains in macroscopically aligned electrospun polymer nanofibers. *Journal of the American Chemical Society* **2007**;129:2777-82.
[63] Liu Y, Zhang X, Xia Y, Yang H. Magnetic field assisted electrospinning of aligned straight and wavy polymeric nanofibers. *Advanced Materials* **2010**;22:2454-7.

[64] Wang H, Tang H, He J, Wang Q. Fabrication of aligned ferrite nanofibers by magnetic-field assisted electrospinning coupled with oxygen plasma treatment. *Materials Research Bulletin* **2009**;44:1676-80.
[65] Yang D, Lu B, Zhao Y, Jiang X. Fabrication of aligned fibrous arrays by magnetic electrospinning. *Advanced Materials* **2007**;19:3702-6.
[66] Matthews JA, Wnek GE, Simpson DG, Bowlin GL. Electrospinning of collagen nanofibers. *Biomacromolecules* **2002**;3:232-8.
[67] Moon S, Farris RJ. How is it possible to produce highly oriented yarns of electrospun fibers ? *Polymer Engineering and Science* **2007**;47:1530-5.
[68] Reneker DH, Yarin AL. Electrospinning jets and polymer nanofibers. *Polymer* **2008**;49:2387-425.
[69] Mathew G, Hong JP, Rhee JM, Leo DJ, Nah C. Preparation and anisotropic mechanical behavior of highly-oriented electrospun poly(butylene terephthalate) fibers. *Journal of Applied Polymer Science* **2006**;101:2017-21.
[70] Kiselev P, Rosell-Llompart J. Highly aligned electrospun nanofibers by elimination of the whipping motion. *Journal of Applied Polymer Science* **2012**;125:2433-41.
[71] Kim K, Lee K, Myung K, Yo H, Kim H. The effect of molecular weight and the linear velocity of drum surface on the properties of electrospun poly(ethylene terephthalate) nonwovens. *Fibers and Polymers* **2004**;5:122-7.
[72] Zussman E, Rittel D, Yarin AL. Failure modes of electrospun nanofibers. *Applied Physics Letters* **2003**;82:3958-60.
[73] Edwards MD, Mitchell GR, Mohan SD, Olley RH. Development of orientation during electrospinning of fibres of poly(e-caprolactone). *European Polymer Journal* **2010**;46:1175-83.
[74] Blond D, Walshe W, Young K, Blighe FM, Khan U, Almecija D, et al. Strong, tough, electrospun polymer-nanotube composite membranes with extremely low density. *Advanced Functional Materials* **2008**;18:2618-24.
[75] Na H, Li Q, Sun H, Zhao C, Yuan X. Anisotropic mechanical properties of hot-pressed PVDF membranes with higher fiber alignments via electrospinning. *Polymer Engineering and Science* **2009**;49:1291-8.
[76] Reneker DH, Yarin AL, Zussman E, Xu H. Electrospinning of nanofibers from polymer solutions and melts. *Advances in Applied Mechanics* **2007**;41:43-195.
[77] Sun Z, Deitzel JM, Knopf J, Chen X, Gillespie Jr. JW. The effect of solvent dielectric properties on the collection of oriented electrospun fibers. *Journal of Applied Polymer Science* **2012**;125:2585-94.
[78] Kessick R, Fenn J, Tepper G. The use of AC potentials in electrospraying and electrospinning processes. *Polymer* **2004**;45:2981-4.
[79] Theron A, Zussman E, Yarin AL. Electrostatic field-assisted alignment of electrospun nanofibres. *Nanotechnology* **2001**;12:384-90.
[80] Bhattarai N, Edmondson D, Veiseh O, Matsen FA, Zhang M. Electrospun chitosan-based nanofibers and their cellular compatibility. *Biomaterials* **2005**;26:6176-84.
[81] Sundaray B, Subramanian V, Natarajan TS, Xiang R-Z, Chang C-C, Fann W-S. Electrospinning of continuous aligned polymer fibers. *Applied Physics Letters* **2004**;84:1222-4.
[82] Carnell LS, Siochi EJ, Holloway NM, Stephens RM, Rhim C, Niklason LE, et al. Aligned mats from electrospun single fibers. *Macromolecules* **2008**;41:5345-9.
[83] Cho SJ, Kim B, An T, Lim G. Replicable multilayered nanofibrous patterns on a flexible film. *Langmuir* **2010**;26:14395-9.
[84] Orlova Y, Magome N, Liu L, Chen Y, Agladze K. Electrospun nanofibers as a tool for architecture control in engineered cardiac tissue. *Biomaterials* **2011**;32:5615-24.

[85] Yang F, Murugan R, Wang S, Ramakrishna S. Electrospinning of nano/micro scale poly(L-lactic acid) aligned fibers and their potential in neural tissue engineering. *Biomaterials* **2005**;26:2603-10.
[86] Tong H-W, Wang M. Electrospinning of aligned biodegradable polymer fibers and composite fibers for tissue engineering applications. *Journal of Nanoscience and Nanotechnology* **2007**;7:3834-40.
[87] Vaquette C, Cooper-White JJ. Increasing electrospun scaffold pore size with tailored collectors for improved cell penetration. *Acta Biomaterialia* **2011**;7:2544-57.
[88] Ner Y, Asemota C, Olson JR, Sotzing GA. Nanofiber alignment on a flexible substrate : hierarchical order from macro to nano. *ACS Applied Materials & Interfaces* **2009**;1:2093-7.
[89] Wu Y, Dong Z, Wilson S, Clark RL. Template-assisted assembly of electrospun fibers. *Polymer* **2010**;51:3244-8.
[90] Lavielle N, Hébraud A, Mendoza-Palomares C, Ferrand A, Benkirane-Jessel N, Schlatter G. Structuring and Molding of Electrospun Nanofibers: Effect of Electrical and Topographical Local Properties of Micro-Patterned Collectors. *Macromolecular Materials and Engineering* **2012**;297:958-68.
[91] Ding Z, Salim A, Ziaie B. Selective nanofiber deposition through field-enhancement electrospinning. *Langmuir* **2009**;25:9648-52.
[92] Zhang D, Chang J. Patterning of electrospun fibers using electroconductive templates. *Advanced Materials* **2007**;19:3664-7.
[93] Wang Y, Hao L, Wang G, Yin T, Wang B, Yu Q. Electrospinning of polymer nanofibers with ordered patterns and architectures. *Journal of Nanoscience and Nanotechnology* **2010**;10:1699-706.
[94] Seo JM, Arumugam GK, Khan S, Heiden PA. Comparison of the effects of an ionic liquid and triethylbenzylammonium chloride on the properties of electrospun fibers, 1 - poly (lactic acid). *Macromolecular Materials and Engineering* **2009**;294:35-44.
[95] Arumugam GK, Khan S, Heiden PA. Comparison of the effects of an ionic liquid and other salts on the properties of electrospun fibers, 2 - poly(vinyl alcohol). *Macromolecular Materials and Engineering* **2009**;294:45-53.
[96] Ye XY, Huang XJ, Xu ZK. Nanofibrous mats with bird's nest patterns by electrospinning. *Chinese Journal of Polymer Science (English Edition)* **2012**;30:130-7.
[97] Yan G, Yu J, Qiu Y, Yi X, Lu J, Zhou X, et al. Self-assembly of electrospun polymer nanofibers: a general phenomenom generating honeycomb-patterned nanofibrous structures. *Langmuir* **2011**;27:4285-9.
[98] Thandavamoorthy S, Gopinath N, Ramkumar SS. Self-assembled honeycomb polyurethane nanofibers. *Journal of Applied Polymer Science* **2006**;101:3121-4.
[99] Ahirwal D, Hébraud A, Kádár R, Wilhelm M, Schlatter G. From self-assembly of electrospun nanofibers to 3D cm thick hierarchical foams. *Soft Matter* **2013**;9:3164-72.
[100] Karageorgiou V, Kaplan D. Porosity of 3D biomaterial scaffolds and osteogenesis. *Biomaterials* **2005**;26:5474-91.
[101] Uecker JC, Tepper GC, Rosell-Llompart J. Ion-assisted collection of Nylon-4,6 electrospun nanofibers. *Polymer* **2010**;51:5221-8.
[102] Kim G, Kim W. Highly porous 3D nanofiber scaffold using an electrospinning technique. . *Journal of Biomedical Materials Research Part B: Applied Biomaterials* **2006**;81B:104-10.
[103] Nam J, Huang Y, Agarwal S, Lanutti J. Improved cellular infiltration in electrospun fiber via engineered porosity. *Tissue Engineering* **2007**;13:2249-57.
[104] Leong MF, Rasheed MZ, Lim TC, Chian KS. In vitro cell infiltration and in vivo cell infiltration and vascularization in a fibrous, highly porous poly(D,L-lactide) scaffold

fabricated by cryogenic electrospinning technique. *Journal of Biomedical Materials Research, Part A* **2009**;91A:231-40.
[105] Srouji S, Kizhner T, Suss-Tobi E, Livne E, Zussmann E. 3D nanofibrous electrospun multilayered construct is an alternative ECM mimicking scaffold. *Journal of Materials Science: Materials in Medicine* **2008**;19:1249-55.
[106] Tzezana R, Zussman E, Levenberg S. A layered ultra-porous scaffold for tissue engineering created via hydrospinning method. *Tissue Engineering Part C-Methods* **2008**;14:281-8.
[107] Blakeney BA, Tambralli A, Anderson JM, Andukuri A, Lim D-J, Dean DR, et al. Cell infiltration and growth in a low density, uncompressed three dimensional electrospun nanofibrous scaffold. *Biomaterials* **2011**;32:1583-90.
[108] Teo W-E, Ramakrishna S. Electrospun nanofibers as a platform for multifunctional, hierarchically organized nanocomposite. *Composites Science and Technology* **2009**;69:1804-17.
[109] Hou Z, Li G, Lian H, Lin J. One-dimensional luminescent materials derived from the electrospinning process: preparation, characteristics and application. *Journal of Materials Chemistry* **2012**;22:5254-76.
[110] Xie J, MacEwan MR, Ray WZ, Liu W, Siewe DY, Xia Y. Radially Aligned, Electrospun Nanofibers as Dural Substitutes for Wound Closure and Tissue Regeneration Applications. *ACS Nano* **2010**;4:5027-36.
[111] Mao M, He J, Liu Y, Li X, Li D. Ice-template-induced silk fibroin–chitosan scaffolds with predefined microfluidic channels and fully porous structures. *Acta Biomaterialia* **2012**;8:2175-84.
[112] Csaderova L, Martines E, Seunarine K, Gadegaard N, Wilkinson CDW, Riehle MO. A Biodegradable and Biocompatible Regular Nanopattern for Large-Scale Selective Cell Growth. *Small* **2010**;6:2755-61.
[113] Dalby MJ, Gadegaard N, Tare R, Andar A, Riehle MO, Herzyk P, et al. The control of human mesenchymal cell differentiation using nanoscale symmetry and disorder. *Nat Mater* **2007**;6:997-1003.
[114] He J, Liu Y, Hao X, Mao M, Zhu L, Li D. Bottom-up generation of 3D silk fibroin–gelatin microfluidic scaffolds with improved structural and biological properties. *Materials Letters* **2012**;78:102-5.
[115] Kim D-H, Lee H, Lee YK, Nam J-M, Levchenko A. Biomimetic Nanopatterns as Enabling Tools for Analysis and Control of Live Cells. *Advanced Materials* **2010**;22:4551-66.
[116] Lee CH, Shin HJ, Cho IH, Kang Y-M, Kim IA, Park K-D, et al. Nanofiber alignment and direction of mechanical strain affect the ECM production of human ACL fibroblast. *Biomaterials* **2005**;26:1261-70.
[117] Yin Z, Chen X, Chen JL, Shen WL, Hieu Nguyen TM, Gao L, et al. The regulation of tendon stem cell differentiation by the alignment of nanofibers. *Biomaterials* **2010**;31:2163-75.
[118] Zong X, Bien H, Chung C-Y, Yin L, Fang D, Hsiao BS, et al. Electrospun fine-textured scaffolds for heart tissue constructs. *Biomaterials* **2005**;26:5330-8.
[119] Panseri S, Cunha C, Lowery J, Del Carro U, Taraballi F, Amadio S, et al. Electrospun micro- and nanofiber tubes for functional nervous regeneration in sciatic nerve transections. *BMC Biotechnology* **2008**;8:39.
[120] Xie J, MacEwan MR, Li X, Sakiyama-Elbert SE, Xia Y. Neurite Outgrowth on Nanofiber Scaffolds with Different Orders, Structures, and Surface Properties. *ACS Nano* **2009**;3:1151-9.
[121] Stitzel J, Liu J, Lee SJ, Komura M, Berry J, Soker S, et al. Controlled fabrication of a biological vascular substitute. *Biomaterials* **2006**;27:1088-94.

[122] Lee CH, Singla A, Lee Y. Biomedical applications of collagen. *International journal of pharmaceutics* **2001**;221:1-22.
[123] Solchaga LA, Dennis JE, Goldberg VM, Caplan AI. Hyaluronic acid-based polymers as cell carriers for tissue-engineered repair of bone and cartilage. *Journal of Orthopaedic Research* **1999**;17:205-13.
[124] Middleton JC, Tipton AJ. Synthetic biodegradable polymers as orthopedic devices. *Biomaterials* **2000**;21:2335-46.
[125] Van Natta F, Hill J, Carothers W. Studies of polymerization and ring formation. XXIII. e-caprolactone and its polymers. *J Am Chem Soc* **1934**;56:455-7.
[126] Bordes P, Pollet E, Avérous L. Nano-biocomposites: biodegradable polyester/nanoclay systems. *Progress in Polymer Science* **2009**;34:125-55.
[127] Woodruff MA, Hutmacher DW. The return of a forgotten polymer—polycaprolactone in the 21st century. *Progress in Polymer Science* **2010**;35:1217-56.
[128] Coulembier O, Degée P, Hedrick JL, Dubois P. From controlled ring-opening polymerization to biodegradable aliphatic polyester: Especially poly (β-malic acid) derivatives. *Progress in Polymer Science* **2006**;31:723-47.
[129] Kehoe S, Zhang X, Boyd D. FDA approved guidance conduits and wraps for peripheral nerve injury: a review of materials and efficacy. *Injury* **2012**;43:553-72.
[130] Cipitria A, Skelton A, Dargaville T, Dalton P, Hutmacher D. Design, fabrication and characterization of PCL electrospun scaffolds—a review. *Journal of Materials Chemistry* **2011**;21:9419-53.
[131] Hutmacher D, Cool S. Concepts of scaffold-based tissue engineering—the rationale to use solid free-form fabrication techniques. *Journal of cellular and molecular medicine* **2007**;11:654-69.
[132] Ishii O, Shin M, Sueda T, Vacanti JP. In vitro tissue engineering of a cardiac graft using a degradable scaffold with an extracellular matrix–like topography. *The Journal of thoracic and cardiovascular surgery* **2005**;130:1358-63.
[133] Yoshimoto H, Shin Y, Terai H, Vacanti J. A biodegradable nanofiber scaffold by electrospinning and its potential for bone tissue engineering. *Biomaterials* **2003**;24:2077-82.
[134] Cottin-Bizonne S, Chakfé N, Beaufigeau M, Le Magnen J, Dieval F, Doillon C, et al. Les polymeres synthetiques resorbables: caracteristiques et applications pour les protheses arterielles. *RBM-News* **1999**;21:62-75.
[135] Engelberg I, Kohn J. Physico-mechanical properties of degradable polymers used in medical applications: a comparative study. *Biomaterials* **1991**;12:292-304.
[136] Van der Schueren L, De Schoenmaker B, Kalaoglu ÖI, De Clerck K. An alternative solvent system for the steady state electrospinning of polycaprolactone. *European Polymer Journal* **2011**;47:1256-63.
[137] Ma Z, Mao Z, Gao C. Surface modification and property analysis of biomedical polymers used for tissue engineering. *Colloids and Surfaces B: Biointerfaces* **2007**;60:137-57.
[138] Hutmacher DW. Scaffolds in tissue engineering bone and cartilage. *Biomaterials* **2000**;21:2529-43.
[139] Xiao L, Wang B, Yang G, Gauthier M. Poly (Lactic Acid)-Based Biomaterials: Synthesis, Modification and Applications. *Biomedical Science, Engineering and Technology* **2012**;11.
[140] Benicewicz BC, Hopper PK. Review: Polymers for Absorbable Surgical Sutures—Part II. *Journal of Bioactive and Compatible Polymers* **1991**;6:64-94.
[141] Gupta B, Revagade N, Hilborn J. Poly (lactic acid) fiber: An overview. *Progress in polymer science* **2007**;32:455-82.
[142] Lunt J, Shafer AL. Polylactic acid polymers from com. Applications in the textiles industry. *Journal of Industrial textiles* **2000**;29:191-205.

[143] Lunt J. Large-scale production, properties and commercial applications of polylactic acid polymers. *Polymer degradation and stability* **1998**;59:145-52.
[144] Rasal RM, Janorkar AV, Hirt DE. Poly(lactic acid) modifications. *Progress in Polymer Science* **2010**;35:338-56.
[145] Martin O, Averous L. Poly (lactic acid): plasticization and properties of biodegradable multiphase systems. *Polymer* **2001**;42:6209-19.
[146] Schlosshauer B, Müller E, Schröder B, Planck H, Müller H-W. Rat Schwann cells in bioresorbable nerve guides to promote and accelerate axonal regeneration. *Brain research* **2003**;963:321-6.
[147] Barone DJ, Raquez JM, Dubois P. Bone-guided regeneration: from inert biomaterials to bioactive polymer (nano) composites. *Polymers for Advanced Technologies* **2011**;22:463-75.
[148] Janorkar AV, Metters AT, Hirt DE. Modification of poly (lactic acid) films: enhanced wettability from surface-confined photografting and increased degradation rate due to an artifact of the photografting process. *Macromolecules* **2004**;37:9151-9.
[149] Brady JM, Cutright DE, Miller RA, Battistone GC, Hunsuck EE. Resorption rate, route of elimination, and ultrastructure of the implant site of polylactic acid in the abdominal wall of the rat. *Journal of biomedical materials research* **1973**;7:155-66.
[150] Reed A, Gilding D. Biodegradable polymers for use in surgery—poly (glycolic)/poly (Iactic acid) homo and copolymers: 2. In vitro degradation. *Polymer* **1981**;22:494-8.
[151] Puppi D, Detta N, Piras AM, Chiellini F, Clarke DA, Reilly GC, et al. Development of Electrospun Three-arm Star Poly (ε-caprolactone) Meshes for Tissue Engineering Applications. *Macromolecular bioscience* **2010**;10:887-97.
[152] Lowery JL, Datta N, Rutledge GC. Effect of fiber diameter, pore size and seeding method on growth of human dermal fibroblasts in electrospun poly (ε-caprolactone) fibrous mats. *Biomaterials* **2010**;31:491-504.
[153] Keun Kwon I, Kidoaki S, Matsuda T. Electrospun nano-to microfiber fabrics made of biodegradable copolyesters: structural characteristics, mechanical properties and cell adhesion potential. *Biomaterials* **2005**;26:3929-39.
[154] Lee E-J, Teng S-H, Jang T-S, Wang P, Yook S-W, Kim H-E, et al. Nanostructured poly (ε-caprolactone)–silica xerogel fibrous membrane for guided bone regeneration. *Acta biomaterialia* **2010**;6:3557-65.
[155] Hsu CM, Shivkumar S. N, N-Dimethylformamide Additions to the Solution for the Electrospinning of Poly (ε-caprolactone) Nanofibers. *Macromolecular Materials and Engineering* **2004**;289:334-40.
[156] Uyar T, Besenbacher F. Electrospinning of uniform polystyrene fibers: The effect of solvent conductivity. *Polymer* **2008**;49:5336-43.
[157] Orlova Y, Magome N, Liu L, Chen Y, Agladze K. Electrospun nanofibers as a tool for architecture control in engineered cardiac tissue. *Biomaterials* **2011**;32:5615-24.
[158] Dvir T, Timko BP, Kohane DS, Langer R. Nanotechnological strategies for engineering complex tissues. *Nat Nano* **2011**;6:13-22.
[159] Stevens MM, George JH. Exploring and engineering the cell surface interface. *Science* **2005**;310:1135-8.
[160] Bae W-G, Kim HN, Kim D, Park S-H, Jeong HE, Suh K-Y. 25th Anniversary article: Scalable multiscale patterned structures inspired by Nature: the role of hierarchy. *Advanced Materials* **2013**;26:675-700.
[161] Geiger B, Spatz JP, Bershadsky AD. Environmental sensing through focal adhesions. *Nature reviews molecular cell biology* **2009**;10:21-33.
[162] Bettinger CJ, Langer R, Borenstein JT. Engineering substrate topography at the micro- and nanoscale to control cell function. *Angew Chem Int Ed* **2009**;48:5406-15.
[163] Anselme K. Osteoblast adhesion on biomaterials. *Biomaterials* **2000**;21:667-81.

[164] Chen CS, Mrksich M, Huang S, Whitesides GM, Ingber DE. Geometric Control of Cell Life and Death. *Science* **1997**;276:1425-8.
[165] Cheng Q, Lee BLP, Komvopoulos K, Li S. Engineering the microstructure of electrospun fibrous scaffolds by microtopography. *Biomacromolecules* **2013**;14:1349-60.
[166] Liu Y, Zhang L, Li H, Yan S, Yu J, Weng J, et al. Electrospun fibrous mats on lithographically micropatterned collectors to control cellular behaviors. *Langmuir* **2012**;28:17134−42.
[167] Ortega I, Ryan AJ, Deshpande P, MacNeil S, Claeyssens F. Combined microfabrication and electrospinning to produce 3-D architectures for corneal repair. *Acta Biomaterialia* **2013**;9:5511-20.
[168] Hamilton DW, Chehroudi B, Brunette DM. Comparative response of epithelial cells and osteoblasts to microfabricated tapered pit topographies in vitro and in vivo. *Biomaterials* **2007**;28:2281-93.
[169] Soscia DA, Sequeira SJ, Schramm RA, Jayarathanam K, Cantara SI, Larsen M, et al. Salivary gland cell differentiation and organization on micropatterned PLGA nanofiber craters. *Biomaterials* **2013**;34:6773-84.
[170] Ghasemi-Mobarakeh L, Prabhakaran MP, Balasubramanian P, Jin G, Valipouri A, Ramakrishna S. Advances in electrospun nanofibers for bone and cartilage regeneration. *Journal of Nanoscience and Nanotechnology* **2013**;13:4656-71.
[171] Parfitt AM. Osteonal and hemi-osteonal remodeling: the spatial and temporal framework for signal traffic in adult human bone. *J Cell Biochem* **1994**;55:273-86.
[172] Giraud Guille MM, Mosser G, Helary C, Eglin D. Bone matrix like assemblies of collagen: From liquid crystals to gels and biomimetic materials. *Micron* **2005**;36:602-8.
[173] Ripamonti U. Biomimetism, biomimetic matrices and the induction of bone formation. *Journal of Cellular and Molecular Medicine* **2009**;13:2953-72.
[174] Rumpler M, Woesz A, Dunlop JWC, van Dongen JT, Fratzl P. The effect of geometry on three-dimensional tissue growth. *Journal of The Royal Society Interface* **2008**;5:1173-80.
[175] Bidan CM, Kommareddy KP, Rumpler M, Kollmannsberger P, Bréchet YJM, Fratzl P, et al. How Linear Tension Converts to Curvature: Geometric Control of Bone Tissue Growth. *PLoS ONE* **2012**;7:e36336.
[176] Bidan CM, Kommareddy KP, Rumpler M, Kollmannsberger P, Fratzl P, Dunlop JWC. Geometry as a factor for tissue growth: towards shape optimization of tissue engineering scaffolds. *Adv Healthcare Mater* **2013**;2:186-94.
[177] George J, Kuboki Y, Miyata T. Differentiation of mesenchymal stem cells into osteoblasts on honeycomb collagen scaffolds. *Biotechnology and Bioengineering* **2006**;95:404-11.
[178] Goh Y-F, Shakir I, Hussain R. Electrospun fibers for tissue engineering, drug delivery, and wound dressing. *Journal of Materials Science* **2013**;48:3027-54.
[179] Sill TJ, von Recum HA. Electrospinning: Applications in drug delivery and tissue engineering. *Biomaterials* **2008**;29:1989-2006.
[180] Tamayol A, Akbari M, Annabi N, Paul A, Khademhosseini A, Juncker D. Fiber-based tissue engineering: Progress, challenges, and opportunities. *Biotechnology Advances* **2013**;31:669-87.
[181] Lavielle N, Hébraud A, Schlatter G, Thöny-Meyer L, Rossi RM, Popa AM. Simultaneous electrospinning and electrospraying: A straightforward approach for fabricating hierarchically structured composite membranes. *ACS Applied Materials and Interfaces* **2013**;5:10090-7.
[182] Daming Z, Jiang C. Electrospinning of three-dimensional nanofibrous tubes with controllable architectures. *Nano Letters* **2008**;8:3283 - 7.

[183] Li D, Wang Y, Xia Y. Electrospinning Nanofibers as Uniaxially Aligned Arrays and Layer-by-Layer Stacked Films. *Advanced Materials* **2004**;16:361-6.
[184] Zhang DM, Chang J. Patterning of electrospun fibers using electroconductive templates. *Advanced Materials* **2007**;19:3664-7.
[185] Ding Z, Salim A, Ziaie B. Selective Nanofiber Deposition through Field-Enhanced Electrospinning. *Langmuir* **2009**;25:9648-52.
[186] Rogers CM, Morris GE, Gould TWA, Bail R, Toumpaniari S, Harrington H, et al. A novel technique for the production of electrospun scaffolds with tailored three-dimensional micro-patterns employing additive manufacturing. *Biofabrication* **2014**;6:035003.
[187] Lukáš D, Sarkar A, Martinová L, Vodsed'álková K, Lubasová D, Chaloupek J, et al. Physical principles of electrospinning (Electrospinning as a nanoscale technology of the twenty-first century. *Textile Progress* **2009**;41:59-140.
[188] Ma Z, Kotaki M, Inai R, Ramakrishna S. Potential of nanofiber matrix as tissue-engineering scaffolds. *Tissue Engineering* **2005**;11:101-9.
[189] Li WJ, Laurencin CT, Caterson EJ, Tuan RS, Ko FK. Electrospun nanofibrous structure: a novel scaffold for tissue engineering. *Journal of biomedical materials research* **2002**;60:613-21.
[190] Madden LR, Mortisen DJ, Sussman EM, Dupras SK, Fugate JA, Cuy JL, et al. Proangiogenic scaffolds as functional templates for cardiac tissue engineering. *Proc Natl Acad Sci U S A* **2010**;107:15211-6.
[191] Salgado AJ, Coutinho OP, Reis RL. Bone tissue engineering: state of the art and future trends. *Macromol Biosci* **2004**;4:743-65.
[192] Pham QP, Sharma U, Mikos AG. Electrospun poly (ε-caprolactone) microfiber and multilayer nanofiber/microfiber scaffolds: characterization of scaffolds and measurement of cellular infiltration. *Biomacromolecules* **2006**;7:2796-805.
[193] Shalumon KT, Chennazhi KP, Nair SV, Jayakumar R. High Thick Layer-by-Layer 3D Multiscale Fibrous Scaffolds for Enhanced Cell Infiltration and It's Potential in Tissue Engineering. *Journal of Biomedical Nanotechnology* **2013**;9:2117-22.
[194] Chen X, Fu X, Shi J-g, Wang H. Regulation of the osteogenesis of pre-osteoblasts by spatial arrangement of electrospun nanofibers in two- and three-dimensional environments. *Nanomedicine: Nanotechnology, Biology and Medicine* **2013**;9:1283-92.
[195] Kim TG, Chung HJ, Park TG. Macroporous and nanofibrous hyaluronic acid/collagen hybrid scaffold fabricated by concurrent electrospinning and deposition/leaching of salt particles. *Acta Biomaterialia* **2008**;4:1611-9.
[196] Teo W, Liao S, Chan C, Ramakrishna S. Remodeling of three-dimensional hierarchically organized nanofibrous assemblies. *Current Nanoscience* **2008**;4:361-9.
[197] Blakeney BA, Tambralli A, Anderson JM, Andukuri A, Lim D-J, Dean DR, et al. Cell infiltration and growth in a low density, uncompressed three-dimensional electrospun nanofibrous scaffold. *Biomaterials* **2011**;32:1583-90.
[198] Jin L, Feng Z-Q, Wang T, Ren Z, Ma S, Wu J, et al. A novel fluffy hydroxylapatite fiber scaffold with deep interconnected pores designed for three-dimensional cell culture. *Journal of Materials Chemistry B* **2014**;2:129.
[199] Wang Z, Cui Y, Wang J, Yang X, Wu Y, Wang K, et al. The effect of thick fibers and large pores of electrospun poly(ε-caprolactone) vascular grafts on macrophage polarization and arterial regeneration. *Biomaterials* **2014**;35:5700-10.
[200] Baker BM, Gee AO, Metter RB, Nathan AS, Marklein RA, Burdick JA, et al. The potential to improve cell infiltration in composite fiber-aligned electrospun scaffolds by the selective removal of sacrificial fibers. *Biomaterials* **2008**;29:2348-58.

[201] Wang K, Zhu M, Li T, Zheng W, Xu LL, Zhao Q, et al. Improvement of Cell Infiltration in Electrospun Polycaprolactone Scaffolds for the Construction of Vascular Grafts. *Journal of Biomedical Nanotechnology* **2014**;10:1588-98.
[202] Leong MF, Rasheed MZ, Lim TC, Chian KS. In vitro cell infiltration and in vivo cell infiltration and vascularization in a fibrous, highly porous poly(D,L-lactide) scaffold fabricated by cryogenic electrospinning technique. *Journal of Biomedical Materials Research Part A* **2009**;91A:231-40.
[203] Simonet M, Schneider OD, Neuenschwander P, Stark WJ. Ultraporous 3D polymer meshes by low-temperature electrospinning: Use of ice crystals as a removable void template. *Polymer Engineering & Science* **2007**;47:2020-6.
[204] Kim MS, Kim GH. Highly porous electrospun 3D polycaprolactone/β-TCP biocomposites for tissue regeneration. *Materials Letters* **2014**;120:246-50.
[205] Nedjari S, Eap S, Hébraud A, Wittmer CR, Benkirane-Jessel N, Schlatter G. Electrospun Honeycomb as Nests for Controlled Osteoblast Spatial Organisation. *Macromolecular Bioscience* **2014**;DOI: 10.1002/mabi.201400226.
[206] Wittmer CR, Hébraud A, Nedjari S, Schlatter G. Well-organized 3D nanofibrous composite constructs using cooperative effects between electrospinning and electrospraying. *Polymer* **2014**;55:5781-7.
[207] Karageorgiou V, Kaplan D. Porosity of 3D biomaterial scaffolds and osteogenesis. *Biomaterials* **2005**;26:5474-91.
[208] Ankam S, Teo BK, Kukumberg M, Yim EK. High throughput screening to investigate the interaction of stem cells with their extracellular microenvironment. *Organogenesis* **2013**;9:128-42.
[209] Gupta K, Kim DH, Ellison D, Smith C, Kundu A, Tuan J, et al. Lab-on-a-chip devices as an emerging platform for stem cell biology. *Lab Chip* **2010**;10:2019-31.
[210] Markert LDA, Lovmand J, Foss M, Lauridsen RH, Lovmand M, Füchtbauer E-M, et al. Identification of distinct topographical surface microstructures favoring either undifferentiated expansion or differentiation of murine embryonic stem cells. *Stem cells and development* **2009**;18:1331-42.
[211] Unadkat HV, Hulsman M, Cornelissen K, Papenburg BJ, Truckenmüller RK, Carpenter AE, et al. An algorithm-based topographical biomaterials library to instruct cell fate. *Proceedings of the National Academy of Sciences* **2011**;108:16565-70.
[212] Ankam S, Suryana M, Chan LY, Moe AAK, Teo BK, Law JB, et al. Substrate topography and size determine the fate of human embryonic stem cells to neuronal or glial lineage. *Acta biomaterialia* **2013**;9:4535-45.
[213] Moe AAK, Suryana M, Marcy G, Lim SK, Ankam S, Goh JZW, et al. Microarray with Micro-and Nano-topographies Enables Identification of the Optimal Topography for Directing the Differentiation of Primary Murine Neural Progenitor Cells. *Small* **2012**;8:3050-61.
[214] Xu C, Inai R, Kotaki M, Ramakrishna S. Electrospun nanofiber fabrication as synthetic extracellular matrix and its potential for vascular tissue engineering. *Tissue Engineering* **2004**;10:1160-8.
[215] Yang F, Murugan R, Wang S, Ramakrishna S. Electrospinning of nano/micro scale poly (L-lactic acid) aligned fibers and their potential in neural tissue engineering. *Biomaterials* **2005**;26:2603-10.
[216] Zhu X, Cui W, Li X, Jin Y. Electrospun fibrous mats with high porosity as potential scaffolds for skin tissue engineering. *Biomacromolecules* **2008**;9:1795-801.
[217] Gallego-Perez D, Higuita-Castro N, Sharma S, Reen RK, Palmer AF, Gooch KJ, et al. High throughput assembly of spatially controlled 3D cell clusters on a micro/nanoplatform. *Lab Chip* **2010**;10:775-82.

[218] Lee HJ, Nam SH, Son KJ, Koh W-G. Micropatterned Fibrous Scaffolds Fabricated Using Electrospinning and Hydrogel Lithography: New Platforms to Create Cellular Micropatterns. *Sensors and Actuators B: Chemical* **2010**;148:504-10.
[219] Nedjari S, Eap S, Hébraud A, Wittmer CR, Benkirane-Jessel N, Schlatter G. Electrospun Honeycomb as Nests for Controlled Osteoblast Spatial Organisation. *Macromolecular Bioscience* **2014**;in press:DOI: 10.1002/mabi.201400226.
[220] Wallin P, Zanden C, Carlberg B, Hellstrom Erkenstam N, Liu J, Gold J. A method to integrate patterned electrospun fibers with microfluidic systems to generate complex microenvironments for cell culture applications. *Biomicrofluidics* **2012**;6:24131.
[221] Wutticharoenmongkol P, Sanchavanakit N, Pavasant P, Supaphol P. Preparation and characterization of novel bone scaffolds based on electrospun polycaprolactone fibers filled with nanoparticles. *Macromolecular bioscience* **2006**;6:70-7.
[222] Francis L, Venugopal J, Prabhakaran MP, Thavasi V, Marsano E, Ramakrishna S. Simultaneous electrospin–electrosprayed biocomposite nanofibrous scaffolds for bone tissue regeneration. *Acta biomaterialia* **2010**;6:4100-9.
[223] Gupta D, Venugopal J, Mitra S, Giri Dev V, Ramakrishna S. Nanostructured biocomposite substrates by electrospinning and electrospraying for the mineralization of osteoblasts. *Biomaterials* **2009**;30:2085-94.
[224] Hench LL. Bioceramics: from concept to clinic. *Journal of the American Ceramic Society* **1991**;74:1487-510.
[225] Kim S-S, Sun Park M, Jeon O, Yong Choi C, Kim B-S. Poly (lactide-< i> co</i>-glycolide)/hydroxyapatite composite scaffolds for bone tissue engineering. *Biomaterials* **2006**;27:1399-409.
[226] Thian ES, Li X, Huang J, Edirisinghe MJ, Bonfield W, Best SM. Electrospray deposition of nanohydroxyapatite coatings: A strategy to mimic bone apatite mineral. *Thin Solid Films* **2011**;519:2328-31.
[227] Huang J, Jayasinghe S, Best S, Edirisinghe M, Brooks R, Bonfield W. Electrospraying of a nano-hydroxyapatite suspension. *Journal of materials science* **2004**;39:1029-32.
[228] Huang J, Best S, Bonfield W, Brooks R, Rushton N, Jayasinghe S, et al. In vitro assessment of the biological response to nano-sized hydroxyapatite. *Journal of Materials Science: Materials in Medicine* **2004**;15:441-5.
[229] Muthutantri A, Huang J, Edirisinghe M. Novel method of preparing hydroxyapatite foams. *Journal of Materials Science: Materials in Medicine* **2008**;19:1485-90.
[230] Venugopal J, Rajeswari R, Shayanti M, Low S, Bongso A, R. Giri Dev V, et al. Electrosprayed hydroxyapatite on polymer nanofibers to differentiate mesenchymal stem cells to osteogenesis. *Journal of Biomaterials Science, Polymer Edition* **2013**;24:170-84.
[231] Kim HW, Song JH, Kim HE. Nanofiber generation of gelatin–hydroxyapatite biomimetics for guided tissue regeneration. *Advanced functional materials* **2005**;15:1988-94.
[232] Donati I, Paoletti S. Material properties of alginates. *Alginates: biology and applications*: Springer; **2009**. p. 1-53.
[233] Daemi H, Barikani M. Synthesis and characterization of calcium alginate nanoparticles, sodium homopolymannuronate salt and its calcium nanoparticles. *Scientia Iranica* **2012**;19:2023-8.
[234] Rowley JA, Madlambayan G, Mooney DJ. Alginate hydrogels as synthetic extracellular matrix materials. *Biomaterials* **1999**;20:45-53.
[235] Dvir-Ginzberg M, Gamlieli-Bonshtein I, Agbaria R, Cohen S. Liver tissue engineering within alginate scaffolds: effects of cell-seeding density on hepatocyte viability, morphology, and function. *Tissue Engineering* **2003**;9:757-66.
[236] Bhattarai N, Li Z, Edmondson D, Zhang M. Alginate-based nanofibrous scaffolds: Structural, mechanical, and biological properties. *Advanced Materials* **2006**;18:1463-7.

[237] Alborzi S, Lim LT, Kakuda Y. Electrospinning of Sodium Alginate-Pectin Ultrafine Fibers. *Journal of food science* **2010**;75:C100-7.
[238] Saquing CD, Tang C, Monian B, Bonino CA, Manasco JL, Alsberg E, et al. Alginate–Polyethylene Oxide Blend Nanofibers and the Role of the Carrier Polymer in Electrospinning. *Industrial & Engineering Chemistry Research* **2013**;52:8692-704.
[239] Porter JR, Ruckh TT, Popat KC. Bone tissue engineering: a review in bone biomimetics and drug delivery strategies. *Biotechnology Progress* **2009**;25:1539-60.
[240] Ng R, Zang R, Yang KK, Liu N, Yang ST. Three-dimensional fibrous scaffolds with microstructures and nanotextures for tissue engineering. *RSC Advances* **2012**;2:10110-24.
[241] Zhang Q, Welch J, Park H, Wu CY, Sigmund W, Marijnissen JCM. Improvement in nanofiber filtration by multiple thin layers of nanofiber mats. *Journal of Aerosol Science* **2010**;41:230-6.
[242] Krishnamoorthy T, Thavasi V, Subodh G M, Ramakrishna S. A first report on the fabrication of vertically aligned anatase TiO 2 nanowires by electrospinning: Preferred architecture for nanostructured solar cells. *Energy and Environmental Science* **2011**;4:2807-12.
[243] Soliman S, Pagliari S, Rinaldi A, Forte G, Fiaccavento R, Pagliari F, et al. Multiscale three-dimensional scaffolds for soft tissue engineering via multimodal electrospinning. *Acta Biomaterialia* **2010**;6:1227-37.
[244] Simonet M, Stingelin N, Wismans JGF, Oomens CWJ, Driessen-Mol A, Baaijens FPT. Tailoring the void space and mechanical properties in electrospun scaffolds towards physiological ranges. *J Mater Chem B* **2014**;2:305-13.
[245] Shim IK, Suh WH, Lee SY, Lee SH, Heo SJ, Lee MC, et al. Chitosan nano-/microfibrous double-layered membrane with rolled-up three-dimensional structures for chondrocyte cultivation. *J Biomed Mater Res A* **2009**;90:595-602.
[246] Zhang DM, Chang J. Electrospinning of Three-Dimensional Nanofibrous Tubes with Controllable Architectures. *Nano Letters* **2008**;8:3283-7.
[247] Yokoyama Y, Hattori S, Yoshikawa C, Yasuda Y, Koyama H, Takato T, et al. Novel wet electrospinning system for fabrication of spongiform nanofiber 3-dimensional fabric. *Materials Letters* **2009**;63:754-6.
[248] Reis TC, Correia IJ, Aguiar-Ricardo A. Electrodynamic tailoring of self-assembled three-dimensional electrospun constructs. *Nanoscale* **2013**;5:7528-36.
[249] Sun DH, Chang C, Li S, Lin LW. Near-field electrospinning. *Nano Letters* **2006**;6:839–42.
[250] Huang Y, Bu N, Duan Y, Pan Y, Liu H, Yin Z, et al. Electrohydrodynamic direct-writing. *Nanoscale* **2013**;5:12007-17.
[251] Kim H-Y, Lee M, Park KJ, Kim S, Mahadevan L. Nanopottery: Coiling of Electrospun Polymer Nanofibers. *Nano Letters* **2010**;10:2138–40.
[252] Dalton PD, Vaquette C, Farrugia BL, Dargaville TR, Brown TD, Hutmacher DW. Electrospinning and additive manufacturing: converging technologies. *Biomaterials Science* **2013**;1:171-85.
[253] Theron SA, Zussman E, Yarin AL. Experimental investigation of the governing parameters in the electrospinning of polymer solutions. *Polymer* **2004**;45:2017-30.
[254] Silberstein MN, Pai CL, Rutledge GC, Boyce MC. Elasticplastic behavior of non-woven fibrous mats. *Journal of the Mechanics and Physics of Solids* **2012**;60:295-318.
[255] Bryers JD, Giachelli CM, Ratner BD. Engineering biomaterials to integrate and heal: The biocompatibility paradigm shifts. *Biotechnol Bioeng* **2012**;109:1898-911.
[256] Madden LR, Mortisen DJ, Sussman EM, Dupras SK, Fugate JA, Cuy JL, et al. Proangiogenic scaffolds as functional templates for cardiac tissue engineering. *PNAS* **2010**;107:15211-6.

# Publications Lists and communications

## Articles in international peer reviewed journal:

**Salima Nedjari,** Guy Schlatter, Anne Hébraud, **"Thick Honeycomb Electrospun Scaffold with Controlled Pore Size",** accepted in *Material Letters*,DOI:10.1016/j.matlet.2014.11.118, 2014

**Salima Nedjari**, Sandy Eap, Anne Hébraud, Corinne R. Wittmer, Nadia Benkirane-Jessel, Guy Schlatter, **"Electrospun Honeycomb as Nests for Controlled Osteoblast Spatial Organization**, *Macromolecular Bioscience*, 2014,Vol. 14, 1580–1589

Corinne R. Wittmer, Anne Hébraud, **Salima Nedjari**, Guy Schlatter, **"Well-Organized 3D Nanofibrous Constructs using Cooperative Effects between Electrospinning and Electrospraying",***Polymer*, 2014, Vol. 55, 5781-5787

## Book chapter:

**Salima Nedjari**, Anne Hébraud, Guy Schlatter, **"Organized assembly of electrospun nanofibers: from 1D to 3D"** Book chapter under press in *Electrospinning: Principles, possibilities and practice*, Eds. Royal Society of Chemistry, ISBN 13: 9781849735568, ISBN 10: 1849735565, 2014.

## Communications:

Oral presentation in international conference:

**S. Nedjari,** S. Eap, A. Hébraud, N. Benkirane-Jessel, G. Schlatter, **"Micro-weaving of honeycomb nanofibrous membranes : application to bone regeneration"**, Istanbul Textile Congress, 30$^{th}$ may-1$^{er}$ june 2013, Istanbul, Turkey.

Posters:

**Best poster price: S. Nedjari,** S. Eap, A. Hébraud, N. Benkirane-Jessel, G. Schlatter, **"Micro-tissage de membranes nanofibreuses : application à la régénération osseuse",** 41$^{ème}$ Colloque National du GFP, Groupe Français des Polymères, 19-22 november 2012, Grenoble, France.

**Best poster price: S. Nedjari,** S. Eap, A. Hébraud, N. Benkirane-Jessel, G. Schlatter, **"3D Micro-weaving of honeycomb of electrospun nanofibers: application to bone regeneration",** Conference « Electrospinning, Principles, Practice and Possibilities », Institute of Physics, 21-22 march 2012, London, UK.

**S. Nedjari**, C. R. Wittmer, S. Eap, A. Hébraud, N. Benkirane-Jessel, S. Geffray, G.Schlatter, **"3D micro-weaving of electrospun nanofibers: Design and fabrication of nanostructured biochips for tissue engineering applications"**, Journées Nationales des Nanosciences et des Nanotechnologies, 4-6 november 2013, Marseille, France.

Salima NEDJARI

# Microstructuration of nanofibrous membranes by electrospinning: Application to tissue engineering

**Résumé :** L'objectif de cette thèse était de développer de nouveaux biomatériaux nanofibreux architecturés (2D ou 3D) grâce à la méthode d'électrospinning puis d'étudier l'influence de ces structures nanofibreuses sur le comportement des cellules osseuses. L'électrospinning est une technique qui permet d'obtenir des nanofibres en projetant sous l'action d'un champ électrique intense une solution de polymère sur un collecteur. Les nanofibres sont alors généralement disposées aléatoirement sous forme de mats (ou scaffolds). Ces scaffolds trouvent des applications en ingénierie tissulaire grâce à leur structure mimant la matrice extracellulaire des tissus vivants. Toutefois, il a été montré que lorsque le collecteur est micro-structuré, il est alors possible de contrôler l'organisation des fibres lors de leur dépôt grâce à la perturbation locale du champ électrique au voisinage de la surface du collecteur. Ces collecteurs architecturés jouent ainsi le rôle de « templates » électrostatiques. Dans un premier temps, nous avons développé des scaffolds 2D nanofibreux monocomposants en forme de nids d'abeilles grâce à l'utilisation d'un collecteur micro-structuré en nids d'abeilles lors du procédé d'électrospinning. Ces scaffolds ont été développés à partir de deux biopolyesters le poly(ε-caprolactone) (PCL) ou le poly(lactic acid) (PLA). Nous avons prouvé que la morphologie des nanofibres de PCL (distribution bimodale du diamètre des fibres) conduisait à un scaffold présentant un relief beaucoup plus marqué alors qu'avec les fibres de PLA, qui présentent une distribution monomodale du diamètre des fibres, les scaffolds obtenus sont beaucoup plus plats. Nous avons montré qu'il est possible de contrôler l'organisation spatiale de cellules osseuses de type MG-63, des ostéoblastes, en jouant sur le relief et l'architecture du scaffold. Puis, nous avons démontré qu'en couplant la micro-structuration des nanofibres de PCL (par l'utilisation d'un collecteur en nid d'abeilles lors du procédé d'électrospinning) avec les propriétés d'auto-assemblage du PCL, nous pouvions élaborer de nouveaux scaffolds nanofibreux 3D ayant la particularité de présenter des pores de tailles contrôlées ainsi qu'un gradient de porosité dans l'épaisseur du scaffold. Puis nous nous sommes intéressés à l'élaboration de membranes composites micro-structurées 2D et 3D. En couplant le procédé d'électrospinning avec le procédé d'électrospraying sur des collecteur micro-structurés, nous avons démontré que nous pouvions déposer de manière contrôlée les particules spécialement sur les murs des nids d'abeilles grâce notamment à la présence d'une très fine couche de fibres électrospinnées au préalable sur le collecteur. Cette fine couche de nanofibres joue le rôle de « template électrostatique » pour le dépôt des particules. Nous avons ensuite appliqué cette technique pour développer des membranes composites nanofibreuses bicouches à base de nanofibres de PCL et de microparticules d'hydroxyapatite (HA). Ces membranes composées de 21 microarchitectures différentes (barres, plots, hexagones, labyrinthe) ont ensuite été intégrées dans des mini plaques de culture cellulaire, formant ainsi un nouveau type de biopuce, appelés biochips, qui permettent pour le screening des microarchitectures nanofibreuses. Enfin, en combinant simultanément l'électrospinning de nanofibres et l'électrospraying de particules sur des collecteur micro-structurés en nid d'abeilles, des scaffolds composites 3D présentant des pores cylindriques de tailles contrôlées ont été élaborés.

**Abstract:** The aim of this thesis was to develop new architectured nanofibrous biomaterials (2D or 3D) using the electrospinning method and to study the influence of these nanofibrous structures on bone cells behaviors. Electrospinning is a technique allowing the production of nanofibers by projecting, under the action of a strong electric field, a polymer solution on a collector. The nanofibers are generally randomly deposited and form mats or scaffolds. These scaffolds are interesting for tissue engineering applications because of their structure mimicking the extracellular matrix of living tissues. However, it has been shown that when the collector is microstructured, it is possible to control the organization of the fibers during their deposition through the local perturbation of the electric field at the vicinity of the surface of the collector. These micropatterned collectors act as "electrostatic templates". First, 2D honeycomb nanofibrous scaffolds were elaborated using micropatterned honeycomb collectors during the electrospinning process. These scaffolds were made either with poly(ε-caprolactone) (PCL) or poly(lactic acid) (PLA). We showed that the morphology of the PCL nanofibers (bimodal distribution of the fiber diameter) led to a scaffold with a strong relief. Despite, with PLA fibers which presented a monomodal distribution of the fiber diameter, the obtained scaffolds were much flatter. It was possible to control the spatial organization of bone-like cells MG-63 (osteoblasts), playing on the relief and the architecture of the scaffold. Subsequently, 3D materials were elaborated using micropatterned collectors in order to open new paths for the development of filling materials for bone regeneration. Microstructuration of PCL nanofibers (by the use of micropatterned honeycomb collector during the electrospinning process) coupled with the self-assembling properties of the PCL lead to the development of new 3D nanofibrous scaffolds, with controlled pore size and porosity gradient in the thickness of the scaffold. Afterwards, micropatterned composite 2D and 3D membranes were elaborated. By coupling the process of electrospinning with the process of electrospraying on micropatterned collector, we demonstrated that we can deposit the particles in a controlled way, especially on the walls of honeycomb patterns thanks to the presence of a thin fiber layer first deposited on the collector. This thin nanofiber layer plays the role of an "*electrostatic template*" for the particles deposition. Thereafter, this technique was applied to develop bilayers composite nanofibrous membranes containing PCL nanofibers and hydroxyapatite (HA) microparticles. These membranes consisted of 21 different microarchitectures (bars, blocks, hexagons, maze) were then incorporated into a small cell culture plate, thereby forming a new type of biochip for the screening of nanofibrous architectures. Indeed, these biochips allowed the screening of nanofibrous microarchitectures to identify the most relevant for bone regeneration. It turned out that the HA hexagonal structures (with an average diameter of 300 microns) and circular HA structures (with an average diameter of 150 microns) are the structures that enhance the most the mineralization process of bone cells.